DNA Recognition by the Enantiomers of $Rh(en)_2phi^{3+}$: Recognition through Hydrogen Bonding and van der Waals Contacts.

Thesis by

Thomas P. Shields

In Partial Fulfillment of the Requirements

for the Degree of

Doctor of Philosophy

California Institute of Technology

Pasadena, California

1995

(Submitted March 1, 1995)

ACKNOWLEDGEMENTS

First and foremost I would like to thank my advisor, Professor Jackie Barton for her support, encouragement and insight during the course of my research at CalTech. Jackie has always been a positive force in moving this project forward and indeed, if there is any logical progression apparent in the following pages, it is to her credit. Jackie has been an inspiration not only through her relentlessly positive attitude, but her dedication to her group and her science. I would also like to thank my undergraduate advisor, Professor A. Graham Lappin at Notre Dame, for encouraging me to attend CalTech and being a great guy in general.

I would like to thank the members of the "small molecule group" - Dr. Louis Kuo, Dr. Achim Krotz, Dr. J. Grant Collins and Brian Hudson for their help and advise over the past 5 years. I must also thank the entire Barton group, past and present, for their companionship and camaraderie. Anna Marie Pyle first introduced me to Jackie's lab, and watched over me for a summer when I was a naive kid from the country. Christy Chow was always a good friend to me, as were Dr. Alan Friedman, Dr. Eric Long and Dr. Takashi Morii. Dr. Louis Kuo helped me out tremendously in my early years, and Dr. Achim Krotz provided several of the compounds used in these experiments. Tim Johann was always willing to discuss binding constants, and also encouraged me to take up ice hockey. Bob Terbreuggen injected a spark into our lab, and is a decent guy for a Michigan alum. Finally, Mo Renta has been a good friend and an incredible source of help and information.

During my years here at CalTech, I have managed to find several diversions from the demands of laboratory life. The Hogs, the Chemistry soccer team, and the Caltech Hockey club have provided atheletic outlets for my frustrations and energies. In addition, I

will always cherish those deafening jam sessions with Resbit, as well as our few live gigs. While these antics have helped to keep me sane, they have also provided me with opportunities to develop outside of science. Tim Herzog and Mike Abrams deserve special credit for not only being fine Hogs, but tremendous house mates.

I could never fully express my gratitude to my family, who have provided the love and stability that are my cornerstones. My parents, who have made countless sacrifices in order to provide me with the educational opportunities I have enjoyed, have also shown me how to lead lives guided by love and care for others. Finally, the completion of this thesis would not have been possible without the love and understanding of Aaiysha Khursheed. She has shown incredible patience these last few months, and has provided me with unerring support during the trying times of thesis writing.

ABSTRACT

The enantiomers of $Rh(en)_2phi^{3+}$ (en = ethylene diamine, phi = 9,10-phenanthrene-quinone diimine) have been prepared in order to explore systematically the contributions of hydrogen bonding and van der Waals contacts to sequence selective DNA binding. Both enantiomers bind strongly to DNA via intercalation of the aromatic phi ligand, and produce direct strand scission upon irradiation with near-UV light. The cleavage mechanism is consistent with the direct abstraction of the C3'-H atom from the major groove of DNA by a bound, photoexcited $Rh(phi)^{3+}$ species. Elements of the sequence specificity of Λ- and Δ-$Rh(en)_2phi^{3+}$ were established by comparing recognition characteristics to those of several $Rh(phi)^{3+}$ complexes containing ancillary saturated amines and a thioether, and by cleavage of oligonucleotide targets containing O^6methylguanine, 7-deazaguanine and deoxyuracil substitutions. Both enantiomers display a strong sensitivity to the inclusion or removal of a single methyl group in the major groove of DNA. Δ-$Rh(en)_2phi^{3+}$ displays relatively high selectivity in targeting 5'-GC-3' steps and this selectivity is the result of hydrogen bonding between the axial amines of the metal complex and the O^6 position of guanine residues. In contrast, Λ-$Rh(en)_2phi^{3+}$ is less selective; besides binding to 5'-GC-3' steps, the Λ-enantiomer also recognizes 5'-TX-3' steps through a positive van der Waals contact between the ancillary methylene groups and the 5-methyl group of thymine. The structural basis for these enantioselective elements of recognition have also been investigated via 1D- and 2D- ^1H NMR methods. Both Λ- and Δ-$Rh(en)_2phi^{3+}$ bind to $d(GTGCAC)_2$ by classical intercalation, and 2D-NOESY studies of the Δ-$Rh(en)_2phi^{3+}$: $d(GTGCAC)_2$ complex demonstrate specific intercalation at the central 5'-GC-3' site. Molecular models show that deep intercalation of the phi ligand ideally locates the ancillary ethylene diamine ligands for the proposed hydrogen bonding and van der Waals contacts. While illustrating the importance of hydrogen bonding and van der Waals contacts in achieving site specificity, the current work also suggests a modular approach to the design of molecules capable of recognizing larger DNA sequences.

TABLE OF CONTENTS

LIST OF FIGURES

LIST OF TABLES

Chapter 2 :

LIST OF SCHEMES

Chapter 1: Introduction.

1.1. The general features of protein : DNA recognition.

Over 40 years ago, Watson and Crick identified deoxyribonucleic acid (DNA) as the primary source of genetic information.[1] Consisting of a series of hydrogen bonded base pairs stacked together like rungs on a twisting ladder, the DNA double helix encodes all the information necessary for cellular life. DNA binding proteins, due to their central role in accessing and maintaining this storehouse of information, play an equally critical role in cellular development, differentiation and growth. Understanding those factors which contribute to the sequence specific recognition of DNA by proteins is therefore a fascinating and alluring area of research.[2-4]

Figure 1.1. Watson Crick GC and AT base pairs.

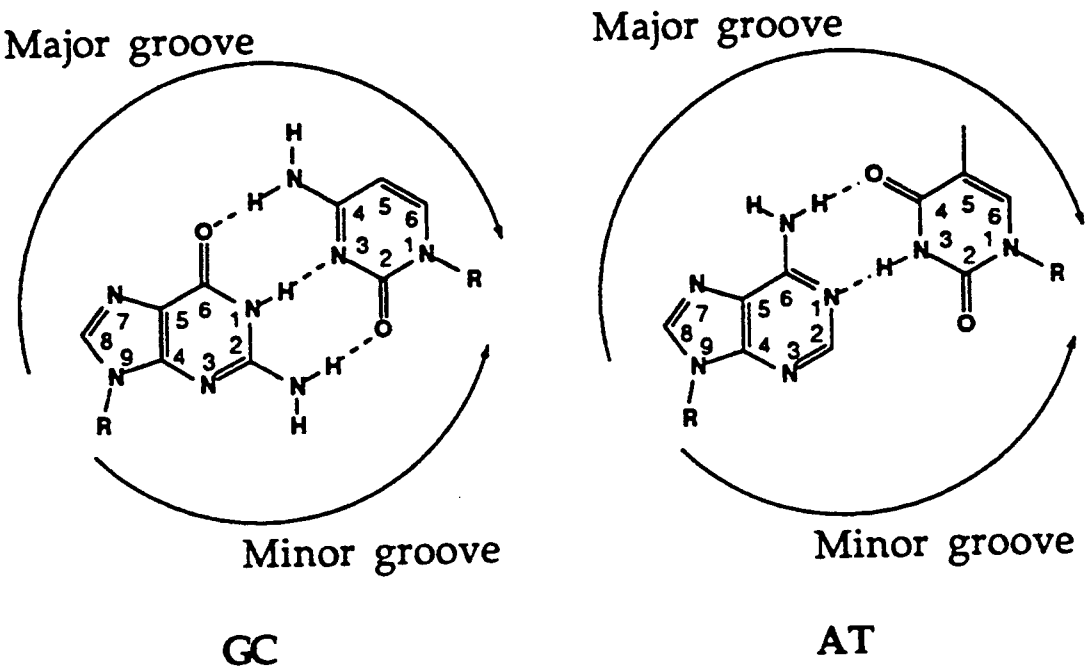

Figure 1.2. The structure of double helical DNA. This picture illustrates the right-handed helical nature of B-form DNA. The negatively charged sugar phosphate backbone, colored in green, spirals upward, enclosing the base pairs. The structure of the duplex is held together by the hydrogen bonding of the base pairs (shown in red), as well as the stacking of the aromatic bases in the extended π-system along the helical axis.

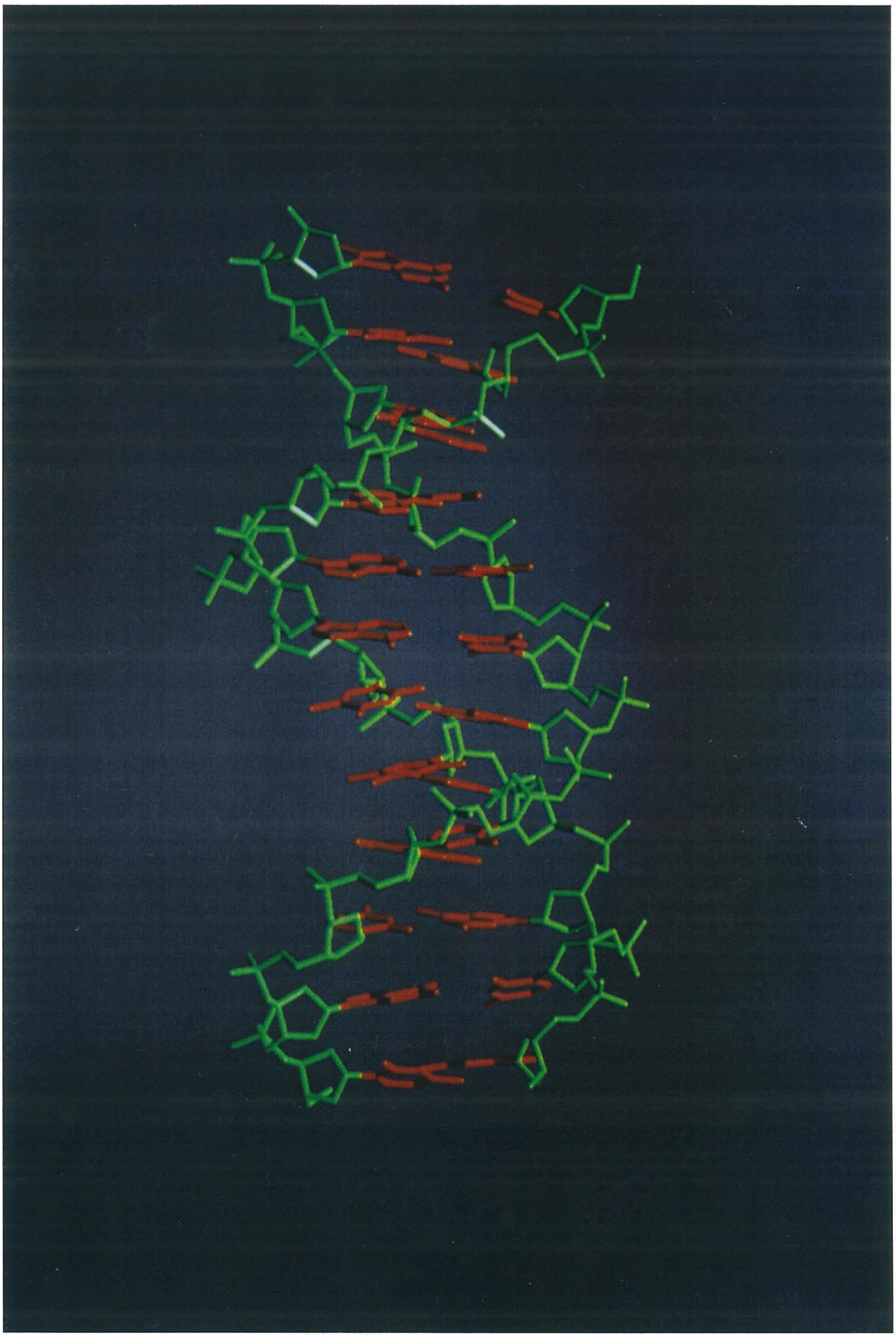

While the DNA genome represents a tremendous library of information, this information must somehow be accessed, in order to translate the primary sequence information into proteins capable of cellular functions. DNA transcription factors control the most basic cellular processes of transcription, replication and repair of the genome by binding to their target sequences with high affinity and specificity.[4] This recognition is achieved by an impressive array of weak non-covalent interactions with DNA - electrostatic attractions, salt bridges, hydrogen bonding and van der Waals contacts. In addition to these direct interactions, the importance of overall shape complementarity between a protein and DNA is also emerging as an important factor in achieving sequence specific DNA recognition. Finally, transcription factors often engage in protein - protein dimerization, in order to increase their total binding energy as well as to enlarge the range of DNA targets through both hetero- and homo-dimerization.

An amazing result from the study of DNA transcription factors is that nature has solved the crucial problem of DNA recognition several times. Both phylogenetic and structural studies have illustrated that transcription factors may be grouped into a number of families, often characterized by the motif employed to engage in sequence specific contacts. Thus, instead of a single alphabet or code for the recognition of the DNA bases, there appear to be multiple means to achieving the same recognition. In the current database of structurally characterized DNA : protein complexes, there are several different motifs utilized to recognize either the GC or AT base pair, and likewise, the same amino acid does not always recognize the same base pair. In spite of the wide variances noted between different families of DNA transcription factors, there are several unifying themes upon which sequence specific DNA recognition appears to rest. One such underlying theme is that sequence specific recognition of DNA most often occurs in the major groove of DNA. Nature has likely chosen the major groove for its larger size (about size of a single α-helix) as well as the unique disposition of potential hydrogen bonding and van der Waals functionality encoded by the GC and AT base pairs.[5]

Although the sequence of DNA represents a direct source of encoded information, it also represents an indirect source of information through the polymorphism of sequence dependent DNA structure.[6] Likewise, DNA binding proteins seem to be capable of both direct and indirect readout of the DNA helix.[4,7,8] While the elements of direct readout direct readout - hydrogen bonding and van der Waals contacts - are familiar to every chemist, the importance of indirect readout was not initially expected, and is still not well understood. Two transcription factors exemplifying this dual recognition are the Zif268 and TATA-box binding proteins.

The co-crystal structure of the zinc finger protein Zif268 bound to its 9 base pair (bp) recognition sequence represents a paradigm for the direct readout of DNA.[7] In the crystal structure, three zinc fingers aligned in tandem recognize three base pair regions of DNA through a network of hydrogen bonding contacts between amino acid side chains and 6 guanine residues. Amazingly, 5 of these 6 contacts are made between arginine side chains and guanine residues through a unique bidentate hydrogen bond. Since there are no interactions between the three fingers, the Zif268 structure illustrates how a large sequence may be recognized through the modular array of smaller recognition motifs.

As opposed to the direct readout employed by the Zif268 protein, the TATA-box binding protein (TBP) is an example of the power of indirect readout.[8] Although the protein binds an 8 bp consensus recognition sequence with high affinity (K_d = 2-4 x 10^{-9} M), there are relatively few direct protein : DNA interactions. Instead, a large part of the stability of the protein : DNA complex appears to rest in the ability of the DNA sequence to deform with little energetic penalty, in order to complement the shape of the TBP protein. Thus the DNA in the co-crystal is bent and untwisted to an unprecedented degree towards the major groove to allow greater access to the normally shallow, convex minor groove. This structure is further interesting because it reveals sequence specific contacts from the protein to DNA bases in the minor groove, whereas the majority of protein : DNA complexes employ major groove contacts.[4]

Figure 1.3. Schematic representation of the base contacts present in the Zif268 crystal structure.[7] Note that the protein recognizes the 9 base pair sequence primarily through interaction with the G-rich strand. Of the 6 specific contacts, 5 employ arginine side chains to recognize guanine residues.

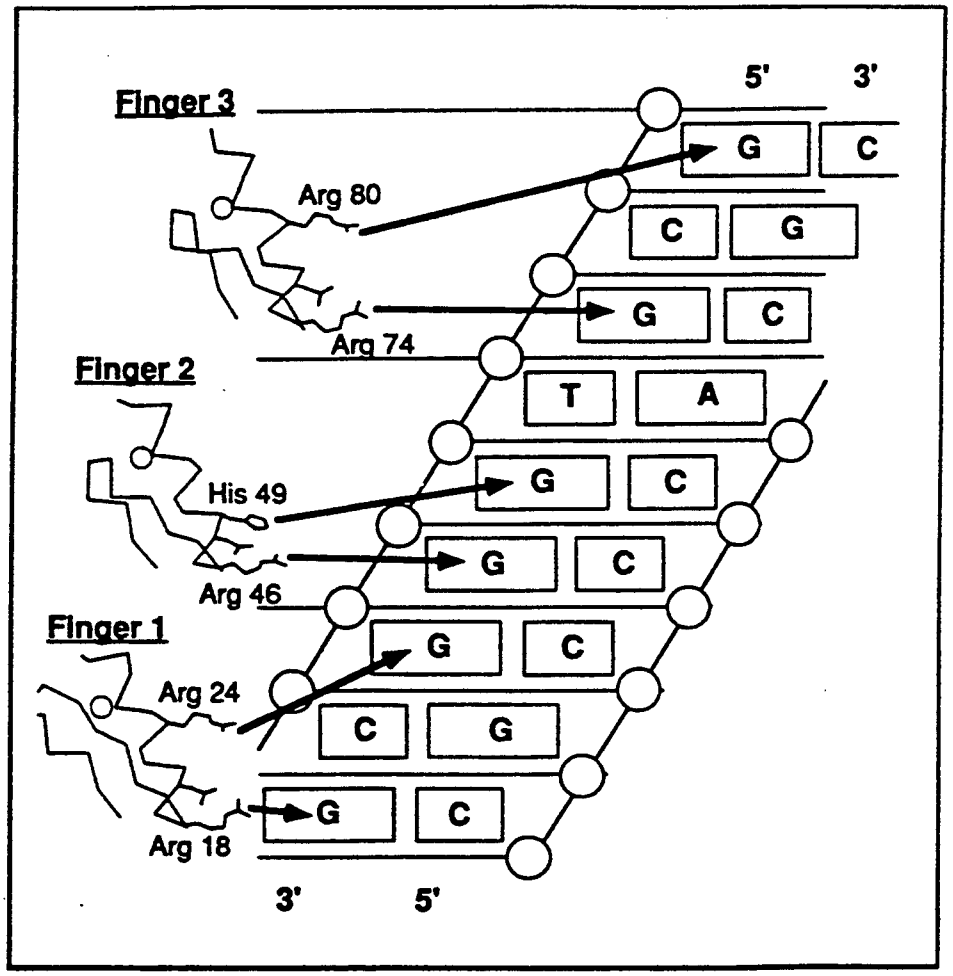
5'
3'
Finger 3
Arg 80
Arg 74
Finger 2
His 49
Arg 46
Finger 1
Arg 24
Arg 18
G
C
C
G
G
C
T
A
G
C
G
C
G
C
C
G
G
C
3'
5'

The importance of sequence dependent DNA structure in protein : DNA recognition, illustrated dramatically in the TBP structure, is also exemplified by the 434 repressor and cro proteins, both of which are helix-turn-helix (HTH) proteins.[9] These proteins bind to DNA as dimers, and although numerous direct hydrogen bonding and van der Waals contacts are employed to recognize the consensus sequences, sequence specific binding is also strongly affected by non-contacted bases in the middle of the two half-sites. As with the TBP structure, this result emphasizes the role of DNA structure in achieving high affinity recognition.

The tremendous advances in molecular and structural biology over the past decade have revolutionized the way scientists investigate protein : DNA recognition. This fantastic problem is now approached routinely in atomic detail, and tremendous strides have been made towards understanding the factors which determine the. However, we are still far from a state where the predictive, *de novo* design of proteins containing novel specificity is possible. Therefore, we must attack this problem with renewed vigor and determination.

1.2. The use of transition metal complexes to mimic protein : DNA recognition.

In the Barton group, we attempt to construct transition metal complexes capable of the sequence specific recognition of DNA.[10] Our central aim is to utilize the power and versatility of inorganic chemistry to approach the fundamental problem of how a protein recognizes a specific target site along the DNA duplex. This research not only provides the foundation for novel chemotherapeutic agents, but also offers hope for the development of new tools for biotechnology.

Several properties of transition metal complexes make them ideal for the task of exploring sequence specific DNA recognition. First, the coordination complexes of Ru(II) and Rh(III) shown in Figure 1.4 are substitutionally inert and coordinatively saturated, so that they, like DNA binding proteins, bind to DNA non-covalently. Figure

1.5 shows three common modes of interaction between transition metal complex and DNA - electrostatic attraction to the phosphate groups, hydrophobic interaction in the minor groove, and intercalation from the major groove. Secondly, the photochemical properties or Ru(II) and Rh(III) complexes may be used to great advantage as reporter groups. The luminescence of a Ru(II) complex is quite sensitive to its environment, and Rh(III) complexes are potent photo oxidants. The capability of Rh(III) complexes to cleave DNA upon photoactivation allows one to assay affinity for a wide array of binding sites through the photocleavage of end labeled DNA fragments, followed by analysis by denaturing polyacrylamide gel electrophoresis. Thirdly, one may utilize the octahedral metal complex as a versatile scaffold to present a diverse family of structures to the DNA helix. Using this approach to investigate the recognition of DNA, we have developed molecules with well defined three-dimensional shapes that probe both basic and subtle aspects of DNA structure. In addition, metal complexes developed in our labs mimic such important elements of protein : DNA recognition as shape selectivity, non-covalent dimerization, and the importance of hydrogen bonding and van der Waals interactions.

The most basic element of DNA structure which may be probed by coordinatively saturated transition metal complexes is the helical nature of duplex DNA. In an equilibrium dialysis experiment, the Δ-enantiomer of $Ru(phen)_3^{2+}$ displays a preference for right-handed helical DNA due to the complementary fit of the intercalated Δ-enantiomer and the right-handed DNA helix.[3] By utilizing complexes with more structurally diverse shapes, aspects of DNA tertiary structure may also be recognized. The complex $Rh(DIP)_3^{3+}$, with its bulky hydrophobic ancillary ligands, recognizes elements of DNA tertiary structure such as cruciforms and Holliday junctions.[11a] $Rh(DIP)_3^{3+}$ also recognizes the GU base pair mismatch, and important structural element in tRNA and other RNA structure.[11b] Finally, $Rh(DIP)_3^{3+}$ has been developed as a probe for elements of nucleic acid structure which were previously unknown.[11c]

Figure 1.4. Several complexes developed in the Barton group as probes of nucleic acid conformation and structure. $Ru(TMP)_3^{2+}$ binds in the minor groove of A-form DNA, while $Rh(DIP)_3^{3+}$ probes DNA and RNA tertiary structure. $Rh(phen)_2phi^{3+}$ binds to DNA and RNA sites where the major groove is open, whereas $Rh(phi)_2bpy^{3+}$ binds DNA in a sequence neutral fashion, making it a powerful footprinting tool. Finally, two derivatives of $Rh(phen)_2phi^{3+}$, $Rh(DPB)_2phi^{3+}$ and Λ-$Rh(MGP)_2phi^{3+}$, combine the power of shape selective recognition with the recognition elements of non-covalent dimerization and hydrogen bond donation respectively to achieve level of specificity rivaling that of DNA binding proteins.

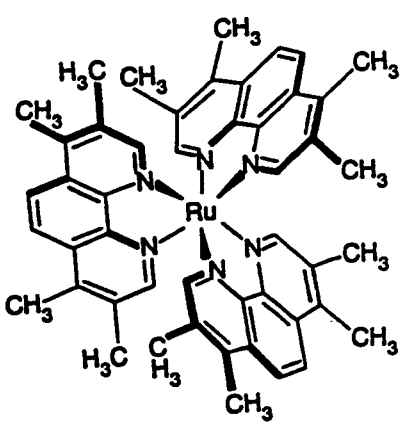
2+
Ru
CH3
H3C

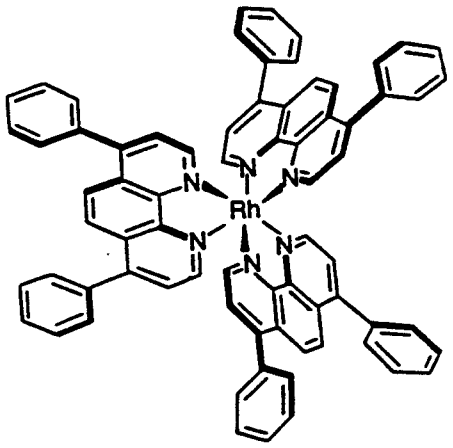
3+
Rh

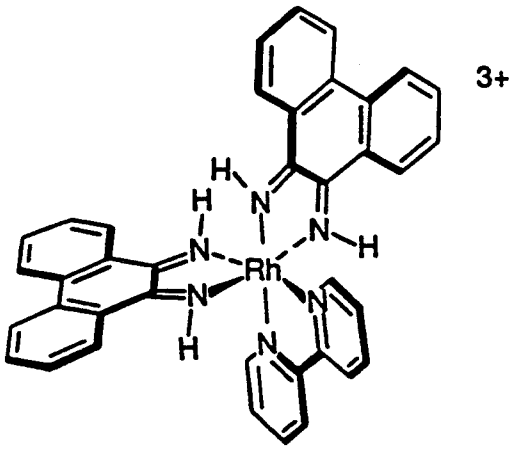
3+
Rh
H
N

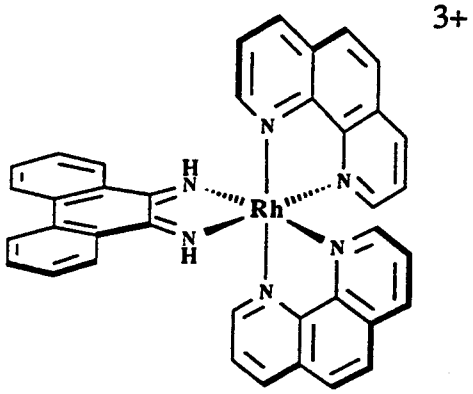
3+
Rh
H
N

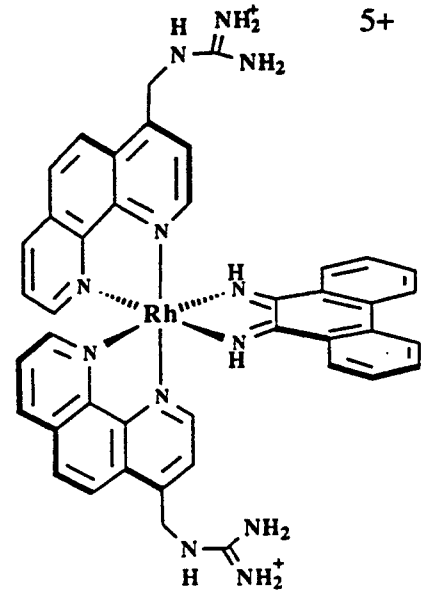
5+
Rh
NH2
NH2+

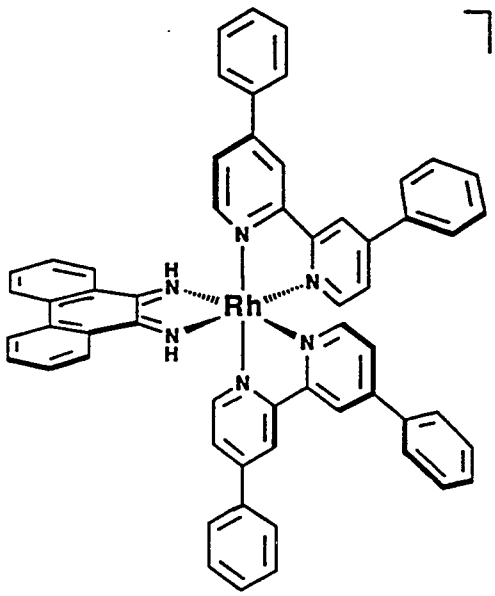
3+
Rh

Figure 1.5. Three modes of interaction between chiral transition metal complexes and duplex DNA. Shown are three metal complexes engaging in either electrostatic attraction with the phosphate group (top), intercalation from the major groove (middle), and surface binding in the minor groove (bottom).

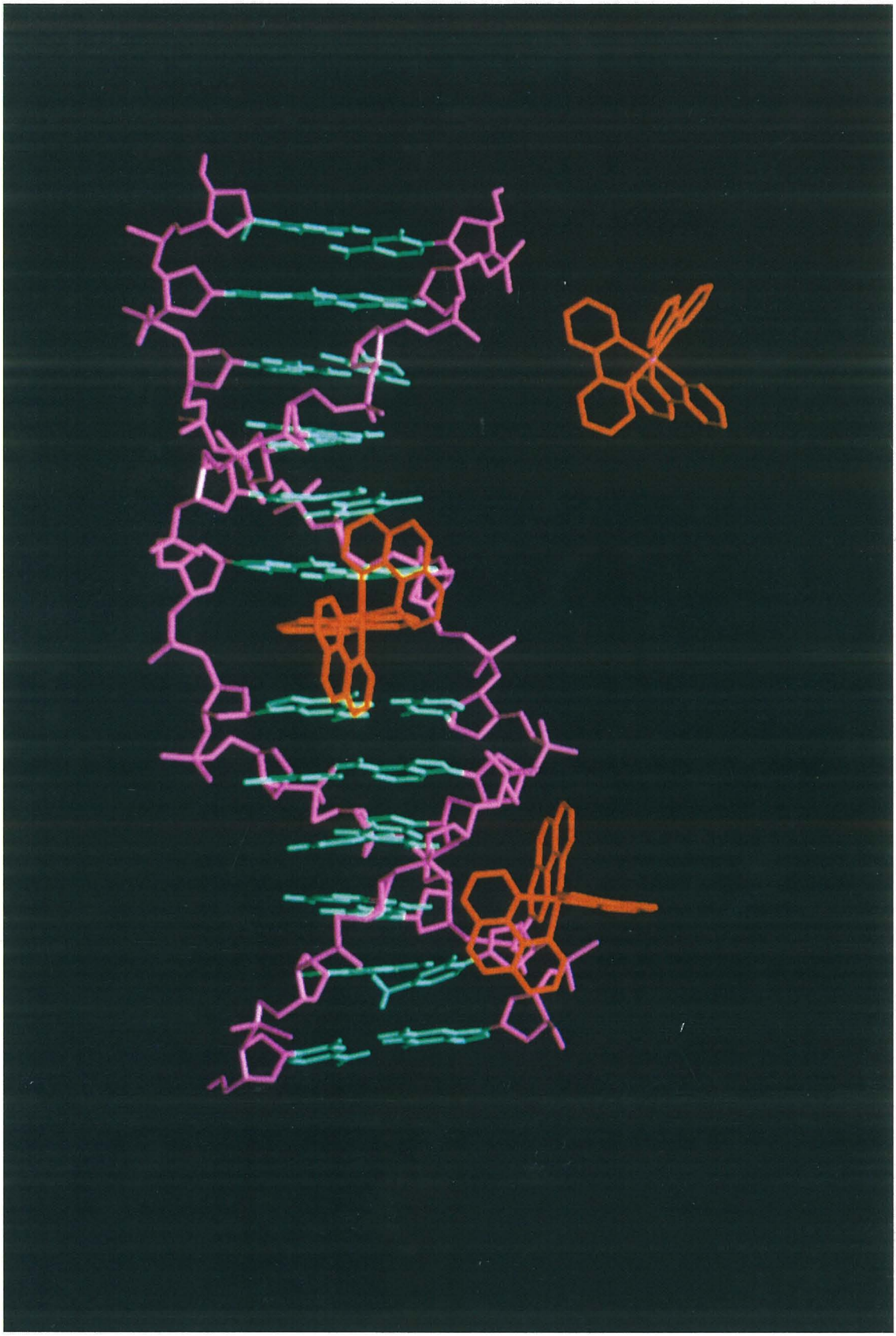

Figure 1.6. Chiral discrimination in the binding of Λ- and Δ-$Ru(phen)_3^{2+}$ to DNA. DNA is shown as a ribbon model, while the metal complexes are shown as propellers. Intercalative binding favors interaction of the Δ-enantiomer in the major groove, whereas groove binding is favored by the Λ-enantiomer.

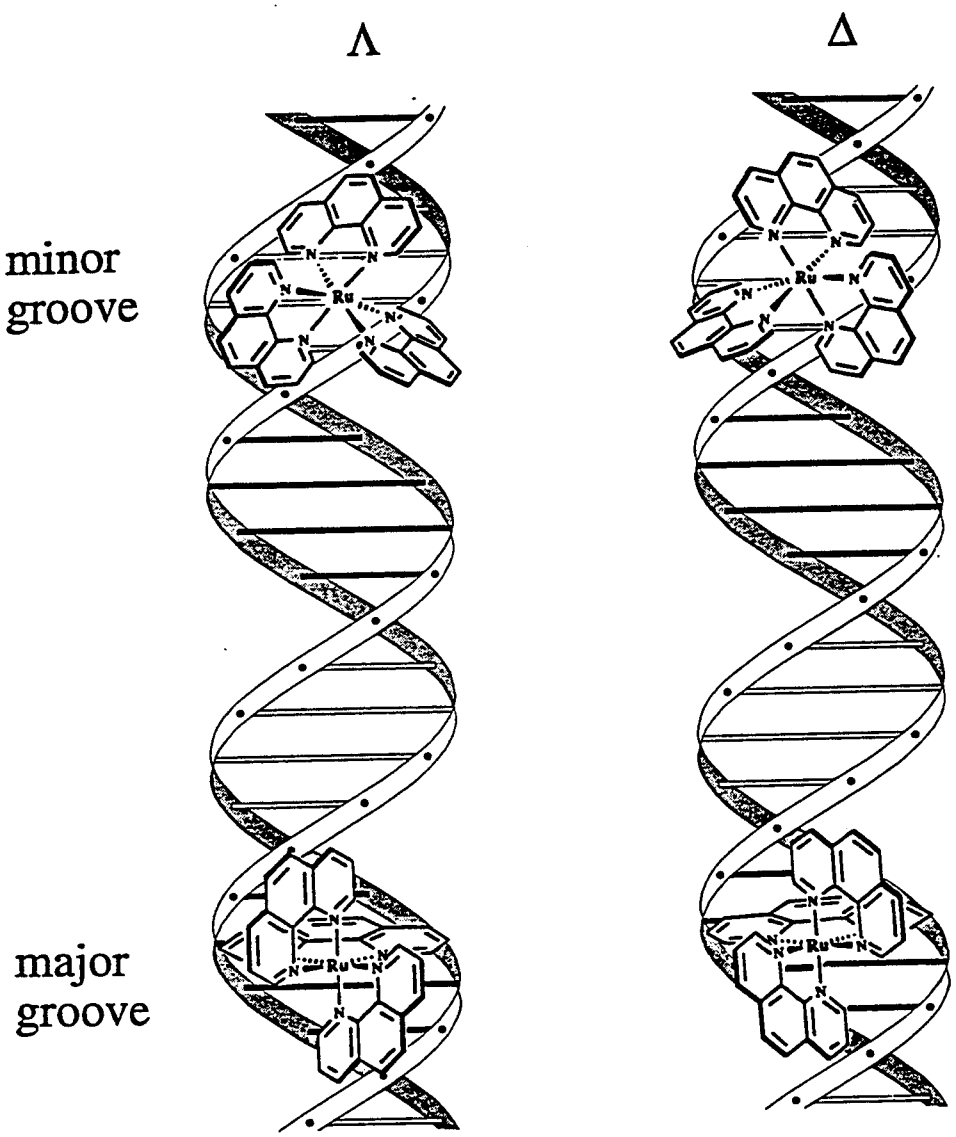
Λ
Δ
minor groove
major groove

In order to probe more subtle features of DNA structure, we have recently focused upon Rh(III) complexes of phenanthrenequinone diimine (phi) ligand.[12] Based on biophysical, mechanistic, and NMR characterization, these complexes which bind to DNA primarily through intercalation of the phi ligand into the base stack of DNA. The high affinity ($K_a > 10^7\ M^{-1}$) and the potential for high specificity of these complexes makes them potential competitors with proteins for sites along the DNA helix. Further, since $Rh(phi)^{3+}$ complexes bind to DNA via intercalation from the major groove,[12] as opposed to minor groove binding drugs such as netropsin, distamycin[2] or bleomycin,[13] the study of their recognition properties probes recognition in the major groove of DNA.

The power of shape selection is illustrated in the comparison of DNA recognition by $Rh(phen)_2phi^{3+}$ and $Rh(phi)_2bpy^{3+}$.[12b] Although both complexes bind DNA strongly and cleave DNA upon photoactivation, they exhibit drastically different sequence selectivities. Figure 1.6 illustrates that, for $Rh(phen)_2phi^{3+}$, the positioning of the phen (2,9) protons relative to the intercalating phi ligand gives rise to steric clashes at most DNA sites. In contrast, $Rh(phi)_2bpy^{3+}$ is able to bind to all sites along the DNA helix since the steric bulk of the ancillary ligands is pulled away from the plane of intercalation. Due to its combination of sequence neutral DNA binding and efficient photoactivated cleavage, $Rh(phi)_2bpy^{3+}$ is a useful photo footprinting reagent,[14] while $Rh(phen)_2phi^{3+}$ acts as a probe of sites along the DNA helix where differential propeller twisting of the base pairs results in the opening of the major groove.[12c] $Rh(phen)_2phi^{3+}$ also specifically recognizes of triple base sites, bulges and mismatches in RNA structure, which are also characterized by an opening of the major groove of the A-form helix.[12d]

Perhaps the best example of achieving sequence selectivity through the combination of strong intercalative binding coupled with the steric constraints of the ancillary ligands is given by the recognition of the 8 bp sequence 5'-CTCTAGAG-3' by $Rh(DPB)_2phi^{3+}$.[15] This site actually represents two overlapping 6 bp site, 5'-CTCTAG-3', where the $Rh(phi)^{3+}$ complex intercalates between the central CT base step. The high

affinity for binding at the 8 bp site relative to an isolated 6 bp site is due to the cooperative binding of two molecules as a non-covalent dimer. This dimer is stabilized by the overlap of two phenyl rings on the ancillary ligands of adjacent intercalated complexes, yielding a 2 kcal/mol preference for the 8 bp site over an isolated 6 bp site.

Finally, we have begun to explore the potential of direct readout of DNA sequences through the addition of hydrogen bonding guanidinium groups onto the $Rh(phen)_2phi^{3+}$ framework, as well as the different approach of tethering small peptides onto the $Rh(phi)_2bpy^{3+}$ framework. The complex Λ-1-$Rh(MGP)_2phi^{3+}$ recognizes the 6 bp sequence 5'-CATATG-3' , and the importance of hydrogen bonding has been demonstrated by the use of the modified DNA base 7-deazaguanine.[16] Binding of the complex at its recognition site requires a large unwinding and twisting of the DNA, similar to the case of the TATA-box binding protein discussed above.

An exciting approach for the recognition of DNA sites is the construction of chimeric molecules consisting of a sequence neutral metal complex, e.g. $Rh(phi)_2bpy^{3+}$, and a covalently tethered small peptide.[17] Such a scheme has been employed to investigate the specificity of single recognition helices from the DNA binding proteins P_{22} repressor and the 434 repressor. The small, synthetic metal complex is capable of replacing the bulk of the DNA binding protein in achieving the delivery and orientation of the peptide to the DNA helix. Such a system provides the basis for the development of artificial repressors targeted for a specific gene.

Figure 1.7. Shape selectivity as the basis for the sequence selectivities of $Rh(phen)_2phi^{3+}$ and $Rh(phi)_2bpy^{3+}$. Steric clashes between the (2,9) protons of the ancillary phenanthroline ligands results in a high level of selectivity for $Rh(phen)_2phi^{3+}$. In contrast, $Rh(phi)_2bpy^{3+}$ displays a low level of selectivity since the steric bulk of the ancillary ligands is pulled away from the plane of intercalation.

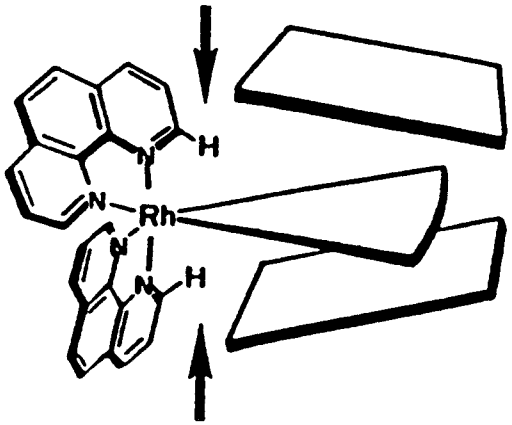

$[Rh(phen)_2(phi)]^{3+}$

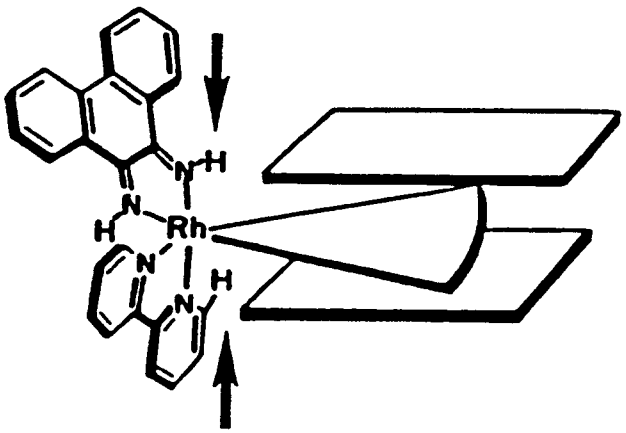

$[Rh(phi)_2(bpy)]^{3+}$

Figure 1.8. The recognition of an 8 base pair site, 5'-CTCTAGAG-3', by the non-covalent dimerization of two molecules of $Rh(DPB)_2phi^{3+}$.

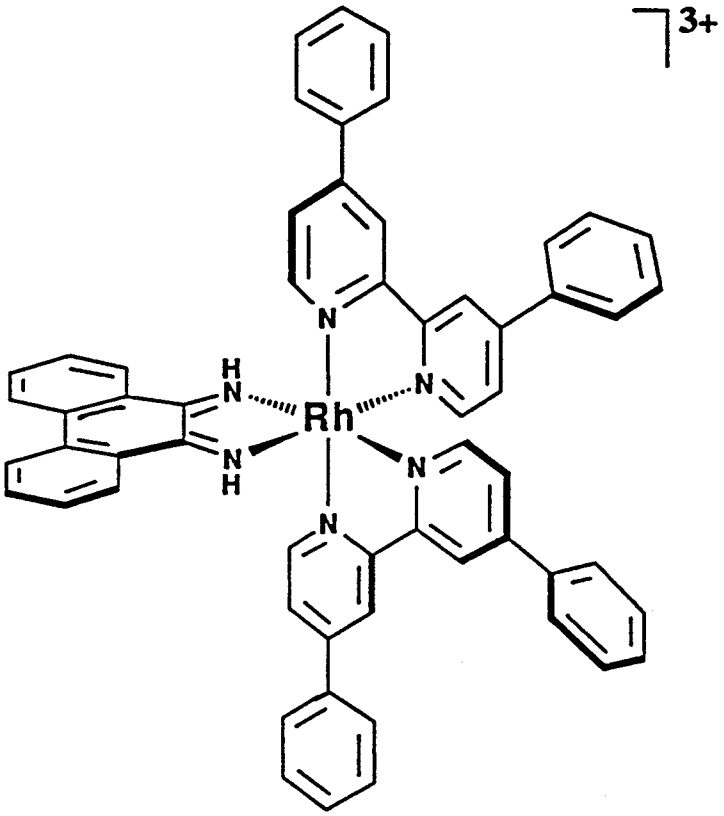
3+
N
H
N
Rh
N
H
N
N
N

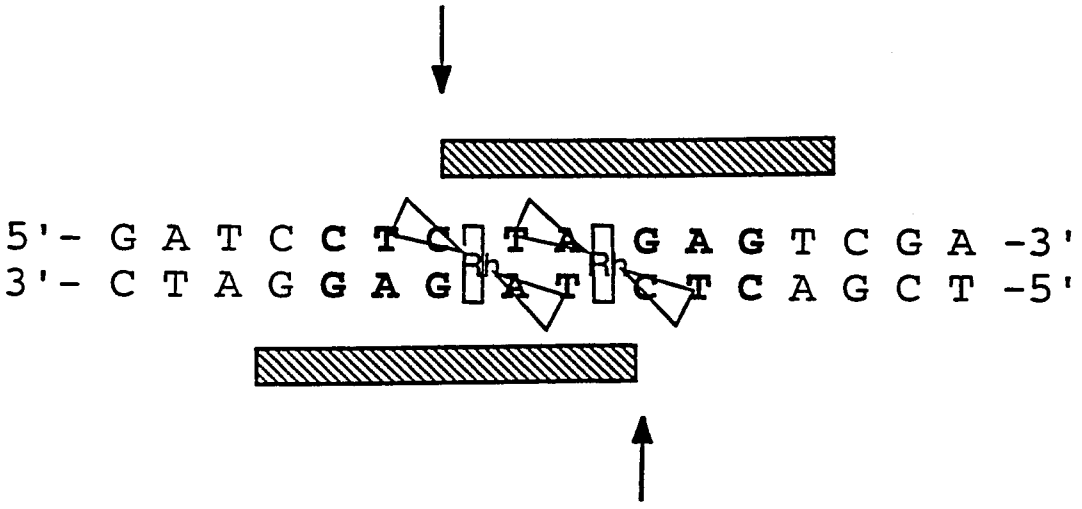
5'- G A T C C T C T A G A G T C G A -3'
3'- C T A G G A G A T C T C A G C T -5'
Rh
Rh

Although the recognition of DNA by $Rh(phen)_2phi^{3+}$ and its derivatives has illustrated the importance of shape selectivity in the targeting of DNA sites by metallointercalators, a predictive design strategy based solely upon shape selective recognition is not feasible, given the limited information regarding the sequence dependent structural variation of DNA.[6] Therefore, efforts have turned recently into exploring more direct readout of DNA bases by the intercalating metal complex. Although the complex $Rh(MGP)_2phi^{3+}$ described above employs hydrogen bonding contacts in achieving very specific recognition, we also desired a route to examine the importance of hydrogen bonding and van der Waals contacts in the relative absence of such a dominating recognition feature as shape selectivity. Therefore, the complexes of $Rh(en)_2phi^{3+}$ were developed. These complexes maintained the intercalative phi ligand, as well as the Rh(III) center to provide structural stability and photochemical reactivity. The ancillary ethylene diamine ligands were chosen as the simplest combination of hydrogen bonding and van der Waals potential elements.

Chapter 2 of this thesis describes the basic interactions of $Rh(en)_2phi^{3+}$ with DNA. As with the parent $Rh(phen)_2phi^{3+}$, $Rh(en)_2phi^{3+}$ binds to DNA via intercalation, and cleaves DNA upon photoactivation with near-UV light. Importantly, $Rh(en)_2phi^{3+}$ displays a lack of shape selectivity by binding to both DNA and RNA polymers with high affinity. The mechanism of photoactivated DNA cleavage is consistent with the direct abstraction of the C3'-H from the deoxyribose moiety and the subsequent degradation of the sugar phosphate backbone.

The sequence specific recognition of DNA by these complexes is investigated in Chapter 3. Elements of the sequence specificity of Λ- and Δ-$Rh(en)_2phi^{3+}$ were established by comparing recognition characteristics to those of several $Rh(phi)^{3+}$ complexes containing ancillary saturated amines and a thioether, and by cleavage of oligonucleotide targets containing O^6methylguanine, 7-deazaguanine and deoxyuracil substitutions. Both enantiomers display a strong sensitivity to the inclusion or removal of

a single methyl group in the major groove of DNA. Δ-$Rh(en)_2phi^{3+}$ displays relatively high selectivity in targeting 5'-GC-3' steps and this selectivity is the result of hydrogen bonding between the axial amines of the metal complex and the O^6 position of guanine residues. In contrast, Λ-$Rh(en)_2phi^{3+}$ is less selective; besides binding to 5'-GC-3' steps, the Λ-enantiomer also recognizes 5'-TX-3' steps through a positive van der Waals contact between the ancillary methylene groups and the 5-methyl group of thymine.

The structural basis for this enantioselectivity is probed in Chapter 4 via 1D- and 2D- NMR methods. The enantiomers of $Rh(en)_2phi^{3+}$ bind to the oligonucleotide duplex $d(GTGCAC)_2$ in a fundamentally similar manner - through the full intercalation of the phi ligand into the base stack of DNA. While Λ-$Rh(en)_2phi^{3+}$ binds to the oligomer in a sequence neutral fashion, 2D-NOESY experiments support the specific intercalation of Δ-$Rh(en)_2phi^{3+}$ at the central 5'-GC-3' steps of the duplex, consistent with the photocleavage studies of Chapter 3. Molecular modeling indicates that the deep intercalation of the phi ligand serves not to create steric clashes between the ancillary ligands and DNA, but to ideally locate the ethylene diamine ligands for hydrogen bonding and positive van der Waals contacts.

Finally, Chapter 5 discusses a scheme for the recognition of larger DNA sites, based on the simple non-covalent contacts employed by Λ- and Δ-$Rh(en)_2phi^{3+}$. While the enantiomers of $Rh(en)_2phi^{3+}$ are not themselves highly specific molecules, the principles illustrated in this thesis serve as the foundation for the predictive recognition of larger DNA sequences.

Figure 1.9. The enantiomers of $Rh(en)_2phi^{3+}$. While maintaining the Rh(III) center and the intercalative phi ligand, $Rh(en)_2phi^{3+}$ is designed for a low level of shape selectivity due to the small ancillary ethylene diamine ligands. However, these ligands also represent the simplest possible combination of potential hydrogen bonding and van der Waals functionalities.

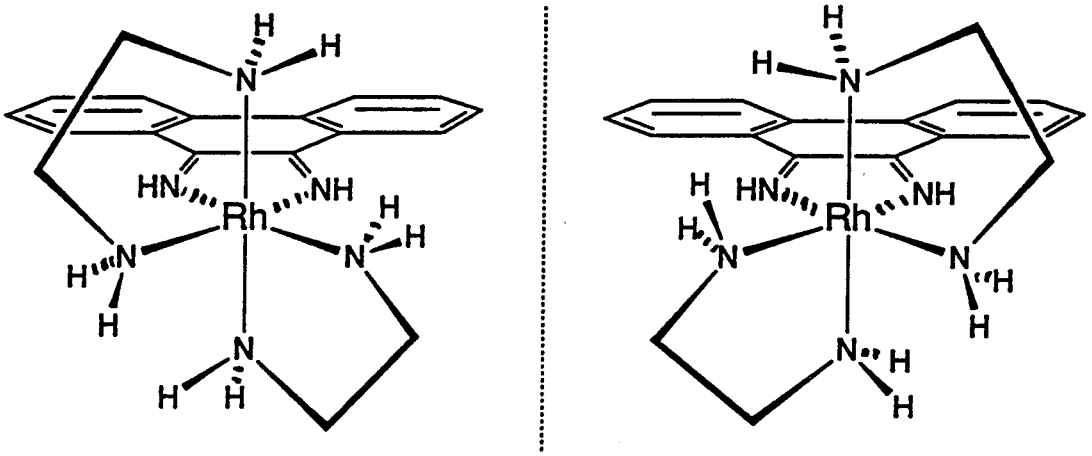

Δ- Rh(en)2phi3+ Δ- Rh(en)2phi3+

References and Footnotes

1. Watson, J.D.; Crick, F.H.C. *Nature*, **1953**, *171*, 737.
2. Dervan, P. B. *Science* **1986**, *232*, 464.
3. Barton, J.K. *Science*, **1986**, *233*, 727.
4. (a) Pabo, C. O.; Sauer, R. T. *Ann. Rev. Biochem.* **1992**, *61*, 1053. (b) Steitz, T.A. *Q. Rev. Biophys.* **1990**, *23*, 205.
5. Seeman, N.C.; Rosenberg, J.M.; Rich, A. *Proc. Nat Acad Sci USA* **1976**, *73*, 804.
6. Saenger, W. *Principles of Nucleic Acid Structure*, Springer-Verlag, 1984.
7. Pavletich, N.P.; Pabo, C.O. *Science*, **1993**, *261*, 1701.
8. (a) Kim, Y.; Geiger, S.H.; Hahn, S., Sigler, P.S. *Nature* **365**, *512*, 1993. (b) Kim, J.L.; Nikolov, D.B.; Burley, S.K. *Nature* **1993**, *365*, 520.
9. Harrison, S.C.; Aggarwal, A.K. *Ann. Rev. Biochem.* **1990**, *59*, 933.
10. (a) Pyle, A. M. ; Barton, J. K. *Prog. Inorg. Chem.* **1990**, *38*, 413. (b) Dupureur, C.M.; Barton. J.K. *Comp. Supromolecular Chem.* in press.
11. (a) Kirshenbaum, M.R.; Tribolet, R.; Barton, J.K. *Nucl. Acids Res.* **1988**, *16*, 7943. (b) Chow, C. S.; Barton, J. K. *J. Amer. Chem. Soc.* **1990**, *112*, 2839. (c) Lee, I.; Barton, J.K. *Biochem.*. **1993**, *32*, 6121.
12. (a) Pyle, A. M.; Long, E. C.; Barton, J. K. *J. Amer. Chem. Soc.* **1989**, *111*, 4520. (b) Sitlani, A.; Long, E. C.; Pyle, A. M.; Barton, J. K. *J. Amer. Chem. Soc.* **1992**, *114*, 2303. C. Campisis (d) Chow, C. S.; et al. *Biochem.* **1992**, *31*, 972.
13. Subbe, J.; Kozarich, J. *Chem. Rev.* **1987**, *87*, 1107.
14. Uchida, K.; Pyle, A.M.; Morii, T.; Barton, J.K. *Nucl. Acids Res.* **1989**, *17*, 259.
15. Sitlani, A.S.; Dupureur, C.M.; Barton, J.K. *J. Am. Chem. Soc.* **1993**, *115*, 12589.
16. Terbreuggen, R.H.; Barton, J.K. submitted for publication.
17. Sardesai, N.Y.; Zimmerman, K.; Barton, J.K. *J. Am. Chem. Soc.* **1994**, *116*, 7502.

Chapter 2: The DNA Binding and Cleavage Characteristics of $Rh(en)_2phi^{3+}$.

2.1. Introduction

There is substantial interest in delineating those factors which contribute to DNA site recognition by both small molecules and proteins.[1,2] High affinity DNA recognition involves both direct readout of DNA sequence through hydrogen bonding and van der Waals contacts, as well as indirect readout based upon less tenable but equally powerful tools such as shape selection or innate DNA flexibility. Despite the tremendous knowledge garnered from both crystal and NMR structures of several DNA : protein[3] and DNA : drug[4] complexes, a complete understanding of the principles which govern DNA recognition remains a fascinating and alluring area of research.

Our laboratory has focused on the design and development of transition metal complexes which display DNA sequence selectivity based primarily upon shape selection[5-7], in which the overall shape complimentarity between a metal complex and a particular DNA site directs sequence specific recognition. Most recently we have explored DNA recognition by a family of mixed ligand polypyridyl complexes of Rh(III) containing the phenanthrenequinone diimine (phi)† ligand.[6,7] Mechanistic, NMR and DNA binding studies have shown that these complexes associate with DNA with high affinity through the intercalation of the phi ligand into the major groove. When irradiated with UV light in the presence of DNA these phi complexes of Rh(III) complexes demarcate the site of binding through direct strand scission of the sugar phosphate backbone through a mechanism involving H- abstraction of the C_3'-H atom located in the major groove of DNA.[6]

Complexes such as $Rh(phen)_2phi^{3+}$ display site selectivity based on the steric constraints of the non-intercalated ancillary ligands, and have been developed as probes

of sites in DNA where the major groove is open.[6] While the sequence specific recognition of DNA by $Rh(phen)_2phi^{3+}$ mimics such elements of protein : DNA recognition as shape selectivity and indirect readout, $Rh(phen)_2phi^{3+}$ is not capable of sequence selectivity based on more direct readout, since the ancillary phenanthroline ligands lack the potential for extensive hydrogen bonding and van der Waals contacts. Although the use of modified phenanthroline ligands has provided a mimic of protein : protein dimerization[7a] as well as a complex capable of probing DNA twistability,[7b] the sequence selectivity of these complexes is still largely influenced by shape selectivity.

In order to study the importance of hydrogen bonding and van der Waals contacts to DNA recognition in the relative absence of such dominating a feature as shape selectivity, we have designed and synthesized the enantiomers of $Rh(en)_2phi^{3+}$. The ancillary ethylenediamine ligands were predicted to be capable of both donating hydrogen bonds from the coordinated amines, as well as engaging in van der Waals contacts between the methylene groups and DNA residues such as the thymine methyl group. $Rh(en)_2phi^{3+}$ should retain the overall stability of $Rh(phen)_2phi^{3+}$, since it also is a substitutionally inert d^6 transition metal complex which is coordinatively saturated. $Rh(en)_2phi^{3+}$ contains the intercalating phi ligand in order to maintain the high overall affinity for DNA of the parent $Rh(phen)_2phi^{3+}$, as well as the DNA photocleavage chemistry used to demark binding along the DNA helix.

Since the enantiomers of $Rh(en)_2phi^{3+}$ are smaller than polypyridyl complexes such as $Rh(phen)_2phi^{3+}$, spanning only a single base step when intercalated into double helical DNA, the expected level of sequence selectivity due to shape selection is small. However, we shall see (Chapters 3 & 4) that the enantiomers of $Rh(en)_2phi^{3+}$ provide a route to examine systematically the contributions of hydrogen bonding and van der Waals contacts to sequence selectivity through the disposition of their ancillary ethylenediamine ligands.

Figure 2.1. The structures of $Rh(phen)_2phi^{3+}$ and $Rh(en)_2phi^{3+}$.

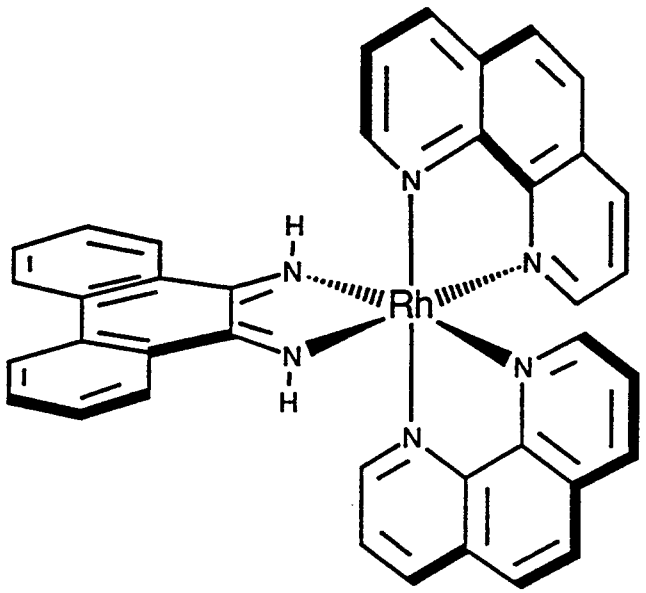

Δ-$Rh(phen)_2phi^{3+}$

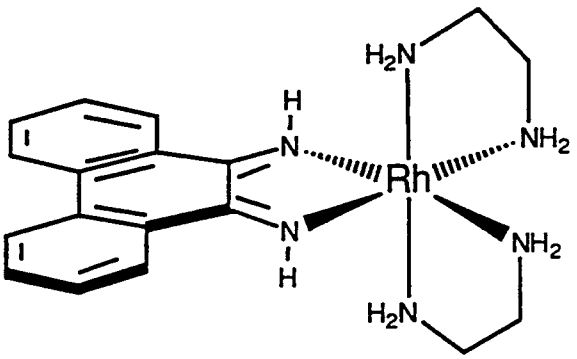

Δ-$Rh(en)_2phi^{3+}$

The first step in examining sequence selective DNA recognition by the enantiomers of $Rh(en)_2phi^{3+}$ was to characterize the basic DNA binding and photocleavage properties of these molecules. UV-Vis binding titrations and plasmid unwinding experiments establish that $Rh(en)_2phi^{3+}$, as well as several other $Rh(phi)^{3+}$ complexes containing saturated amines and a thioether, bind strongly to DNA through the intercalation of the phi ligand. The photocleavage of DNA by $Rh(en)_2phi^{3+}$ was characterized in terms of end product analyses, stoichiometry and quantum efficiency, and in all cases analogy to the parent $Rh(phen)_2phi^{3+}$ is presented and discussed. The cleavage reaction may best be described by a model where a photoexcited phi cation radical directly abstracts the C_3'-H atom from the deoxyribose sugar, ultimately leading to the release of a free nucleic acid base and direct DNA strand scission.

2.2. Experimental

Materials: Calf thymus DNA and poly rI · poly rC were purchased from Pharmacia LKB. Plasmid pBR322 was purchased from Gibco BRL. Terminal deoxy Transferase (TdT) and Polynucleotide Kinase (PNK) were purchased from Boehringer Mannheim as parts of 3'- and 5'-end labeling kits respectively. γ- [^{32}P]-dATP was from Dupont-NEN and α-[^{32}P] ddATP was from Amersham. The oligonucleotide $d(GAGTGCACTC)_2$ was prepared on an ABI Model 392 DNA synthesizer using phosphoramidite chemistry and purified using established protocols.[8] Phosphoramidites, solid supports and reagents for solid phase DNA oligonucleotide synthesis were purchased from ABI (Foster City, CA) and Glen Research (Sterling, VA).

$[Rh(en)_2phi^{3+}](ClO_4)_3$ was prepared as previously described.[9,10] The complexes $[Rh(NH_3)_4phi]Cl_3$, [Rh(cyclen)phi]Cl_3, and $[Rh(S_4\text{-cyclen})phi]Cl_3$ were prepared by Dr. Achim Krotz. Λ- and Δ-$Rh(phen)_2phi^{3+}$ were graciously provided by Dr. Cindy Dupureur. Free base standards cytosine (C), guanine (G), thymine (T) and adenine (A) were obtained from US Biochemical and quantitated by UV-Vis spectroscopy. H_2O was

purified with a Millipore Milli-Q Plus system, and was ≥ 18 MΩ resistance. All other enzymes, buffers, salts and sequencing reagents were obtained from commercial sources and were of the highest purity available.

Instrumentation: UV-Vis spectra were recorded either on a Hewlett Packard 8452A Diode Array Spectrophotometer or on a Cary 2200 Spectrophotometer stored with Spectrocalc program. Circular dichroism spectra were recorded on a JASCO J500A spectrometer. All spectra were recorded in 1 cm path length quartz cells.

The light source used in photocleavage experiments was a Oriel Model 6140 1000 Watt Hg/Xe lamp equipped with a Model 6123 IR filter, and either a Model 77250 (1/8 m) or Model 77200 (1/4 m) monochromator. A 305 nm cutoff filter was utilized in photocleavage studies with the 1/8 m monochromator to avoid DNA damage by extraneous UV light. Alternatively a 325 nm Liconix Model 4240 NB He-Cd laser was used as a light source for photocleavage.

High Performance Liquid Chromatography (HPLC) was performed on a Waters 600E Multi Solvent Delivery System and monitored with either a Model 996 diode array detector (processed with Waters Millennium software) or with a Model 484 tunable wavelength detector. Phosphorimagery was performed on a Molecular Dynamics PhosphorImager and images were processed using Image Quant software.

Resolution of Δ- and Λ- Rh(en)$_2$phi^{3+} : Rac- [Rh(en)$_2$phi^{3+}] $(ClO_4)_3$ (32.4 mg), was pre-loaded onto 5 mL of Sephadex SP C-25 resin, which was then loaded onto a 40 x2.5 cm Sephadex column prepared in the HCl form. The column was first washed with 300 mL H_2O , and then the enantiomers were separated utilizing 0.15 M solution of potassium antimonyl tartrate as eluent. After ~800 mL antimonyl tartrate solution had passed down the column, a peristaltic pump was employed to recirculate the eluent, and two distinct bands were evident on the second pass down the column. At this point, the pump was removed and 600 mL H_2O was washed down the column to remove the excess antimonyl tartrate. The resin was then physically removed from the column and the two

bands were cut out and separated. Δ- and Λ-$Rh(en)_2phi^{3+}$ were obtained by eluting the resin with 1 M HCl, followed by desalting twice on a Sep-Pak columns (Dupont). Concentrations of enantiomers were quantitated by UV-Vis spectroscopy ($\varepsilon_{376\ nm}$ = 13,500 M^{-} cm^{-} at pH 7.0) and the isomeric purity was checked by CD, ($\Delta\varepsilon_{310\ nm} = \pm 240$ deg M^{-1} cm^{-1}).[10-12] Yields : 9.5 mg Δ-$[Rh(en)_2phi]Cl_3$ (80%), 10.9 mg Λ-$[Rh(en)_2phi]Cl_3$. (92%). M.W. $[Rh(en)_2phi](ClO_4)_3$ = 727.25 g/mol, $[Rh(en)_2phi]$ Cl_3 = 535.25 g/mol.

UV-Vis Binding Titrations : A 600 μL buffered solution of 20-35 μM $Rh(phi)^{3+}$ complex was titrated with aliquots of DNA or RNA solution (~ 1- 5 mM base pairs stock solution) until the hypochromicity and red shift effects were saturated (typically > 10 base pairs / Rh molecule). The DNA or RNA solution added to the $Rh(phi)^{3+}$ complex also contained 20-35 μM Rh complex such that the [Rh] was held constant as the [DNA] increased. To probe only the changes in the electronic spectrum of the $Rh(phi)^{3+}$ complex, an equivalent amount of DNA or RNA was added to the reference cell at each point in the titration.

Unwinding Assays : Plasmid pBR322 DNA (0.5 μg) was incubated with increasing amount of Rh complex (0.1- 10 μM) for 30-45 min. in 20 μL total volume. 2 μL 10x non-denaturing loading dye was added to each tube, and the samples were directly loaded onto non-denaturing 1% agarose gels. Samples were electrophoresed for 2 hr. at 500 Volts, and stained with either ethidium bromide or $Ru(bpy)_2dppz^{2+}$.

Photocleavage of Oligonucleotide DNA : The DNA oligonucleotide $d(GAGTGCACTC)_2$ was either 5'- [^{32}P] end-labeled with γ- [^{32}P]-ATP and polynucleotide kinase, or 3'- [^{32}P] end-labeled with α- [^{32}P]-ddATP and terminal deoxytransferase. Labeled oligomers were purified on 10% polyacrylamide prep gels (0.8 mM thick spacers, full size), and then isolated by electroelution of gel pieces in a Schleicher and Schuell Elutrap (250 Volts, 15 min.). End-labeled material was stored

frozen in buffered solution (30 mM Tris·borate, 0.33 mM EDTA, pH 8.3) and used within 7-14 days of isolation.

DNA stock solutions were prepared in 1.7 mL pre-siliconized eppendorf tubes by mixing cold oligonucleotide with a small amount of labeled strand (~100-150K cpm / sample). To afford suitable mixing of labeled strand with unlabeled carrier, stock solutions were heated at 37° C for 10 min., followed by cooling to room temperature. Amounts of DNA and buffer were added such that when a 15 μL aliquot of the annealed DNA stock solution was extracted and diluted to a final volume of 20 μL with the appropriate $Rh(phi)^{3+}$ complex, the 20 μL solution would contain 1x buffer, as well as the desired metal and DNA concentrations.

Samples (20 μL) were irradiated by placing the uncapped tube in the beam of the Hg-Xe lamp such that the sample volume resided at the focal point of the Hg-Xe lamp. Photocleavage reactions were quenched by removal from light, although typically 1.5 μL of a 5 mM base pairs calf thymus DNA solution was added to each photocleavage sample in order to allow more facile denaturation of the strands upon electrophoresis by competing with the labeled oligomer for the $Rh(phi)^{3+}$ complex. After irradiation, 3-5 μL (20-30,000 cpm) of the samples were removed and dried, resuspended in loading dye, and directly electrophoresed on 20% denaturing polyacrylamide gels at 3000 volts for 1.5 hours. Following electrophoresis, the samples were exposed to photostimulable storage phosphor plates for 12-18 hours. The phophorimaged gels were quantitated with the ImageQuant software package (Molecular Dynamics).

Quantum yields for Free Base Release : Samples for free base release experiments were prepared to be 800 μL total volume containing 50 μM $Rh(phi)^{3+}$ complex, 500 uM calf thymus DNA base pairs, pH 7.0, 10 mM NaCacodylate, 40 mM NaCl, in a 1.0 cm quartz UV-Vis cell equipped with a small teflon stir bar. The cell was placed in the beam of the Hg-Xe lamp such that the focal point of the lamp was in the center of the cell. To avoid bleaching a particular sample volume, cells were stirred

vigorously during irradiation, and also were shifted vertically 3 times. After irradiation, samples were divided into several eppendorf tubes and frozen on dry ice for later HPLC analysis. Samples were injected onto a reverse phase C18 HPLC column and free base products were eluted with 0.05 M ammonium formate, pH 7.0 at 260 nm. After 10 minutes, an acetonitrile gradient (0 to 30 %, 10 min; 20 to 50%, 10 min; hold at 50% for 5 min.) was initiated to remove uncut DNA and $Rh(phi)^{3+}$ complex from the HPLC column. Calibration curves for C, G & T were constructed in order to calculate the moles free base produced in each reaction. The identity of the free base products was confirmed by co-injection with authentic standards.

The photon flux of the Hg-Xe lamp was measured through ferrioxalate actinometry.[13] An 800 μL stirred solution of 0.001 M $Fe(C_2O_4)_3^{3-}$ (pH controlled with 0.001 M H_2SO_4) was irradiated in the same geometry as the Rh:DNA samples, and the cell was again moved three times during irradiation to avoid bleaching. 20 μL of the $Fe(C_2O_4)_3^{3-}$ solution was extracted and, after the addition of 500 μL phenanthroline solution (0.2% by weight in water) and 125 μL buffer (pH 2.0, H_2SO_4 : NaOAc), diluted to a final volume of 10 mL. Lamp intensity was then quantitated based on the quantum yield for the photoreduction of $Fe(C_2O_4)_3^{3-}$ (1.24 at 313 nm) and the extinction coefficient of the $Fe(phen)_3^{2+}$ complex formed (1.1×10^4 M^{-1} cm^{-1} at 510 nm). The photon flux of the Hg-Xe lamp varied between 3-5 x 10^{-6} Einsteins / min. Care was taken to measure photon flux at short times where the yield of $Fe(phen)_3^{2+}$ was linear.

Experiments Establishing the Stoichiometry of the DNA cleavage reaction:

A. Photoanation in the presence of DNA. Samples were prepared in 1.7 mL eppendorf tubes with 250 μL total volume containing 20 μM $Rh(en)_2phi^{3+}$, 25 μM DNA duplex, and buffered with 10 mM NaCacodylate, 40 mM NaCl, pH 7.0. Samples were irradiated at 4° C for 10 - 40 min at 313 nm with the Hg-Xe lamp. Immediately following irradiation, the UV-Vis spectrum of each sample was measured and the sample was removed from the UV-Vis cell and frozen for later HPLC analysis. For comparison,

the loss of phi absorbance was also measured in the absence of DNA at identical times and concentrations in order to investigate the influence of DNA binding on the photochemistry of the complex. The moles $Rh(en)_2phi^{3+}$ lost during irradiation was calculated by comparison of the irradiated samples versus dark control samples, using the extinction coefficient for $Rh(en)_2phi^{3+}$ at 402 nm, where the extinction coefficient for free and bound $Rh(en)_2phi^{3+}$ were identical.

B. Free base release. The sample in A above was injected onto a C18 reverse phase column (Microsorb-MV, Rainin Instruments, C18, 5 mM x 20 cm length, 100 Å pore size, Model # 86-200-C5) for analysis of free base products. Free bases were eluted with 0.05 M, pH 7.0 Ammonium formate buffer (10 min, isocratic) followed by an acetonitrile gradient (0 to 20%, 10 min; 20 to 50%, 10 min; hold at 50% for 5 min.) to remove uncut DNA oligomer as well as $Rh(phi)^{3+}$ complex. Free base products C,G, and T were observed at 4.2, 10.8 and 15.6 min. respectively and quantitated via calibration curves created with authentic standards.

C. Oligonucleotide strand cleavage. Samples were prepared in 1.7 mL eppendorf tubes with 250 µL total volume containing 20 µM $Rh(en)_2phi^{3+}$, ~500,000 cpm 3'-labeled $d(GAGTGCACTC)_2$, 25 µM DNA duplex, pH 7.0, 10 mM NaCacodylate, 40 mM NaCl. Samples were irradiated at 4° C for 40 min at 313 nm. An 8 µL aliquot from each sample (~25,000 cpm) was removed, dried, then resuspended in 3.5 µL denaturing loading dye. Samples were heated at 90° C 4 minutes, then loaded onto 20% denaturing polyacrylamide gels. Samples were electrophoresed at 2500 V for 2 hours, transferred to a blank film and exposed to photostimulable storage phosphor plates for 12-18 hours. The exposed plates were scanned on a molecular Dynamics phosphorimager, and were quantitated with the ImageQuant software program.

2.3. Results

2.3.1. Resolution of Λ- and Δ- enantiomers of $Rh(en)_2phi^{3+}$.

The synthesis and crystal structure of $Rh(en)_2phi^{3+}$ is already published and discussed.[9,10] For reference, the ORTEP model, along with relevant bond distance and angle information, is presented here. (Figure 2.2) The UV-Vis spectrum of rac-$Rh(en)_2phi^{3+}$, as well as the circular dichroism spectra of the Λ- and Δ- enantiomers are presented in Figure 2.3. The assignment of Δ-$Rh(en)_2phi^{3+}$ as having negative ellipticity at 310 nm is based on comparison to both $Rh(en)_3^{3+}$ and $Rh(phen)_3^{3+}$,[12] as well as to the crystal structures of several diastereomeric $Rh(phi)^{3+}$ complexes.[11b]

2.3.2. Assays for intercalation and unwinding of DNA by $Rh(en)_2phi^{3+}$.

A. UV-Vis Binding Assays. Upon intercalation into double stranded DNA, an organic chromophore will often experience hypochromism and a red shift in its absorption maximum. This observation is consistent with the fact that the DNA bases themselves experience ~ 30-40% hypochromicity at 260 nm upon stacking in the double helix.[14] Figure 2.4 shows the electronic spectrum of Λ-$Rh(en)_2phi^{3+}$ upon the sequential addition of calf thymus DNA. The spectra display a strong red shift (~12 nm) along with substantial hypochromicity in the phi centered transition at 350 - 400 nm. A similar degree of hypochromicity is observed at 300- 275 nm, but the strong absorbance of DNA in both sample and reference cell makes this area of the spectrum less informative than the π-->π* transition. Isosbestic behavior is observed, with both free and bound complexes absorbing equally at 405 nm.

Figure 2.2. Structure of $Rh(en)_2phi^{3+}$ with relevant bond distances and angles.

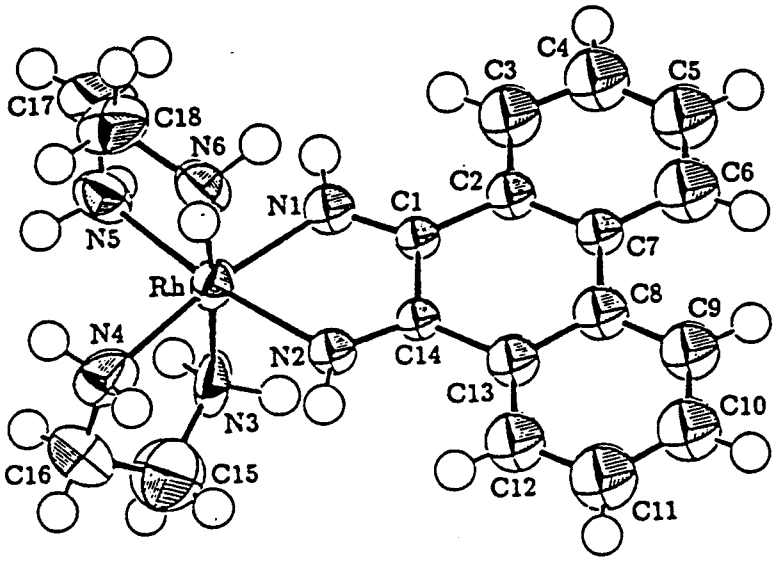

Relevant Bond Distances (Å) and Angles (°)

Rh-N1	1.996 (15)	N1-Rh-N2	77.1 (6)	N2-Rh-N6	92.6 (6)
Rh-N2	2.007 (14)	N1-Rh-N3	92.2 (6)	N3-Rh-N4	83.3 (6)
Rh-N3	2.066 (15)	N1-Rh-N4	172.0 (6)	N3-Rh-N5	94.6 (6)
Rh-N4	2.058 (16)	N1-Rh-N5	96.5 (6)	N3-Rh-N6	176.0 (6)
Rh-N5	2.065 (16)	N1-Rh-N6	91.2 (6)	N4-Rh-N5	90.5 (6)
Rh-N6	2.029 (16)	N2-Rh-N3	90.2 (6)	N4-Rh-N6	93.6 (6)
		N2-Rh-N4	96.3 (6)	N5-Rh-N6	82.9 (6)
		N2-Rh-N5	172.1 (6)		

Figure 2.3. UV-Vis and circular dichroism spectra of $Rh(en)_2phi^{3+}$. All spectra were measured at pH 7.0, 10 mM NaCacodylate, 40 mM NaCl in 1 cm pathlength quartz cells. The UV-Vis spectrum displays maxima at 376 nm (ε = 13,500 M^{-1} cm^{-1}), 271 nm (26,300 M^{-1} cm^{-1}), 252 nm (18,600 M^{-1} cm^{-1}), 229 nm (36,700 M^{-1} cm^{-1}), as well as shoulders at 389 nm (12,400 M^{-1} cm^{-1}), 283 nm (12,000 M^{-1} cm^{-1}) and 263 nm (22,500 M^{-1} cm^{-1}). A ratio of ~ 2 : 1 between the absorbances at 271 and 376 nm is characteristic of a pure sample.

The circular dichroism spectra display peaks at 272 nm ($\Delta\varepsilon$ = ±180 deg M^{-} cm^{-}), 308 nm (± 240 deg M^{-} cm^{-}), 385 nm (± 70 deg M^{-} cm^{-}) and 480 nm (± 15 deg M^{-} cm^{-}). The assignment of Δ-$Rh(en)_2phi^{3+}$ as having negative ellipticity at 310 nm is consistent with the assignments established for similar complexes.[11b, 12]

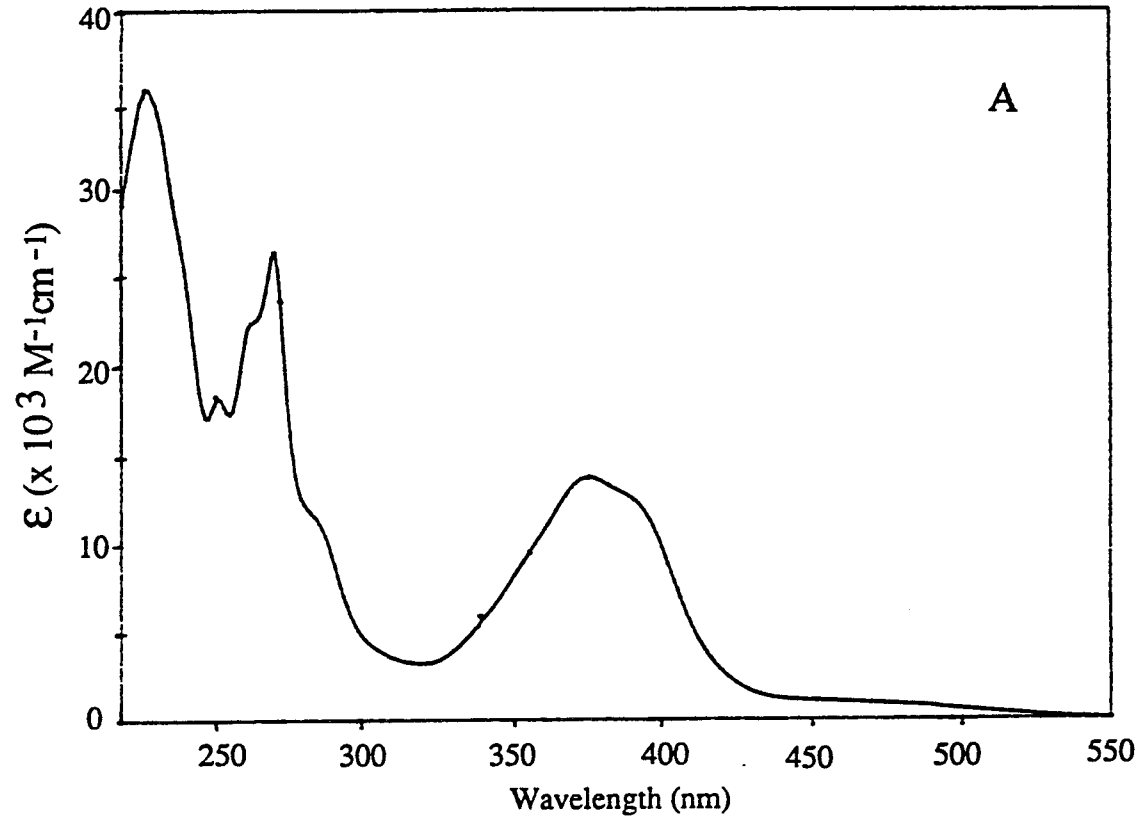
A
ε (x 10^3 M^-1cm^-1)
40
30
20
10
0
250
300
350
400
450
500
550
Wavelength (nm)

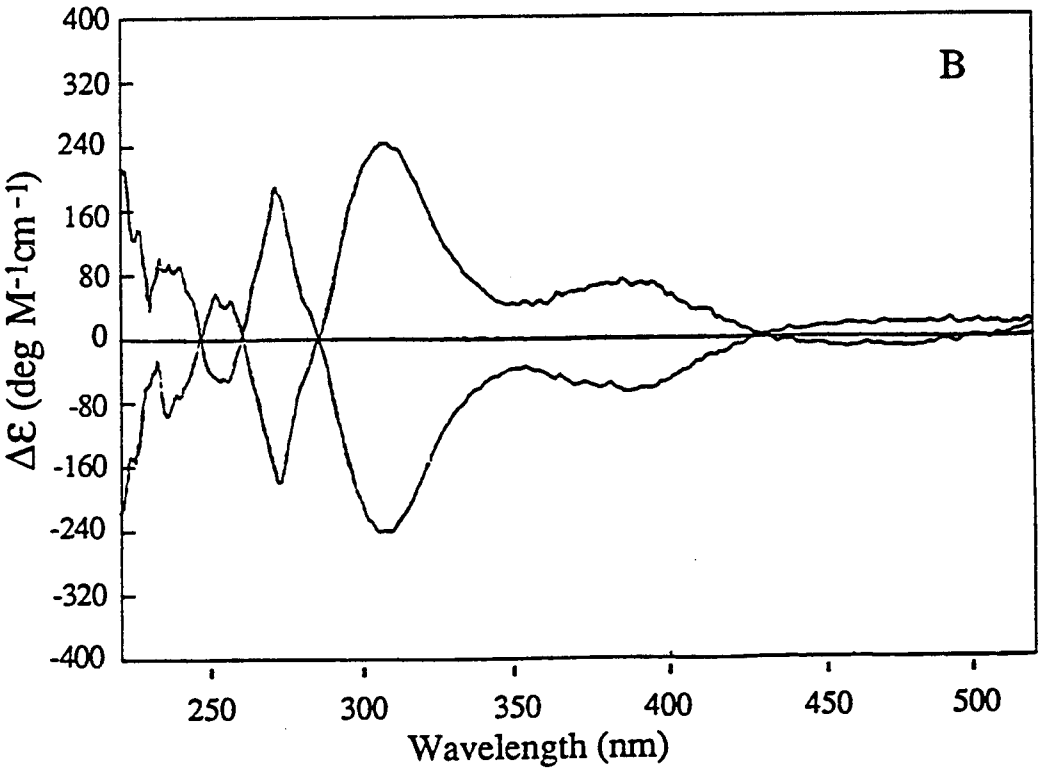
B
Δε (deg M^-1cm^-1)
400
320
240
160
80
0
-80
-160
-240
-320
-400
250
300
350
400
450
500
Wavelength (nm)

Figure 2.4. UV-Vis titration of Λ-$Rh(en)_2phi^{3+}$ with calf thymus DNA. Metal concentration in every spectrum was 17.5 μM. Spectra are shown at 0, 26.6, 53.0, 79.2, 105.3, 131.1, 195.1 and 398.1 μM DNA base pairs, although the last two spectra are essentially superimposed. Upon addition of DNA, the spectrum of Λ-$Rh(en)_2phi^{3+}$ displays a clear red shift along with substantial hypochromicity in the phi centered π-->π^* transition at 320 - 400 nm. Isosbestic behavior is observed, with an isosbestic point at 406 nm.

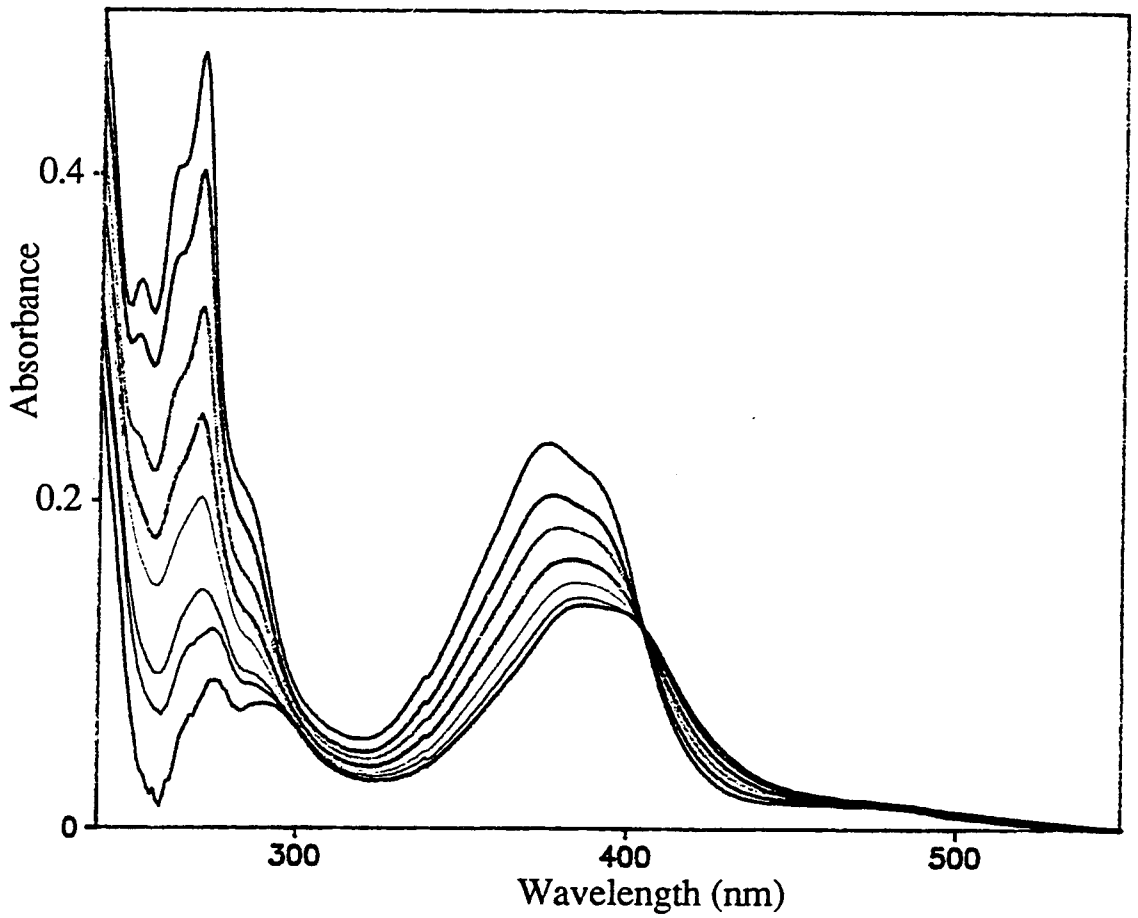
0.4
0.2
0
Absorbance
300
400
500
Wavelength (nm)

Figure 2.5. Analyses of UV-Vis titration data. Data is plotted as the change in maximum extinction coefficient of the phi centered π-->π^* transition versus [DNA] / [Rh]. For Λ-Rh(en)$_2$phi^{3+} (Panel A), Δ-Rh(en)$_2$phi^{3+} (Panel B), Rh(cyclen)phi^{3+} (Panel C), as well as Rh(S_4-cyclen)phi^{3+} (Panel D), the hypochromic effects saturate at a level of ~8 DNA nucleotides per Rh(phi)$^{3+}$ molecule.

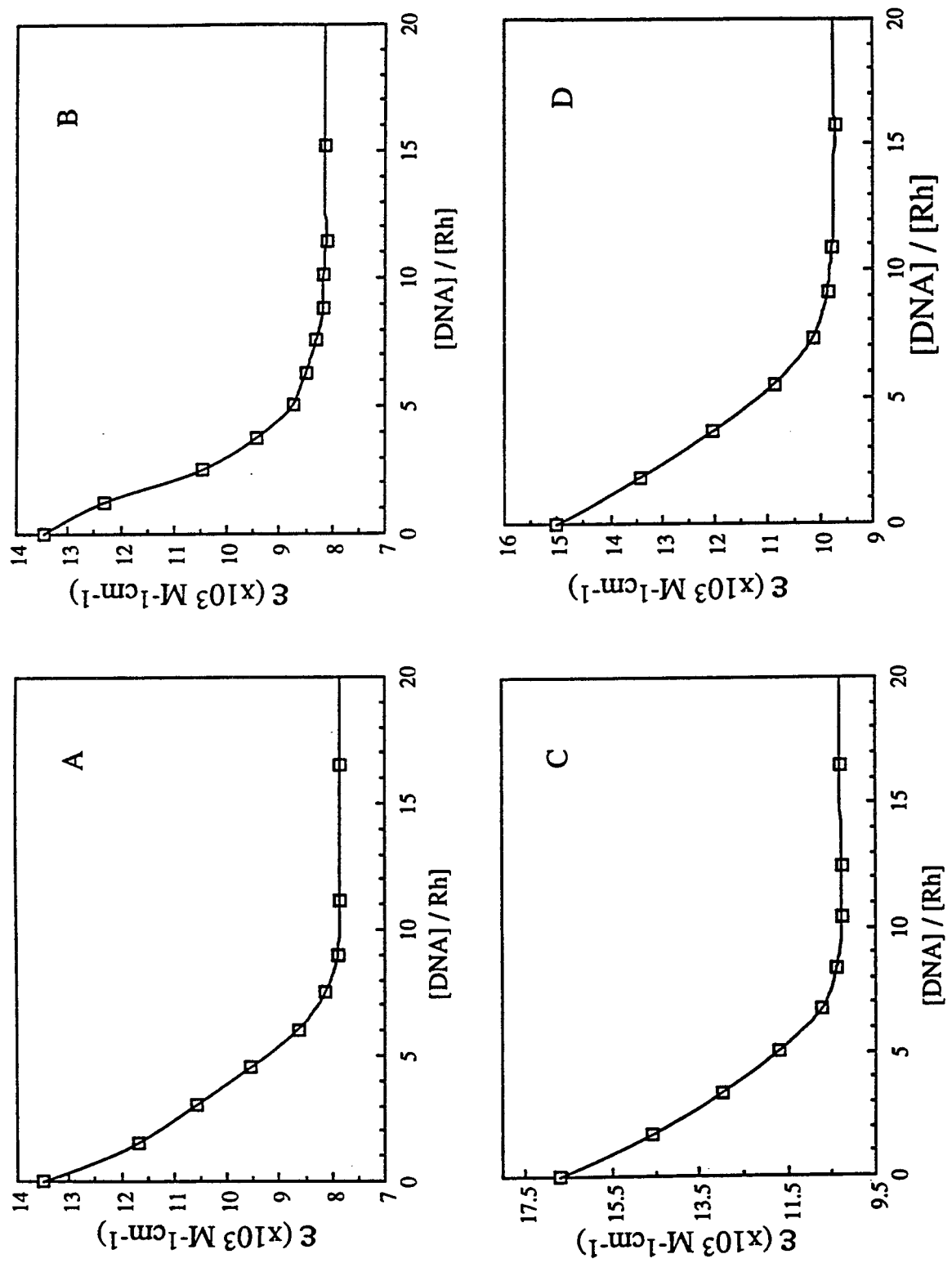
A
B
C
D
ε (x10³ M⁻¹cm⁻¹)
[DNA] / [Rh]

Results from titrations of Λ-Rh(en)$_2$phi^{3+}, Δ-Rh(en)$_2$phi^{3+}, Rh(cyclen)phi^{3+} and Rh(S$_4$-cyclen)phi^{3+} with calf thymus DNA are listed in Table 2.1, and the hypochromicity and red shift previously reported [6] for Rh(phen)$_2$phi^{3+} is included for comparison. The Rh(phi)$^{3+}$ complexes containing ancillary saturated amines and a thioether interact with DNA all display red shifts in absorbance maximum along with strong hypochromicity similar to Rh(phen)$_2$phi^{3+}. In order to view the saturation of the hypochromic effect, the change in maximum extinction coefficient may be plotted as a function of [DNA] / [Rh] ratio. Such plots for the Rh(phi)$^{3+}$ complexes examined are shown in Figure 2.5. In all three graphs, saturation of the hypochromic effect is observed at ~8 DNA nucleotides per Rh.

Table 2.1. UV-Vis titrations of various Rh(phi)$^{3+}$ complexes with calf thymus DNA.

Rh(phi)$^{3+}$ complex	Red Shift [a]	Hypochromicity [b]	Isosbestic Point
Λ- Rh(en)$_2$phi^{3+}	12 nm	42.0 %	406 nm
Δ-Rh(en)$_2$phi^{3+}	12 nm	42.6 %	405 nm
Rh(cyclen)$_2$phi^{3+}	13 nm	38.8 %	385 nm
Rh(S$_4$-cyclen)$_2$phi^{3+}	9 nm	33.5 %	423 nm
Rh(phen)$_2$phi^{3+} [c]	16 nm	42.3 %	391 nm

a. Red shift = absorption maximum bound - free.

b. Hypochromicity = 100 x (ε_{free} - ε_{bound}) / ε_{free}

c. Data taken from reference 6.

Figure 2.6 shows the UV-Vis spectrum of rac-$Rh(en)_2phi^{3+}$ upon the sequential addition of poly rI · poly rC, a rather generic RNA homopolymer. Again, the $Rh(phi)^{3+}$ complex displays a substantial red shift and hypochromicity upon the addition of the polynucleotide. Results for the titrations of $Rh(NH_3)_4phi^{3+}$, $Rh(en)_2phi^{3+}$ and $Rh(phen)_2phi^{3+}$ with poly rI · poly rC are summarized in Table 2.2. An important difference between $Rh(phen)_2phi^{3+}$ and either $Rh(en)_2phi^{3+}$ or $Rh(NH_3)_4phi^{3+}$ becomes apparent when plots of extinction coefficient versus [RNA] / [Rh] ratio are compared. In Figure 2.7, the saturation of the hypochromic effect for both polyamine complexes saturate occurs at approximately half the RNA : Rh ratio required for $Rh(phen)_2phi^{3+}$. Note that for the polyamine complexes the saturating ratio with poly rI · poly rC is similar to that observed with calf thymus DNA.

Table 2.2 Titrations of $Rh(phi)^{3+}$ complexes with poly rI · poly rC .

$Rh(phi)^{3+}$ complex	Red Shift [a]	Hypochromicity [b]	Isosbestic Point
$Rh(NH_3)_4phi^{3+}$	8 nm	37.6 %	400 nm
$Rh(en)_2phi^{3+}$	9 nm	36.8 %	405 nm
$Rh(phen)_2phi^{3+}$	15 nm	23.8 %	376 nm

a. Red shift = difference in absorption maximum of bound and free complex.

b. Hypochromicity = $100 \times (\varepsilon_{free} - \varepsilon_{bound}) / \varepsilon_{free}$.

Figure 2.6. UV-Vis titration of rac-$Rh(en)_2phi^{3+}$ with poly rI · poly rC. Metal concentration in every spectrum was 27.9 μM. Spectra are shown at 0, 14.9, 29.8, 44.5, 59.1, 73.6, 95.3, 116.7, 179.7 μM base pairs. Upon addition of poly rI · poly rC, the spectrum of $Rh(en)_2phi^{3+}$ displays a clear red shift along with substantial hypochromicity in the phi centered π-->π^* transition at 320 - 420 nm. Isosbestic behavior is observed, with an isosbestic point at 405 nm.

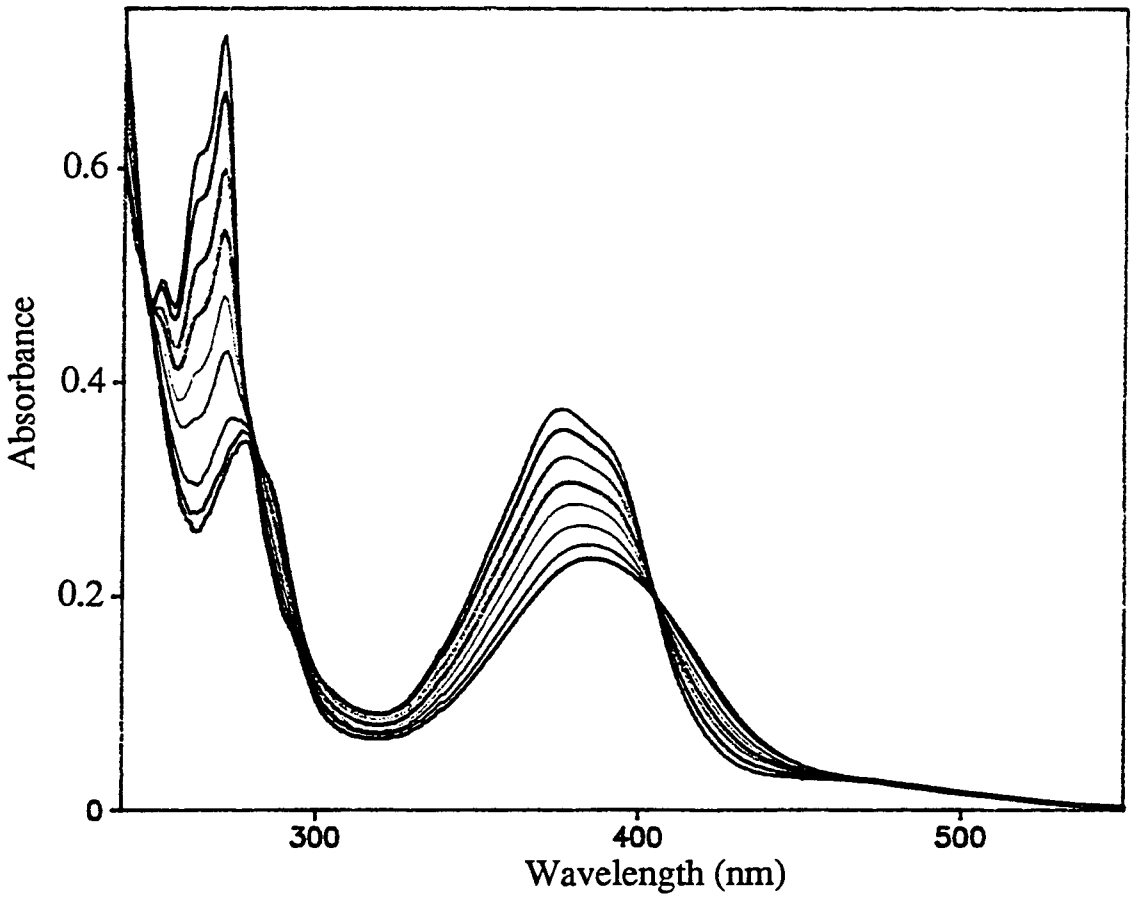
Absorbance
0.6
0.4
0.2
0
300
400
500
Wavelength (nm)

Figure 2.7. Analyses of UV-Vis titrations of poly rI · poly rC. Data is plotted as the change in maximum extinction coefficient of the π-->π* transition versus [DNA] / [Rh]. Plots are shown for $Rh(NH_3)_4phi^{3+}$ (Panel A), $Rh(en)_2phi^{3+}$ (Panel B), as well as $Rh(phen)_2phi^{3+}$ (Panel C). While the hypochromic effects saturate at a level of ~8 DNA nucleotides per $Rh(phi)^{3+}$ complex for $Rh(NH_3)_4phi^{3+}$ and $Rh(en)_2phi^{3+}$, the hypochromicity of $Rh(phen)_2phi^{3+}$ does not saturate until a higher ratio is reached (~15 DNA nucleotides / Rh molecule).

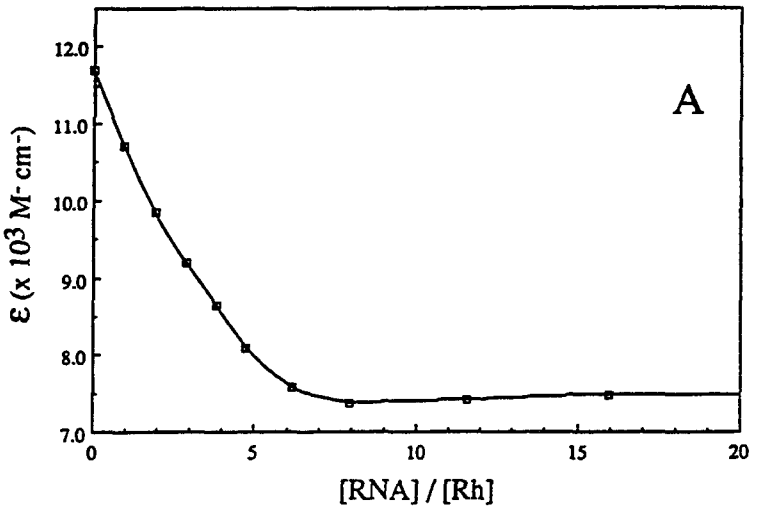
A
12.0
11.0
10.0
9.0
8.0
7.0
ε (x 10³ M⁻ cm⁻)
0
5
10
15
20
[RNA] / [Rh]

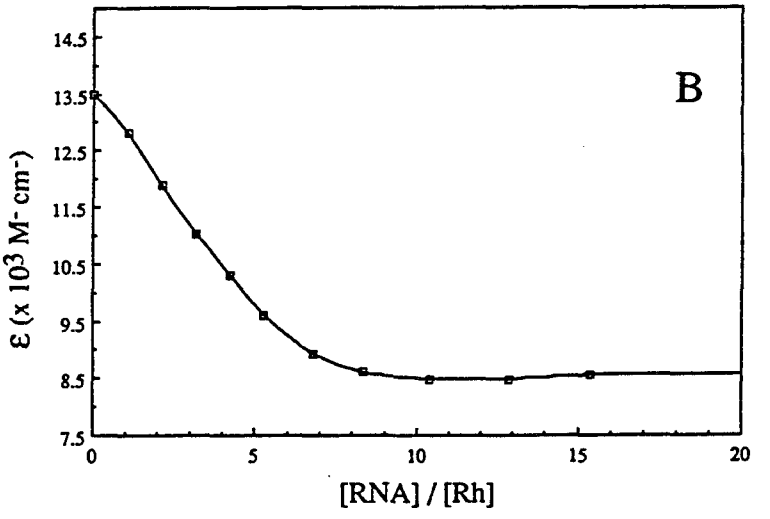
B
14.5
13.5
12.5
11.5
10.5
9.5
8.5
7.5
ε (x 10³ M⁻ cm⁻)
0
5
10
15
20
[RNA] / [Rh]

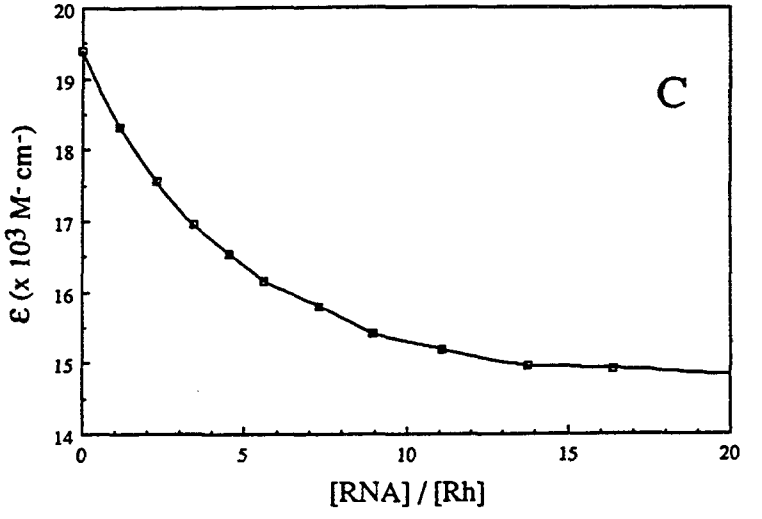
C
20
19
18
17
16
15
14
ε (x 10³ M⁻ cm⁻)
0
5
10
15
20
[RNA] / [Rh]

B. Unwinding assays. When an intercalator binds to the DNA helix, the π-stacked bases separate by 3.4 Å to allow the stacking of the flat aromatic intercalator into the helix.[16] The DNA helix also unwinds, to allow better stacking between the DNA bases and the intercalating ligand and relieve strain on the phosphodiester backbone.[17] The progressive unwinding of supercoiled plasmid DNA by Λ- and Δ-$Rh(en)_2phi^{3+}$ is shown in Figure 2.8. The addition of metal complex causes plasmid pBR322 DNA to unwind, thus altering the electrophoretic mobility of the supercoiled Form I DNA to that of the relaxed, (nicked circular) form II DNA. This comigration indicates that the Form I DNA has been unwound by the metal complex, thus removing the supercoiling responsible for the faster migration of Form I DNA through the agarose gel matrix. In Figure 2.8, some gel retardation of Form II nicked plasmid is noted, although this effect is substantially smaller than the unwinding effect.

One may compare the concentration required to relax all 11 supercoils of pBR322 as a measure of the effective unwinding per metal complex. In Table 2.3, this parameter is compared for several $Rh(phi)^{3+}$ complexes under identical conditions. At concentrations of 6 μM metal complex, both Λ-$Rh(en)_2phi^{3+}$ and Δ-$Rh(en)_2phi^{3+}$, cause the form I supercoiled DNA to migrate with the Form II nicked DNA. $Rh(phen)_2phi^{3+}$, which unwinds DNA by ~ 21° per bound Rh molecule,[6] also has a parameter of 6 μM in this assay.

Although the results in Table 2.3 indicate that the enantiomers of $Rh(en)_2phi^{3+}$ unwind DNA as well as $Rh(phen)_2phi^{3+}$, the effect is less than that predicted by ~20° unwinding per bound molecule. In order to unwind all 11 supercoils of plasmid pBR322, assuming an average binding constant of $1 \times 10^5\ M^{-1}$, the degree of unwinding is ~ 10° / $Rh(phi)^{3+}$ complex. However, the reported values likely represent underestimates of the unwinding potential of these $Rh(phi)^{3+}$ molecules because the reversible dissociation of these complexes throughout the course of electrophoresis would allow a free $Rh(phi)^{3+}$ complex to be drawn away from the Rh:DNA complex to the negative anode terminal.

Figure 2.8. The unwinding of plasmid pBR322 DNA by Λ- and Δ-$Rh(en)_2phi^{3+}$. Lanes 1 - 10 correspond to the incubation of 0.5 mg pBR322 plasmid DNA with 0, 1, 2, 4, 5, 6, 8, 10, 15 and 20 μM $Rh(en)_2phi^{3+}$. In the lane corresponding to 6 μM total [Rh], the retarded Form I DNA migrates with the free Form II DNA shown in the 0 μM Rh lanes. Although the Form II DNA also displays gel retardation upon binding by $Rh(en)_2phi^{3+}$, this effect is less than the unwinding of the supercoiled Form I species.

A

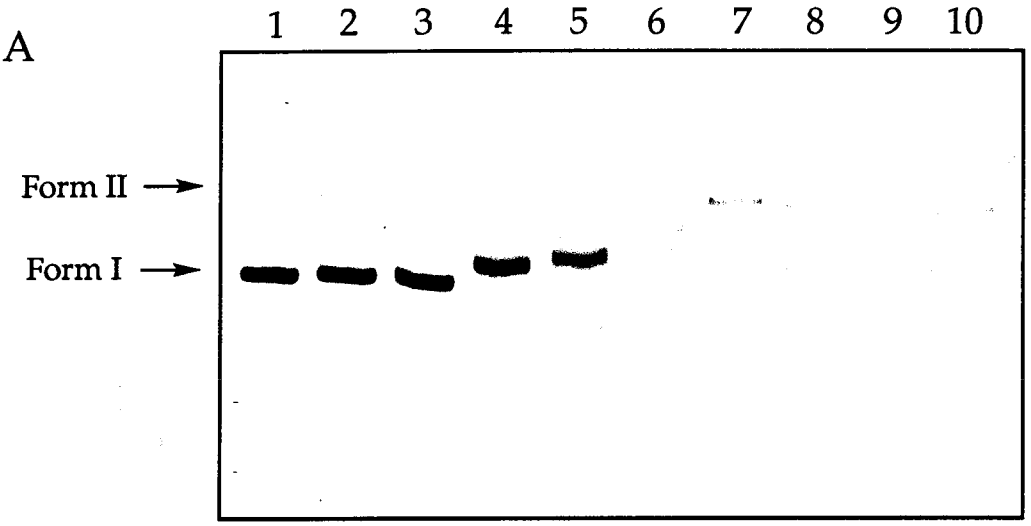

B

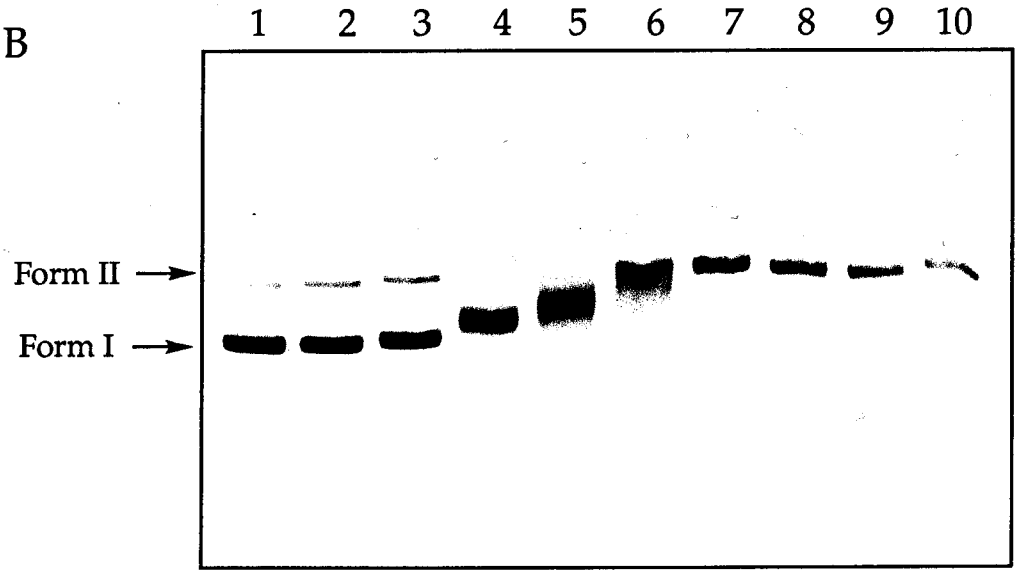

Table 2.3. Unwinding of plasmid pBR322 by $Rh(phi)^{3+}$ complexes.

$Rh(phi)^{3+}$ Complex	Unwinding [Rh][a]
$Rh(NH_3)_4phi^{3+}$	6 μM
Λ-$Rh(en)_2phi^{3+}$	6 μM
Δ-$Rh(en)_2phi^{3+}$	6 μM
$Rh(cyclen)phi^{3+}$	8 μM
$Rh(S_4\text{-cyclen})phi^{3+}$	8 μM
$Rh(phen)_2phi^{3+}$	6 μM

a. This value represents the concentration $Rh(phi)^{3+}$ at which the comigration of bound Form I with free Form II plasmid DNA was observed.

2.3.3. Photocleavage of d(GAGTGCACTC)$_2$ by the enantiomers of Rh(en)$_2$phi^{3+}.

In addition to binding strongly to both DNA and RNA and unwinding plasmid DNA, Rh(en)$_2$phi^{3+} promotes DNA cleavage upon photoactivation with near-UV light. To examine the DNA termini produced in photocleavage experiments, 3'- [^{32}P] or 5'- [^{32}P] end-labeled d(GAGTGCACTC)$_2$ (10 μM DNA duplex) was irradiated in the presence of either 10 μM Rh(en)$_2$phi^{3+} or 5 μM Rh(phen)$_2$phi^{3+} in 20 μL total volume for 10 - 15 minutes at 313 nm. In both 3'- and 5'-end-labeled experiments, the termini produced by Λ- and Δ-Rh(en)$_2$phi^{3+} photocleavage were compared to termini produced by Λ- and Δ-Rh(phen)$_2$phi^{3+}.

An image of a 20% denaturing polyacrylamide gel (Figure 2.9.A) reveals that photocleavage of 3'- [^{32}P] end-labeled d(GAGTGCACTC)$_2$ by the enantiomers of both Rh(en)$_2$phi^{3+} and Rh(phen)$_2$phi^{3+} produces only 5' - phosphate termini, which comigrate with termini produced in Maxam-Gilbert sequencing reactions.[8] Figure 2.9.B directly compares photocleavage of 5'- [^{32}P] end-labeled d(GAGTGCACTC)$_2$ by Λ-and Δ-Rh(en)$_2$phi^{3+} to cleavage by Λ- and Δ-Rh(phen)$_2$phi^{3+}. Again, both Λ- and Δ-Rh(en)$_2$phi^{3+} produce primarily 3'-phosphate termini which comigrate with the 3'-termini produced in the Maxam-Gilbert sequencing reactions.[8] However, at several sites in Figure 2.9.B, there is also a secondary band, denoted with the letter b, which migrates significantly slower than the corresponding primary phosphate band (e.g. G_3 = G_3 phosphate, G_3- b = G_3 secondary band) . For Λ-Rh(en)$_2$phi^{3+} production of this secondary product is evident at positions G_3, T_4, C_6 and T_9, while the Δ- enantiomer produces a secondary band at T_4, C_6 and T_9. At higher exposures of Figure 2.9.B., there is also a secondary band accompanying the weak cleavage by Δ-Rh(en)$_2$phi^{3+} at G_3. Importantly, both Λ-Rh(phen)$_2$phi^{3+} and Δ-Rh(phen)$_2$phi^{3+} also produce this secondary band at positions G_3, T_4, C_6, and A_7 in photocleavage of d(GAGTGCACTC)$_2$. This terminus has been assigned as the 3'- phosphoglycaldehyde termini produced in photocleavage of DNA by Rh(phen)$_2$phi^{3+}.[6] The secondary phosphoglycaldehyde

terminus is the only non-phosphate terminus observed under these conditions. (e.g. no phosphoglycolate terminus observed).

Figure 2.9. Analysis of DNA end products derived from $Rh(en)_2phi^{3+}$ photocleavage. A. Cleavage of 3'- [^{32}P] end-labeled $d(GAGTGCACTC)_2$. Lanes 1 and 2, Maxam-Gilbert G and C+T reactions respectively; lane 3, DNA incubated in the presence of 5 μM Δ-$Rh(en)_2phi^{3+}$; lane 4, DNA irradiated in the absence of $Rh(phi)^{3+}$ complex; lanes 5 and 6, photocleavage for 15 min. by 10 μM Λ- and Δ- $Rh(en)_2phi^{3+}$ respectively; lanes 7 and 8, photocleavage for 10 min. by 5 μM Λ- and Δ-$Rh(phen)_2phi^{3+}$ respectively. All four $Rh(phi)^{3+}$ complexes produce solely 5' -phosphate termini, as judged by comigration of photocleavage bands with those produced by Maxam Gilbert sequencing reactions.

B. Photocleavage of 5'- [^{32}P] end-labeled $d(GAGTGCACTC)_2$. Lanes are identical to those described for Panel A. All four $Rh(phi)^{3+}$ complexes produce primarily 3'-phosphate termini, as judged by comigration with Maxam Gilbert sequencing reactions. However, there is also clear production of a secondary photocleavage product at numerous sites (denoted with the letter b).

A

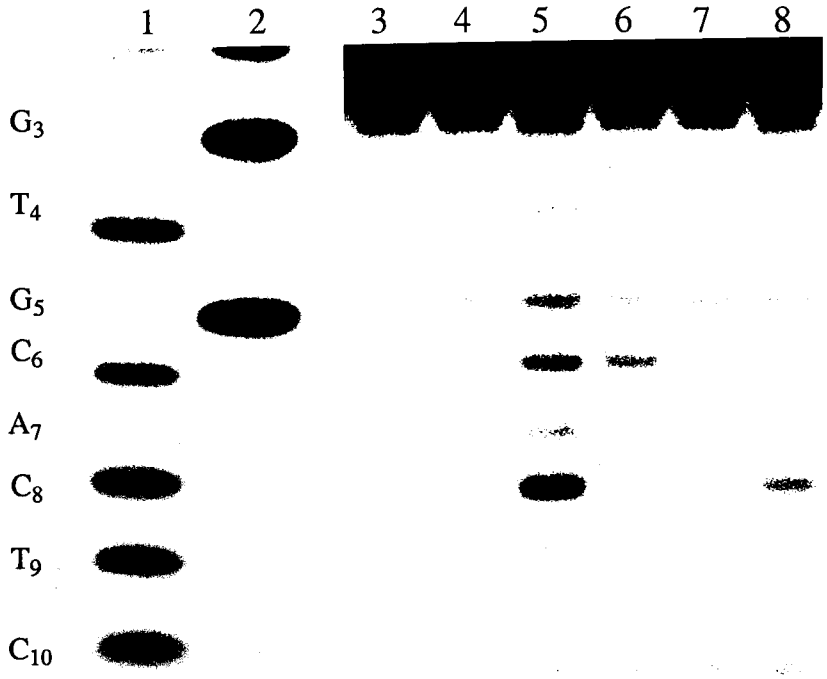
1
2
3
4
5
6
7
8
G3
T4
G5
C6
A7
C8
T9
C10

B

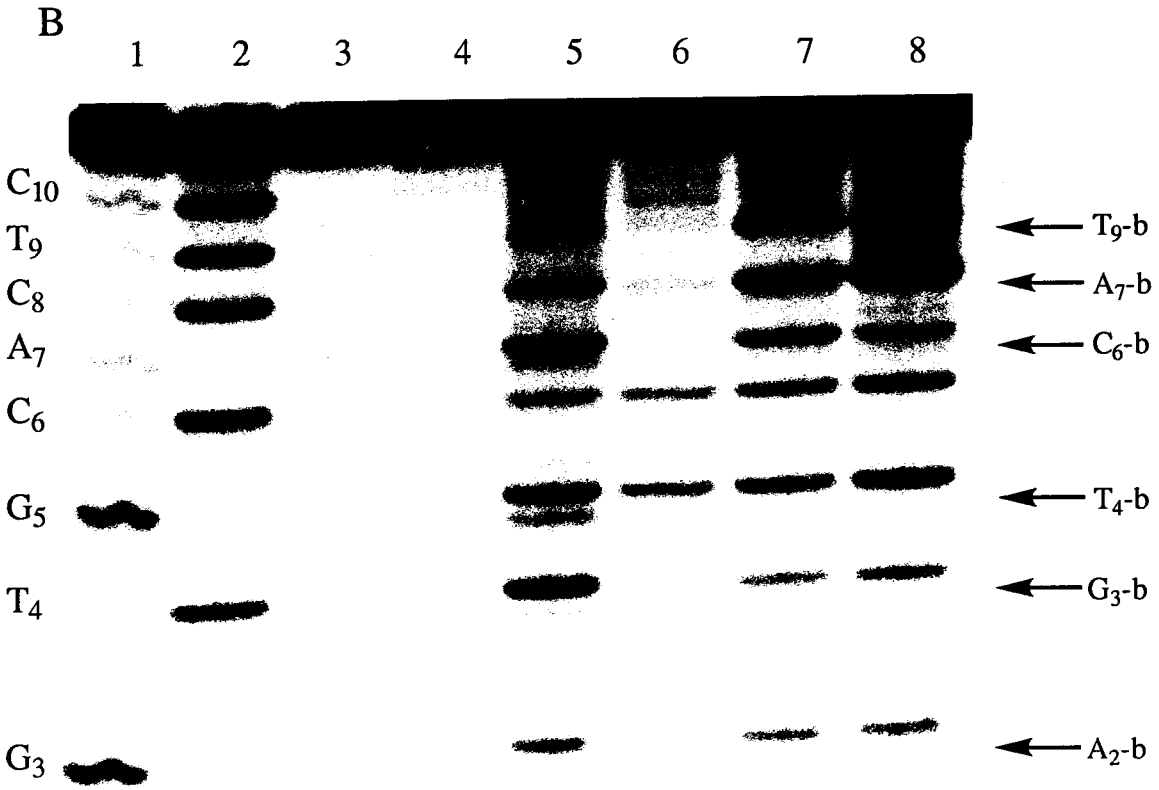
1
2
3
4
5
6
7
8
C10
T9
C8
A7
C6
G5
T4
G3
T9-b
A7-b
C6-b
T4-b
G3-b
A2-b

Quantitation of the results of Figure 2.9.B is listed in Table 2.4. The fraction cleavage at a base n is defined by equation 1:

$$I_n = \left(\frac{I_{n,raw} - I_{bkgd}}{I_{tot} - I_{tot,bkgd}} \right) - \left(\frac{I_{lc,raw} - I_{bkgd}}{I_{lc,tot} - I_{tot,bkgd}} \right) , \quad (1)$$

where I_n is the fraction of DNA strands cleaved at base n, $I_{n,raw}$ is the raw volume intensity of the band n, I_{bkgd} is the intensity measured for the same area placed on an ostensibly blank part of the image, $I_{n,lc}$ is the volume intensity for band n in the light control, I_{tot} an $I_{lc,tot}$ are the total volume intensities measured in either a cleavage or light control lane, including individual bands as well as uncut oligonucleotide, and $I_{tot,bkgd}$ is the corresponding correction for the larger background intensity of the rectangle used to quantitate total loading in a lane. Values reported are the average of two independent trials which differed by < 5-10 %.

The secondary phosphoglycaldehyde band accounts for ~30-50% of the cleavage by Λ-Rh(en)$_2$phi^{3+}, a higher percentage than is produced by either Λ- or Δ-Rh(phen)$_2$phi^{3+}. It is significant that while the strong cleavage by the Δ-Rh(en)$_2$phi^{3+} complex at position G_5 is accompanied by no phosphoglycaldehyde product, cleavage at position C_6 produces significant amounts of phosphoglycaldehyde product. Also, the weaker cleavage by the Δ-enantiomer at T_4 and G_3 produce secondary bands which it accounts for ~50% of the total cleavage at these weak sites.

Table 2.4. Phosphoglycaldehyde production in photocleavage of d(GAGTGCACTC)$_2$.[a]

Base	Λ-Rh(en)$_2$phi^{3+} fraction cleavage (% b) [a,b]	Δ-Rh(en)$_2$phi^{3+} fraction cleavage (% b)	Λ-Rh(phen)$_2$phi^{3+} fraction cleavage (% b)	Δ-Rh(phen)$_2$phi^{3+} fraction cleavage (% b)
G_3	0.23 (29.3)	0.03 (44.0)	0.19 (21.0)	0.21 (18.3)
T_4	0.58 (27.9)	0.13 (48.4)	0.22 (27.9)	0.27 (21.9)
G_5	0.40 (ND)[d]	0.18 (ND)	0.28 (ND)	0.42 (ND)
C_6	0.44 (49.8)	0.22 (32.1)	0.31 (22.8)	0.43 (21.9)
A_7	0.48 (NR)[e]	0.07 (NR)	0.31 (NR)	0.31 (NR)
C_8	0.34 (NR)	0.11 (NR)	0.82 (NR)	1.95 (NR)
T_9	0.63 (49.1)	0.25 (61.0)	0.33 (21.8)	0.83 (41.5)

a. Values reported are the average of two trial which differed by < 5-10%.

b. Fraction cleavage = 100 x (total intensity at base n / total intensity in that lane).

c. (% b) = percent of cleavage at base n due to phosphoglycaldehyde product.

d. ND = band not detectable. e. NR = band not resolved.

2.3.4. Quantum yields for free base release.

Figure 2.10 shows a typical HPLC trace following photocleavage of calf thymus DNA by *rac*-$Rh(en)_2phi^{3+}$ and $Rh(cyclen)phi^{3+}$. The free base products cytosine, guanine and thymine (labeled **C**, **G** & **T**) were eluted with retention times of 3.2, 5.3 and 7.5 minutes respectively. Although the free base A was occasionally observed at ~12-14 minutes, the peak was always quite broad and thus not suitable for quantitation. The peak at 2 min. was highly variant between injections, and is likely a combination of base propenoates, buffer salts and air. For both reasons, the reported quantum yields represent underestimates of the true values.

The quantum yields for free base release of cytosine, guanine, and thymine by several $Rh(phi)^{3+}$ complexes are presented in Table 2.5. Quantum yields were calculated by equation 2:

$$\Phi_{313} = \frac{\text{mol free bases}}{\text{mol hv absorbed}} = \frac{\text{mol C, G, \& T}}{(t)(I_\lambda)[(100 - \%T)/100]} \quad , \qquad (2)$$

where Φ_{313} is the quantum yield for free base release at 313 nm, t is irradiation time (min), I_λ is the light intensity at 313 nm in Einsteins / min, and [(100 -%T) / 100] is the correction for the fraction of light absorbed by the Rh:DNA solution at 313 nm. Light intensity, as measured by ferrioxalate actinometry, was typically 3-5 x 10^{-6} Ein / min. Following quantitation of the HPLC traces, the moles free base produced by each complex was determined using calibration curves constructed with authentic standards. All values listed are the average of two trials which differed by < 5-10%.

The value of 12 x 10^{-4} previously reported[6] for the quantum yield of free base release by $Rh(phen)_2phi^{3+}$ is provided in Table 2.5 for reference. In general, the quantum yields for phi complexes of Rh(III) containing saturated amines as ancillary ligands are an order of magnitude less than the quantum yield for $Rh(phen)_2phi^{3+}$.

Figure 2.10. HPLC analysis of free base release by $Rh(en)_2phi^{3+}$ and $Rh(cyclen)phi^{3+}$. Shown are HPLC traces following photocleavage of 500 μM base pairs calf thymus DNA by 40 μM $Rh(en)_2phi^{3+}$ (Trace A) or $Rh(cyclen)phi^{3+}$ (Trace B) for 40 minutes, pH 7.0, 10 mM NaCacodylate, 40 mM NaCl. Trace C displays the HPLC trace obtained upon irradiation of calf thymus DNA in the absence of $Rh(phi)^{3+}$ complex. The free bases cytosine, guanine, and thymine are labeled **C**, **G** and **T** respectively. Note the variance in the peak marked **1**, which is likely due to base propenoates, buffer salts and air from the injection port.

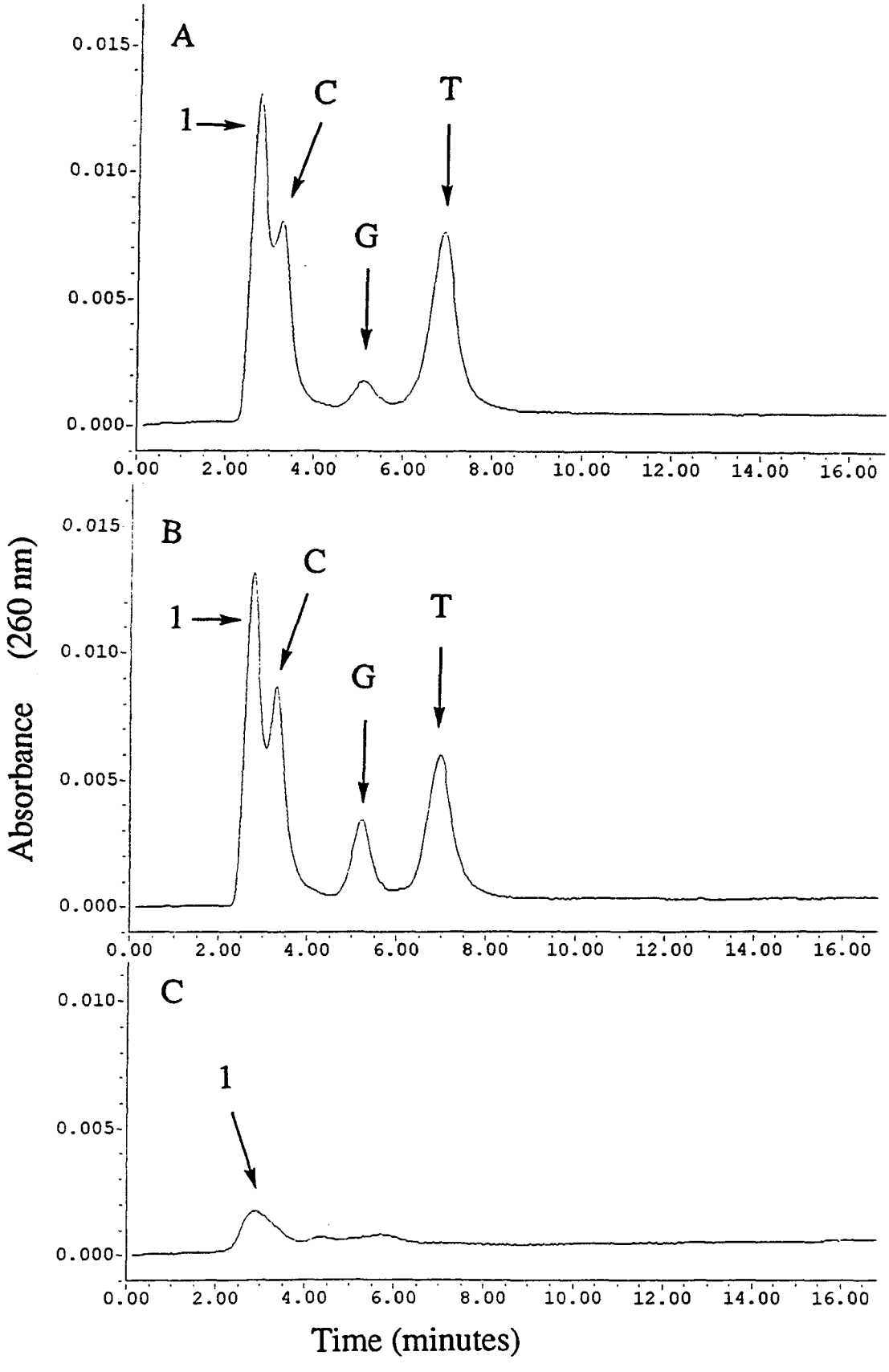
A
B
C
1
C
G
T
0.015
0.010
0.005
0.000
0.00
2.00
4.00
6.00
8.00
10.00
12.00
14.00
16.00
Absorbance (260 nm)
Time (minutes)

Table 2.5. Quantum yields for free base release by $Rh(N_4)phi^{3+}$ complexes.

$Rh(phi)^{3+}$ Complex	$\Phi_{313\ nm}$ (x 10^4)
$Rh(NH_3)_4phi^{3+}$	0.6
$Rh(en)_2phi^{3+}$	1.0
$Rh(cyclen)phi^{3+}$	1.2
$Rh(S_4\text{-cyclen})phi^{3+}$	0.3
$Rh(phen)_2phi^{3+}$	12 [a]

a. Data taken from reference 6.

2.3.5. Establishing the stoichiometry of DNA cleavage by $Rh(en)_2phi^{3+}$. Quantitative photoanation, free base release and strand cleavage experiments on identical samples.

Figure 2.11 shows the UV-Vis spectrum of 20 μM solution of $Rh(en)_2phi^{3+}$ irradiated in the absence (A) and presence (B) of 25 μM duplex $d(GAGTGCACTC)_2$. The photolysis of $Rh(phi)^{3+}$ complexes from 313 nm to 365 nm results in the preferential loss of the phi ligand, which may be monitored by the absorbance loss in the phi centered π-->π^* transition of the UV-Vis spectrum. Quantitation of the loss of phi complex during photolysis was measured by the absorbance change at the isosbestic point of the phi centered π - π^* band. Note that the spectrum of $Rh(en)_2phi^{3+}$ in the presence of $d(GAGTGCACTC)_2$, (Figure 2.11.B) displays a 12 nm red shift and ~35 % hypochromicity in the π - π^* band relative to the spectrum of the free metal complex, indicating that the $Rh(en)_2phi^{3+}$ is fully bound. While photolysis of $Rh(en)_2phi^{3+}$ in the absence of DNA resulted in a 17 % loss in absorbance at 376 nm (0.83 nmoles Rh), the photolysis of the bound complex results in a ~12 % (0.60 nmoles) loss.

Figure 2.12 shows typical HPLC traces obtained upon injection of the above samples on a C-18 analytical HPLC column. The free bases cytosine (C), guanine (G), and thymine (T) were detected at 4.2, 10.8 and 15.6 minutes respectively, and were assigned by comparison to authentic standards. Under the gradient used, the uncut DNA migrates at 21.5 min, and free Rh complex, distinguished by its long wavelength absorption, migrates at 22.8 min. Some $Rh(en)_2phi^{3+}$ also elutes with the uncleaved DNA peak, indicating that it is tightly associated with the DNA under HPLC conditions.

In order to relate the amount of strand cleavage with the amount of photoanation and the amount of free base released, photocleavage of 3' - [^{32}P] end-labeled $d(GAGTGCACTC)_2$ was performed at the same conditions as the cold irradiations. The cleavage reactions were analyzed by 20% denaturing polyacrylamide gel electrophoresis, and the fraction cleavage at each resolved base was calculated as described in section

2.3.2. The sum of the fractions at each individual base was multiplied by a correction (10 / 8) for bases not resolved to yield the total fraction of DNA strands cleaved. The amount of strand cleavage was then calculated as the total fraction cleaved multiplied by the concentration of DNA strands (50 μM) and the irradiation volume (250 mL). Thus 8 out of 10 bases were quantitated, and 3.8% of the oligonucleotide strands were cleaved, corresponding to 0.58 nmoles strand cleavage reported in Table 2.6.

Table 2.6 is a summary of the results from the three experiments described above. The results indicate that a 1:1:1 stoichiometry exists between the loss of phi absorbance, the release of a free base and the cleavage of a DNA strand. Therefore, the reduced quantum efficiency of $Rh(en)_2phi^{3+}$ relative to $Rh(phen)_2phi^{3+}$ reflects a difference in the photoantion effeiciency, since it appears that every $Rh(en)_2phi^{3+}$ molecule which is excited (and therefore undergoes photoanation) also cleaves the DNA strand. While the amount of free base products listed in Table 2.6 appears to be less than that expected by either the loss of phi absorbance or the amount of strand cleavage, it was not possible to quantitate the release of the free base adenine in the HPLC analysis of the reaction, and thus the minor discrepancy is likely a reflection of cleavage at adenine residues.

Table 2.6. Quantitation of photocleavage of d(GAGTGCACTC) by $Rh(en)_2phi^{3+}$.

Experiment	Product (nmoles)
Photoanation	0.60 [a,d]
Free base release	0.48 [b,d]
Strand cleavage	0.58 [c,e]

a. Quantitated at 402 nm, where ε_{free} and ε_{bound} for $Rh(en)_2phi^{3+}$ are identical.

b. Determined by integration of the peaks for C, G and T and comparison to calibration curves constructed with authentic samples.

c. Calculated as (percentage cleaved) x (DNA strand concentration) x (250 μL) x (1.25).

d. The average of three trials. e. The average of four trials.

Figure 2.11. Photolysis of 20 μM $Rh(en)_2phi^{3+}$ in the absence and presence of 25 μM duplex $d(GAGTGCACTC)_2$. A. UV-Vis spectra before (top) and after (bottom) the photolysis of a 20 μM solution of $Rh(en)_2phi^{3+}$, (pH 7.0, 10 mM NaCacodylate, 40 mM NaCl), for 40 minutes in the absence of DNA. B. UV-Vis spectra of the photolysis of $Rh(en)_2phi^{3+}$ in the presence of 25 μM duplex $d(GAGTGCACTC)_2$ at the same conditions. In both Panel A and B, the inset region is an expansion of the changes in the phi centered π-->π^* band.

Note that the spectrum of $Rh(en)_2phi^{3+}$ in Panel B display the red shift (~12 nm) and hypochromism (~35 % loss) associated with DNA binding. The isosbestic point of $Rh(en)_2phi^{3+}$ for the oligonucleotide duplex is 402 nm. In the absence of DNA, photolysis produces a 17 % loss in $Rh(en)_2phi^{3+}$ absorbance at 402 nm, whereas the same photolysis in the presence of DNA yields a 12 % loss.

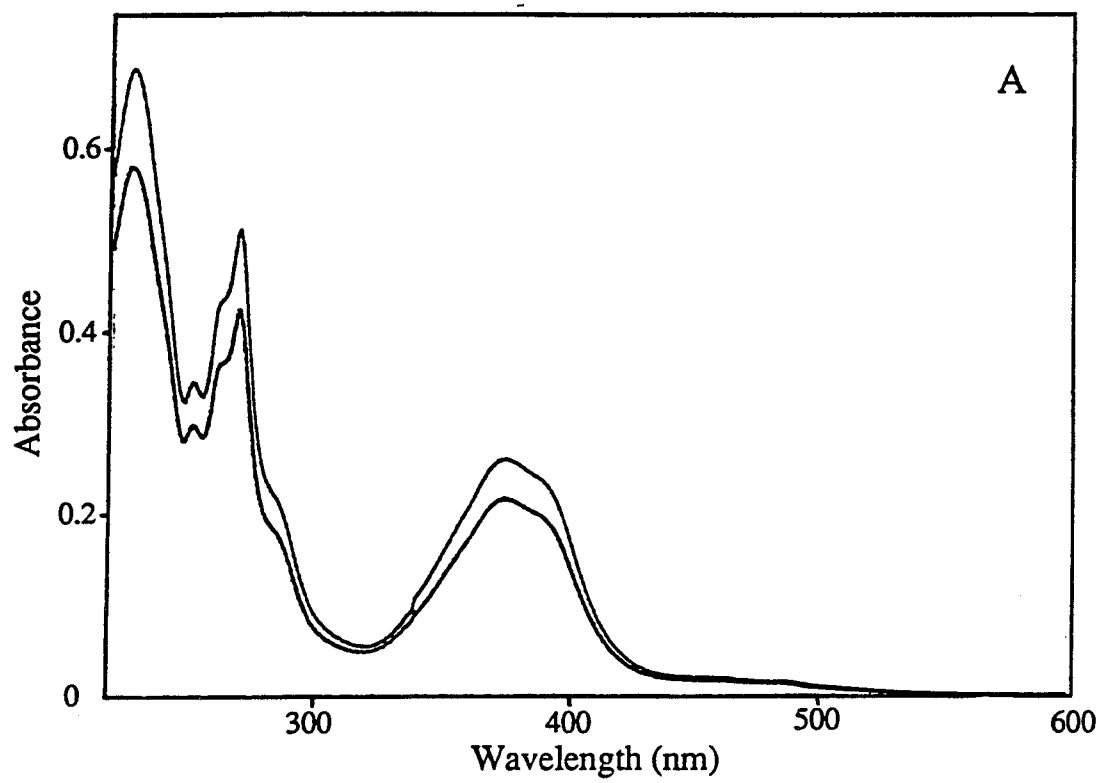
A
Absorbance
0.6
0.4
0.2
0
300
400
500
600
Wavelength (nm)

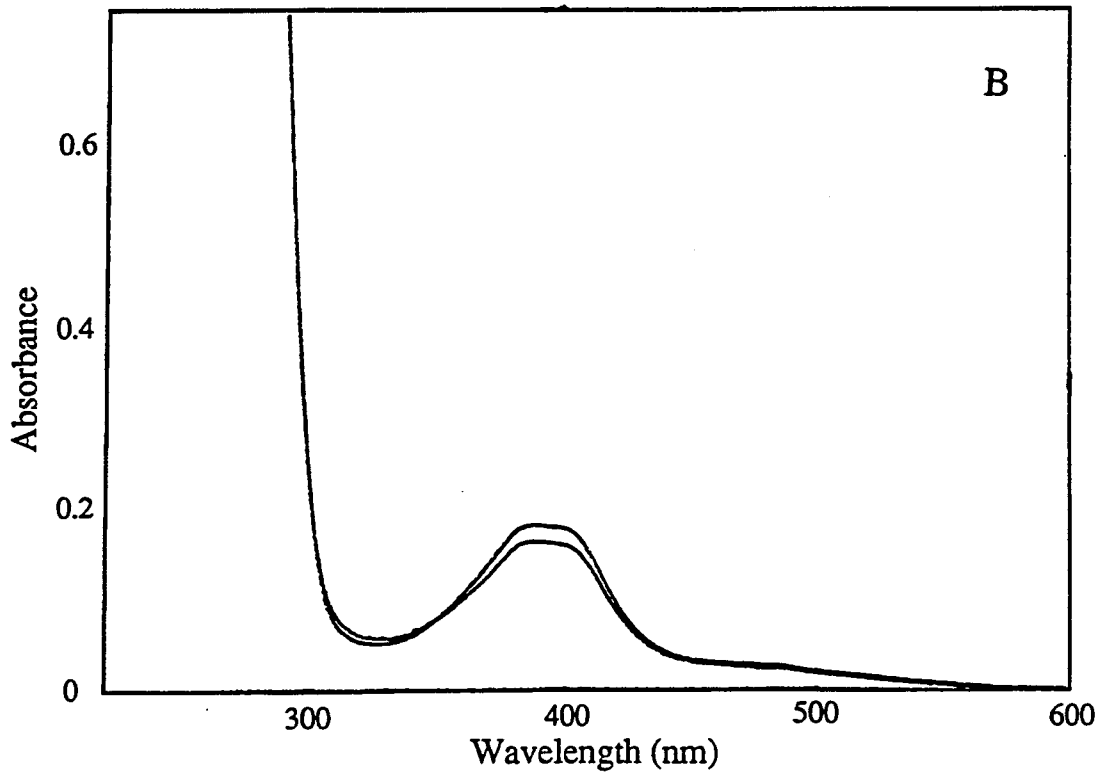
B
Absorbance
0.6
0.4
0.2
0
300
400
500
600
Wavelength (nm)

Figure 2.12. HPLC analysis of the photocleavage of d(GAGTGCACTC)$_2$ by Rh(en)$_2$phi^{3+}. Trace A is the analysis of products obtained by irradiation for 40 min at 313 nm of a solution containing 20 μM Rh(en)$_2$phi^{3+} and 25 μM duplex oligonucleotide d(GAGTGCACTC)$_2$, while Trace C is the analysis of the same solution with no irradiation. Trace B is the analysis of the cleavage of 25 μM duplex oligonucleotide in the absence of metal complex. All solutions were pH 7.0, 10 mM NaCacodylate, 40 mM NaCl. The free base products cytosine (C), guanine (G), and thymine (T) were detected at 4.2, 10.8 and 15.6 minutes respectively, and were assigned by comparison to authentic standards. Although not shown in the figure, the uncut DNA migrates at 21.5 min, and free Rh(en)$_2$phi^{3+}, distinguished by its long wavelength absorption, migrates at 22.8 min. Some Rh(en)$_2$phi^{3+} complex also elutes with the uncleaved DNA peak, indicating that it is tightly associated with the DNA under the conditions of HPLC analysis.

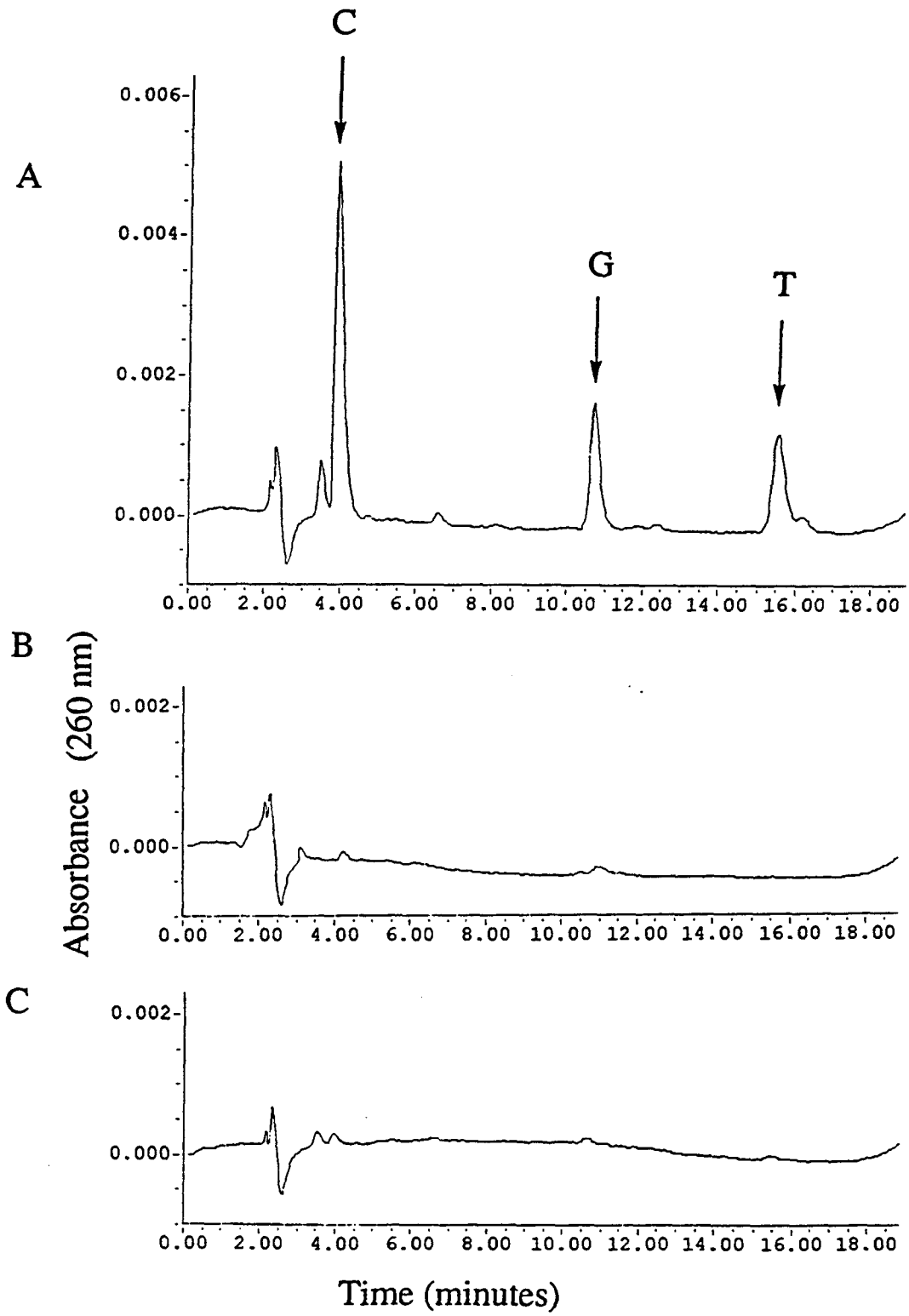
A
B
C
C
G
T
0.006
0.004
0.002
0.000
0.00 2.00 4.00 6.00 8.00 10.00 12.00 14.00 16.00 18.00
Absorbance (260 nm)
Time (minutes)

2.4. Discussion

2.4.1. The structure of $Rh(en)_2phi^{3+}$.

While the synthesis and characterization of $Rh(en)_2phi^{3+}$ has been previously published and discussed,[9,10] mention is made here of structural features relevant to the cleavage of DNA by $Rh(en)_2phi^{3+}$, as well as the capability of the ancillary ethylene diamine ligands to engage in hydrogen bonding and van der Waals contacts with DNA. First, the Rh-N bonds are ~ 0.05 Å shorter for the phi ligand than for the ethylenediamine ligand. This indicates that coordination of the phi ligand (responsible for the photoactivated DNA cleavage) involves substantial mixing of the metal and phi ligand orbitals.

Secondly, the N_{ax}-Rh-N_{ax} angle[18] directly affects the ability of these axial amines to donate hydrogen bonds to DNA since it determines their spatial orientation relative to the plane of the phi ligand. The small bite size of the ethylenediamine ligand causes a small distortion from pure octahedral geometry, but the N_{ax}-Rh-N_{ax} angle of 176° places the axial amines directly above and below the plane of the phi ligand. Further, the apparent flexibility of the 5-membered chelate ring (see below) leads to the conclusion that the axial amines of both enantiomers occupy substantially the same space for hydrogen bonding.

One final aspect of the crystal structure is that the two ethylenediamine ligands display two different ring puckers. Since altering the ring pucker affects the position of the methylene groups of the ethylenediamine ligands relative to the intercalative phi ligand, the potential of making van der Waals contacts between $Rh(en)_2phi^{3+}$ and DNA is dependent on the state of these rings. However, since both the possible low energy conformations are observed in the crystal structure, it is likely that a low energy barrier exists between the two states and that the 5 membered rings are likely fluxional in solution.

The resolution of enantiomers of $Rh(phi)^{3+}$ complexes by cation exchange chromatography with a chiral eluent is essentially a modification of the work of Yoshikawa and Yamizaki.[15] Cation chromatography provides a tremendous advantage over previous resolution methods based on co-crystallization of a particular enantiomer with a chiral salt (e.g. $Co(L\text{-cysteinesulfanate})_3^{3-}$) since column chromatography allows clear visualization of the two enantiomers. Although separations such as the one described here are now common in the Barton laboratory, the separation of Λ- and Δ-$Rh(en)_2phi^{3+}$ represented the first use of cation exchange chromatography to resolve enantiomers of a $Rh(phi)^{3+}$ compound.[10] The availability of milligram quantities of the enantiomers of $Rh(en)_2phi^{3+}$ has allowed the detailed study of their sequence specific binding and cleavage of DNA.

2.4.2. $Rh(phi)^{3+}$ complexes containing ancillary saturated amine and a thioether bind to DNA by intercalation.

Since the enantiomers of $Rh(en)_2phi^{3+}$, as well as the derivatives $Rh(NH_3)_4phi^{3+}$, $Rh(cyclen)phi^{3+}$, and $Rh(S_4\text{-cyclen})phi^{3+}$ maintained the octahedral d^6 Rh(III) center and the intercalative phi ligand of the parent molecule $Rh(phen)_2phi^{3+}$, it was expected that they would bind to DNA with high affinity through intercalation. This hypothesis is correct, as judged by the strong similarities between $Rh(N_4)phi^{3+}$ complexes and $Rh(phen)_2phi^{3+}$ both in terms of changes in UV-Vis spectra upon binding to DNA as well as the ability to unwind supercoiled plasmid DNA.

In titrations of $Rh(en)_2phi^{3+}$ and derivatives with calf thymus DNA, it appears that the polyamine $Rh(phi)^{3+}$ complexes experience a 10 -15 nm red shift and 30 - 40 % hypochromism in their phi centered π-π^* transition. This effect is similar to the 16 nm red shift and 42% hypochromicity observed with $Rh(phen)_2phi^{3+}$,[6] and thus indicates that a general similarity exists between mode of DNA binding of these new $Rh(phi)^{3+}$ complexes and the parent $Rh(phen)_2phi^{3+}$. Although Λ- and Δ-$Rh(en)_2phi^{3+}$ exhibit similar hypochromic and red shift effects, this UV-Vis assay would not be expected to

detect enantioselective interactions between the metal complexes and calf thymus DNA due to the strong affinity of both enantiomers for calf thymus DNA, which contains strong binding sites for both Λ- and Δ-$Rh(en)_2phi^{3+}$. Further, the small size of Λ- and Δ-$Rh(en)_2phi^{3+}$ relative to the helical groove width would eliminate the enantioselectivity favoring Δ-enantiomers commonly observed with tris(polypridyl) metal complexes.

An important feature of $Rh(en)_2phi^{3+}$ was that the smaller ancillary ligands were designed to impart less shape selectivity to the complex, in order to better isolate and explore the importance of hydrogen bonding and van der Waals contacts to sequence selective DNA binding. Although $Rh(N_4)phi^{3+}$ complexes display a high degree of similarity to $Rh(phen)_2phi^{3+}$ in their interaction with calf thymus DNA, there is a pronounced difference in their binding to RNA. The result that $Rh(N_4)phi^{3+}$ complexes bind an RNA polymer with similar bulk affinity to a DNA polymer, indicates that the small complexes are unable to sense the differences in size, shape and groove depth between the A-form and B-form helices. In contrast, the larger (more shape selective) $Rh(phen)_2phi^{3+}$ binds an RNA duplex with a lower affinity than a DNA duplex, likely due to the poor fit of the bulky ancillary phenanthroline ligands and the narrow and deep major groove of A-form RNA. Thus it appears that, as judged by simple UV-Vis titrations, the polyamine $Rh(phi)^{3+}$ complexes display less shape selectivity than $Rh(phen)_2phi^{3+}$.

The degree of unwinding of the DNA helix upon intercalation is a critical aspect of any intercalative model of drug : DNA interaction, as it relates to the stacking between the DNA bases and the intercalating ligand.[16,17] The degree of unwinding by $Rh(en)_2phi^{3+}$ is further important since it affects the spatial position of the DNA moieties which will engage in hydrogen bonds and van der Waals contacts with the ethylenediamine ligands. The current results clearly suggest that the polyamine $Rh(phi)^{3+}$ complexes are capable of unwinding plasmid DNA to a similar degree as $Rh(phen)_2phi^{3+}$, approximately ~20° per bound molecule.

In total, while the observations of hypochromicity, red shifts and plasmid unwinding are by no means conclusive proof of intercalation by $Rh(en)_2phi^{3+}$ and its derivatives, the present results do testify to a strong electronic interaction between the phi ligand and DNA, as well as a significant unwinding of DNA upon binding. These assays are further useful in their favorable comparison of the novel polyamine $Rh(phi)^{3+}$ complexes with the established metallointercalator $Rh(phen)_2phi^{3+}$.

2.4.3. The mechanism of DNA photocleavage by $Rh(en)_2phi^{3+}$.

In terms of both end products and stoichiometry, the photocleavage of DNA by $Rh(en)_2phi^{3+}$ is consistent with a mechanism analogous to that described for $Rh(phen)_2phi^{3+}$. As illustrated in Scheme 2.1, this photochemical generation of a phi centered cation radical which is energetically and stereospecifically competent to abstract the C3'-H atom from the major groove, causing degradation of the deoxyribose sugar by either an O_2-dependent or O_2-independent pathway, and ultimately leading to the direct scission of the DNA strand.

The observation of the release of free nucleic acid base in photocleavage of DNA by $Rh(en)_2phi^{3+}$ and its derivatives establishes that, as with $Rh(phen)_2phi^{3+}$, the target for photoactivated damage of DNA by phi complexes of Rh(III) is the deoxyribose sugar moiety. However, it was not possible to isolate and identify any modified base species (e.g. base propenoic acids) in photocleavage by $Rh(en)_2phi^{3+}$, as had been observed with $Rh(phi)_2bpy^{3+}$.[6] Since several pathways of DNA cleavage following H-atom abstraction involve the release of free nucleic acid bases,[18,19] further interpretation of free base release in mechanistic detail is prohibited.

However, any strand cleavage of DNA leads to the production of two new termini, and the nature of these two termini are highly informative as to the site of the initial DNA lesion.[6,18,19] The production of 5'-phosphate termini is common to several DNA lesions, and thus is not a potentially discriminating factor in determining the initial site of H atom abstraction. In contrast, the production of several non-phosphate 3'-termini may be correlated with initial H-atom abstraction from the C1', C3', C4', and C5' positions of the deoxyribose sugar. These modified termini all result from the inclusion of from 1 to 3 carbons of the damaged sugar into the newly formed 3'-terminus.

Scheme 2.1. Mechanism of DNA degradation following C3'-H atom abstraction. Species in solid boxes have been identified in cleavage by both $Rh(en)_2phi^{3+}$ and $Rh(phen)_2phi^{3+}$, while the dashed box indicates products identified in cleavage by $Rh(phen)_2phi^{3+}$, but not $Rh(en)_2phi^{3+}$. Modified from Reference 6.

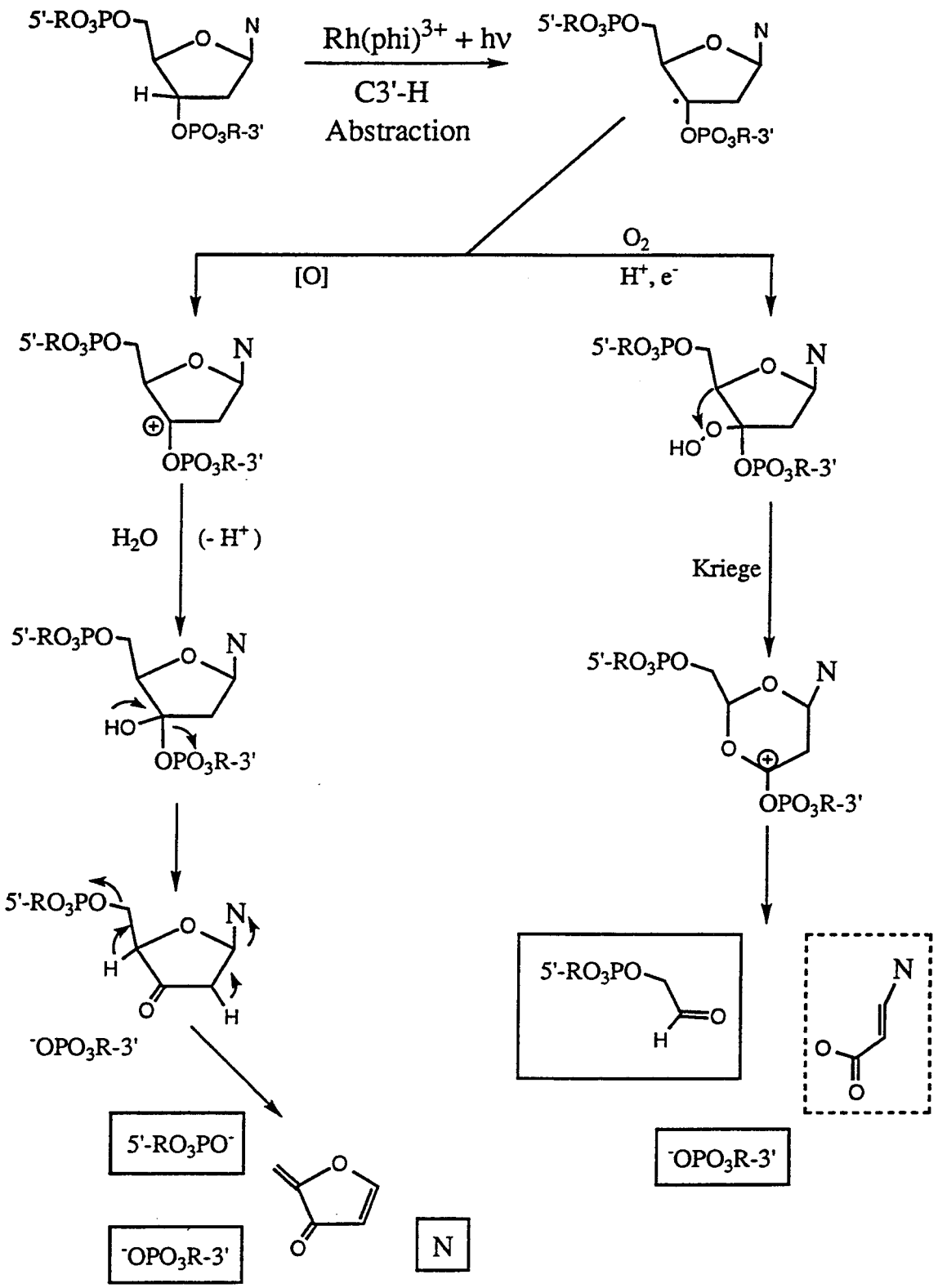
5'-RO3PO
Rh(phi)3+ + hν
C3'-H
Abstraction
OPO3R-3'
O2
[O]
H+, e-
H2O
(- H+)
Kriege
HO
-OPO3R-3'
5'-RO3PO-
N

In photocleavage of 5'- [^{32}P] end-labeled d(GAGTGCACTC)$_2$ by the enantiomers of Rh(en)$_2$phi^{3+}, there is clear production of secondary, non- phosphate termini, in addition the predominant 3'-phosphate termini. Cleavage of the oligonucleotide duplex by Rh(phen)$_2$phi^{3+} yields the same secondary product, which has been assigned as the 3'-phosphoglycaldehyde terminus, produced following C3'-H abstraction by Rh(phen)$_2$phi^{3+} and subsequent degradation of the deoxyribose sugar along the O_2 dependent pathway.[6] The production of 3' phosphoglycaldehyde termini by the enantiomers of Rh(en)$_2$phi^{3+} indicates that the cleavage mechanism established for Rh(phen)$_2$phi^{3+} may also arise with the polyamine Rh(phi)$^{3+}$ complexes.

It was possible to examine directly the stoichiometry of the photocleavage reaction by comparing the amounts of Rh(en)$_2$phi^{3+} photoanation, free base release, and DNA strand cleavage under identical conditions. Interestingly, there appears to be little or no non-productive photoreaction of Rh(en)$_2$phi^{3+} since, in support of the proposed mechanism, the cleavage of DNA by Rh(en)$_2$phi^{3+} is characterized by a stoichiometric relationship between the release of free base, strand scission and loss of phi absorbance. A stoichiometric relationship between the DNA side and the metal complex side of the photocleavage reaction is also supported by the similarity of the quantum yields for photoanation and free base release of Rh(en)$_2$phi^{3+} (see below). This result leads to the important conclusion that a single Rh(phi)$^{3+}$ complex cleaves the DNA a single time DNA and not in any catalytic fashion. This conclusion is further supported in Chapter 3 by cleavage of a number of DNA substrates by Rh(en)$_2$phi^{3+}, where there is no evidence for cleavage by a diffusible species.

Since Rh(en)$_2$phi^{3+}, as well as derivatives Rh(NH$_3$)$_4$phi^{3+}, Rh(cyclen)phi^{3+} and Rh(S4-cyclen)phi^{3+}, retained the aromatic phi ligand and the Rh(III) center of Rh(phen)$_2$phi^{3+}, it was not surprising that they also maintained the characteristics of strong intercalative binding and DNA photocleavage. However, the effect of the variation of ancillary ligand upon cleavage efficiency was of interest both in practical

terms, as well in terms of what any effect would reveal about the photochemistry of the $Rh(phi)^{3+}$ moiety. In practice, $Rh(phen)_2phi^{3+}$ displays a much greater absorbance than $Rh(en)_2phi^{3+}$ at the irradiation wavlength used in photocleavage studies (e.g. 18,500 $M^{-1}cm^{-1}$ vs. 3,000 $M^{-1}cm^{-1}$ at 313 nm). However, the quantum efficiency (which corrects for the relative absorbances at 313 nm) for free base release of the polyamine $Rh(phi)^{3+}$ complexes are an order of magnitude less than the value for $Rh(phen)_2phi^{3+}$. This lower efficiency may be understood in light of the pH dependence of $Rh(phi)^{3+}$ complex photochemistry illustrated in Table 2.8.

Table 2.8. Comparison of quantum yields for photoanation and free base release.

		Photoanation [a] (x 10^4)			Free base release (x 10^4)
$Rh(phi)^{3+}$ Complex	pKa	$\Phi_{325\ nm}$ pH 4	$\Phi_{325\ nm}$ pH 7	$\Phi_{325\ nm}$ pH 10	$\Phi_{313\ nm}$ pH 7
$Rh(NH_3)_4phi^{3+}$	9.2	--	0.3	6.4	0.6
$Rh(en)_2phi^{3+}$	9.1	--	0.3	10	1.0
$Rh(cyclen)phi^{3+}$	9.0	--	0.7	2.1	1.2
$Rh(S_4\text{-cyclen})phi^{3+}$	4.7	0.4	2.1	--	0.3
$Rh(phen)_2phi^{3+}$	6.2	0.04	5.2	--	12 [b]

a. Data taken from Ref. 11a. b. Data taken from Ref. 6.

The photocleavage efficiencies of $Rh(phi)^{3+}$ are remarkably similar to their photochemical efficiencies in the absence of DNA at pH 7.0 . Not only does this comparison clearly link the reactions of photoanation and DNA photocleavage, it argues that $Rh(en)_2phi^{3+}$ does not cleave DNA as efficiently as $Rh(phen)_2phi^{3+}$ mainly because it is significantly more protonated at pH 7.0. This in turn supports the existence of a phi

cation radical generated by a ligand to metal charge transfer (LMCT) since a deprotonated phi ligand would be more likely to engage in a LMCT. Thus, instead of suggesting a fundamental difference in the photochemistry of $Rh(phen)_2phi^{3+}$ and $Rh(en)_2phi^{3+}$, the lower efficiency of $Rh(N_4)phi^{3+}$ complexes provides support for the phi cation radical proposed in the DNA cleavage mechanism of both complexes.

Finally, investigation of the DNA cleavage mechanism of $Rh(en)_2phi^{3+}$ has once again shown that the chemical details DNA cleavage are inexorably tied to the intimacies and intricacies of DNA binding. In photocleavage of the same oligonucleotide duplex by $Rh(en)_2phi^{3+}$ and $Rh(phen)_2phi^{3+}$, the greater production of the 3'- phosphoglycaldehyde terminus as a percentage of total cleavage by $Rh(en)_2phi^{3+}$ may be attributed to an increased accessibility of O_2 to the initial lesion afforded by the smaller size of $Rh(en)_2phi^{3+}$. A similar relationship was noted in the comparison of $Rh(phen)_2phi^{3+}$ and $Rh(phi)_2bpy^{3+}$, where the greater production of 3'-phosphoglycaldehyde termini by $Rh(phi)_2bpy^{3+}$ correlated well with the way in which the shapes of these complexes controlled access of O_2 to the initial C3'-lesion. The difference in shape between these two complexes allowed more O_2 to reach the initial lesion for $Rh(phi)_2bpy^{3+}$, and ultimately led to a greater partitioning of strand cleavage through the O_2 dependent pathway.

In light of the small size of the ancillary ethylenediamine ligands, (not likely to affect O_2 access to the damaged sugar), it might be expected that $Rh(en)_2phi^{3+}$ would also produce more O_2 dependent cleavage than $Rh(phen)_2phi^{3+}$. The increased percentage of cleavage by the O_2 dependent pathway is therefore a reflection of the smaller size of ethylenediamine relative to phenanthroline ligands. Once again it appears that the chemistry of DNA cleavage is strongly affected by the structural details of DNA binding.

2.5. Conclusions.

The results presented in this chapter establish the basic elements of DNA binding and photocleavage by the enantiomers of $Rh(en)_2phi^{3+}$, as well the derivatives $Rh(NH_3)_4phi^{3+}$, $Rh(cyclen)phi^{3+}$ and $Rh(S_4\text{-cyclen})phi^{3+}$. These molecules bind to DNA strongly via intercalation of the aromatic phi ligand into the stacked bases of the DNA helix, and this intercalation is marked by a pronounced unwinding of the DNA helix. Importantly, $Rh(en)_2phi^{3+}$ appears to be less shape selective than $Rh(phen)_2phi^{3+}$, as judged by its similar affinity for both a DNA and RNA polymer.

Product analyses and relative photoefficiencies suggest that the cleavage of DNA by $Rh(en)_2phi^{3+}$ proceeds by a mechanism analogous to that described for $Rh(phen)_2phi^{3+}$. Direct abstraction of the C3'-H atom by a phi centered cation radical species is followed by degradation of the sugar phosphate backbone to afford direct strand scission of DNA at the site of binding. Due to the higher pK_a values of the immine N atoms in $Rh(en)_2phi^{3+}$, this cleavage (as well as the photoanation in the absence of DNA) proceeds with a lower efficiency than $Rh(phen)_2phi^{3+}$. Importantly, a 1:1:1 stoichiometry is observed between the loss of phi absorbance, the release of free base, and the cleavage of DNA strands. The observation of cleavage chemistry at the C3'- position of the deoxyribose ring argues for a major groove orientation, and this will be supported in Chapter 3.

The enantiomers of $Rh(en)_2phi^{3+}$ therefore are anchored to DNA by the intercalation of the phi ligand, and the ancillary ethylenediamine ligands well positioned to engage in hydrogen bonding and van der Waals contacts with DNA. We may examine how these weak non-bonded contacts contribute to the sequence selective binding and photocleavage of DNA by $Rh(en)_2phi^{3+}$.

References and Footnotes

1. (a) Pyle, A. M. ; Barton, J. K. *Prog. Inorg. Chem.* **1990**, *38*, 413. (b) Moser, H. E.; Dervan, P. B. *Science* **1987**, *238*, 645. (c) Dervan, P. B. *Science* **1986**, *232*, 464. (d) Nicholaou, K. C. ; Dai, W. M. ; Tsay, S. C. ; Estevez, V. A. ; Wrasidlo, W. *Science* **1992**, *256*, 1172. (e) Zein, N.; Sinham, McGahren, W. J.; Ellestad, G. A. *Science* **1988**, *240*, 1198. (f) Hecht, S. M. *Acc. Chem. Res.* **1986**, *19*, 383. (g) Sigman, D. S. *Science* **1987**, *217*, 1197.

2. (a) Pabo, C. O.; Sauer, R. T. *Ann. Rev. Biochem.* **1992**, *61*, 1053. (b) Steitz, T.A. *Q. Rev. Biophys.* **1990**, *23*, 205. (c) Desjarlais, J. R.; Berg, J. M. *Proc. Natl. Acad. Sci. U.S.A.* **1992**, *89*, 7345.

3. (a) Kim, Y.; Geiger, S.H.; Hahn, S., Sigler, P.S. *Nature* **365**, *512*, 1993. (b) Kim, J.L.; Nikolov, D.B.; Burley, S.K. *Nature* **1993**, *365*, 520. (c) Schulz, S.C.; Shields, G.C.; Steitz, T.A. *Science* **1991** *253*, 1001. (d) Somers, W.S.; Phillips, S.E.V. *Nature* **1992**, *359*, 387. (e) Jordan, S.R.; Pabo, C.O. *Science* **1988**, *242*, 893. (f) Anderson, J.E.; Ptashne, M.; Harrison, S.C. *Nature* **1987**, *326*, 846.

4. (a) Pelton, J.G.; Wemmer, D.E. *Proc. Natl Acad. Sci. U.S.A.* **1989**, *86*, 5723. (b) Wu, W.; Vanderwall, D.E.; Stubbe, J.A.; Kozarich, J.W.; Turner, C.W. *J. Amer. Chem. Soc.* **1995**, *116*, 10843. (c) Gao, X.; Patel, D.J. *Biochem.* **1989**, *28*, 751. (d) Searle, M.S. *Prog. NMR Spec.* **1993**, *25*, 403.

5. (a) Chow, C. S.; Barton, J. K. *Meth. Enzym.* **1992**, *212*, 219. (b) Barton, J. K. *Science* **1986**, *233*, 727. (c) Kirshenbaum, M. R.; Tribolet, R.; Barton, J. K., *Nuc. Acids Res.* **1988**, *16*, 7943. (d) Mei, H. Y.; Barton, J. K. *Proc. Natl Acad. Sci. U.S.A.* **1988**, *85*, 1339. (e) Chow, C. S.; Barton, J. K. *J. Amer. Chem. Soc.* **1990**, *112*, 2839.

6. (a) Pyle, A. M.; Long, E. C.; Barton, J. K. *J. Amer. Chem. Soc.* **1989**, *111*, 4520. (b) Sitlani, A.; Long, E. C.; Pyle, A. M.; Barton, J. K. *J. Amer. Chem. Soc.* **1992**, *114*, 2303. (c) Pyle, A. M.; Morii, T.; Barton, J. K. *J. Amer. Chem. Soc.* **1990**, *112*,

9432 - 9434. (d) Chow, C. S.; Behlen, E. S.; Uhlenbeck, O. C.; Barton, J. K. *Biochem.* **1992**, *31*, 972.

7. (a) Sitlani, A.S.; Dupureur, C.M.; Barton, J.K. *J. Am. Chem. Soc.* **1993**, *115*, 12589. (b) Terbreuggen, R.H.; Barton, J.K. submitted for publication.
8. Maniatis, T.; Fritsch, E. F.; Sambrook, J. *Molecular Cloning: A Laboratory Manual,* 2nd ed.; Cold Spring Harbor Laboratory, 1989.
9. Schaefer, W. P.; Krotz, A. H.; Kuo, L.Y.; Shields, T. P.; Barton, J. K. *Acta Cryst.* **1992**, *C48*, 2071.
10. Krotz, A.H.; Kuo, L.Y.; Shields, T.P.; Barton, J.K. *J. Am. Chem Soc.* **1993** , *115*, 3877.
11. (a) Krotz, A.H.; Kuo, L.Y.; Barton, J.K. *Inorg. Chem.* **1993**, *32*, 5963. (b) Krotz, A.H.; Barton, J.K. *Inorg. Chem.* **1994**, *33*, 1940.
12. (a) Galbsol, F. *Inorg. Synth.* **1970**, *12*, 269. (b) Bosnich, B. *Acc. Chem. Res.* **1969**, *2*, 266.
13. Calvert, J.G.; Pitts, J.N. *Photochemistry*, John Wiley and Sons, New York, 1967.
14. Saenger, W. *Principles of Nucleic Acid Structure*, Springer-Verlag, 1984.
15. Yoshikawa, Y.; Yamasaki, K. *Coord. Chem. Rev.* **1979**, *28*, 205.
16. Lerman, L.S. *J. Mol. Biol.* **1961**, *3*, 18.
17. (a) Wang, A.H.J.; Nathans, J.; van der Marel, G.; van Boom, J.H.; Rich, A. *Nature* **1978**, *276*, 471.
18. N_{ax} and Neq refer to the ligated N atoms either in axial or equatorial positions relative to the plane of the phi ligand.
19. Subbe, J.; Kozarich, J. *Chem. Rev.* **1987**, *87*, 1107.
20. Dedon, P.C.; Goldberg, I.H. *Chem. Res. Toxicol.* **1992**, *5*, 311.
21. The exclusive production of 5' - phosphate termini is consistently seen in cleavage by the enantiomers of $Rh(en)_2phi^{3+}$ over a wide range of oligonucleotide substrates. (Data shown in Chapter 3)

Chapter 3. Sequence selective DNA cleavage by the enantiomers of $Rh(en)_2phi^{3+}$: Recognition through hydrogen bonding and van der Waals contacts in the major groove.†

3.1. Introduction.

The design of synthetic complexes capable of the sequence specific recognition of DNA is a topic of tremendous importance to biochemistry today.[1-3] Such complexes not only possess tremendous pharmaceutical potential, but also allow us to probe the fundamental question of how DNA recognition proceeds in nature. In the Barton group, the power and versatility of inorganic chemistry is applied to understanding those factors which contribute to the sequence specific recognition of DNA by proteins.[4-11] The importance of shape selectivity has been established in our investigations of DNA recognition by substitutionally inert transition metal complexes comprising a vast array of well-defined shapes.[5-8] The development of phenanthrenequinone diimine (phi) complexes of Rh(III), which bind strongly to DNA by intercalation from the major groove has allowed us to explore shape selective recognition of DNA in greater detail,[6] as well as to develop complexes capable of mimicking protein : DNA interactions.[8]

In Chapter 2, the sequence selective photocleavage of DNA by enantiomers of $Rh(en)_2phi^{3+}$ is examined. Although they display a low level of sequence selectivity due to their small size, the enantiomers of $Rh(en)_2phi^{3+}$ provide a unique system in which to explore discrete elements of molecular recognition within the major groove of DNA. Once anchored in the major groove by metallointercalation, the enantiomers of $Rh(en)_2phi^{3+}$ position coordinated amines for potential hydrogen bonding to the DNA helix and methylene groups for positive van der Waals contacts with the DNA bases. We have examined specifically how these enantiomers discriminate among DNA sequences through this combination of hydrogen bonding and van der Waals interactions.

The importance of hydrogen bonding and van der Waals contacts to the sequence selective binding and cleavage of DNA by $Rh(en)_2phi^{3+}$ will be probed with two complementary techniques. First, the photocleavage selectivities of Λ- and Δ-$Rh(en)_2phi^{3+}$ will be compared to a series of $Rh(N_4)phi^{3+}$ complexes (N_4 = $(NH_3)_4$, $(en)_2$, cyclen, S_4-cyclen). Chapter 2 established that the members of this family all bind to DNA through the intercalation of the aromatic phi ligand and cleave DNA by the same mechanism upon irradiation with near-UV light. Thus the changes in DNA recognition properties between several $Rh(phi)^{3+}$ complexes containing saturated amines and a thioether as ancillary ligands may be rationalized in terms of variations in the type and orientation of their ancillary ligands. These simple metallointercalators therefore offer a route to examine systematically the contributions of hydrogen bonding and van der Waals contacts to site specificity, since they differ only in the kind and symmetry of functional group placement with respect to the DNA groove.

Secondly, the DNA moieties involved in hydrogen bonding and van der Waals contacts with the enantiomers of $Rh(en)_2phi^{3+}$ will be pinpointed through photocleavage of oligonucleotides containing modified or unnatural bases. Photocleavage of oligonucleotides containing O^6methylguanine and deoxyuracil substitutions for guanine and thymine residues will probe the effect of the addition or removal of a single methyl group in the major groove of DNA. The results not only firmly place the enantiomers of $Rh(en)_2phi^{3+}$ in the major groove of DNA, but show that both hydrogen bonding and positive van der Waals interactions are crucial elements in determining the sequence specificity of these complexes. The elucidation of these contacts makes it possible to utilize a modular approach for the recognition of larger DNA sequences based on these simple hydrogen bonding and van der Waals contacts.[11]

† Adapted in part from Krotz, A.K.; Kuo, L.Y.; Shields, T.P.; and Barton, J.K. *J.Am. Chem. Soc.*, **1993**, *115*, 3877.

3.2. Experimental

Materials: Calf thymus DNA was purchased from Pharmacia LKB and plasmid pUC18 was purchased from Gibco BRL. Terminal deoxy Transferase (TdT), Klenow fragment and Polynucleotide Kinase (PNK) were purchased from Boehringer Mannheim as parts of either their 3'- and 5'-end labeling kits. γ-^{32}P-dATP and α-^{32}P-dATP was from Dupont NEN and α-^{32}P ddATP was from Amersham. Stock solutions of dGTP, dCTP and dTTP were from Boehringer Mannheim. Oligonucleotide DNA was prepared on an ABI Model 392 DNA synthesizer using phosphoramidite chemistry and purified by reversed phase HPLC. Phosphoramidites, solid supports and reagents for solid phase DNA synthesis were from ABI (Foster City, CA) and Glen Research (Sterling, VA).

Λ- and Δ- Rh(en)$_2$phi^{3+} were prepared as previously described.[9] Rh(cyclen)phi^{3+}, Rh(S$_4$-cyclen)phi^{3+} and Rh(NH$_3$)$_4$phi^{3+} were prepared by Dr. Achim Krotz.[10] Λ- and Δ-Rh(phen)$_2$phi^{3+} were graciously provided by Dr. Cindy Dupureur. All metal complexes were quantitated by UV-Vis spectroscopy using published extinction coefficients. H_2O was purified with a Millipore Milli-Q system, and was $\geq$ 18 MOhms resistance. All other enzymes, buffers, salts and sequencing reagents were obtained from commercial sources and were of the highest purity available.

Instrumentation: UV-Vis spectra were recorded either on a Hewlett Packard 8452A Diode Array Spectrophotometer or on a Cary 2200 Spectrophotometer stored with Spectrocalc program. Circular dichroism spectra were recorded on a JASCO J500A spectrometer. All spectra were recorded in 1 cm path length quartz cells.

The light source used in photocleavage experiments was a Oriel Model 6140 1000W Hg/Xe lamp equipped with a Model 6123 IR filter, and either a Model 77250 (1/8 m) or Model 77200 (1/4 m) monochromator. A 305 nm cutoff filter was utilized in photocleavage studies with the 1/8 m monochromator to avoid DNA damage by extraneous UV light. Alternatively a 325 nm Liconix Model 4240 NB He-Cd laser was used as a light source for photocleavage.

High Performance Liquid Chromatography (HPLC) was performed on a Waters 600E Multi Solvent Delivery System and monitored with either a Model 996 diode array detector (processed with Waters Millennium software) or with a Model 484 tunable wavelength detector. Phosphorimagery was performed on a Molecular Dynamics Phosphorimager and images were processed using Image Quant software.

Photocleavage of Oligonucleotide DNA : Oligonucleotide DNA was either 5' end-labeled with γ-^{32}P-ATP and polynucleotide kinase, or 3' end-labeled with α-^{32}P-ddATP and terminal deoxytransferase using standard protocols.[12,13] Labeled oligonucleotides were purified on 10% polyacrylamide prep gels (8 mM thick, full size, native or denaturing). End-labeled DNA was isolated from gel pieces by electroelution in a Schleicher and Schuell Elutrap chamber (250 volts, 30 min.), stored frozen in buffered solution (pH 7.0, 0.3X TBE) and used within 7-14 days of isolation.

An annealed DNA stock solution was prepared in 1.7 mL pre-siliconized eppendorf tubes by mixing an equivalent amount of the two strands with a small amount of labeled strand (~100-150K cpm / sample) and heating at 90° C for 4 min, followed by slow cooling to room temperature over at least 45 minutes. The amounts of DNA and buffer added were such that when a 15 µL aliquot of the annealed DNA stock solution was extracted and diluted to a final volume of 20 µL with the appropriate Rh(phi)$^{3+}$ complex, the 20 µL solution would contain 1x buffer, as well as the desired metal and DNA concentrations. Unless otherwise noted, the conditions for examining the sequence selectivity of oligonucleotide cleavage by enantiomers of Rh(en)$_2$phi^{3+} were 100 µM base pairs DNA, 5 µM Rh(phi)$^{3+}$ complex, pH 7.0, 10 mM NaCacodylate, 40 mM NaCl, irradiation for 15 minutes at 313 nm. In order to accurately sample cleavage by the metal complex, a small amount of 3'-[^{32}P] end-labeled oligomer (~120-150,000 cpm / sample) was annealed with a large excess of cold duplex.

20 µL samples were irradiated by opening the cap and placing the tube such that the back end resided at the focal point of the Hg-Xe lamp. Alternatively, the opened

tubes were placed in the beam of the 325 nm laser. Photocleavage reactions were quenched by removal from light, although typically 1.5 μL of a 5 mM base pairs calf thymus DNA solution was added to each photocleavage sample in order to allow more facile denaturation of the strands upon electrophoresis by competing with the labeled oligomer for the metal complex. After irradiation, 3-5 μL (20-30,000 cpm) of the samples were removed and dried, then resuspended in loading dye to a concentration of 10,000 cpm / μL dye. Samples were heated at 90° C for 4.5 minutes, then directly electrophoresed on 20% denaturing polyacrylamide gels at 2500-2800 volts for 3.5 hours.

Photocleavage of restriction fragments : The 140- and 180- base pair EcoRI / PvuII restriction fragments of pUC18 were either 3' end-labeled with Klenow fragment and α-^{32}P-dATP, or 5' end-labeled with polynucleotide kinase and γ-^{32}P dATP as previously described.[12] Labeled fragments were purified by electrophoresis on small, 0.8 mM thick, 8% native polyacrylamide gels at 1000 volts for 2 hours. The two fragments were excised from the gel and isolated by electroelution at 250 volts for 1.5 hours. Samples were divided into 1.5 million cpm sections, ethanol precipitated and stored at -20° C.

DNA stock solutions were prepared in 1.7 mL pre-siliconized eppendorf tubes which contained calf thymus DNA, 5'- or 3'- end-labeled restriction fragment (~60 -100,000 cpm / sample), water and buffer. The amounts of calf thymus DNA and buffer added were such that when a 15 μL aliquot of the DNA stock solution was extracted and diluted to a final volume of 20 μL with the appropriate Rh(phi)$^{3+}$ complex, the 20 μL solution would contain 1x buffer, as well as the desired metal and DNA concentrations. Samples were irradiated as described above, then precipitated by the addition of 1.5 μL of a 5 mM base pairs calf thymus DNA solution, 15 μL 5 M NH_4OAc, and 400 μL EtOH. Samples were placed on dry ice for 30 minutes, then spun down and the supernatant removed. The DNA pellet was rinsed with 400 μL of 80% EtOH and then dried on a Savant rotary speed-vac.

Dried samples were resuspended in loading dye such that the solution was ~10K cpm / μL dye. Samples were heated for 4.5 minutes at 90° C, then 2-3 μL aliquots were separated by electrophoresis on 8% denaturing polyacrylamide gels for 2 hours at 2000 volts. Gels were transferred to paper and dried for 45 min on a Biorad Model 583 gel dryer.

Quantification of Cleavage results via phosphorimagery: Both 20% and 8% denaturing polyacrylamide gels were quantitated with a Molecular Dynamics PhosphorImager. Gels were exposed to photostimulable storage phosphor screens for 12-18 hours, and developed using the ImageQuant program. The fraction cleavage at a base n is defined by equation 1:

$$I_n = \left(\frac{I_{n,raw} - I_{bkgd}}{I_{tot} - I_{tot,\,bkgd}} \right) - \left(\frac{I_{lc,raw} - I_{bkgd}}{I_{lc,\,tot} - I_{lc,bkgd}} \right) , \qquad (1)$$

where I_n is the fraction of DNA strands cleaved at base n. In equation (1), $I_{n,raw}$ is the integrated volume intensity of the photocleavage band n, $I_{n,lc}$ is the volume intensity for band n in the light control, and I_{bkgd} is the intensity measured for the same area placed on an ostensibly blank part of the image. Likewise, I_{tot} an $I_{lc,\,tot}$ are the total volume intensities in either a cleavage or light control lane, including individual bands as well as uncut oligonucleotide, and $I_{tot,bkgd}$ is the corresponding correction for the larger background intensity of the rectangle used to quantitate total loading in a lane. Therefore, photocleavage produced by a $Rh(phi)^{3+}$ complex is characterized by an intensity I_n which is corrected for background, loading errors, as well as light control damage.

Determination of site specific binding constants: Sequence specific binding constants were determined by a modification of the methods developed by Singleton and Dervan.[14a] Photocleavage of a [^{32}P] end-labeled restriction fragment was performed over a gradient of metal concentrations spanning four orders of magnitude (0.005 μM --> 10 μM), and the cleavage intensities at the resolved bases in each lane were quantitated as described above. Typically, 80 bases were well resolved under the conditions used in

these experiments. An average binding constant (K_b) for the Rh(phi)$^{3+}$ complex over the entire DNA fragment was determined by fitting a plot of total cleavage intensity in a lane (the numeric sum of I_n values for all resolved bases) versus total metal concentration ($[Rh]_{tot}$) to the following form of the Langmuir binding isotherm :

$$\sum I_n = I_{total}\left(\frac{\overline{K}_b \bullet [Rh]_{tot}}{1 + \overline{K}_b \bullet [Rh]_{tot}}\right) , \qquad (2)$$

where ΣI_n is the sum of the corrected intensities over all the resolved bases at a concentration Rh_{tot}. The two adjustable parameters determined by the least squares fit of the data were I_{total}, which is the theoretical maximal cleavage of the target DNA, and K_b, which is the average binding constant of the complex over the restriction fragment. Average affinity constants determined in this manner were wholly consistent with values predicted from the UV-Vis titrations described in Chapter Two. This average K_b value was used to estimate a $[Rh]_{free}$ value for each $[Rh]_{tot}$ by solving the quadratic expression :

$$\overline{K}_b = \frac{x}{([Rh]_{tot} - x)([DNA]_{tot} - x)} , \qquad (3)$$

where x = [Rh:DNA] complex, $[DNA]_{tot}$ = the concentration of DNA sites,[15] and $[Rh]_{free} = [Rh]_{tot} - x$. These $[Rh]_{free}$ values were then used to find sequence specific binding constants ($K_{b,n}$) for all sites n along the restriction fragment. Corrected cleavage intensity at an individual base ($I_{n,Rh}$) was plotted against the $[Rh]_{free}$, and the plot was again fit to a Langmuir binding isotherm (Equation 4) :

$$I_n = I_{sat,n}\left(\frac{K_{b,n} \bullet [Rh]_{free}}{1 + K_{b,n} \bullet [Rh]_{free}}\right) . \qquad (4)$$

Molecular Modeling. All molecular modeling was performed with the InsightII program (Biosym Technologies, La Jolla, CA) on a Silicon Graphics Iris Indigo Workstation. The coordinates of Rh(en)$_2$phi^{3+}, Rh(NH$_3$)$_4$phi^{3+}, Rh(cyclen)phi^{3+} and Rh(S$_4$-cyclen)phi^{3+} were taken from their crystal structures.[9a,10] Models of DNA intercalation sites were either based on the crystal structure of the metallointercator

(terpyridyl)(ethanethiolato)Pt(II) bound to $d(CG)_2$,[16] or created in the Biopolymer subroutine of InsightII.[17]

3.3. Results

3.3.1. Comparison of the sequence selectivity of several $Rh(phi)^{3+}$ complexes containing ancillary saturated amines and a thioether ligand.

In order to define the basic principles underlying the recognition of DNA by the enantiomers of $Rh(en)_2phi^{3+}$, photocleavage by Λ- and Δ-$Rh(en)_2phi^{3+}$ was compared to several other $Rh(phi)^{3+}$ complexes which differed only in the type and placement of ancillary ligands. Comparison of the recognition patterns of these complexes offers a means to identify the structural elements of $Rh(en)_2phi^{3+}$ enantiomers responsible for sequence selective recognition of DNA. For the substrate in this study, an oligonucleotide duplex (Y_1:Y_2) was designed to contain, on each strand, all ten possible base steps as well as their complements. This oligonucleotide therefore presented a near-random DNA sequence with which to assay the general recognition properties of the enantiomers of $Rh(en)_2phi^{3+}$ and their derivatives.

Photocleavage of the duplex Y_1:Y_2 by Λ- and Δ-$Rh(en)_2phi^{3+}$, as well as the complexes $Rh(NH_3)_4phi^{3+}$, $Rh(cyclen)phi^{3+}$ and $Rh(S_4\text{-cyclen})phi^{3+}$, is shown in Figure 3.2 for the case where duplex cleavage is sampled by 3'- [^{32}P] end-labeled strand Y_1. Cleavage of the duplex by Δ-$Rh(en)_2phi^{3+}$ is very specific, with strong sites of cleavage concentrated at G,C base pairs, e.g. at bases $C_9G_{10}G_{11}G_{12}$; $G_{16}C_{17}$; $G_{20}C_{20}C_{21}$; and $C_{27}G_{28}$ of Figure 3.2. When strand Y_2 is labeled, (data not shown) strong cleavage is found in the complementary G,C regions.

Figure 3.1. The $Rh(N_4)phi^{3+}$ complexes used in this study.

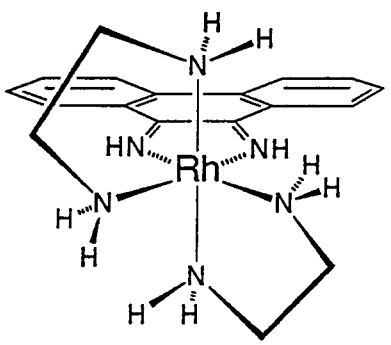

Λ-$Rh(en)_2phi^{3+}$

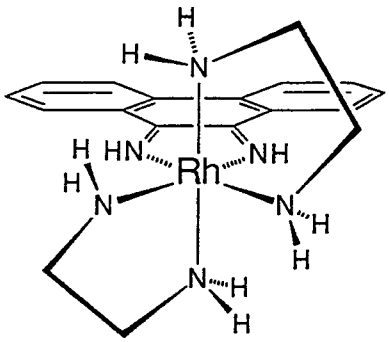

Δ-$Rh(en)_2phi^{3+}$

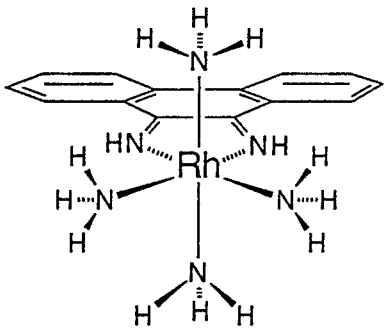

$Rh(NH_3)_4phi^{3+}$

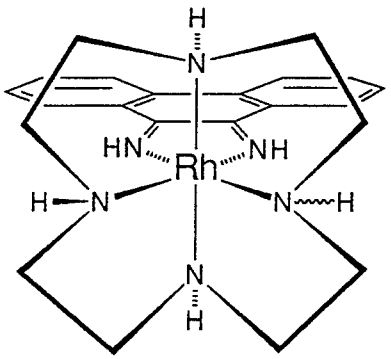

$Rh(cyclen)phi^{3+}$

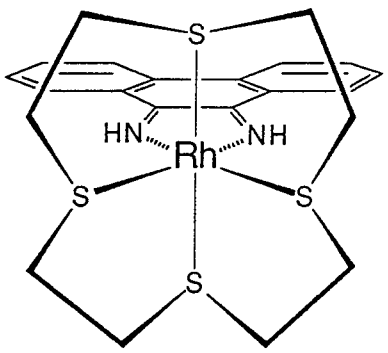

$Rh(S_4\text{-cyclen})phi^{3+}$

Recognition of Y_1:Y_2 by $Rh(NH_3)_4phi^{3+}$, which lacks the potential for making extensive van der Waals contacts with DNA, closely parallels the sequence selectivity of Δ-$Rh(en)_2phi^{3+}$ (compare lanes 4 and 5 of Figure 3.2). In fact there are no sites on Y_1:Y_2 which are cleaved by Δ-$Rh(en)_2phi^{3+}$ and not also recognized by $Rh(NH_3)_4phi^{3+}$, indicating that axial amine ligands direct recognition of G,C regions, while the Δ-orientation of the methylene groups provides no recognition. Photocleavage by $Rh(cyclen)phi^{3+}$, which contains axial amine ligands as well as methylene groups similar to both Λ- and Δ-$Rh(en)_2phi^{3+}$, again shows strong cleavage in all G,C regions of the duplex, in addition to weaker cleavage at bases $T_{13}T_{14}$ and $A_{24}A_{25}$ of Y_1.

In contrast to the sequence specific cleavage of the Δ-enantiomer, Λ-$Rh(en)_2phi^{3+}$ produces cleavage at nearly every residue along the duplex, indicating a low degree of selectivity. Thus, while Λ-$Rh(en)_2phi^{3+}$ also recognizes G,C regions of the oligomer Y_1:Y_2 (e.g. $G_{20}C_{21}C_{22}$ in Figure 3.2), strong cleavage also occurs enantioselectively within T,A stretches of the duplex. Finally, Λ-$Rh(en)_2phi^{3+}$ recognizes 5'-ACG-3' and 5'-GTG-3' sites strongly, producing cleavage at positions A_8 and C_9, as well as T_{19} and G_{20} of Y_1. However, other 5'-CG-3' and 5'-TG-3' steps are not cleaved strongly, and thus this recognition is attributed to shape selectivity. Shape selective cleavage of Λ-$Rh(en)_2phi^{3+}$ has been noted previously at both at 5'-ACG-3' and 5'-GTG-3' sites.[9b]

The complex $Rh(S_4\text{-cyclen})phi^{3+}$, which lacks axial amines for donating hydrogen bonds, does not recognize the G,C regions of the duplex Y_1:Y_2. $Rh(S_4\text{-cyclen})phi^{3+}$ cleaves the oligomer poorly, with a single strong cleavage site in Figure 3.2 at base C_9. In contrast to the generally symmetric cleavage patterns of both Λ- and Δ-$Rh(en)_2phi^{3+}$, there is no corresponding cleavage of the complementary strand when cleavage of 3'- [^{32}P] end-labeled Y_2 is examined (data not shown) indicating that the binding of $Rh(S_4\text{-cyclen})phi^{3+}$ at this site is characterized by a canting of the metal complex toward one strand. Similarly, the only strong cleavage of 3'-[^{32}P] end-labeled

Y_2 by Rh(S_4-cyclen)phi^{3+} again appears at a C residue of a 5'-ACG-3' site, (data not shown) and again there is no strong cleavage at the complementary site in Figure 3.2 (base C_{17}). Recognition of these 5'- ACG-3' sites by Rh(S_4-cyclen)phi^{3+} is ascribed to shape selectivity, since the duplex Y_1:Y_2 contains eight repeats of the dinucleotide 5'-CG-3', yet only two 5'-ACG-3' sites are recognized strongly.

The photocleavage of oligomer Y_1:Y_2 by Λ- and Δ-Rh(en)$_2$phi^{3+} may be characterized by the percent enantiomeric excess (% e.e.) of cleavage at each base.

$$\% \text{ e.e.} = \left(\frac{I_{n,\Lambda} - I_{n,\Delta}}{I_{n,\Lambda} + I_{n,\Delta}} \right) * 100 \quad , \qquad (5)$$

where $I_{n,\Lambda}$ and $I_{n,\Delta}$ are the corrected cleavage intensities of Λ- and Δ-Rh(en)$_2$phi^{3+} at site n, calculated as described in the experimental section. The photocleavage of Y_1:Y_2 is summarized in Figure 3.3, a histogram displaying the cleavage on both strands as measured by the percent enantiomeric excess (% e.e.) at each base.

The histogram illustrates graphically the basis for recognition of DNA of general sequence by Λ- and Δ-Rh(en)$_2$phi^{3+}. At the G,C regions of the Y_1:Y_2 duplex, values of % e.e. are low and varied indicating that there is little energetic difference between the binding of Λ- and Δ-Rh(en)$_2$phi^{3+} at these sites. However, high levels of % e.e. are observed within the T,A regions of the duplex, indicating that there is an enantioselective preference of the Λ-enantiomer for T,A regions of the DNA. There are two remaining regions of Y_1:Y_2 which display relatively high % e.e. levels due to shape selective recognition by Λ-Rh(en)$_2$phi^{3+} at these overlapping 5'-ACG-3' and 5'-GTG-3' sites.

Thus in cleavage of a DNA duplex of general sequence, all Rh(phi)$^{3+}$ complexes containing axial amine ligands strongly recognize G,C regions of DNA, while a complex lacking hydrogen bond donors in the axial position does not cleave G,C regions strongly. Furthermore, the Λ-positioning of ancillary ligands directs enantioselective recognition of DNA, as seen primarily in the increased affinity of Λ-Rh(en)$_2$phi^{3+} for T,A regions of the duplex, as well as the shape selective recognition of 5'-ACG-3' and 5'-GTG-3' sites.

Figure 3.2 . Recognition of an oligonucleotide designed to contain all ten possible base steps. An image of a 20% denaturing polyacrylamide gel after photocleavage of oligonucleotide Y_1:Y_2 by Λ- and Δ-Rh(en)$_2$phi^{3+} and several derivatives. Irradiation conditions were 100 μM base pairs Y_1:Y_2, ~120-150,000 cpm / sample 3'-[^{32}P] end-labeled Y_1, 5 μM Rh(phi)$^{3+}$ complex, 50 mM NaCacodylate, pH 7.0, 20 minutes irradiation at 325 nm. Lane 1, untreated oligomer; lane 2, oligomer irradiated in the absence of metal complex; lane 3 - 7, oligomer irradiated in the presence of Λ-Rh(en)$_2$phi^{3+}, Δ-Rh(en)$_2$phi^{3+}, Rh(NH$_3$)$_4$phi^{3+}, Rh(cyclen)phi^{3+} and Rh(S$_4$-cyclen)phi^{3+} respectively.

The sequence of Y_1:Y_2 is give below :

Y_1 5'- ATA TCG CAC GGA TTA GCG TGC CTA ATC GAT AT -3'
Y_2 3'- TAT AGC GTG CCT AAT CGC ACG GAT TAG CTA TA -5'

Note that Δ-Rh(en)$_2$phi^{3+} cleaves specifically in G,C rich regions of the oligomer, and that this specificity is paralleled in both Rh(NH$_3$)$_4$phi^{3+} as well as Rh(cyclen)phi^{3+}. Rh(S$_4$-cyclen)phi^{3+} does not cleave the duplex in G,C regions, but instead cleaves the oligomer shape selectively at base C$_9$ of an 5'-ACG-3' site. Λ-Rh(en)$_2$phi^{3+} cleaves the oligomer with a low degree of selectivity, since it also recognizes G,C regions, as well as cleaving enantioselectively within T,A regions and at 5'-ACG-3' and 5'-GTG-3' sites.

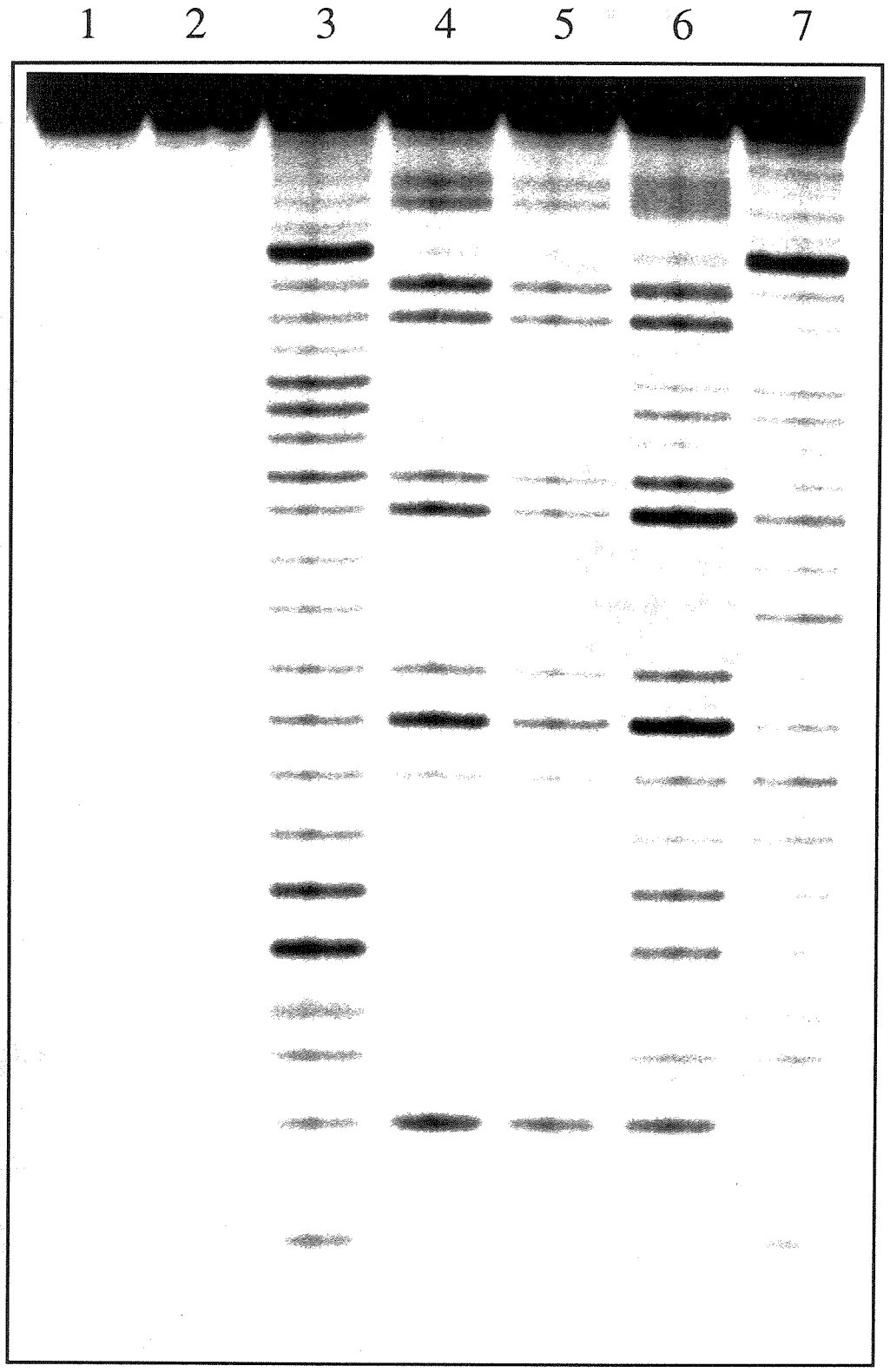
1
2
3
4
5
6
7
A - 5'
T
A
T
C
C
C
G
G
A
T
T
A
G
C
G
T
G
C
C
T
A
A
T
C
G
A
T
A
T - 3'

Figure 3.3. A histogram illustrating the cleavage by Λ- and Δ-$Rh(en)_2phi^{3+}$ on the oligonucleotide duplex Y_1:Y_2. Photocleavage data was quantitated via phosphorimagery, and values of % e.e. were calculated as described by equation (5) such that positive % e.e. at a base corresponds to greater cleavage by Λ-$Rh(en)_2phi^{3+}$. Data is presented for experiments employing both 3'- [^{32}P] end-labeled strand Y_1 (Panel B) as well as strand Y_2 (Panel C). The bars representing % e.e. values are shaded in terms of T,A regions displaying high % e.e., (solid bars); G,C regions displaying low or varied % e.e., (dashed bars); and two remaining regions which display moderate % e.e. due to shape selective recognition of 5'-ACG-3' and 5'-GTG-3' sites by Λ-$Rh(en)_2phi^{3+}$ (bold bars).

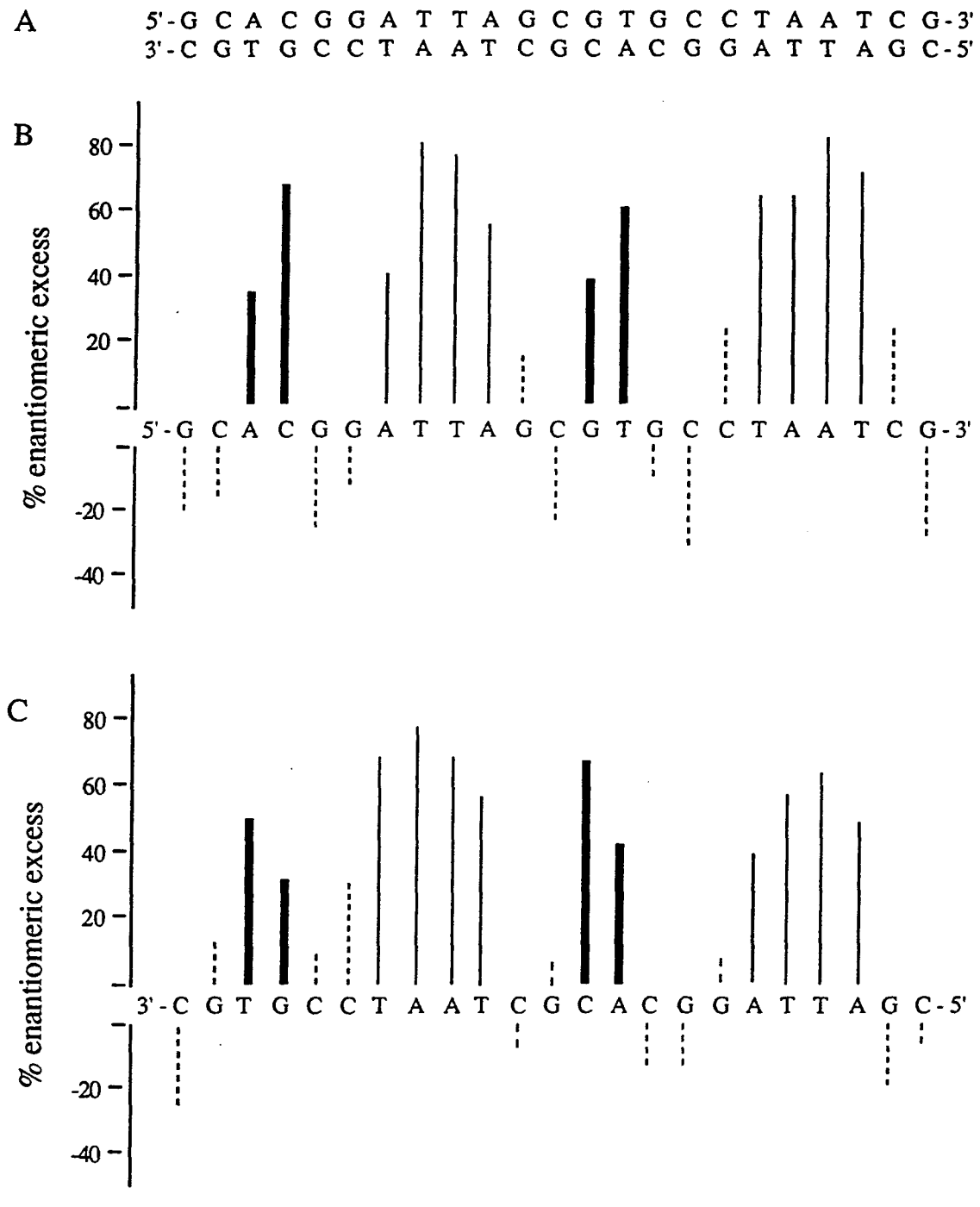
A
5'-G C A C G G A T T A G C G T G C C T A A T C G-3'
3'-C G T G C C T A A T C G C A C G G A T T A G C-5'
B
% enantiomeric excess
80
60
40
20
-20
-40
5'-G C A C G G A T T A G C G T G C C T A A T C G-3'
C
% enantiomeric excess
80
60
40
20
-20
-40
3'-C G T G C C T A A T C G C A C G G A T T A G C-5'

3.3.2. Enantioselective cleavage by Λ- and Δ-Rh(en)$_2$phi^{3+} of an oligonucleotide duplex designed to contain strong binding sites.

In order to examine in more detail the DNA recognition properties of Λ- and Δ-Rh(en)$_2$phi^{3+}, an oligonucleotide duplex (B_1:B_2) was designed to contain several 5'-GC-3' steps, predicted to be strong sites for Δ-Rh(en)$_2$phi^{3+}, as well as a T,A stretch predicted to contain strong sites for enantioselective recognition by Λ-Rh(en)$_2$phi^{3+} The sequence of B_1:B_2 is given below :

```
B1   5'-  ATG CAA TAT AAG TGC ACA TGC AAC TGC AGT GCA C  -3'
B2   3'-  TAC GTT ATA TTC ACG TGT ACG TTG ACG TCA CGT G  -5'
```

Photocleavage of B_1:B_2 by the enantiomers of Rh(en)$_2$phi^{3+}, displayed in Figure 3.4, closely follows the recognition patterns established in cleavage of the oligomer Y_1:Y_2. When strand B_2 is 3'- [^{32}P] end-labeled, Δ-Rh(en)$_2$phi^{3+} cleaves the duplex very selectively at three 5'-GC-3' steps - $G_{14}C_{15}$, $G_{20}C_{21}$, and $G_{26}C_{27}$. At these sites, as was noted in cleavage at the $G_{16}C_{17}$ step of Y_1:Y_2, two strong cleavage bands are observed corresponding to the 5'- and the 3'- sugars of the 5'-GC-3' intercalation step. Interestingly, cleavage intensity at the 3'-C residue is typically twice the intensity at the 5'-G residue. This recognition is in contrast to photocleavage of DNA by Rh(phen)$_2$phi^{3+}, which produces a single cleavage band at the 5'- base of the intercalation site.[6]

Recognition of the oligomer B_1:B_2 by Λ-Rh(en)$_2$phi^{3+} again displays a low degree of sequence selectivity, cleaving the duplex at nearly every base. Λ-Rh(en)$_2$phi^{3+} cleaves very strongly within T,A stretches of the duplex (e.g. bases T_{24}-T_{30} of Figure 3.4) as well as recognizing 5'-GC-3' sites (although not as well as the Δ-enantiomer). Interestingly, the enantioselective cleavage of T,A regions is stronger in the middle of the T,A stretch than at either the 5'- or 3'- edges. Finally, strong cleavage of B_1:B_2 occurs at 5'-TG-3' steps which are within 5'-ATG-3' sites, (e.g. base T_{17} in Figure 3.4). Since other

5'-TG-3' steps are not cleaved with similar intensity, the selectivity for this site is again assigned as shape selective. It is noted that similar shape selective cleavage has been observed at 5'-ATG-3' sites in cleavage of restriction fragments by Λ-$Rh(en)_2phi^{3+}$.[9b]

In Figure 3.5, the quantitated photocleavage of the B_1:B_2 oligomer by Λ- and Δ-$Rh(en)_2phi^{3+}$ is presented in histogram format. Since this oligonucleotide was designed to contain strong cleavage sites for both Λ-and Δ-$Rh(en)_2phi^{3+}$, it is informative to view the cleavage by each complex separately and in terms of enantioselective ratio. The histogram illustrates that for both enantiomers, strong cleavage of one strand of the duplex is accompanied by strong cleavage of the complementary strand, indicating the absence of canting of the metal complex towards one strand within the intercalation site. Thus, the cleavage by Λ-$Rh(en)_2phi^{3+}$ within T,A stretches is strong on both strands, and the recognition of 5'-GC-3' steps by Δ-$Rh(en)_2phi^{3+}$ is characterized by strong cleavage at all four residues. Interestingly, the recognition of 5'-GC-3' steps by Δ-$Rh(en)_2phi^{3+}$ displays a distinct 3'-asymmetry in its cleavage pattern, commonly associated with minor groove binding molecules such as MPE·Fe(II).[1] However, the cleavage pattern displayed by Δ-$Rh(en)_2phi^{3+}$ is not due to a minor groove orientation, but instead due to the weighting of cleavage from the major groove at 5'-GC-3' steps towards the 3'-C residue on both strands (*vide infra*). Finally, in the shape selective recognition of 5'-ATG-3' sites by Λ-$Rh(en)_2phi^{3+}$, there is perhaps some evidence of canting , although such an assignment is made difficult due to the overlap of 5'-ATG-3' sites on both B_1 and B_2 strands, as well as the low overall sequence selectivity of the Λ-enantiomer.

Figure 3.4. Recognition of a duplex designed to contain strong binding sites for Λ- and Δ-Rh(en)$_2$phi^{3+}. An image of a phosphorimaged screen of a 20% denaturing polyacrylamide gel after photocleavage of the oligonucleotide B_1:B_2 by the enantiomers of Rh(en)$_2$phi^{3+}. Irradiation conditions were 100 μM base pairs B_1:B_2 ~120-150,000 cpm / tube 3'-[^{32}P] end-labeled strand B_1, 5 μM Rh(en)$_2$phi^{3+} or 2.5 μM Rh(phen)$_2$phi^{3+}, 50 mM NaCacodylate, pH 7.0, 15 minutes irradiation (10 min. for Rh(phen)$_2$phi^{3+}) at 313 nm. Lanes 1 and 2, Maxam Gilbert G and C+T sequencing reactions respectively; lane 3, oligomer incubated in the presence of Δ-Rh(en)$_2$phi^{3+}, no irradiation; lane 4, oligomer irradiated in the absence of metal complex; lanes 5 -8, oligomer irradiated in the presence of Λ-Rh(en)$_2$phi^{3+}, Δ-Rh(en)$_2$phi^{3+}, Λ-Rh(phen)$_2$phi^{3+} and Δ-Rh(phen)$_2$phi^{3+} respectively.

Note that Δ-Rh(en)$_2$phi^{3+} cleaves the oligomer very specifically at three 5'-GC-3' sites, and that this recognition is marked by cleavage at both the 5'-G and 3'-C residues. Λ-Rh(en)$_2$phi^{3+} cleaves the oligomer with a strongly within the T,A stretch, in addition to recognizing 5'-ATG-3' sites strongly.

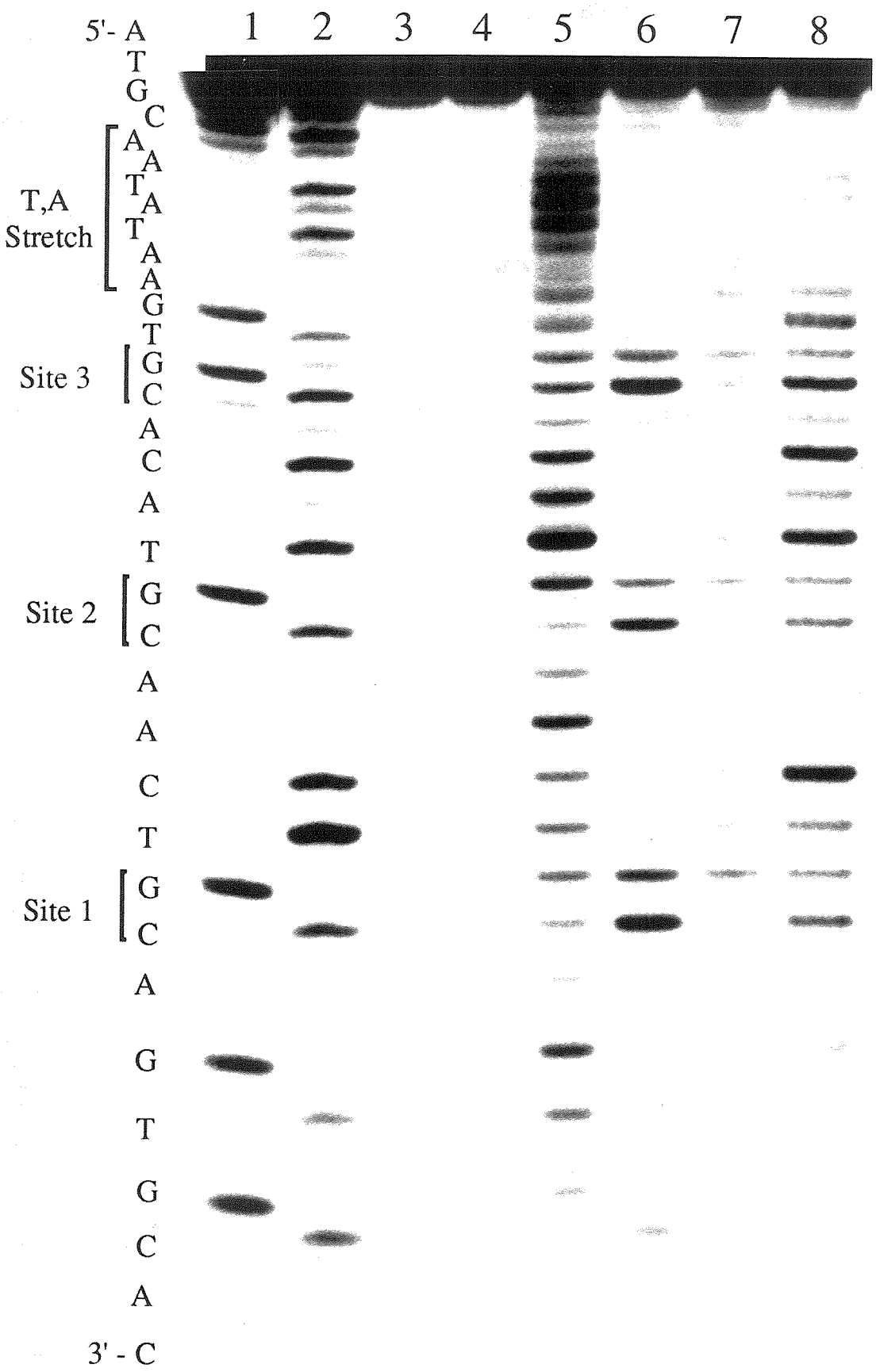
5'- A
T
G
C
A
A
T
A
T
A
A
G
T
G
C
A
C
A
T
G
C
A
A
C
T
G
C
A
G
T
G
C
A
3' - C
1
2
3
4
5
6
7
8
T,A Stretch
Site 3
Site 2
Site 1

Figure 3.5. A histogram displaying photocleavage of the oligomer B_1:B_2 by Λ- and Δ-Rh(en)$_2$phi^{3+} (Panels B and C respectively). Cleavage intensity was quantitated as described in Section 2.3.1, and normalized to the intensity at the strongest cleavage site of Λ-Rh(en)$_2$phi^{3+} on each strand. The high level of selectivity of Δ-Rh(en)$_2$phi^{3+} for 5'-GC-3' sites is dramatically illustrated in this histogram, as is the low overall sequence selectivity displayed by Λ-Rh(en)$_2$phi^{3+}. In general, recognition of a site along one strand is paralleled by recognition of the complementary site indicating the absence of canting of the metal complex towards one strand within the intercalation site, although the strong cleavage of 5'-ATG-3' sites by Λ-Rh(en)$_2$phi^{3+} appears to be canted towards the ATG strand and away from the CAT strand.

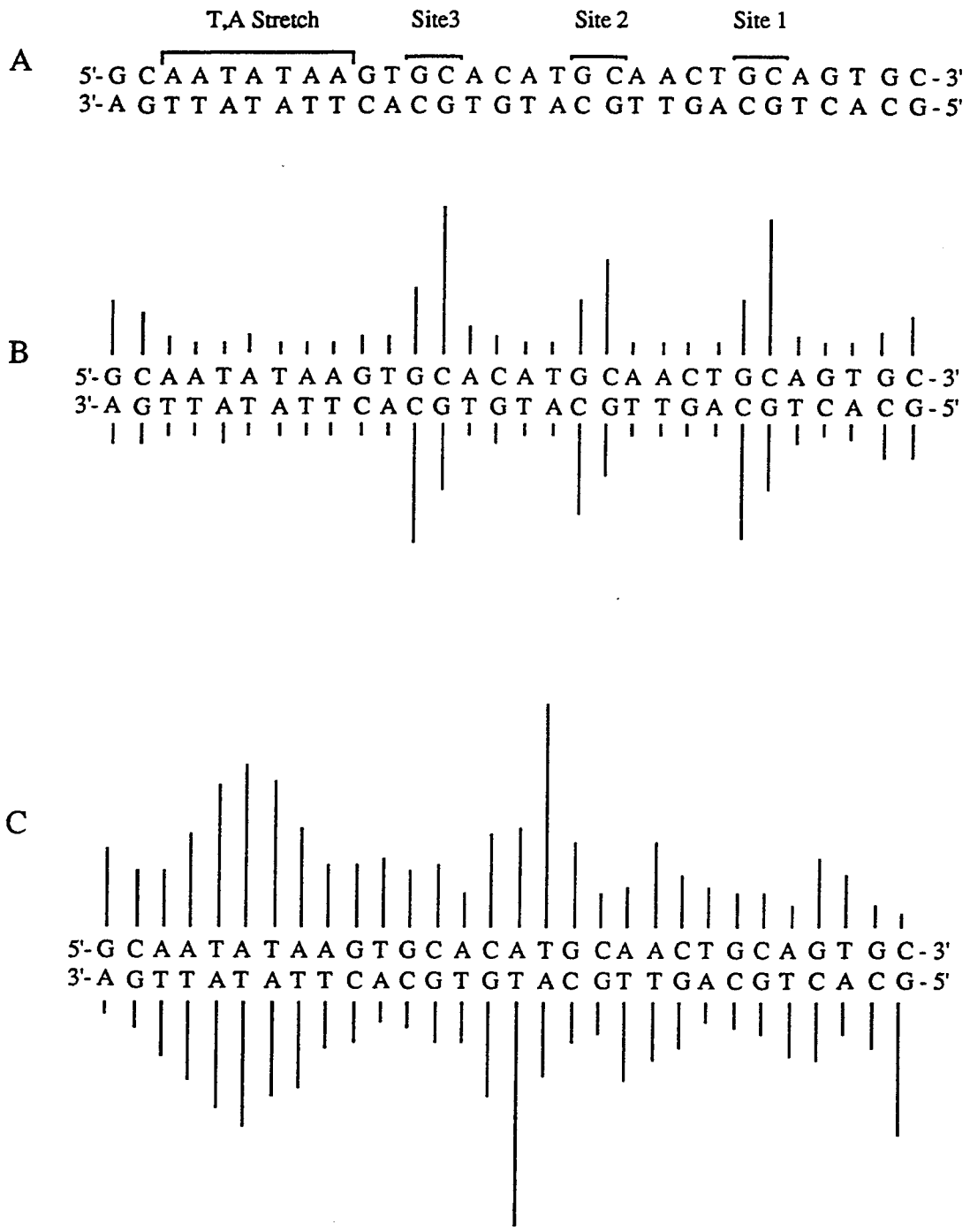
T,A Stretch
Site3
Site 2
Site 1
A
5'-G C A A T A T A A G T G C A C A T G C A A C T G C A G T G C-3'
3'-A G T T A T A T T C A C G T G T A C G T T G A C G T C A C G-5'
B
5'-G C A A T A T A A G T G C A C A T G C A A C T G C A G T G C-3'
3'-A G T T A T A T T C A C G T G T A C G T T G A C G T C A C G-5'
C
5'-G C A A T A T A A G T G C A C A T G C A A C T G C A G T G C-3'
3'-A G T T A T A T T C A C G T G T A C G T T G A C G T C A C G-5'

3.3.3. Site specific affinity constants from photocleavage experiments: Determining the energetic contributions of discrete elements of molecular recognition.

To determine the energetic contributions of hydrogen bonding and van der Waals contacts to sequence selective DNA recognition by the enantiomers of $Rh(en)_2phi^{3+}$, the site specific affinity constants of the enantiomers were determined for the sites available on a140-base pair restriction fragment of pUC18. It was hoped that these values would place limits on the energetic contributions of hydrogen bonding and van der Waals contacts to sequence selectivity. However, both the low overall sequence selectivity and inefficient cleavage chemistry of $Rh(en)_2phi^{3+}$ were considerable obstacles in the design and quantitative analysis of these experiments.

In order to first determine the optimal conditions for the extraction of affinity constants from photocleavage data, experiments were carried out to explore the effect of carrier (non-labeled) DNA concentration, as well as length of irradiation upon the cleavage intensity strong recognition sites. The effect of the concentration of the carrier DNA (calf thymus DNA) upon photocleavage of a 5'- [^{32}P] end-labeled restriction fragment by $Rh(cyclen)phi^{3+}$ is shown in Figure 3.6. As expected, strong cleavage is observed at several 5'-GC-3' steps (denoted with asterisks) along the labeled DNA target. At low concentrations of carrier DNA, (lanes 3-7), there is only a slight difference between the cleavage in the 5 μM and 0.5 μM $Rh(cyclen)phi^{3+}$ lanes indicating that these sites are fully bound at a concentration of 0.5 μM $Rh(cyclen)phi^{3+}$. This observation places a lower limit on the affinity constant of $Rh(cyclen)phi^{3+}$ for these sites of 2×10^6 M^{-1}. Importantly, as the concentration of carrier DNA increases, there is a bleaching of cleavage by $Rh(cyclen)phi^{3+}$ in the 0.5 μM Rh lanes due to the competition for $Rh(cyclen)phi^{3+}$ between carrier DNA and end-labeled fragment. At a concentration of 75 μM calf thymus DNA base pairs, there is little cleavage apparent at 0.5 uM $Rh(cyclen)phi^{3+}$, indicating that the complex is largely bound to the carrier DNA.

Figure 3.6. Effect of carrier DNA concentration on the occupancy of strong sites. Photocleavage of 5'- [^{32}P] end-labeled 140-mer by Rh(cyclen)phi^{3+} is shown at several concentrations of carrier DNA. Lanes 1-3, 1 μM calf thymus DNA, lanes 4 and 5, 5 μM calf thymus DNA, lanes 6 and 7, 15 μM calf thymus DNA, lanes 8-10, 75 μM calf thymus DNA. Irradiation conditions were either 0 μM (lanes 1 and 10), 5 μM (lanes 2,4,6 and 8), or 0.5 μM (lanes 3,5,7 and 9) Rh(cyclen)phi^{3+}, 10 mM NaCacodylate, 40 mM NaCl, pH 7.0, 5 minutes irradiation at 313 nm.

Note that at low concentrations of carrier DNA, (lanes 3-7), cleavage by 5 μM and 0.5 μM Rh(cyclen)phi^{3+} is very similar, placing a lower limit for the K_b at strongly recognized sites of ~ 2 x 10^6 M^{-1}. However, at higher concentrations of carrier DNA, there is a bleaching of cleavage in the 0.5 μM Rh(cyclen)phi^{3+} lanes, indicating that the carrier DNA is competing with the radiolabeled probe for the metal complex, thus lowering the observed affinity of Rh(cyclen)phi^{3+} for its strong binding sites.

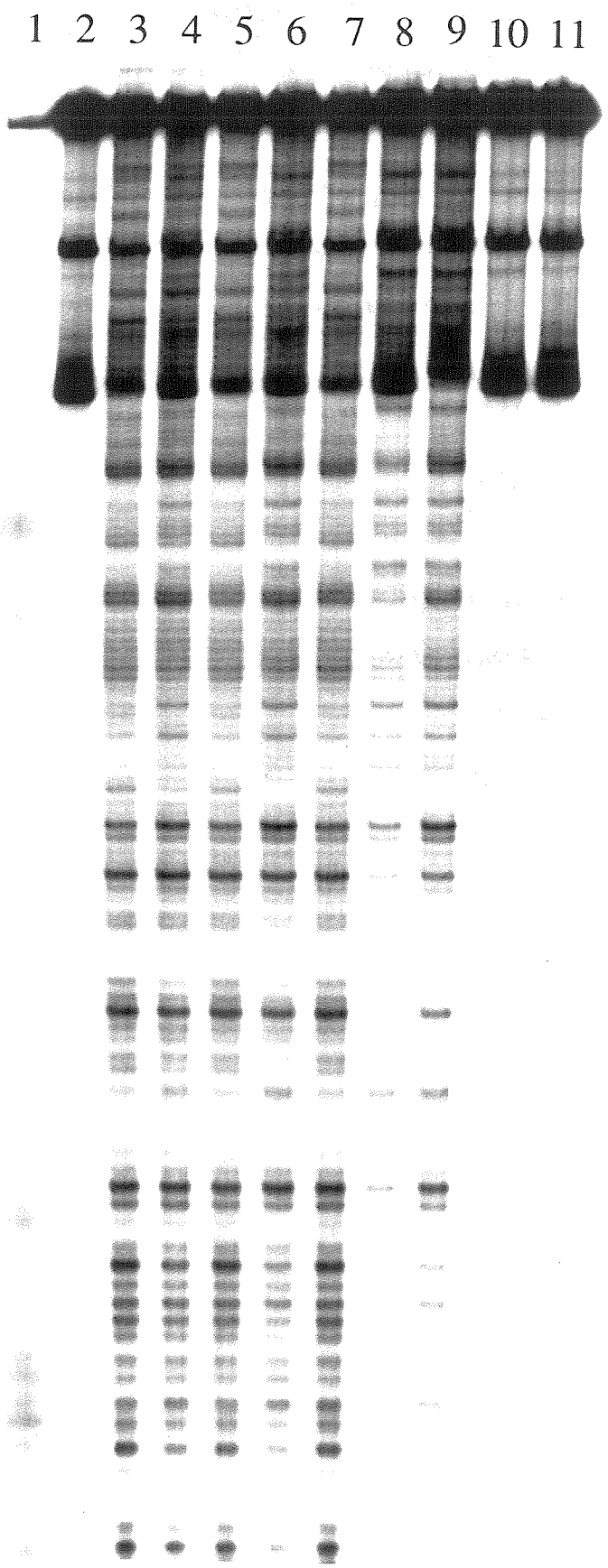
1 2 3 4 5 6 7 8 9 10 11

Thus the apparent affinity of $Rh(N_4)phi^{3+}$ complexes for sites along a DNA duplex may be decreased by the existence of binding sites on the carrier DNA. Given that, as illustrated in Chapter 2, these complexes display a high affinity for both DNA and RNA polynucleotides, there will likely be no carrier to which they will not bind strongly. This result presents both an obvious practical problem, but also a theoretical problem for extraction of affinity constants from the quantitative analysis of photocleavage experiments.

In both quantitative affinity cleavage as well as footprinting techniques, it is possible to obtain accurate affinity constants based solely on the measure of fractional site occupancy and the total ligand concentration.[14,18] This simple relationship rests, however, on the crucial approximation that the total ligand concentration, $[L]_{tot}$, may be substituted for the free ligand concentration, $[L]_{free}$ if the concentration of DNA binding sites is small with respect to the lowest concentration of probe utilized. However, since Λ- and Δ-$Rh(en)_2phi^{3+}$ bind as strongly to sites on the carrier DNA as to sites on the target DNA, this is certainly not valid over most points of a photocleavage titration, since the concentration of sites is only slightly lower than the concentration of carrier DNA base pairs. However, it is possible to obtain a useful approximation of $[Rh]_{free}$ at each $[Rh]_{tot}$ based upon the average affinity constant of the metal complex for the DNA target. This average K_b could be determined spectrophotometrically, or as illustrated here, through the sum of cleavage over the entire strand. Calculated Rh_{free} values may then be used to fit the empirical binding isotherms using equation (4) to determine the sequence specific binding constants of the enantiomers of $Rh(en)_2phi^{3+}$.

Another important requirement for the accurate portrayal of site occupancy through photocleavage is maintaining single hit conditions. At equal levels of binding, overcleavage of the DNA will lead to a false distribution of labeled products in favor of shorter DNA fragments, since only products still connected to the end-label may be observed on a polyacrylamide gel. In order to avoid this distortion of the sequence

selectivity of a $Rh(phi)^{3+}$ complex, cleavage levels must be maintained at a level of one hit per strand, often denoted as single hit conditions. The effect of higher levels of cleavage are evidenced in Figures 3.7.B, where cleavage intensity at several strong sites appears to decrease at very high metal concentrations.

The optimal conditions for the observation of site occupancy and saturation through DNA photocleavage would therefore appear to be a) the highest concentration of carrier DNA which does not compete with labeled fragment for $Rh(phi)^{3+}$ complex, and b) an irradiation time which neither undercleaves sites which are occupied, nor skews the cleavage results in favor of smaller fragments due to overcleavage. Such conditions are achieved for the $Rh(N_4)phi^{3+}$ complexes at a carrier DNA concentration of 5 μM base pairs and 5 minute irradiation. Cleavage over four orders of magnitude in metal concentration (10 μM to 0.005 μM) allows observation of site saturation at strong recognition sites while avoiding serious problems due to overcleavage. These conditions were used to determine the sequence specific affinity constants of Λ- and Δ-$Rh(en)_2phi^{3+}$ for binding sites present on 3'- [^{32}P] end-labeled restriction fragments. The cleavage intensity at each base was quantitated by phosphorimagery, and the data was fit to a theoretical binding curve described by expression (5) in the experimental section. The adjustable parameters I_{sat} and $K_{b,n}$ were provided by a least squares fitting routine.

Figure 3.7 displays cleavage of a 3'- [^{32}P] 140 base pair end-labeled restriction fragment by Λ- and Δ-$Rh(en)_2phi^{3+}$ over four orders of magnitude concentration. The sequence selectivity of both complexes matches the selectivities observed in cleavage of oligonucleotide substrates Y_1:Y_2 and B_1:B_2. Δ-$Rh(en)_2phi^{3+}$ recognizes 5'-GC-3' sites (highlighted in the partial sequence listing), while Λ-$Rh(en)_2phi^{3+}$ cleaves with little sequence selectivity. The occupancy of strong sites for both Λ- and Δ-$Rh(en)_2phi^{3+}$ is well demonstrated by the saturation of cleavage at strong binding sites. However, this saturating level of cleavage is often decreased at higher metal concentrations due to both the population of weaker sites as well as the overcleavage of the labeled target DNA.

Figure 3.7.A. Cleavage of restriction fragment DNA by Λ-Rh(en)$_2$phi^{3+} over four orders of magnitude metal concentration. Irradiation conditions were 10 μM calf thymus DNA base pairs, 80-100,000 cpm / sample 3'- [^{32}P] end-labeled 140-mer restriction fragment, 10 mM NaCacodylate, 40 mM NaCl, pH 7.0, 10 minutes irradiation at 313 nm. Lanes 1, 2, and 3, Maxam Gilbert G, G+A and C+T sequencing reactions respectively; lane 4, incubation of DNA with Δ-Rh(en)$_2$phi^{3+}, no irradiation; lanes 5-16, cleavage at 10, 5, 3, 2, 1.5, 1, 0.5, 0.25, 0.1, 0.05, 0.01, 0.005 μM metal complex; lane 17, irradiation of DNA in the absence of metal complex.

Note that there is saturation of numerous cleavage sites by the 0.5 μM level of metal concentration. In parallel with its sequence selectivity on oligonucleotide substrates, Λ-Rh(en)2phi3+ exhibits little sequence specificity on a restriction fragment substrate, but a high level of overall affinity overall.

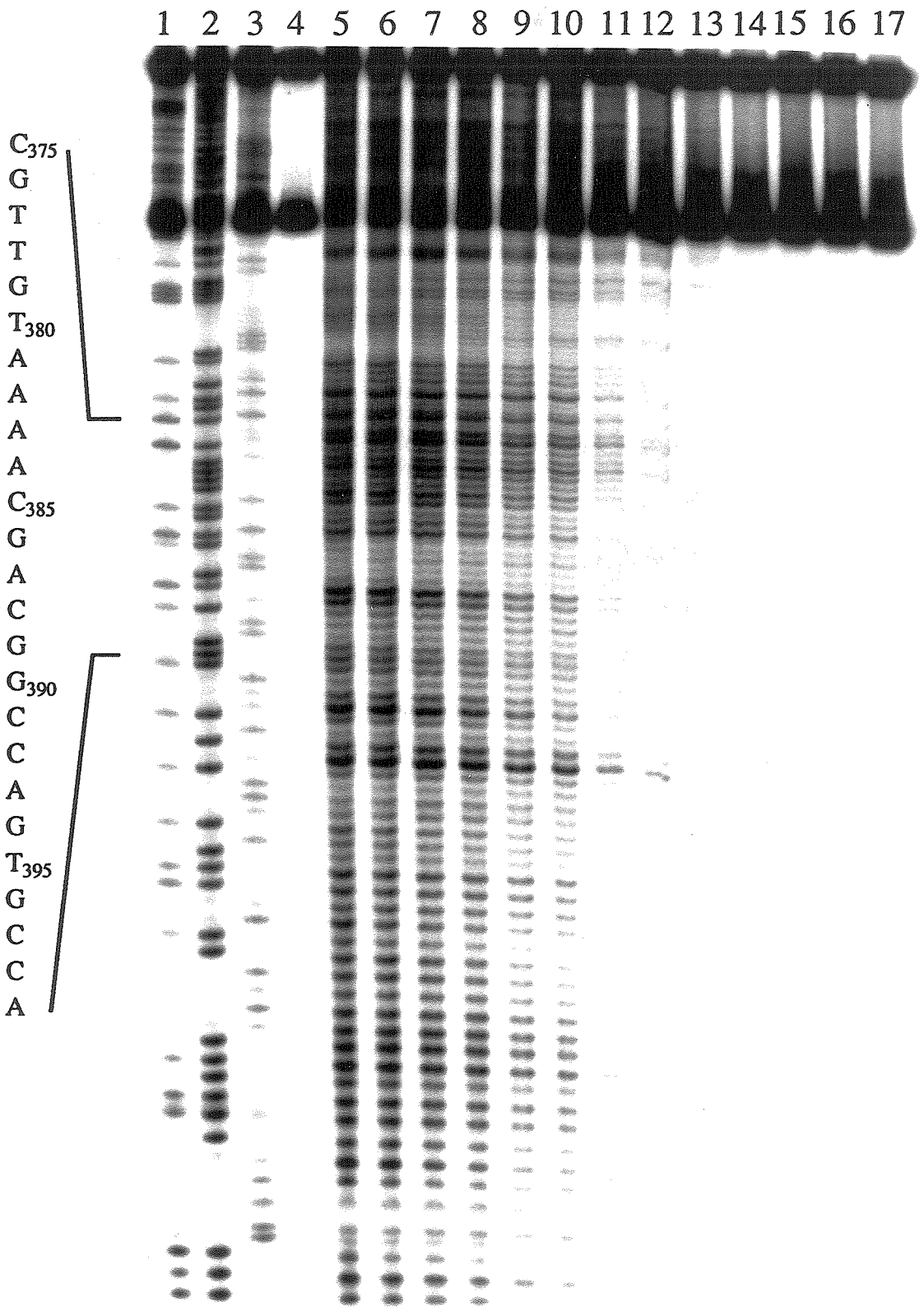
1 2 3 4 5 6 7 8 9 10 11 12 13 14 15 16 17
C375
G
T
T
G
T380
A
A
A
A
C385
G
A
C
G
G390
C
C
A
G
T395
G
C
C
A

Figure 3.7.B. Cleavage of restriction fragment DNA by Δ-Rh(en)$_2$phi^{3+} over four orders of magnitude metal concentration. Irradiation conditions were 10 μM calf thymus DNA base pairs, 80-100,000 cpm / sample 3'-[^{32}P] end-labeled 140-mer restriction fragment, 10 mM NaCacodylate, 40 mM NaCl, pH 7.0, 10 minutes irradiation at 313 nm. Lanes 1 and 2, Maxam Gilbert A+G and C+T sequencing reactions respectively, lane 3, incubation of DNA with Δ-Rh(en)$_2$phi^{3+}, no irradiation; lane 16, irradiation of DNA in the absence of metal complex; lanes 4-15 cleavage at 10, 5, 3, 2, 1.5, 1, 0.5, 0.25, 0.1, 0.01, 0.01, 0.005 μM metal complex.

Note that there is a clear saturation of several strong 5'-GC-3' cleavage sites by the 0.5 μM level of metal concentration. However, cleavage intensity at these sites become bleached at higher metal concentrations due to the population of weaker sites as well as the overcleavage of DNA at these higher levels of Rh(en)$_2$phi^{3+}.

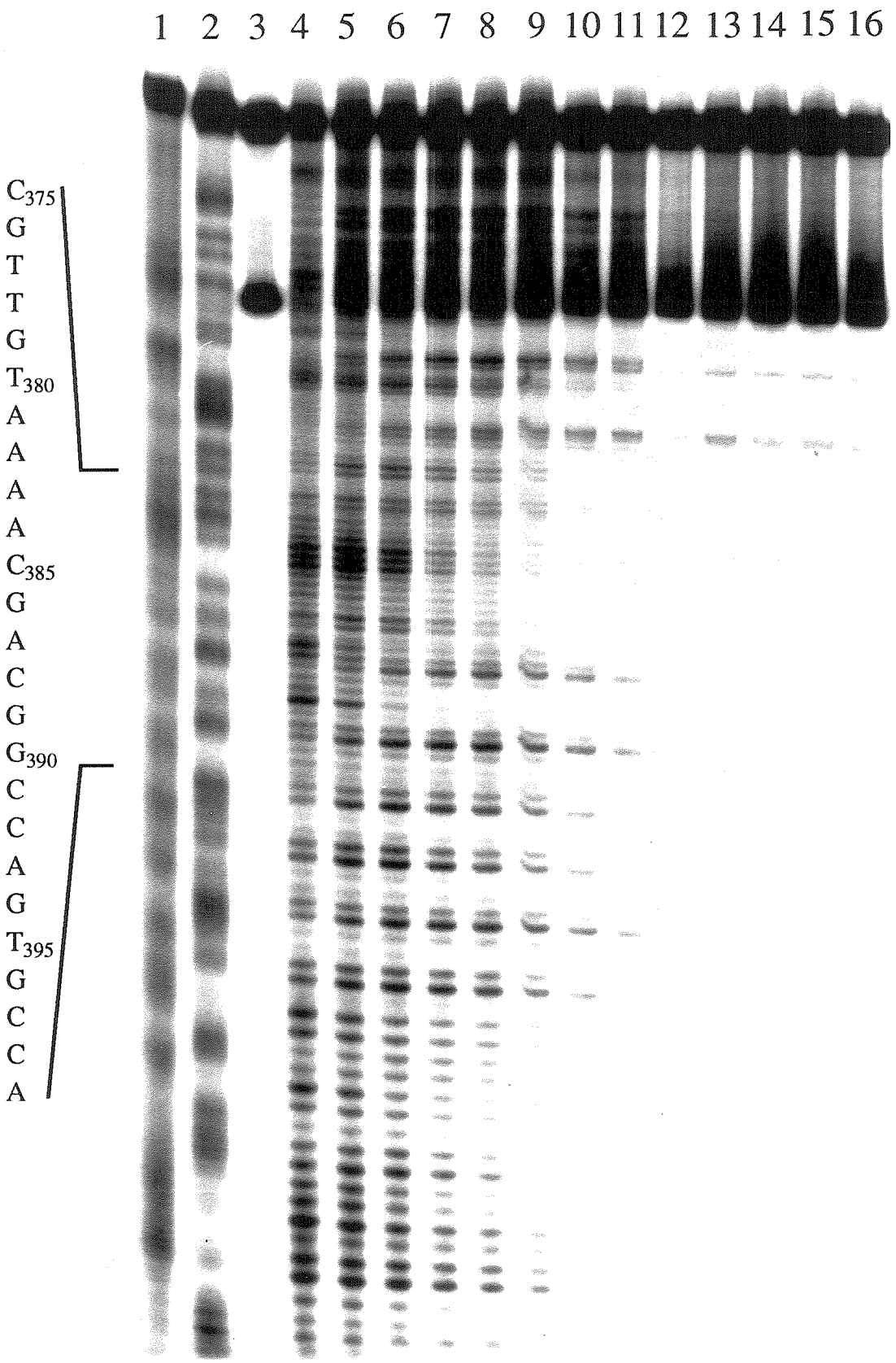
1 2 3 4 5 6 7 8 9 10 11 12 13 14 15 16
C375
G
T
T
G
T380
A
A
A
A
C385
G
A
C
G
G390
C
C
A
G
T395
G
C
C
A

Figure 3.8. Representative binding isotherms for Λ- and Δ-$Rh(en)_2phi^{3+}$. Cleavage intensity data was quantitated as described in the experimental section, and fit to the theoretical binding curve given by Equation (5). Cleavage intensity was then normalized by the value of I_{sat} provided by the least squares fit, and then replotted as Θ ($\Theta = I_n / I_{sat,n}$) versus $[Rh]_{free}$. Data is shown at two bases (T_{377} and C_{391} of pUC18), and in both panels, the open triangles represent Δ-$Rh(en)_2phi^{3+}$, while the open squares represent Λ-$Rh(en)_2phi^{3+}$. Although the curve fitting appears reasonable, the affinity constants calculated likely represent underestimates of the true binding constants due to the decrease in cleavage intensity at higher concentrations of metal complex.

A

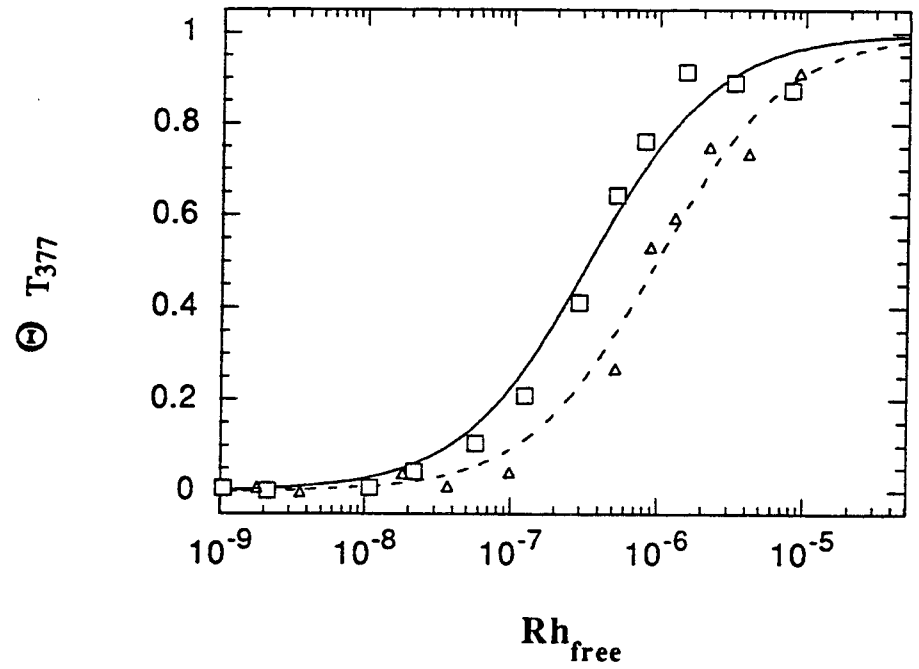
1
0.8
0.6
0.4
0.2
0
10^{-9}
10^{-8}
10^{-7}
10^{-6}
10^{-5}
ΘT_{377}
Rh_{free}

B

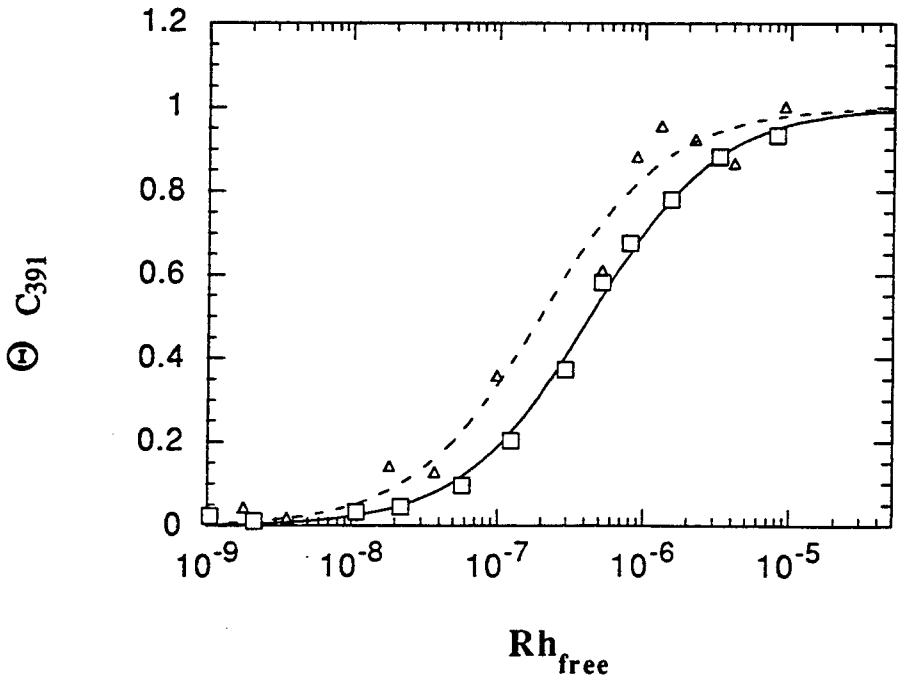
1.2
1
0.8
0.6
0.4
0.2
0
10^{-9}
10^{-8}
10^{-7}
10^{-6}
10^{-5}
ΘC_{391}
Rh_{free}

Table 3.1. Site specific K_b values of Λ- and Δ-$Rh(en)_2phi^{3+}$ for selected sites of the 140-base pair restriction fragment. The bases are numbered by their position in the sequence of pUC18. $K_{b,n}$ values are listed for analysis using $[Rh]_{free}$ values as described .

Base	Λ-$Rh(en)_2phi^{3+}$ $K_{b,n}$ (x 10^{-6} M^{-1})[a]	Δ-$Rh(en)_2phi^{3+}$ $K_{b,n}$ (x 10^{-6} M^{-1})[a]
C_{375}	3.3	1.0
G	3.2	0.8
T	3.3	1.0
T	3.2	1.2
G	3.0	1.4
T_{380}	2.8	1.6
A	3.1	1.5
A	3.1	1.2
A	2.1	1.2
A	1.8	1.1
C_{385}	1.9	1.3
G	1.6	1.5
A	1.7	1.5
C	1.7	0.5
G	1.1	0.4
G_{390}	1.7	0.8
C	2.7	5.0
C	1.9	0.8
A	1.6	0.3
G	1.7	0.3
T_{395}	1.7	0.7
G	1.8	3.3
C	2.9	7.7
C	2.2	2.0
A	1.7	0.9

a. Data is presented as the average of two independent determinations, with uncertainty of ~ 0.5 x 10^6 M^{-1}.

Table 3.1 displays $K_{b,n}$ values of Λ- and Δ-Rh(en)$_2$phi^{3+} for selected sites along a 3'- [^{32}P] end-labeled 140-mer restriction fragment, while Table 3.2 summarizes the data over these selected sites. Importantly, the $K_{b,n}$ values follow the recognition patterns established in oligonucleotide photocleavage, and are consistent with the overall binding strength estimated for Rh(cyclen)phi^{3+} based on Figure 3.6. While Δ-Rh(en)$_2$phi^{3+} displays K_b values for several 5'-GC-3' sites relative to its average affinity, the overall low selectivity of Λ-Rh(en)$_2$phi^{3+} is evidenced by the small difference between the highest and the lowest K_b values over the selected sites (3.3 versus 1.1 x 10^6 M^{-1}). As expected based upon their small size, the enantiomers of Rh(en)$_2$phi^{3+} display a low level of differential binding energy at all DNA sites. However, this fact points out the strength of the photocleavage assay, since such small energetic differences can be readily detected and analyzed in simple photocleavage experiments.

Table 3.2. A summary of the $K_{b,n}$ values presented in Table 3.1.

	Λ-Rh(en)$_2$phi^{3+}	Δ-Rh(en)$_2$phi^{3+}
Average	2.3 x 10^6 M^{-1}	1.6 x 10^6 M^{-1}
High	3.3 x 10^6 M^{-1}	7.7 x 10^6 M^{-1}
Low	1.1 x 10^6 M^{-1}	0.3 x 10^6 M^{-1}

3.3.4. Probing enantioselective cleavage by Λ- and Δ-Rh(en)$_2$phi^{3+} with oligonucleotides containing deoxyuracil, O^{6}methylguanine and 7-deazaguanine.

In order to probe specifically the importance of hydrogen bonding and van der Waals contacts in the sequence specific recognition of DNA by Λ- and Δ-Rh(en)$_2$phi^{3+}, as well as to pinpoint the DNA moieties involved in these contacts, several derivatives of the oligonucleotides Y_1:Y_2 and B_1:B_2 were synthesized which contained modified or unnatural bases. The substitution of O^{6}methylguanine or 7-deazaguanine for guanine

residues probed the importance of hydrogen bonding in recognition of 5'-GC-3' steps by Δ-Rh(en)$_2$phi^{3+}, while the substitution of deoxyuracil for thymine residues probed the importance of van der Waals contacts in both the enantioselective recognition of 5'-TA-3' steps, as well the shape selective recognition of 5'-ATG-3' sites by Λ-Rh(en)$_2$phi^{3+}.

Figure 3.9. The structure of a) guanine, O^{6}methylguanine and 7-deazaguanine and b) deoxyuracil and thymine.

To probe the importance of the O^6 atom in hydrogen bonding at 5'-GC-3' steps, the oligonucleotide B_1:B_2 was modified by the substitution of O^6methylguanine residues for guanine at a single 5'-GC-3' step along the duplex. Cleavage of the modified duplex is displayed in Figure 3.10 for the case where the 3'-[^{32}P] label is placed on the modified B_2 strand. While Δ-Rh(en)$_2$phi^{3+} strongly cleaves the two unmodified 5'-GC-3' steps (Sites 2 and 3) in Figure 3.10, there is little recognition at the modified 5'-GC-3' step (Site 1). Further, cleavage of the modified 5'-GC-3' step by Δ-Rh(en)$_2$phi^{3+} is drastically decreased relative to cleavage at Site 1 in the wild-type B_1:B_2. Cleavage by Λ-Rh(en)$_2$phi^{3+} at the modified 5'-GC-3' site also is decreased relative to cleavage of unmodified Site 1, although the overall cleavage by Λ-Rh(en)$_2$phi^{3+} at this site is weak on both oligomers .

In addition to the modification probed in Figure 3.10, there are several other possible permutations for the substitution of O^6methylguanine residues for guanine residues at Site 1 of the duplex B_1:B_2. Figure 3.11 is a summary of photocleavage intensities at the three 5'-GC-3' sites of B_1:B_2 and its O^6methylguanine derivatives. The intensities for all three 5'-GC-3' steps of each oligomer are shown to provide an internal standard of comparison between the three 5'-GC-3' sites as well as the external standard of comparison to the unmodified B_1:B_2 duplex. The substitution of the O^6methylguanine residues consistently decreases recognition of Site 1 by a factor of 3-4 fold, indicating that recognition of this site by Δ-Rh(en)$_2$phi^{3+} involves a specific contact to the O^6 atom in the major groove of DNA.

Figure 3.10. Photocleavage of an oligonucleotide duplex containing a O^6methyl-guanine residues at a 5'-GC-3' step. An image of a phosphorimaged screen of a 20% denaturing polyacrylamide gel after photocleavage by Λ- and Δ-Rh(en)$_2$phi^{3+} of a derivative of oligonucleotide B1:B2 where O^6methylguanine has been substituted for guanine residues at a 5'-GC-3' step. The modified duplex is denoted as $B1_m$:$B2_m$, and its sequence is summarized :

meB$_1$ 5'- --- --- --- --- -mGC --- -GC --- -GC --- --- - -3'

meB$_2$ 3'- --- --- --- --- -CmG --- -CG --- -CG --- --- - -5'

where regions identical to the B$_1$:B$_2$ duplex are represented as dashes, and mG denotes the O^6methylguanine residues. The three 5'-GC-3' steps are labeled in the Figure as per the conventions of Figure 3.4, and the modified site corresponds to Site 1.

Irradiation conditions were 100 μM base pairs DNA, ~120-150,000 cpm / tube 3'-[^{32}P] end-labeled strand meB$_2$, 5 μM Rh(en)$_2$phi^{3+}, 10 mM NaCacodylate, 40 mM NaCl, pH 7.0, 15 minutes irradiation at 313 nm. Lanes 1 and 2, Maxam Gilbert G and C+T sequencing reactions respectively; lane 3, oligomer incubated with Δ-Rh(en)$_2$phi^{3+}, no irradiation; lane 4, oligomer irradiated in the absence of metal complex; lanes 5 and 6, oligomer irradiated in the presence of Λ-Rh(en)$_2$phi^{3+} and Δ-Rh(en)$_2$phi^{3+} respectively.

Note that Δ-Rh(en)$_2$phi^{3+} cleaves strongly at the two unmodified 5'-GC-3' steps of the oligomer, but weakly at the third site where O^6methylguanine has been substituted for guanine residues (Site 1). Λ-Rh(en)$_2$phi^{3+} cleavage at the modified site is also slightly lower than cleavage of the similar site in the wild-type oligo.

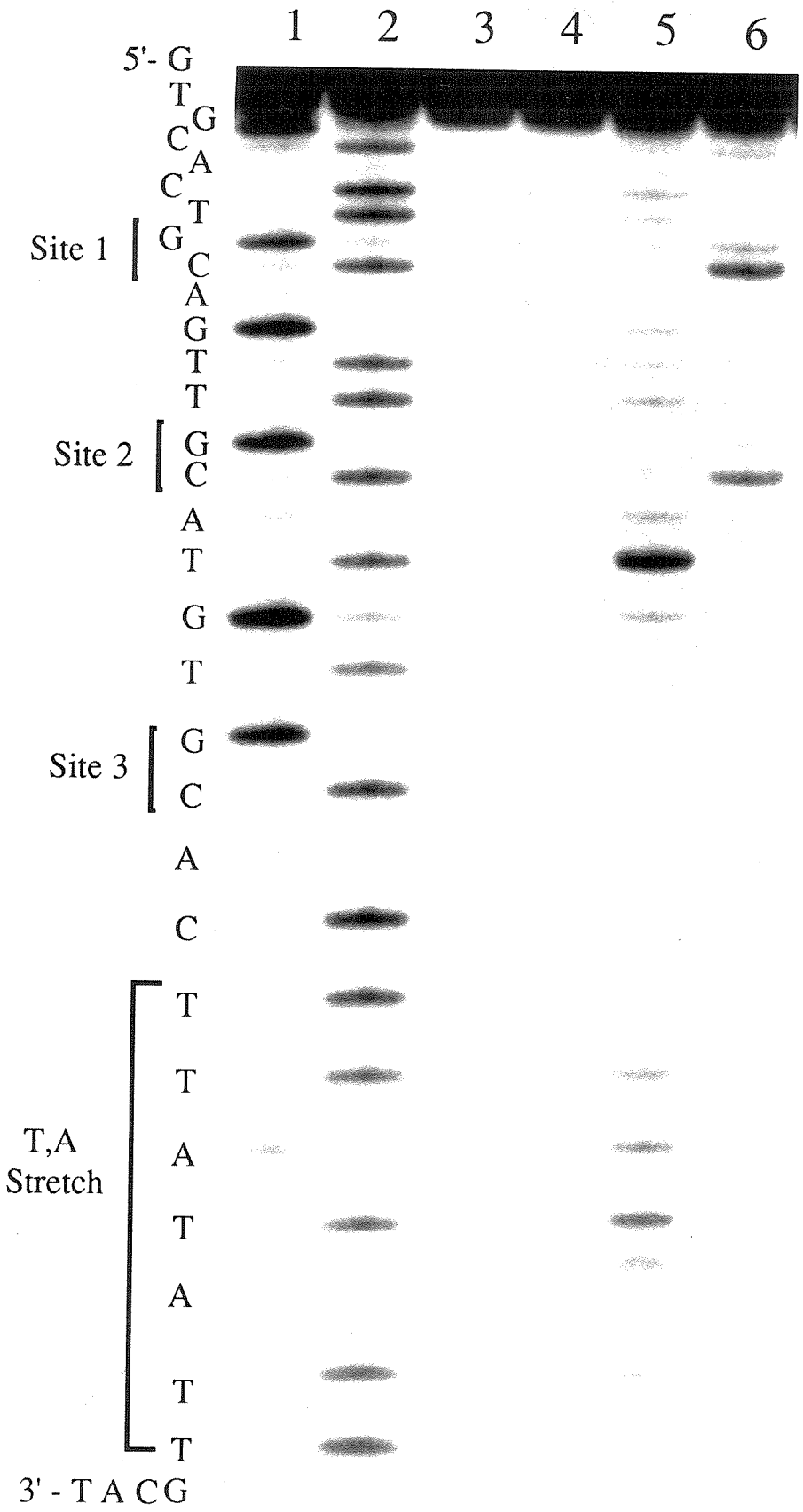
1
2
3
4
5
6
5'- G
T
G
C
A
C
T
Site 1
G
C
A
G
T
T
Site 2
G
C
A
T
G
T
Site 3
G
C
A
C
T
T
T,A
Stretch
A
T
A
T
T
3' - T A C G

Figure 3.11. The effect of substitution of O^6methylguanine at Site 1 of the oligomer B_1:B_2. Cleavage intensity at each base was quantitated as described in the experimental section, and then normalized to the strongest cleavage site of Λ-$Rh(en)_2phi^{3+}$ on either strand. Total cleavage at Sites 1, 2 and 3 represent the summation of normalized cleavage of all four bases of these 5'-GC-3' dinucleotide sites. Data presented is the average of two independent trials.

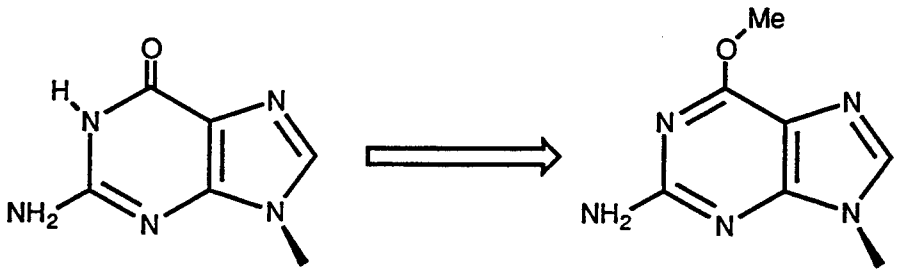

Guanine O^6methylguanine

Sequence	Total cleavage		
Site 1 Site 2 Site 3	Site 1	Site 2	Site 3
5'— G-C — G-C — G-C — 3' 3'— C-G — C-G — C-G — 5'	0.86	0.64	0.83
5'— mG-C — G-C — G-C — 3' 3'— C-G — C-G — C-G — 5'	0.29	0.95	1.18
5'— G-C — G-C — G-C — 3' 3'— C-mG — C-G — C-G — 5'	0.23	0.99	1.15
5'— mG - C — G-C — G-C — 3' 3'— C-mG — C-G — C-G — 5'	0.25	0.93	1.17

The dramatic decrease in Δ-Rh(en)$_2$phi^{3+} cleavage at O^{6}methylguanine residues (Figures 3.10 and 3.11) strongly suggests that the recognition of 5'-GC-3' steps is due to hydrogen bonding from the axial amines of Δ-Rh(en)$_2$phi^{3+} to the O^6 position of guanine residues in the major groove of DNA. However, Δ-Rh(en)$_2$phi^{3+} might also donate a hydrogen bond to the N^7 position of guanine residues, also located in the major groove. Therefore we synthesized another derivative of the B_1:B_2 duplex containing a 5'-GC-3' step substituted with 7-deazaguanine residues.

Due to the instability of oligonucleotides containing 7-deazaguanine residues to irradiation with 313 nm light,[19] it was not possible to examine photocleavage of oligonucleotide duplexes containing deazaguanine substitutions for both guanine residues of a 5'-GC-3' step. However, it was possible to examine the photocleavage of a mixed duplex wherein a strand modified at Site 1 with 7-deazaguanine was annealed to a wild-type strand, and cleavage of this duplex was then assayed by the inclusion of a small amount of 3'-[^{32}P] end-labeled wild-type strand. In Figure 3.12, photocleavage of the mixed duplex N^7B_1:B_2 by Λ- and Δ-Rh(en)$_2$phi^{3+} is compared to cleavage of the similarly constructed mixed duplex meB_1:B_2. The results reveal that Δ-Rh(en)$_2$phi^{3+} is able to recognize a 5'-GC-3' step containing a deazaguanine residue, while cleavage intensity at the same step is lost when a single O^{6}methylguanine residue is placed on the complementary strand. The cleavage of Site 1 substituted with 7-deazaguanine is similar both to the cleavage of Sites 2 and 3 in Figure 3.12, as well as the cleavage of Site 1 in the wild-type duplex. The result obtained with deazaguanine substitutions neatly complements the results of O^{6}methylguanine substitutions, and together they present a strong argument that the recognition of 5'-GC-3' steps by Δ-Rh(en)$_2$phi^{3+} involves a hydrogen bond from the axial amines to the O^6 position of guanine residues above and below the plane of intercalation.

Figure 3.12. Photocleavage of an oligonucleotide containing a 5'-GC-3' step substituted with a single O^6methylguanine or 7-deazaguanine residue. An image of a phosphorimaged screen of a 20% denaturing polyacrylamide gel after photocleavage of the mixed duplex oligonucleotides meB_1:B_2 and N^7B_1:B2 by Λ- and Δ-Rh(en)$_2$phi^{3+}. Irradiation conditions were 100 μM base pairs duplex, ~120-150,000 cpm / tube 3'-[^{32}P] end-labeled strand B_2, 5 μM Rh(en)$_2$phi^{3+} , 10 mM NaCacodylate, 40 mM NaCl, pH 7.0, 15 minutes irradiation at 313 nm. Lanes 1 and 2, Maxam Gilbert G and C+T sequencing reactions respectively; lanes 3 and 7, oligomer irradiated in the presence of Δ-Rh(en)$_2$phi^{3+}; lanes 4 and 8, oligomer irradiated in the presence of Λ-Rh(en)$_2$phi^{3+}; lanes 5 and 9, oligomer irradiated in the absence of metal complex; lanes 6 and 10, oligomer incubated in the presence of Δ-Rh(en)$_2$phi^{3+}, no irradiation.

Note that Δ-Rh(en)$_2$phi^{3+} cleaves strongly at the two unmodified 5'-GC-3' sites of both duplexes, but weakly at a third site where O^6methylguanine has been substituted for the guanine residues. However, when 7-deazaguanine is placed at this 5'-GC-3' site, strong cleavage is again observed similar to that observed at the two unmodified sites. This result indicates that hydrogen bond donation by the axial amines of Rh(en)$_2$phi^{3+} is directed to the O^6 position of guanine, not the N^7 position.

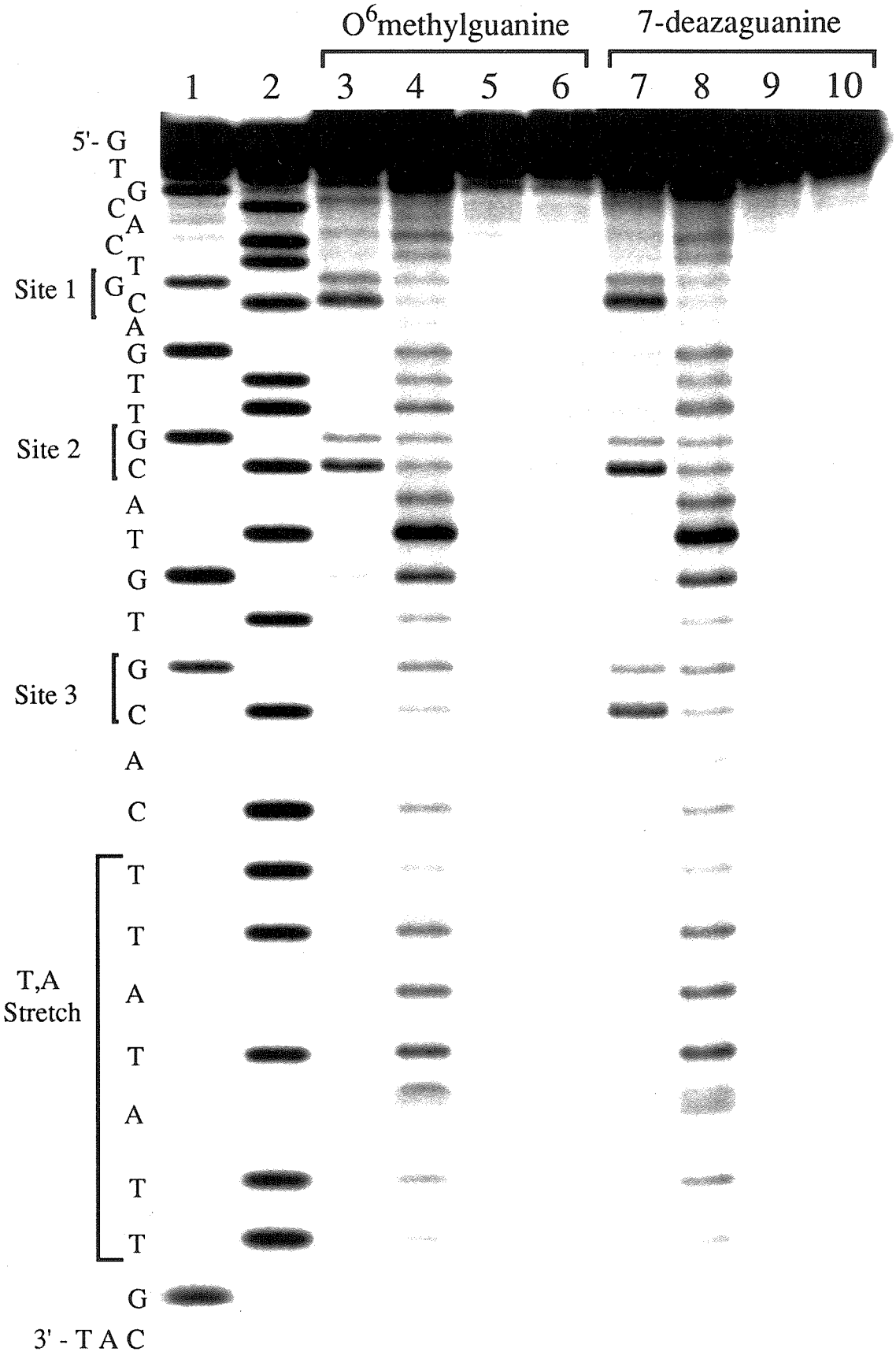
O6methylguanine
7-deazaguanine
1
2
3
4
5
6
7
8
9
10
5'- G
T
G
C
A
C
T
Site 1
G
C
A
G
T
T
Site 2
G
C
A
T
G
T
Site 3
G
C
A
C
T
T
T,A
Stretch
A
T
A
T
T
G
3' - T A C

In addition to probing hydrogen bonding contacts with O^6methylguanine and 7-deazaguanine substitutions, we probed the importance of van der Waals contacts with the thymine methyl moiety in the enantioselective recognition of 5'-TA-3' steps and shape selective recognition of 5'-ATG-3' sites by Λ-Rh(en)$_2$phi^{3+}. Since the two enantiomers present similar hydrogen bond donating axial amines, hydrogen bonding cannot account for this enantioselectivity. However, the preference of Λ-Rh(en)$_2$phi^{3+} for 5'-TA-3' steps, as well as 5'-TX-3' steps in general, suggests the importance of van der Waals contacts between the methylene groups of the ethylenediamine ligands and the thymine methyl group, located in the major groove. As illustrated in Figure 3.13, the disposition of methylene groups for the Λ-enantiomer permits such contact, the Δ-enantiomer does not.

Figure 3.13. ChemDraw model for the enantioselective cleavage by Λ-Rh(en)$_2$phi^{3+} at 5'-TA-3' steps due to the complementarity of the thymine methyl groups and the Λ-disposition of ethylenediamine ligands.

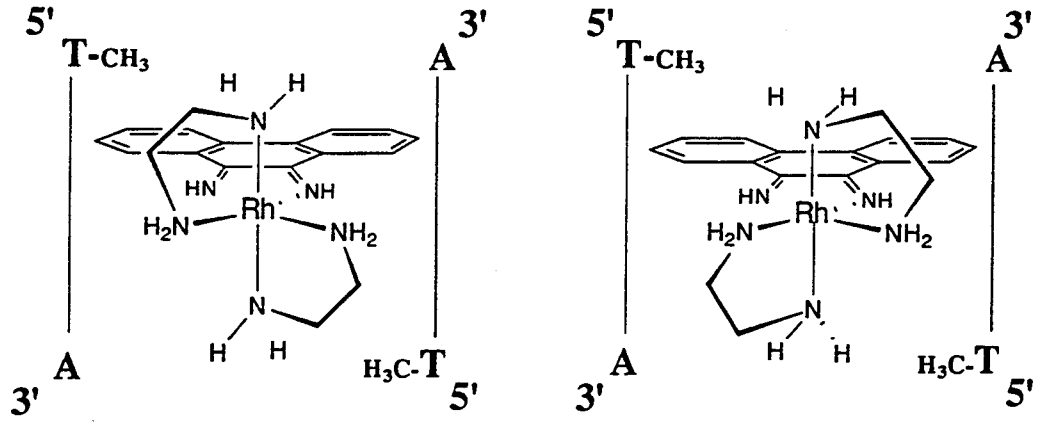

Λ-[Rh(en)$_2$phi]$^{3+}$ Δ-[Rh(en)$_2$phi]$^{3+}$

To demonstrate the involvement of specific methyl-methylene interactions in enantioselective photocleavage by Λ-Rh(en)$_2$phi^{3+}, two 5'-TA-3' sites within the

oligomer Y_1:Y_2 were substituted with deoxyuracil at both thymine residues. Figure 3.14 shows photocleavage by Λ- and Δ-Rh(en)$_2$phi^{3+} of both the modified and wild-type duplexes, and the quantitated data is presented in Table 3.2. Importantly, removal of the methyl group from the major groove of DNA served to eliminate enantioselective cleavage at one 5'-UA-3' step, and reduce it at another. Moreover, as shown in Table 3.2, little effect is seen in photocleavage of other 5'-TX-3' steps, indicating that the local structure of the DNA has been relatively unperturbed by the removal of the methyl groups. The decreases in enantioselectivity at the 3'-A residues of both 5-TA-3' steps indicates that, as with cleavage of 5'-GC-3' sites by Δ-Rh(en)$_2$phi^{3+}, there is access to both sugar residues by Λ-Rh(en)$_2$phi^{3+} at a 5'-TA-3' step.

In addition to 5'-TA-3' steps, enantioselective cleavage by Λ-Rh(en)$_2$phi^{3+} was also observed at several shape selective sites on both Y_1:Y_2 as well as B_1:B_2. Since these complexes span only a single base step when intercalated into DNA, the presence of strong shape selectivity in the recognition of DNA by Λ-Rh(en)$_2$phi^{3+} once again underscores the power of shape selectivity in achieving sequence specific recognition. In an attempt to probe the importance of van der Waals contacts in the shape selective recognition of 5'-ATG-3' sites, the oligonucleotide B_1:B_2 was substituted with deoxyuracil at two 5'-ATG-3' sites. The cleavage of this modified duplex by Λ- and Δ-Rh(en)$_2$phi^{3+} is shown in Figure 3.15 for the case where strand B_2U is 3'-[^{32}P] end-labeled. Surprisingly, there is little change in the cleavage by Λ- Rh(en)$_2$phi^{3+} at the 5'-UG-3' step relative to the corresponding 5'-TG-3' step in the wild-type B_1:B_2 (see Figures 3.4 and 3.5). A similar result was observed when shape selective recognition at a 5'-GTG-3' site was probed by mutation to a 5'-GUG-3' site (data not shown). Thus, the shape selective recognition of 5'-ATG-3' and 5'-GTG-3' sites by Λ-Rh(en)$_2$phi^{3+} does not appear to involve a van der Waals contact, as seen in the enantioselective recognition of 5'-TA-3' steps by the Λ- enantiomer.

Figure 3.14. Photocleavage of oligonucleotides containing 5'-TA-3' and 5'-UA-3' steps. An image of a phosphorimaged screen of a 20% denaturing polyacrylamide gel after irradiation of the oligonucleotides Y_1:Y_2 and Y_1U:Y_2U in the presence of Λ- and Δ-Rh(en)$_2$phi^{3+}. Irradiation conditions were 100 μM base pairs DNA, ~120-150,000 cpm / sample 3'-[^{32}P] end-labeled strand Y_2 or Y_2U, 5 μM Rh(en)$_2$phi^{3+}, 10 mM NaCacodylate, 40 mM NaCl, pH 7.0, 15 minutes irradiation at 313 nm. Lanes 1-6 display cleavage of the 3'-[^{32}P] end-labeled Y_2, lanes 7-12 display cleavage of 3'-[^{32}P] end-labeled Y_2U. Lanes 1 and 7, Maxam-Gilbert G reactions; lanes 2 and 8, Maxam-Gilbert C+T reactions; lanes 3 and 9, untreated DNA; lanes 4 and 10, oligomer irradiated in the absence of metal complex; lane 5 and 11, oligomer irradiated in the presence of Λ-Rh(en)$_2$phi^{3+}; lanes 6 and 12, oligomer irradiated in the presence of Δ-Rh(en)$_2$phi^{3+}. The sequence of the modified duplex is summarized below:

Y_1U 5'- --- --- --- --A TUA --- --- -UA AT- --- -- -3'
Y_2U 3'- --- --- --- --T AAU --- --- -AU TA- --- -- -5'

Note that enantioselective cleavage is constant from one oligomer to the other, except at 5'-TA-3' steps where deoxyuracil substitutions have been made. Here it appears that enantioselectivity either decreases (T_9A_{10}) or is eliminated ($T_{18}A_{19}$), indicating that the enantioselective recognition of these 5'-TA-3' steps by Λ-Rh(en)$_2$phi^{3+} depends upon positive van der Waals contacts made with the methyl group of thymine residues, located in the major groove.

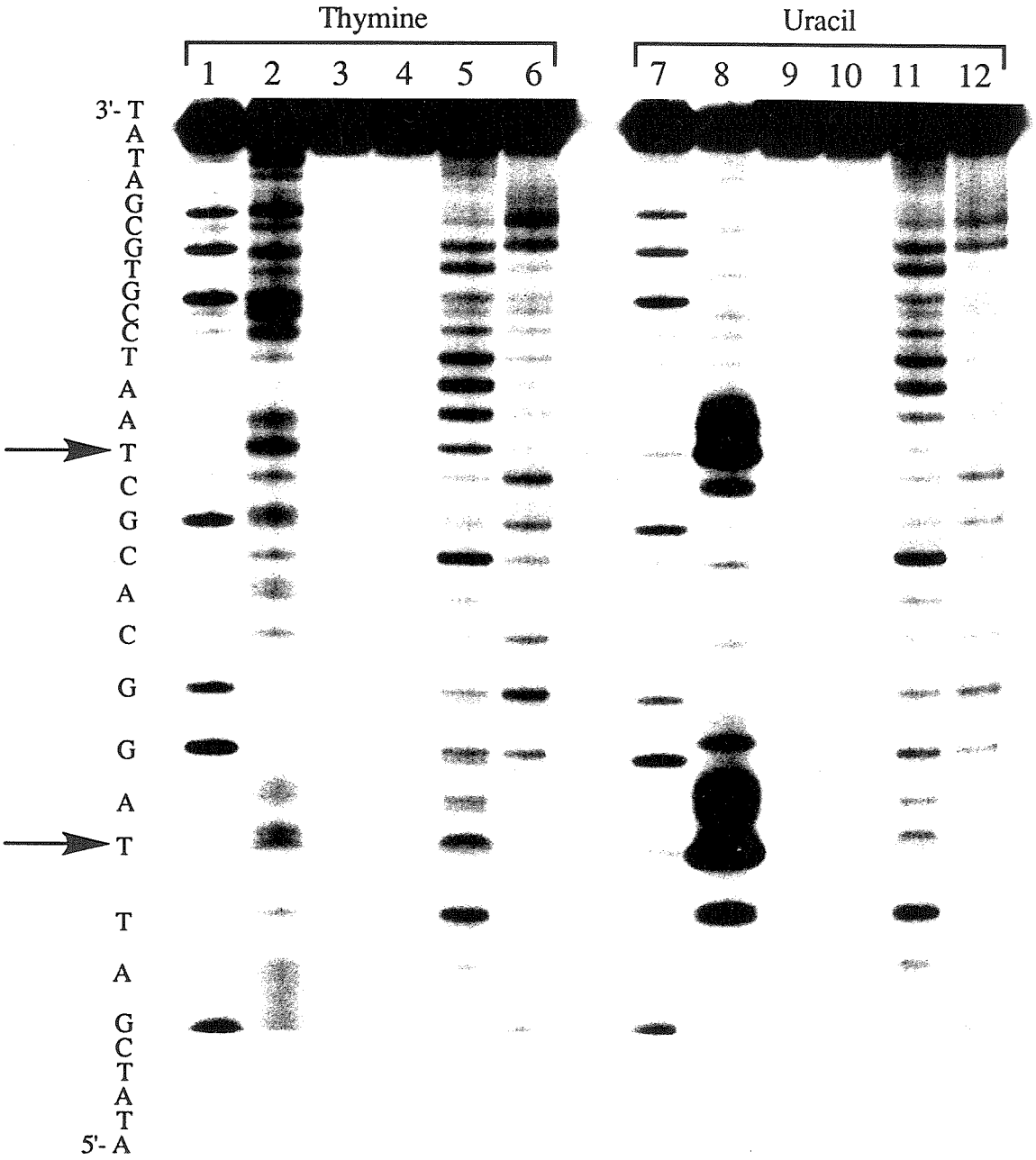
Thymine
Uracil
1 2 3 4 5 6
7 8 9 10 11 12
3'- T
A
T
A
G
C
G
T
G
C
C
T
A
A
T
C
G
C
A
C
G
G
A
T
T
A
G
C
T
A
T
5'- A

Table 3.3. Enantioselectivity in cleavage by $Rh(en)_2phi^{3+}$ at 5'-TX-3' steps. Data is in bold for the two 5'-TA-3' steps which are altered to 5'-UA-3' steps.

Base[a]	5'-TX-3' step	% e.e. - Y_2[b,c]	% e.e. - Y_2U[b,c]
T_8	5'-TT-3'	80	78
T_9	5'-TA-3' [d]	**78**	**59**
A_{10}	5'-TA-3' [d,e]	65	60
A_{14}	5'-TG-3' [e]	24	28
T_{18}	5'-TA-3' [d]	**39**	**5**
A_{19}	5'-TA-3' [d,e]	43	30
A_{20}	5'-TT-3' [e]	52	47
T_{21}	5'-TC-3'	48	48
T_{25}	5'-TG-3'	38	40

a. Bases are numbered by the sequence of strand 2. b. Values of % e.e. were calculated as described in section 2.3.1. Data listed represents the average of two independent determinations which varied by less than 5-10%. c. As a first approximation, cleavage at a 5'-TX-3' base step has been defined by the cleavage intensity at the 5'-residue. d. These 5'-TA-3' steps were substituted with deoxyuracil on Y_2U. e. Cleavage at these A residues reflects recognition of 5'-TX-3' steps on the complementary strand.

Figure 3.15. Photocleavage of an oligonucleotide containing a 5'-AUG-3' step. An image of a phosphorimaged screen of a 20% denaturing polyacrylamide gel after photocleavage of duplex B_1U:B_2U by Λ- and Δ-Rh(en)$_2$phi^{3+}. Irradiation conditions were 100 μM base pairs DNA, 120-150,000 cpm / sample 3'- [^{32}P] end-labeled strand B_2U5 μM Rh(en)$_2$phi^{3+}, 50 mM NaCacodylate, pH 7.0, 15 minutes irradiation at 313 nm. Lanes 1 and 2, Maxam Gilbert G and C+T sequencing reactions respectively; lane 3, oligomer incubated in the presence of Δ-Rh(en)$_2$phi^{3+}, no irradiation; lane 4, oligomer irradiated in the absence of metal complex; lanes 5 and 6, oligomer irradiated in the presence of Λ-Rh(en)$_2$phi^{3+} and Δ-Rh(en)$_2$phi^{3+} respectively. The sequence of the modified duplex B_1U:B_2U can be summarized:

B_1U 5'- --- --- --- --- --- -CA UG- --- --- --- --- - -3'

B_2U 3'- --- --- --- --- --- -GU AC- --- --- --- --- - -5'

Note that upon removal of the thymine methyl group from the 5'-ATG-3' steps, there is still strong recognition of the 5'-ATG-3' site by Λ-Rh(en)$_2$phi^{3+}. This shape selective recognition therefore likely does not involve a positive van der Waals contact similar to that which directs the enantioselective recognition of 5'-TA-3' steps.

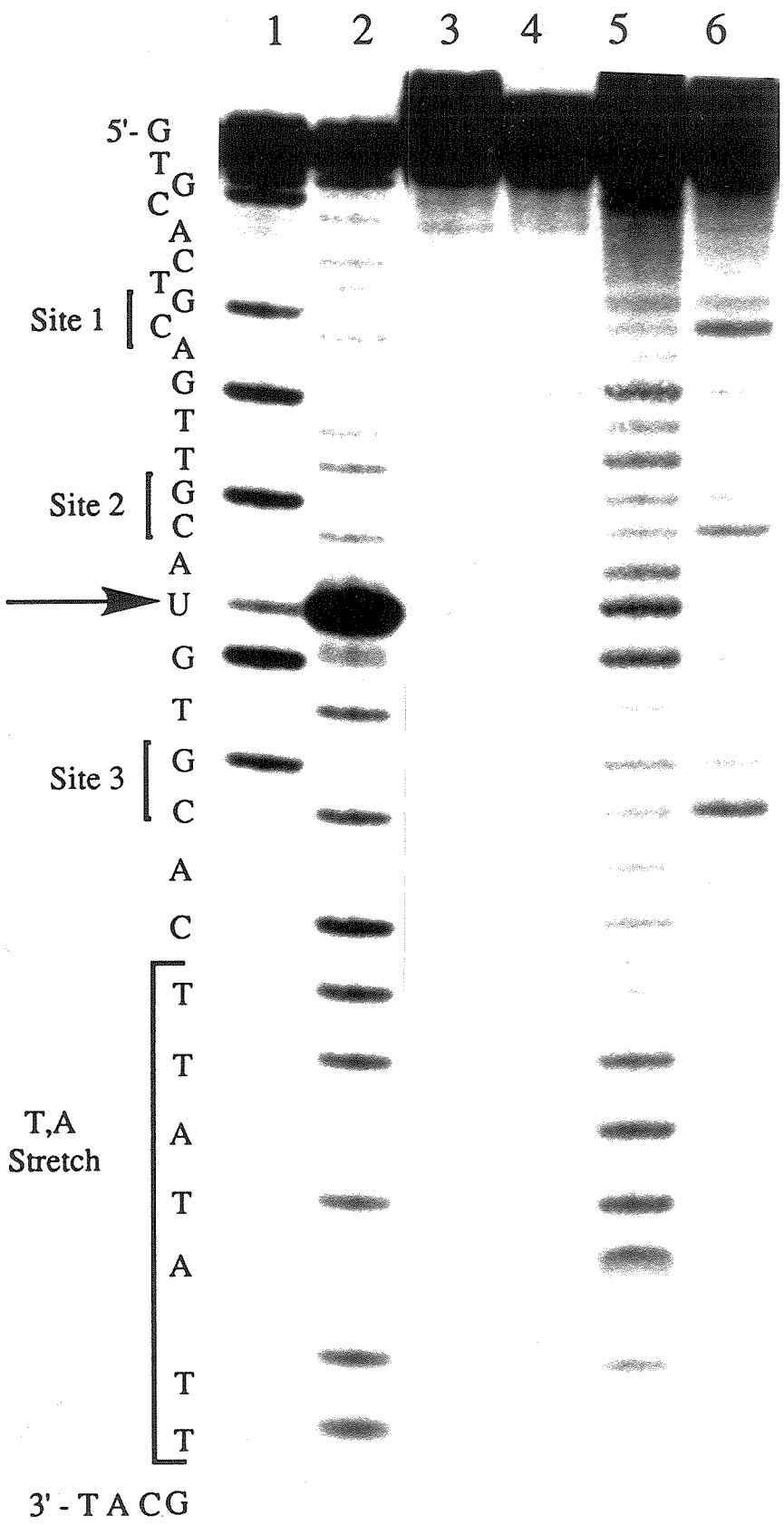
1
2
3
4
5
6
5'- G
T
G
C
A
C
T
G
C
A
G
T
T
G
C
A
U
G
T
G
C
A
C
T
T
A
T
A
T
T
3' - T A C G
Site 1
Site 2
Site 3
T,A
Stretch

3.4. Discussion

The principles governing the sequence selective recognition of DNA by the enantiomers of $Rh(en)_2phi^{3+}$ were explored by two complementary approaches. First, we derived a set of general rules by examination of the sequence selective photocleavage of an oligonucleotide duplex of random sequence by several $Rh(phi)^{3+}$ complexes containing ancillary saturated amines and a thioether. Secondly, cleavage of oligonucleotides containing unnatural or modified residues allowed us to pinpoint the elements of molecular recognition between $Rh(en)_2phi^{3+}$ and DNA.

The enantiomers of $Rh(en)_2phi^{3+}$ display sequence specific photocleavage of DNA through the molecular recognition of the major groove of DNA by the ancillary ethylenediamine ligands. While the intercalative phi ligand imparts a high level of affinity for DNA to both enantiomers, the simple ethylenediamine ligands direct the sequence specificity of the enantiomers through a combination of hydrogen bonding and van der Waals contacts. Only a moderate level of selectivity is observed, as expected given the small size of these complexes with respect to even a dinucleotide DNA intercalation step. However, the simplicity of this system offers a unique opportunity to investigate the basic elements of molecular recognition in discrete units. By delineating the hydrogen bonding and van der Waals interactions available to these complexes and their energetic contribution, one may develop a strategy for constructing transition metal complexes which bind DNA non-covalently with high sequence selectivity.

A crucial observation is that recognition of DNA by $Rh(en)_2phi^{3+}$ occurs within the major groove. Although this conclusion was supported indirectly in Chapter 2 by the observation of DNA cleavage products consistent with H-atom abstraction chemistry from the C3'-H position, it is dramatically supported here by the changes in recognition observed upon the addition or removal of a single methyl group from the major groove of DNA. (Figures 3.10 and 3.14) Given the wealth of biochemical and biophysical evidence,[4-11,16,20] a major groove orientation must now be taken as a general

characteristic of metallointercalation. The placement of the Rh center in the major groove allows one to probe the properties of protein : DNA recognition through the use of simple, structurally defined transition metal complexes. In the present study, the use of the intercalative $Rh(phi)^{3+}$ moiety as a molecular anchor in the major groove has allowed for the exploration of discrete elements of molecular recognition through the use of simple ethylenediamine ancillary ligands capable of donating hydrogen bonds and engaging in van der Waals contacts.

The common positioning of axial amine ligands in Λ- and Δ-$Rh(en)_2phi^{3+}$ directs the recognition of 5'-GC-3' steps through hydrogen bonding from the axial amines of the metal complex to the O^6 position of guanine residues above and below the plane of intercalation. Recognition of G,C regions of DNA is common to all $Rh(phi)^{3+}$ complexes containing ancillary axial amine ligands, while a complex containing a macrocyclic thioether ligand displayed no recognition of G,C regions. Likewise, the placement of a single methyl group at the O^6 position of guanine eliminates the strong recognition of a 5'-GC-3' step by Δ-$Rh(en)_2phi^{3+}$, while the substitution of 7-deazaguanine at that same site had no effect.

In contrast to the common placement of axial amines, the enantiomeric disposition of the methylene groups in $Rh(en)_2phi^{3+}$ presents a motif for the enantioselective recognition of 5'-TA-3' steps by Λ-$Rh(en)_2phi^{3+}$ based upon a positive van der Waals contact. Again, this model for recognition has been tested both by comparison of different metal complexes on a common substrate (Λ-$Rh(en)_2phi^{3+}$ cleaves T,A stretches of DNA, Δ-$Rh(en)_2phi^{3+}$ doesn't), as well as the photocleavage of modified substrates (enantioselectivity is lost at a 5'-UA-3' step relative to a 5'-TA-3' step). Although the energetic value for this contact is slightly lower than expected based on biochemical experiments with larger probes,[20] the result clearly indicates that such a positive van der Waals contact is responsible for the enantioselectivity at 5'-TA-3' steps.

The sequence specific binding constants of Λ- and Δ-Rh(en)$_2$phi^{3+} support the proposed contributions of hydrogen bonding and van der Waals contacts to sequence selectivity. Λ-Rh(en)$_2$phi^{3+} displays a slightly higher overall affinity for most sites along the DNA helix, likely due to its use of both hydrogen bonding and van der Waals contacts. Δ-Rh(en)$_2$phi^{3+}, which is more selective in cleavage of oligonucleotide DNA, likewise displays a higher ratio between the best sites and the average. Given the low values of Δ(ΔG°) between Λ- and Δ-Rh(en)$_2$phi^{3+} evident in these results, it is all the more impressive that we were able probe the hydrogen bonding and van der Waals contacts responsible for sequence specific recognition through oligonucleotide photocleavage. The quantitative analysis of photocleavage titrations, though troubled in its initial application here by the low sequence selectivity of these complexes, should prove useful in examining the energetic contributions to sequence selectivity of other complexes in the Barton group.

The specific non-covalent interactions between the rigid metal complexes and the DNA helix may be illustrated using molecular modeling. Figure 3.16 displays models of Λ- and Δ-Rh(en)$_2$phi^{3+} intercalated into 5'-TA-3' and 5'-GC-3' steps, respectively. As evident in both panels of Figure 3.16, the size of the enantiomers of Rh(en)$_2$phi^{3+} is of the same order, indeed slightly smaller, than the height along the helix axis of an intercalated base pair step. Hence at best, without conformational distortion, two-base site-selectivity is expected for both Λ- and Δ-Rh(en)$_2$phi^{3+}. The two-base site size of Rh(en)$_2$phi^{3+} contrasts the four-base pair site size of Rh(phen)$_2$phi^{3+} and other tris(polypyridyl) complexes, where the size of the complex is comparable to the size of the major groove, and overall enantioselectivities favoring the Δ-isomer are observed with right-handed DNA helices.[4-8]

At the two-base level, the preferences in cleavage by Λ- and Δ-Rh(en)$_2$phi^{3+} are readily illustrated with these models. As evident in Figure 3.16.A, the disposition of methylene groups for Λ-Rh(en)$_2$phi^{3+} complements well the positioning of methyl groups

of thymines above and below the site of intercalation. The methylene groups of the ethylenediamine ligands have been highlighted in red in order to show their proximity to the thymine methyl moieties, also in red. The average C - C non-bonded distance is 4.0 Å in these models. In this model the distances are not too close so as to provide a steric blockade for the Λ-isomer, but sufficiently close to allow a stabilizing van der Waals contact. Clearly, a similar non-bonded contact would not be available with the Δ-isomer at the 5'-TA-3' step. The right-handed helicity of DNA precludes a complementary interaction of the Δ-isomer at a 5'-AT-3' step.

The appropriate positioning of the axial amines of $Rh(en)_2phi^{3+}$ for potential hydrogen bonding to the O^6 position of guanine residues is illustrated in Figure 3.16.B. Although this model describes the hydrogen bonding interactions of Δ-$Rh(en)_2phi^{3+}$ at a 5'-GC-3' base pair step, similar hydrogen bonding interactions would be available for the Λ-isomer. As seen in the Figure, the axial amines (in red) of Δ-$Rh(en)_2phi^{3+}$ are well poised to donate a hydrogen bond to the O^6 position of guanine (also in red). N--O distances of 3.0 Å to the guanines above and below the intercalating phi may be obtained with O··H-N angles of > 160°. It is also noteworthy that the position of the equatorial amines would only permit hydrogen bonding to the phosphate backbone, and canting of the complex towards one strand would be required.

Thus the sequence selectivities determined experimentally are explained through models invoking hydrogen bonding and van der Waals contacts between Λ- and Δ-$Rh(en)_2phi^{3+}$ and the major groove of DNA. The 5'-GC-3' targeting observed with both Λ–and Δ–$Rh(en)_2phi^{3+}$ may be attributed to specific hydrogen bonding by the axial amines of the complex, while the enantioselective targeting of 5'-TA-3' steps by Λ-$Rh(en)_2phi^{3+}$ is attributed to stabilizing van der Waals interactions of the methylene groups of the ethylene diamine ligands with thymine methyl groups in the DNA major groove. Once the orientation of the complex is fixed through intercalation, the orientation of the ancillary groups for potential interaction with DNA becomes well defined.

Figure 3.16. Molecular Modeling of $Rh(en)_2phi^{3+}$ enantiomers in two intercalation sites. In Panel A, Λ-$Rh(en)_2phi^{3+}$ is shown in a 5'-TA-3' step, and in panel B, Δ-$Rh(en)_2phi^{3+}$ is displayed intercalated into a 5'-GC-3' step. The interactions of interest are highlighted in red. The remainder of the metal complex is shown in white, the DNA base pairs in yellow, and the sugar-phosphate backbone in blue.

The hydrogen bonding between axial amines of the complex and the 5'-guanine residues of 5'-GC-3' steps are illustrated on the right. The axial amines (in red) of Δ-$Rh(en)_2phi^{3+}$ are well positioned to donate a hydrogen bond to the O6 of guanine (also in red). Identical interactions are available to the axial amines of the Λ-isomer. The methylene-methyl contacts responsible for enantioselective cleavage by Λ-$Rh(en)_2phi^{3+}$ at 5'-TX-3' steps is illustrated on the left. The disposition of methylene groups for Λ-$Rh(en)_2phi^{3+}$ complements well the positioning of methyl groups of thymines above and below the site of intercalation in a 5'-TA-3' step. The methylene groups of the ethylene diamine ligands have been highlighted in red in order to show their proximity (4 Å) to the thymine methyl moieties, also in red.

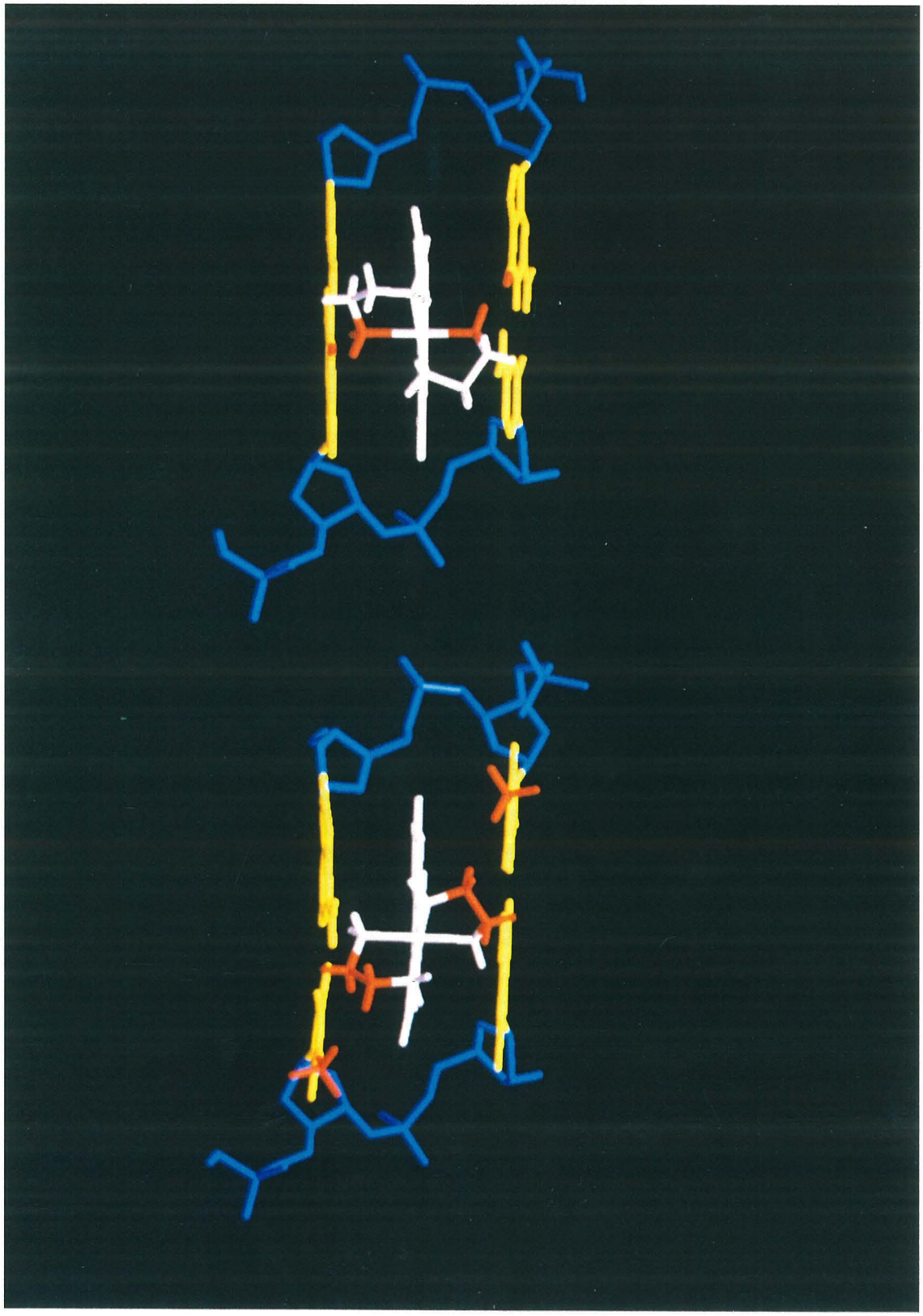

In addition to the models for 5'-GC-3' and 5'-TA-3' recognition proposed above, it is possible to create a model for the shape selective recognition of 5'-ATG-3' sites by Λ-$Rh(en)_2phi^{3+}$. As shown in Figure 3.17, the model entails hydrogen bonding from the axial amine ligands to both the O^4 position of thymine as well as the O^6 position of guanine. However, in order to satisfy the tight fit required by this hydrogen bonding network, it was necessary to twist the molecule within the intercalation site to avoid a steric clash with the thymine methyl group. While this model explains both the canting in cleavage at 5'-ATG-3 sites as well as the lack of sensitivity to the 5'-AUG-3' mutation, it offers no information as to the requirement of a 5'-A residue, which would not be contacted in this model. Such a model awaits a deeper understanding of those factors controlling the sequence dependent structural variations within DNA which lead to such powerful shape selective recognition by such a small complex.

Figure 3.17. Molecular Modeling of Λ-$Rh(en)_2phi^{3+}$ intercalated into a 5'-TG-3' step. The hydrogen bonding contacts are shown in red. Strong recognition of 5'-TG-3' steps is explained by the presence of two optimal hydrogen bonding interactions above and below the plane of intercalation. However, in order to a avoid a steric clash between the ancillary ligand and the thymine methyl moiety, the metal complex has been twisted about an axis roughly parallel to the helical axis of the DNA. This twisting yields a simple explanation for the canting observed in cleavage of 5'-ATG-3' sites by Λ-$Rh(en)_2phi^{3+}$.

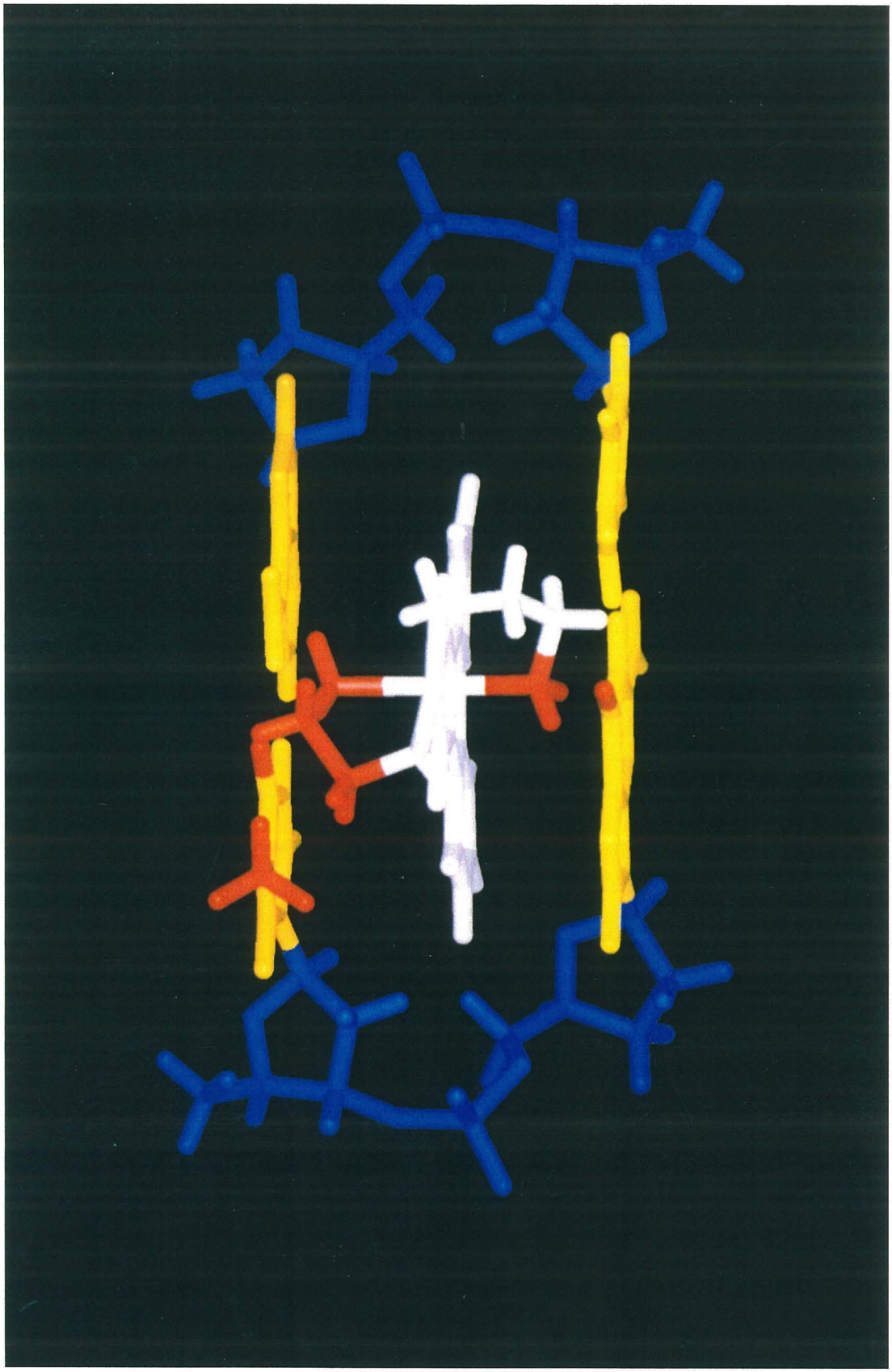

3.5. Conclusions

Λ- and Δ-Rh(en)$_2$phi^{3+} display remarkable enantioselectivity in photocleavage of DNA, given their small size and overall similar shape. Δ-Rh(en)$_2$phi^{3+} displays specificity for 5'-GC-3' steps, due to hydrogen bonding between the axial amines of the metal complex and the O^6 position of the guanine base. Other complexes containing axial amine ligands - Rh(NH$_3$)$_4$phi^{3+}, Rh(cyclen)phi^{3+} and to a lesser extent Λ-Rh(en)$_2$phi^{3+} - all display selectivity for 5'-GC-3' sites, while a complex lacking axial amines, Rh(S$_4$-cyclen)phi^{3+}, shows no selectivity for these sites. The cleavage of DNA oligomers containing the modified bases O^{6}methylguanine and 7-deazaguanine establishes that the hydrogen bonding at 5'-GC-3' steps involves the O^6 but not the N^7 positions of guanine residues above and below the plane of intercalation.

Although Λ-Rh(en)$_2$phi^{3+} displays a low level of sequence selectivity, this observation is recognition of both 5'-GC-3' as well as 5'-TX-3' steps. In contrast to the mutual recognition of 5'-GC-3' steps, the Λ-enantiomer binds 5'-TA-3' steps enantioselectively, due to a positive van der Waals contact between the ancillary ligand and the Me group on thymine. Finally, the less predictable motif of shape selectivity plays a significant role in the sequence selectivity of Λ-Rh(en)$_2$phi^{3+}, particularly in cleavage by the Λ-enantiomer at 5'-ACG-3' and 5'-A/GTG-3' steps.

Finally, a promising assay for the determination of site-specific binding constants from photocleavage gels has been developed. Although the application to the enantiomers to Rh(en)$_2$phi^{3+} is a bit complicated due to the low overall selectivity of these compounds, the methods developed here should provide a useful assay for other more selective complexes used in the Barton group. By delineating the hydrogen bonding and van der Waals interactions available to these complexes and their energetic contribution, one may develop a strategy for constructing transition metal complexes which bind DNA non-covalently with high sequence selectivity.[8b,11]

Footnotes and References

1. (a) Dervan, P. B. *Science* **1986**, *232*, 464. (b) Nicholaou, K. C. ; Dai, W. M. ; Tsay, S. C. ; Estevez, V. A. ; Wrasidlo, W. *Science* **1992**, *256*, 1172. (c) Zein, N.; Sinham, McGahren, W. J.; Ellestad, G. A. *Science* **1988**, *240*, 1198. (d) Hecht, S. M. *Acc. Chem. Res.* **1986**, *19*, 383.

2. (a) Moser, H. E.; Dervan, P. B. *Science* **1987**, *238*, 645. (b) Strobel, S.A.; Dervan, P.B. *Meth. Enzymol.* **1992**, *216*, 309.

3. (a) Pelton, J.G.; Wemmer, D.E. *Proc. Natl Acad. Sci. U.S.A.* **1989**, *86*, 5723. (b) Wu, W.; Vanderwall, D.E.; Stubbe, J.A.; Kozarich, J.W.; Turner, C.W. *J. Amer. Chem. Soc.* **1995**, *116*, 10843.

4. (a) Barton, J.K. *Science*, **1986**, *233*, 727. (b) Pyle, A. M. ; Barton, J. K. *Prog. Inorg. Chem.* **1990**, *38*, 413. (c) Dupureur, C.M.; Barton. J.K. *Comp. Supromolecular Chem.* in press.

5. (a) Chow, C. S.; Barton, J. K. *Meth. Enzym.* **1992**, *212*, 219. (b) Barton, J. K. *Science* **1986**, *233*, 727. (c) Kirshenbaum, M. R.; Tribolet, R.; Barton, J. K., *Nuc. Acids Res.* **1988**, *16*, 7943. (d) Mei, H. Y.; Barton, J. K. *Proc. Natl Acad. Sci. U.S.A.* **1988**, *85*, 1339. (e) Chow, C. S.; Barton, J. K. *J. Amer. Chem. Soc.* **1990**, *112*, 2839.

6. (a) Pyle, A. M.; Long, E. C.; Barton, J. K. *J. Amer. Chem. Soc.* **1989**, *111*, 4520. (b) Sitlani, A.; Long, E. C.; Pyle, A. M.; Barton, J. K. *J. Amer. Chem. Soc.* **1992**, *114*, 2303. (c) Pyle, A. M.; Morii, T.; Barton, J. K. *J. Amer. Chem. Soc.* **1990**, *112*, 9432 - 9434. (d) Campisi, D.; Morii, T.; Barton J.K. *Biochem.* **1994**, *33*, 4130.

7. (a) Chow, C. S.; Behlen, E. S.; Uhlenbeck, O. C.; Barton, J. K. *Biochem.* **1992**, *31*, 972. (b) Chow, C. S.; Hartman, K.M.; Rawlings, S.L.; Huber, P.W.; Barton, J.K. *Biochem.* **1992**, *31*, 3534. (c) Lim, A.-C.; Barton, J.K. *Biochem.* **1993**, *32*, 11029.

8. (a) Sitlani, A.S.; Dupureur, C.M.; Barton, J.K. *J. Am. Chem. Soc.* **1993**, *115*, 12589. (b) Terbreuggen, R.H.; Barton, J.K. submitted for publication.

9. (a) Schaefer, W. P.; Krotz, A. H.; Kuo, L.Y.; Shields, T. P.; Barton, J. K. *Acta Cryst.* **1992**, *C48*, 2071. (b) Krotz, A.H.; Kuo, L.Y.; Shields, T.P.; Barton, J.K. *J. Am. Chem Soc.* **1993** , *115*, 3877.

10. Krotz, A.H.; Kuo, L.Y.; Barton, J.K. *Inorg. Chem* **1993**, 32, 5963.

11. (a) Krotz, A.H.; Hudson, B.P.; Barton, J.K. *J. Am. Chem Soc.* **1993** , *115*, 12577. (b) Hudson, B.P.; Barton, J.K. unpublished results.

12. Maniatis, T.; Fritsch, E. F.; Sambrook, J. *Molecular Cloning: A Laboratory Manual,* 2nd ed.; Cold Spring Harbor Laboratory, 1989.

13. It should be noted that labeling with TdT was often problematic due to the high levels of exonuclease activity and short term stability of labeled products.

14. (a) Singleton, S.F; Dervan, P.B. *J. Am. Chem Soc.* **1992**, *114*, 6957. (b) Singleton, S.F; Dervan, P.B. *Biochem.* **1992**, *31*, 10995.

15. Since Λ-Rh(en)$_2$phi^{3+} is less specific than the Δ-enantiomer, a slightly higher concentration of sites was utilized in iteration of the average K_b expression. Values of 1.0 μM and 2.0 μM were used for the concentration of sites for Λ- and Δ-Rh(en)$_2$phi^{3+}, respectively.

16. (a) Wang, A.H.J.; Nathans, J.; van der Marel, G.; van Boom, J.H.; Rich, A. *Nature* **1978**, *276*, 471.

17. Models of intercalation sites were created within the Biopolymer subroutine of InsightII.

18. (a) Brenowitz, M.; Senear, D.F.; Shea, M.A.; Ackers, G.K. *Methods Enzymol.* **1986**, *130*, 132. (b) Brenowitz, M.; Senear, D.F.; Shea, M.A.; Ackers, G.K. *Proc. Natl. Acad. Sci. U.S.A.* **1986**, *83*, 8462. (c) Senear, D.F.; Brenowitz, M.; Shea, M.A.; Ackers, G.K.Ackers *Biochem.* **1986**, *25*, 7344.

19. The photochemical instability of oligonucleotides containing 7-deazaguanine is likely related its fluorescent properties.

20. (a) Rehmann, J. P.; Barton, J. K. *Biochem.*, **1990**, *29*, 1701; (b) Rehmann, J. P.; Barton, J. K. *Biochem.*, **1990**, *29*, 1710. (c) David, S. D.; Barton, J. K. *J. Am. Chem. Soc.* **1993**, *115*, 2984. (d) Collins, J.G.; Shields, T.P.; Barton, J.K. *J. Am. Chem Soc.* **1994**, *116*, 9840. (e) Dupureur, C.M.; Barton, J.K. *J. Am. Chem. Soc.* **1993**, *116*, 1086.

21. (a) Plaxco, K.W.; Goddard, W.A. *Biochem.* **1994**, *33*, 3050. (b) Aiken, C.R.; Gumport, R.I. *Meth. Enzymol.* **1991**, *208*, 433.

Chapter 4: Investigation of Λ- and Δ-Rh(en)$_2$phi^{3+} bound to the oligonucleotide d(GTGCAC)$_2$: Probing the roots of enantioselectivity via ^{1}H-NMR.

4.1. Introduction.

This chapter describes an investigation into the binding of Λ- and Δ-Rh(en)$_2$phi^{3+} to a small oligonucleotide, d(GTGCAC)$_2$, via one- and two-dimensional (1D- and 2D-) ^{1}H NMR methods. The biophysical and photocleavage studies presented in Chapters 2 and 3 indicate that these complexes bind strongly to DNA via intercalation of the planar aromatic phi ligand from the major groove, and are capable of a relatively high level of enantionselectivity based on hydrogen bonding and van der Waals contacts of the ancillary ethylene diamine ligands. The range of selectivity elements - hydrogen bonding, van der Waals contacts, as well as shape selection - employed by such a simple recognition system bodes well for a scheme wherein sequence selectivity is increased through the modular addition of recognition elements. The ^{1}H NMR experiments described here represent an attempt to obtain detailed structural information regarding the basis for the sequence selective DNA binding and cleavage by the enantiomers of Rh(en)$_2$phi^{3+}.

Photoactivated cleavage of DNA by a sequence specific octahedral metal complex is a powerful assay in its ability to measure simultaneously the relative affinity of a metal complex for a wide range of potential binding sites.[1] However, not unlike other biochemical methods,[2,3] it is an indirect method in terms of understanding the three-dimensional interactions which determine sequence selectivity. Direct structural studies have proven an invaluable aid in providing useful models for DNA : drug complexes.[7,8] In the Barton labs, we have therefore undertaken a series of high resolution structural studies to characterize the details of intercalative binding of different octahedral metal complexes with small helical oligonucleotides.[9-13] These experiments have acted both to

confirm the intercalative binding mode of these metal complexes, and also have provided a structural basis for the observed sequence selectivities of these complexes.

The study of Δ-$Rh(phen)_2phi^{3+}$: $d(GTCGAC)_2$ by 2D- NMR methods first demonstrated the specific intercalation of a $Rh(phi)^{3+}$ complex through the partial insertion of the phi ligand at the central 5'-CG-3' step of the oligomer.[10] Since this binding site corresponded precisely to the site of photocleavage by Δ-$Rh(phen)_2phi^{3+}$, this result cemented the link between shape selective DNA binding and photocleavage. Further, several NOE contacts between ancillary phenanthroline ligands and the DNA pointed to a the major groove orientation of the Rh center. ^{1}H-NMR studies have also provided structural information on the binding modes of $Ru(phen)_2dppz^{2+}$, a complex which does not cleave DNA, and confirmed our intercalative models based upon luminescence spectroscopy.[11] Finally, a recent study of a $Rh(NH_3)_4phi^{3+}$: $d(TGGCCA)_2$ complex confirmed that the smaller $Rh(N_4)phi^{3+}$ complexes bind to DNA through classical intercalation, and that this complete insertion of the phi ligand into the aromatic base stack of DNA orients the axial amine ligands for the hydrogen bonding to the guanine O6 atoms of the central 5'-GC-3' step.[12] Further the slower exchange rates of polyamine $Rh(phi)^{3+}$ complexes relative to $Rh(phi)^{3+}$ complexes containing polypyridyl ancillary ligands makes them suitable for full NMR structural determination.[13] All these studies have contributed to a more structurally based understanding of those forces which contribute to the sequence dependent recognition of DNA by metallointercalators.

Therefore, we undertook here to study the structure of Λ- and Δ-$Rh(en)_2phi^{3+}$ bound to $d(GTGCAC)_2$ via 1D- and 2D- NMR methods in order to investigate the structural details of enantioselectivity. Several important questions we sought to probe were a) do the enantiomers of $Rh(en)_2phi^{3+}$ bind to DNA in a fundamentally similar manner, b) is the depth of intercalation consistent with the proposed hydrogen bonding and van der Waals contacts of the ethylene diamine ligands and c) does ^{1}H NMR provide any useful information about the structure of the DNA at the intercalation site ?

4.2. Experimental.

Materials. Enantiomers of $Rh(en)_2phi^{3+}$ were prepared as previously described,[14] and metal concentrations were quantitated by UV-Visible spectroscopy. The self-complementary deoxyoligonucleotide $d(GTGCAC)_2$ was synthesized on an ABI Model 392 DNA synthesizer using phosphoramidite chemistry, purified by reverse phase HPLC and FPLC, and quantitated with an extinction coefficient of 6,600 M^{-1} cm^{-1} per nucleotide at 260 nm.

Instrumentation. UV-visible spectra were measured either on a Hewlett Packard 8452A Diode Array Spectrophotometer or a Cary 2200 spectrometer. High performance liquid chromatography (HPLC) was performed with a Waters 600/600E Multi Solvent Delivery System equipped with a Waters 484 Tunable Wavelength Detector and a VYDAC Protein & Peptide C18 column. FPLC was performed on a Pharmacia FPLC system equipped with a LCC-500 Plus Controller, an LKB 2141 Variable Wavelength Detector and a PepRC 15 uM HR 16/10 (C18) column.

NMR Experiments. NMR spectra were obtained in 99.96% D_2O, (Cambridge Scientific) and all samples were in phosphate buffer (10 mM $NaHPO_4$ / Na_2PO_4, 20 mM NaCl, pH 7.0). DNA samples were dissolved in 0.5 mL phosphate buffer and repeatedly lyophilized from 99.8% D_2O, and then finally resuspended in 99.96% D_2O. Aliquots of a stock solution of Λ- or Δ-$Rh(en)_2phi^{3+}$ were titrated directly into the NMR tube.

^1H-NMR spectra were recorded on a Bruker AMX-500 spectrometer operating at 500 MHz. Chemical shifts are referenced to sodium 3-(trimethylsilyl)-1-propanesulfonate (TSP) at the corresponding temperature. The two-dimensional (2D) ^1H-COSY and NOESY experiments were acquired in the phase-sensitive mode using the time proportional phase incrementation method.[15] The spectra were recorded with the carrier frequency placed on the HDO resonance using 2048 points in t2 for 512 t1 values and a pulse repetition rate of 1.6 s. NOESY spectra were acquired for mixing times values of 200 and 300 ms. A presaturation pulse was utilized to suppress the HDO resonance. One-dimensional (1D) and

2D-NMR spectra were processed with the FELIX software package (Biosym Technologies, San Diego, CA). 1D-NMR spectra were apodized with a simple exponential multiplication (1 Hz line broadening) prior to Fourier transformation, while 2D-NMR spectra were apodized with a shifted sine bell or a squared sine bell, zero filled twice in t1 and Fourier transformed in both dimensions.

Model Building and Molecular Modeling (energy minimization). Molecular modeling was performed on a Silicon Graphics Iris Indigo Workstation using the Biosym modeling package (Biosym Technologies, San Diego, CA). The coordinates of $Rh(en)_2phi^{3+}$ and $Rh(NH_3)_4phi^{3+}$ were obtained from their crystal structures.[14a,16] Models of $d(GTGCAC)_2$ and $d(TGGCCA)_2$ containing intercalation sites were constructed using either the crystal structure of a dinucleotide intercalation site[17] or the Biopolymer program of the InsightII package. The DNA structures were minimized for 100 steps with a Steepest Descents algorithm before placing the Rh(phi) complex into the intercalation site.

For the energy minimized models of $Rh(NH_3)_4phi^{3+}$: $d(TGGCCA)_2$, the overall 3+ charge of the rhodium complex was spread among the rhodium center and the ligands. AM1 calculations were used to calculate the partial charges on each atom of the neutral and protonated forms of ligands, and these were used to estimate the partial atomic charges in the $Rh(NH_3)_4phi^{3+}$ complex.[18] A distance dependent dielectric ($\varepsilon = 4R_{ij}$) and partially neutralized phosphates were employed in order more accurately to estimate the electrostatic energy term.[19] During minimizations, the coordinates of the rhodium complex were fixed, although the ammine ligands were allowed to rotate about the Rh--N bonds. Hydrogen bonds between the base pairs were included as distance constraints using 50 kcal/mol / $Å^2$, and a force constant of 50 kcal/mol / $Å^2$ was employed for experimentally observed NOE contacts. Several starting structures were examined, and each $Rh(NH_3)_4phi^{3+}$: $d(TGGCCA)_2$ starting structure was minimized for 100 steps using a steepest gradients algorithm, followed by 2,000 steps with a conjugate gradients algorithm. A model was considered to be minimized when the maximum derivative was below 0.1 kcal mol^{-1} $Å^{-1}$.

4.3. Results.

4.3.1. ^{1}H-NMR of free d(GTGCAC)$_2$.

The resonances of the free haxanucleotide were assigned from NOESY and COSY spectra according to established methods[20,21] and are in agreement with results obtained at 300 MHz.[9] Since each base's aromatic resonance displays stronger NOE cross peak to its own sugar H2'2" resonances than to the sugar of the 5'-flanking residue , the oligonucleotide may be described by a B-type conformation (e.g. C2'-endo sugar puckers).

4.3.2. 1D-NMR titration of d(GTGCAC)$_2$ with Λ & Δ-Rh(en)$_2$phi^{3+}.

The ^{1}H-NMR titration of d(GTGCAC)$_2$. with Δ-Rh(en)$_2$phi^{3+} at 295 K is presented in Figure 4.1. As aliquots of metal complex are added to the oligomer, the resonances of DNA base H8 / H6 and sugar H1' protons exhibit substantial changes in chemical shift (-0.04 to -0.46 ppm), but remain sharp, resolved peaks. Since the bound resonances of the C_4 H6 (5.864 ppm), A_5 H1' (6.172 ppm) and T_2 Me (1.314 ppm) protons increase stoichiometrically with added metal complex, it is concluded that there is a single binding site for Δ-Rh(en)$_2$phi^{3+} on the oligomer. The retention of C_2-symmetry in both the DNA and phi ligand protons further argues that this binding site is the central G_3C_4 step. Since both the metal complex and the DNA retain their C_2-symmetry upon complex formation, this binding occurs without canting of the complex towards one strand within the 5'-G_3C_4-3' binding site, a result which is consistent with the photocleavage results described in Chapter 3. Binding at the G_3-C_4 steps is also supported by the large changes in shifts of the C_4 H5 and C_4 H6 protons relative to the similar protons of the C_6 residue. Table 4.1 lists the free and bound chemical shifts of DNA base H8 / H6, as well as sugar H1' H2', H2" and H3' protons.

Figure 4.1. 1D-NMR titration of $d(GTGCAC)_2$ with Δ-$Rh(en)_2phi^{3+}$. 500 MHz ^1H NMR spectra are displayed at metal to duplex ratios of (A) 0, (B), 0.2, (C) 0.4, (D), 0.6, (E), 0.8 and (F) 1.0. The spectrum of free $Rh(en)_2phi^{3+}$ under identical solution conditions is given in spectra (G).

Note that upon addition of the metal complex, the resonances remain sharp and resolved, indicative of slow exchange. Separate free and bound resonances are observed for several protons, most notably those of C_4 H6 (7.350 and 7.564), A_5 H1' (6.226 and 6.172), and T_2 Me (1.401 and 1.314). Also indicative of slow exchange is the growth of the phi ligand protons at a single bound chemical shift. The resonances of phi protons are given in spectra D (bound) and G (free). Both DNA and phi ligand protons retain their C_2-symmetry upon binding, which argues in support of binding at the central G_3-C_4 step.

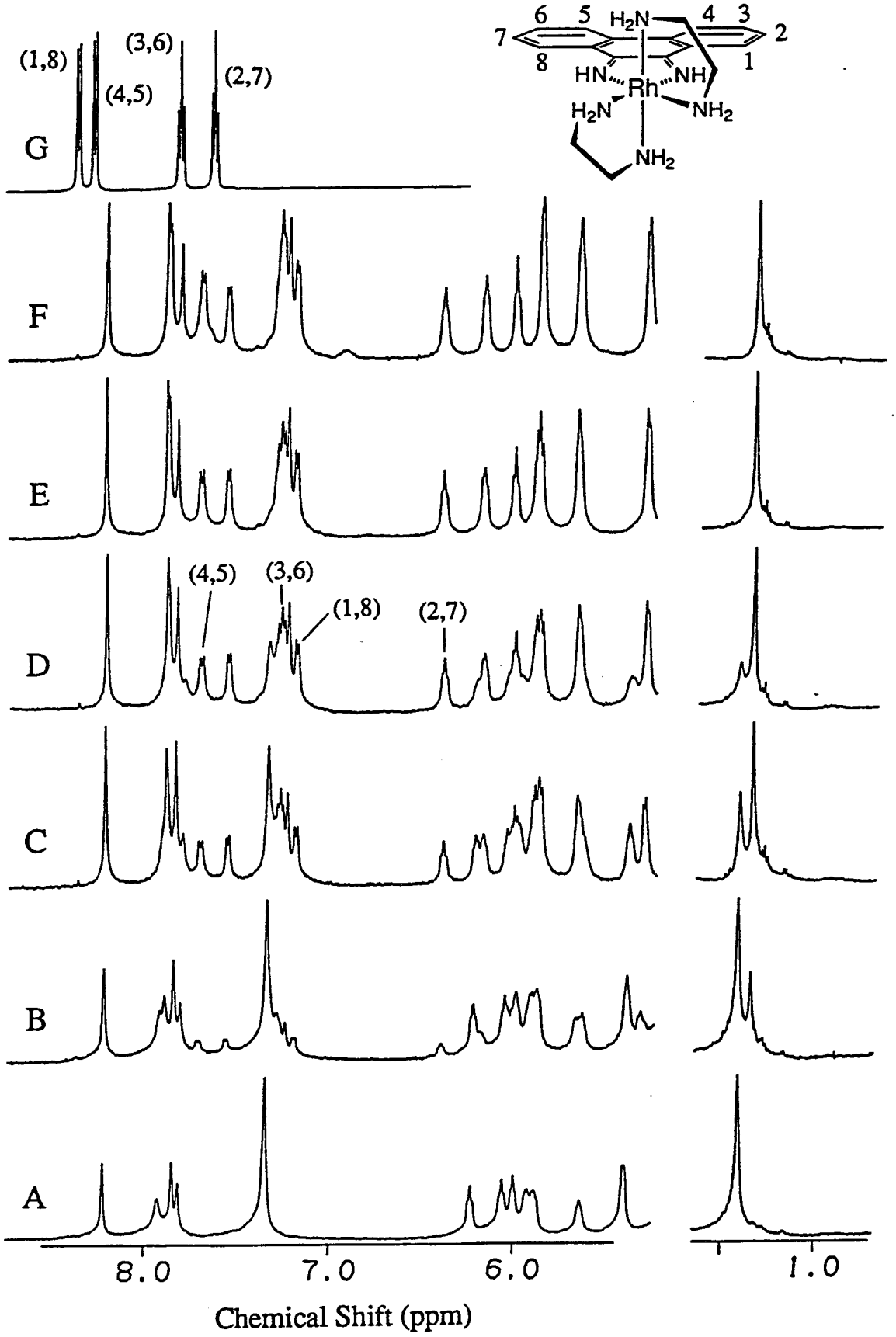
(1,8)
(4,5)
(3,6)
(2,7)
G
F
E
D
C
B
A
(4,5)
(3,6)
(1,8)
(2,7)
6 5 H2N 4 3
7 2
8 1
HN Rh NH
H2N NH2
NH2
8.0
7.0
6.0
1.0
Chemical Shift (ppm)

Table 4.1. Chemical shifts of d(GTGCAC)$_2$ protons at 295 K.[a,b]

A. Free DNA duplex.

Base	H8 / H6	H5/H2 /Me	H1'	H2'	H2"	H3'
G_1	7.842	--	5.98	2.65	2.80	4.81
T_2	7.335	1.40	5.92	2.22	2.55	4.90
G_3	7.875	--	5.87	2.64	2.73	4.98
C_4	7.350	5.40	5.63	2.05	2.39	4.81
A_5	8.220	7.92	6.23	2.67	2.87	4.98
C_6	7.316	5.33	6.05	2.11	2.11	4.46

B. Δ-Rh(en)$_2$phi^{3+} : d(GTGCAC)$_2$ complex.

Base	H8 / H6	H5/H2 /Me	H1'	H2'	H2"	H3'
G_1	7.88	--	5.88	2.58	2.73	4.80
T_2	7.24	1.31	5.66	1.72	2.18	4.78
G_3	7.89	--	5.66	2.62	2.73	5.03
C_4	7.56	5.86	5.29	2.16	2.41	4.76
A_5	8.22	7.84	6.17	2.72	2.86	4.99
C_6	7.27	5.30	6.01	2.06	2.12	4.41

a. All chemical shift data is listed in ppm and referenced to TSP at 295 K.

b. Assignments are based on a combination of 2D-NOESY and COSY spectra.

The lack of significant broadening of the spectra upon addition of Δ-$Rh(en)_2phi^{3+}$, as well as the existence of free and bound resonances for several DNA protons, indicates that the metal complex is in the slow exchange regime with the oligonucleotide at 295 K. This observation is in contrast to many classical intercalators, which typically bind to DNA with intermediate exchange kinetics.[22] An approximation of the exchange rate, (the effective dissociation rate), of the metal complex for the duplex may be made based upon the resolution of the free and bound species of several protons in Figure 4.1, since the condition of slow exchange requires that the dissociation rate of Δ-$Rh(en)_2phi^{3+}$ with the duplex be significantly less than the 45 Hz chemical shift difference between the free and bound thymine methyl resonances.[20] This calculation yields an approximate exchange rate on the order of 5 s^{-1} at 295 K for these protons, which is well within the regime of slow exchange kinetics.

The aromatic phi protons of Δ-$Rh(en)_2phi^{3+}$ were assigned based 2D-NOESY and COSY spectra of the 1:1 complex, as well as the melting experiments described in Section 4.3.3. Consistent empirically with intercalation, the phi proton resonances display large upfield chemical shift movements upon binding to $d(GTGCAC)_2$. The magnitude of shifts (phi (1,8), 1.18 ppm; (2,7), 1.25 ppm; (3,6), 0.55 ppm; and (4,5), 0.58 ppm) indicates that all the phi protons are inserted into the aromatic base stack of DNA upon binding. The relative ordering of these chemical shift movements provides a means to estimate the orientation of the phi ligand within the base stack of DNA. The largest shifts are observed for the phi (1,8) and (2,7) protons, indicating that these protons are located near the center, but in a plane above or below, the center of the G_3 residue where the ring current effects of the aromatic DNA base would most strongly.[23] Such a model necessarily places the (3,6) and (4,5) protons at the edge of the base pair, consistent with their smaller upfield shifts.

In contrast to the sharp, well-resolved resonances of the Δ-Rh(en)$_2$phi^{3+} : d(GTGCAC)$_2$ complex, the titration of the oligonucleotide with Λ-Rh(en)$_2$phi^{3+} yields a pronounced broadening of DNA resonances. As illustrated in Figure 4.2, this broadening occurs at all aromatic and H1' protons, consistent with the low level of sequence selectivity exhibited in the photocleavage studies of Chapter 3. However, the thymine methyl region displays two relatively well-resolved resonances upon addition of Λ-Rh(en)$_2$phi^{3+} (chemical shifts = 1.41 ppm and 1.35 ppm). At a stoichiometry of 1 metal per duplex, it appears that the two forms are present in roughly equivalent amounts, although quantitative integration is not possible due to the broad nature of even these resolved resonances. This result indicates that, despite the low overall selectivity of the Λ-enantiomer, there appears to be a preferential binding site of the complex at the T_2-G_3 step of the oligomer. In such a complex, the removal of the C_2-symmetry of the DNA duplex might be expected to yield two methyl resonances, one resonance shifted by intercalation of Λ-Rh(en)$_2$phi^{3+}, and another resonance very similar to the free oligomer. Further support for this model arises from the spectra of the 1:1 complex at low temperature (Figure 4.3, spectra A, B and C), where two resonances are likewise observed for the A_5 H8 resonance. Binding at this site on the oligomer d(GTGCAC)$_2$ is further consistent with the photocleavage studies presented in Chapter 3, where Λ-Rh(en)$_2$phi^{3+} bound enantioselectively at 5'-GTG-3' sites.

Despite the broad nature of the 1:1 Λ-Rh(en)$_2$phi^{3+} : d(GTGCAC)$_2$ complex at 295 K, assignments of the chemical shifts the phi ligand protons were possible based upon 2D-COSY studies of the 1:1 complex at 285 K. Again, consistent with intercalation, the aromatic protons of the phi ligand display strong upfield movements in chemical shift upon addition to the oligomer. In contrast to the differences noted between the general appearance of Λ- and Δ-Rh(en)$_2$phi^{3+} complexes with d(GTGCAC)$_2$, their apparent binding selectivities, as well as their slightly different exchange rates, there is a remarkable similarity in the upfield chemical shifts between the two enantiomers. The

results, listed in Table 4.2, indicate that the two enantiomers intercalate to a common depth into the base stack of DNA, and therefore the difference in sequence selectivity evident in the spectra of Λ- and Δ-$Rh(en)_2phi^{3+}$: d $(GTGCAC)_2$ complexes is due largely to the interactions of the ancillary ethylene diamine ligands with DNA.

Table 4.2. Chemical shift movements of phi ligand protons upon binding to $d(GTGCAC)_2$ at 295 K.[a,b]

Proton	$Rh(en)_2phi^{3+}$ δ	Λ-$Rh(en)_2phi^{3+}$: DNA δ (change)	Δ-$Rh(en)_2phi^{3+}$: DNA δ (change)
(1,8)	8.37	7.23 (-1.14)	7.18 (-1.19)
(4,5)	8.28	7.67 (-0.61)	7.70 (-0.58)
(3,6)	7.81	7.13 (-0.68)	7.27 (-0.54)
(2,7)	7.63	6.48 [c] (-1.15)	6.38 (-1.25)

a. All data is listed in ppm, referenced to TSP at 295 K.

b. Assignments were based on 2D- NOESY and COSY spectra.

c. This value represents the average of the two phi (2,7) resonances.

Importantly, the phi (2,7) protons appear as two broad resonances at 6.53 and 6.43 ppm in Figure 4.2. While the inequivalence of the phi (2,7) protons may be due to the global loss of C_2-symmetry upon binding of Λ-$Rh(en)_2phi^{3+}$ at the T_2G_3 step, a more likely possibility is that the inequivalence reflects canting of the molecule toward one strand of the helix within an intercalation site. This conclusion is consistent with the observation in Chapter 3 that shape selective recognition by Λ-$Rh(en)_2phi^{3+}$ is accompanied by an unsymmetrical photocleavage pattern, indicative of canting. However, given the broad nature of the DNA and phi proton resonances in the 1:1 complex as well as the low photocleavage selectivity of the Λ-enantiomer, yet another

Figure 4.2. ^{1}H NMR titration of d(GTGCAC)$_2$ with Λ-Rh(en)$_2$phi^{3+} at 295 K. 500 MHz ^{1}H NMR spectra are displayed at metal to duplex ratios of (A) 0, (B), 0.2, (C) 0.4, (D), 0.6, (E), 0.8 and (F) 1.0. The spectrum of free Rh(en)$_2$phi^{3+} under identical solution conditions is given in spectra (G).

In contrast to the Δ-enantiomer, addition of Λ-Rh(en)$_2$phi^{3+} to d(GTGCAC)$_2$ results in broadening of resonances of both the base H8 / H6 and sugar H1' regions. This broadening reflects both the low sequence selectivity of Λ-Rh(en)$_2$phi^{3+} as well as a slightly faster inherent exchange rate. Importantly, there is a loss of C_2-symmetry in both the metal complex (noted in the phi (2,7) protons at 6.43 and 6.53 ppm and the T_2 Me resonance (at R = 1.0, 2 species are clearly present).

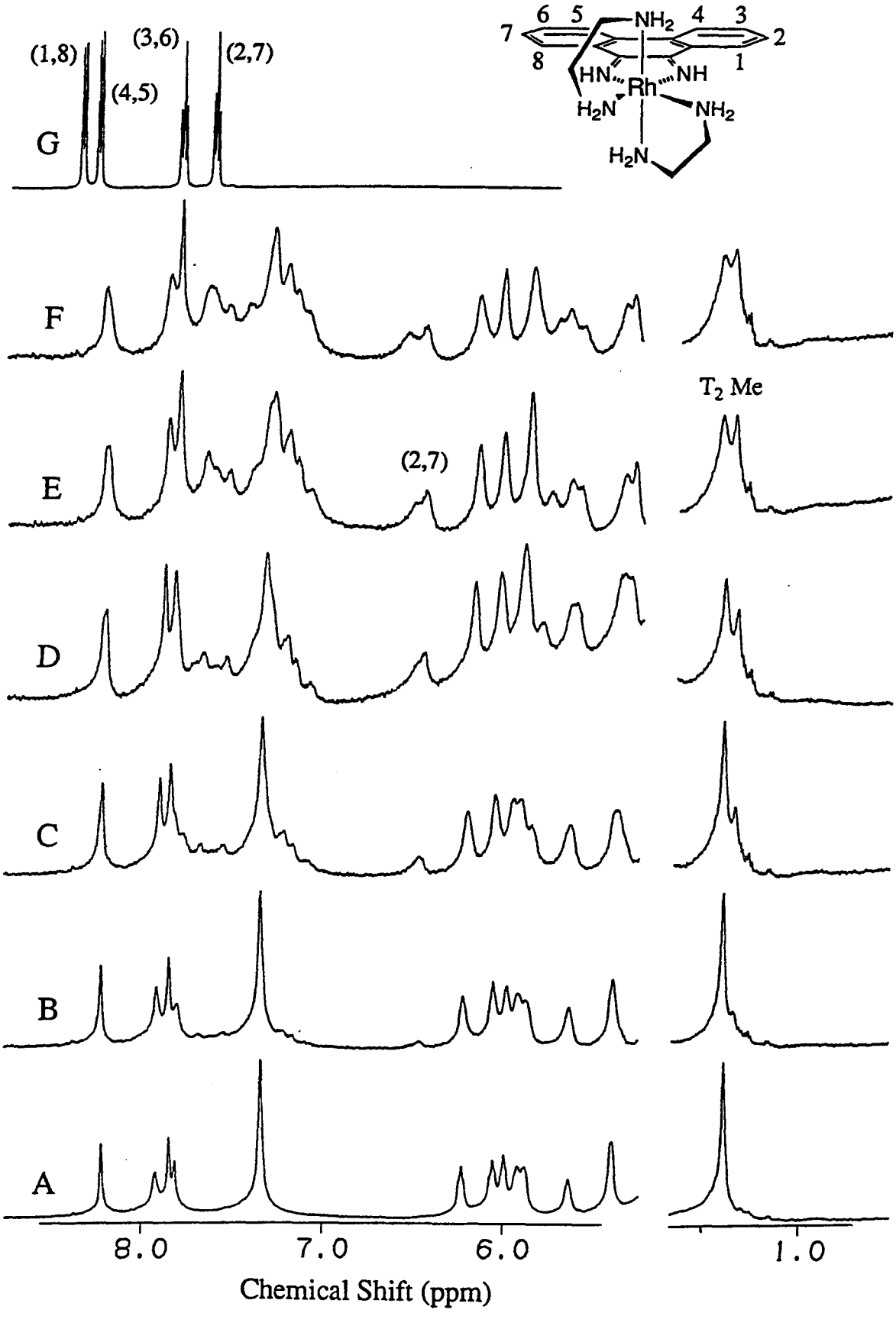
(1,8)
(3,6)
(2,7)
(4,5)
G
F
E
D
C
B
A
(2,7)
T2 Me
8.0
7.0
6.0
1.0
Chemical Shift (ppm)
NH2
HN
NH
Rh
H2N
NH2
H2N

possible interpretation is that the inequivalence of the phi (2,7) protons reflects binding at an alternate site.

Although visual inspection of Figure 4.2 seems to indicate that the complex is in intermediate exchange with the DNA oligomer, a simple estimation of the exchange rate based on the chemical shift difference of two resolved resonances is not possible due to the broadening of resonances and the lack of a single binding site. However, variable temperature experiments described below provide suitable estimates of the exchange rate.

4.3.3. VT-NMR Experiments with of free d(GTGCAC)$_2$, as well as 1:1 complexes with Λ- and Δ- Rh(en)$_2$phi^{3+}.

The binding of intercalators to duplex DNA results in an increase in the duplex melting temperature due to the stabilization of the helix by intercalation.[22,24] Variable temperature ^{1}H-NMR experiments therefore offered a chance to test the hypothesis that the enantiomers of Rh(en)$_2$phi^{3+} bind to DNA through a common motif (full intercalation of the aromatic phi ligand) but with different sequence selectivities due to hydrogen bonding and van der Waals contacts of the ancillary ethylene diamine ligands. Such a model would predict that, despite their differing sequence selectivities, Λ- and Δ-Rh(en)$_2$phi^{3+} should stabilize the helix to a similar degree.

A 1D-NMR variable temperature experiment with free d(GTGCAC)$_2$ is shown in Figure 4.3, while similar experiments with the 1:1 complexes of Λ- and Δ-Rh(en)$_2$phi^{3+} are presented in Figures 4.4 and 4.5 respectively. Spectra were recorded from 280 K to 360 K in increments of 5° K, but the data are displayed at 10° K increments for clarity. As seen in Figure 4.3, a strong melting transition occurs in the free DNA duplex with its center around 330° K. This transition is marked by a strong downfield shifting of the aromatic and H1' resonances as well as pronounced sharpening of the peaks. In Figures 4.4 and 4.5, the melting of the Λ- and Δ-Rh(en)$_2$phi^{3+}: d(GTGCAC)$_2$ complexes also displays a strong melting transition, characterized by the sharpening and shifting of the aromatic and H1' resonances as the temperature increases from 300 K to 360 K. Due to

the broad appearance of resonances in the Λ-$Rh(en)_2phi^{3+}$: $d(GTGCAC)_2$ complex, it is not possible to completely assign the aromatic region of the spectra at all temperatures. However, a direct comparison between the Λ- and Δ-$Rh(en)_2phi^{3+}$ complexes is possible over the entire temperature range for several DNA resonances, as well as the phi (2,7) protons. These results are illustrated graphically as melting curves in Figure 4.7. Importantly, the position of the strong melting transition for in both 1:1 metal DNA complexes is at 335 - 340 K, indicating that the binding of both enantiomers has produced a 5-10° K net stabilization of the duplex, a value consistent with intercalation. Therefore, it appears that both enantiomers stabilize the helix to a similar degree.

In the traces of chemical shift versus temperature shown in Figure 4.4, the A_5 H8 protons in both 1:1 $Rh(en)_2phi^{3+}$: $d(GTGCAC)_2$ complexes exhibit a pre-melting transition between 280 - 320 K. This pre-transition is characterized by a small upfield movement in chemical shift preceding the larger downfield transition associated with duplex melting. Similar pre-transitions are observed in melting curves of several protons in the free DNA (data not shown). Such a pre-transition might be assigned to the fraying of the DNA ends, but the phenomena is not restricted to the G_1 or C_6 residues. It is possible that, given the small size of the oligomer, this pre-transition corresponds to a subtle change in the DNA structure such as an alteration in base pair propeller twisting.

The variable temperature experiments offer a chance to estimate more rigorously the exchange rate of Λ-$Rh(en)_2phi^{3+}$ protons for the duplex according to the relationship:

$$k_c \leq \frac{\pi}{\sqrt{2}} (\Delta \nu_0) \quad , \qquad (1)$$

where k_c is the exchange rate at the coalescence temperature and $\Delta\upsilon_0$ is the chemical shift difference in the slow exchange limit.[25] Based on the difference in chemical shift of the A_5 H8 resonances at 280 K, an upper limit of 55 s^{-1} is placed on the exchange rate at the coalescence temperature of 300 K. Similarly, a value of 100 s^{-1} at 310 K may be estimated based upon the inequivalence of the phi (2,7) resonances at 290 K.

Figure 4.3. Variable temperature study of free $d(GTGCAC)_2$, (Panel A), as well as Λ- and Δ-$Rh(en)_2phi^{3+}$ complexes (Panels B and C). 500 MHz ^1H NMR spectrum (A) - (G) were measured at 280 -360 K in 10° K intervals. In all three panels, a strong melting transition is seen in the sharpening and downfield shifting of the DNA base H8 / H6 and sugar H1' protons. In panels B and C, a similar transition is also observed in the resonances of the phi ligand, most notably the phi (2,7) protons.

Figure 4.3.A. Free d(GTGCAC)$_2$ melting spectra.

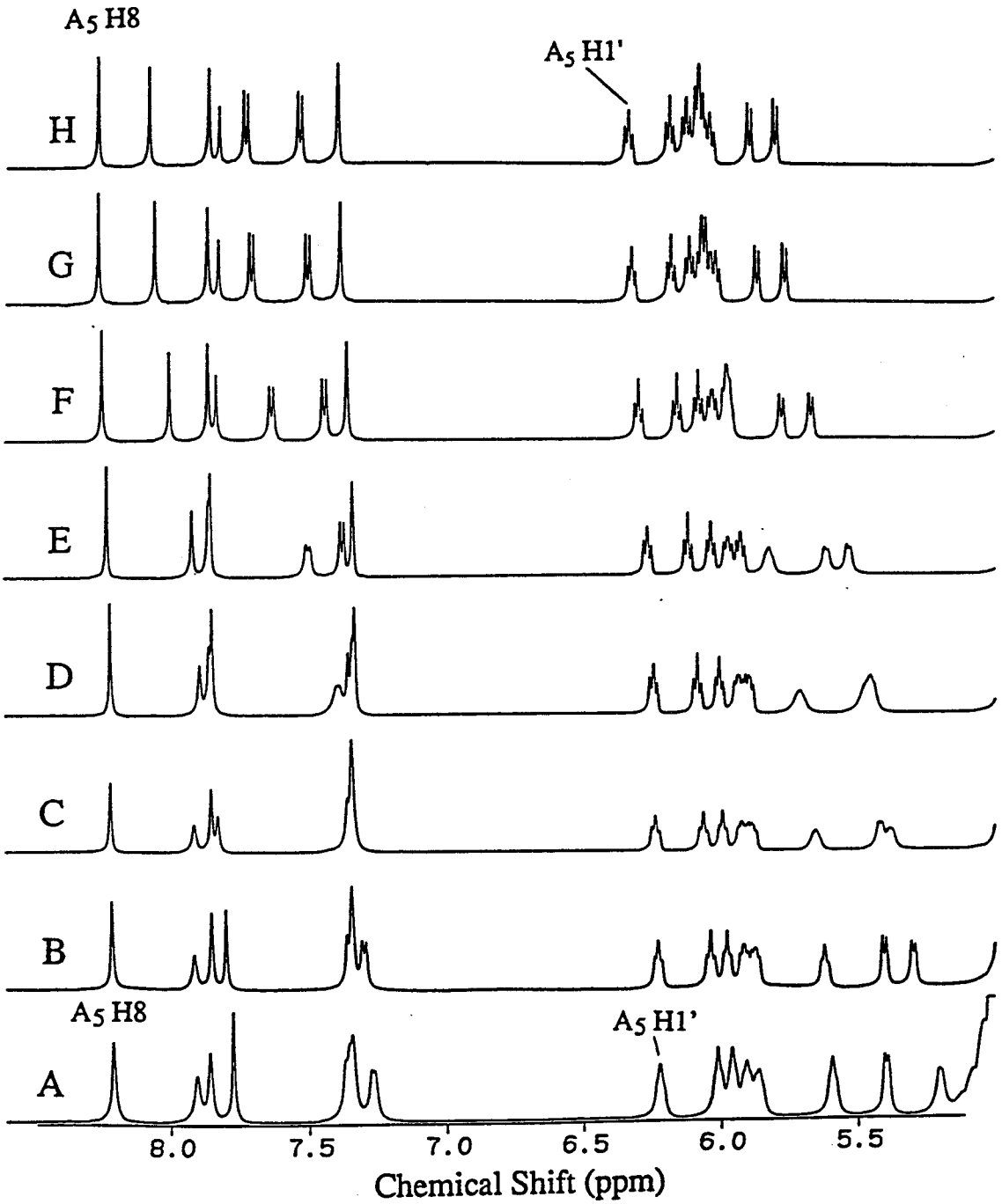

Figure 4.3.B. Λ-Rh(en)$_2$phi^{3+}:d(GTGCAC)$_2$ melting temperature spectra.

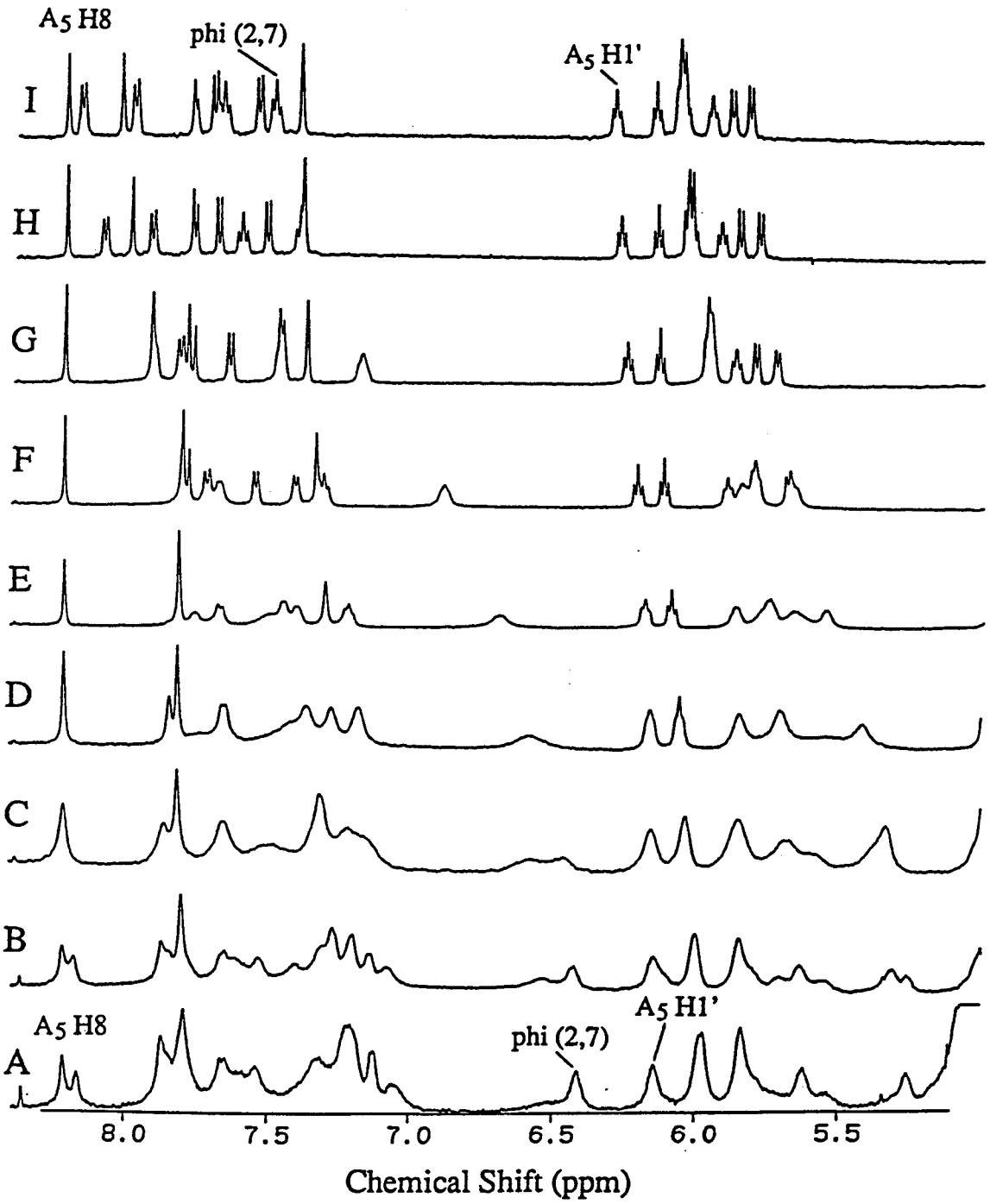

Figure 4.3.C. Δ-Rh(en)$_2$phi^{3+}:d(GTGCAC)$_2$ melting temperature spectra.

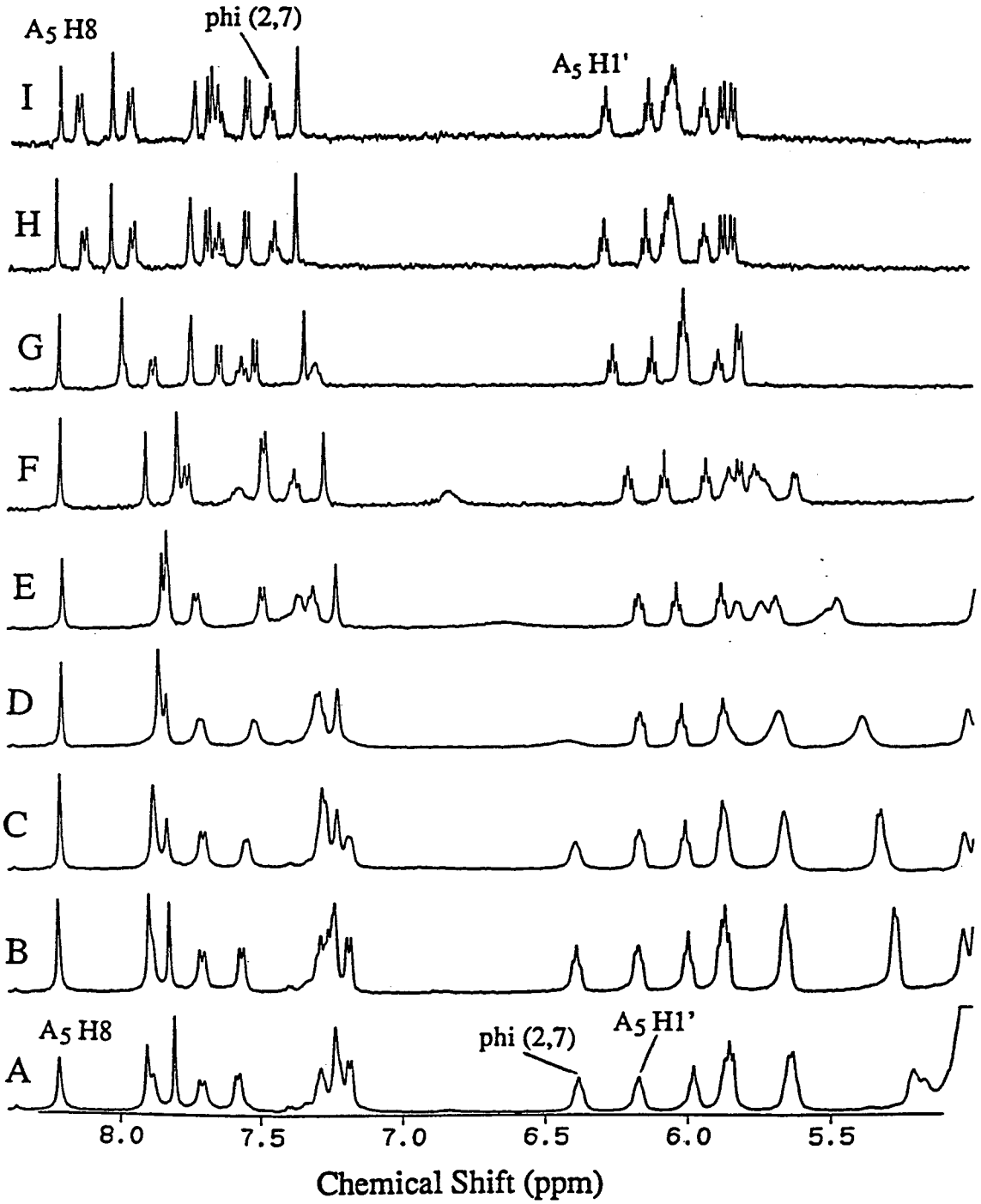

Figure 4.4. Melting curves of free d(GTGCAC)$_2$ duplex, and Λ- and Δ-Rh(en)$_2$phi^{3+} : d(GTGCAC)$_2$ complexes. Spectra in Figure 4.3 were analyzed and the data is displayed here as plots of chemical shift versus temperature for the A_5 H8 , A_5 H1' and phi (2,7) resonances in Panels A, B, and C respectively. In all three panels, free duplex protons are indicated with open circles, while protons from Λ- and Δ-Rh(en)$_2$phi^{3+} : d(GTGCAC)$_2$ complexes are shown with open squares and triangles respectively. Melting points for the complexes may be estimated from the inflection points of these curves.

Note that for both the A_5 H8 and A_5 H1' protons, the Λ- and Δ-Rh(en)$_2$phi^{3+} : d(GTGCAC)$_2$ complexes are stabilized by 5 - 10° K relative to the free duplex. Furthermore, the position of the melting transition of the 1:1 metal : DNA complexes are similar for all three protons shown.

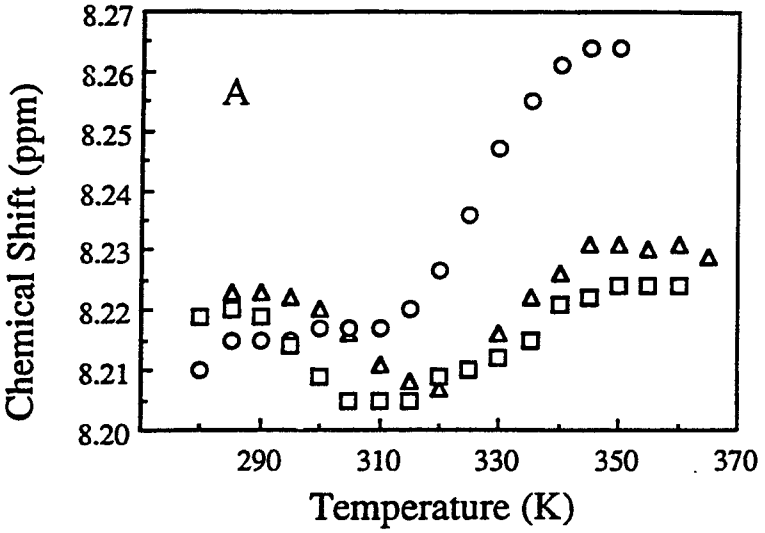
A
Chemical Shift (ppm)
8.27
8.26
8.25
8.24
8.23
8.22
8.21
8.20
290
310
330
350
370
Temperature (K)

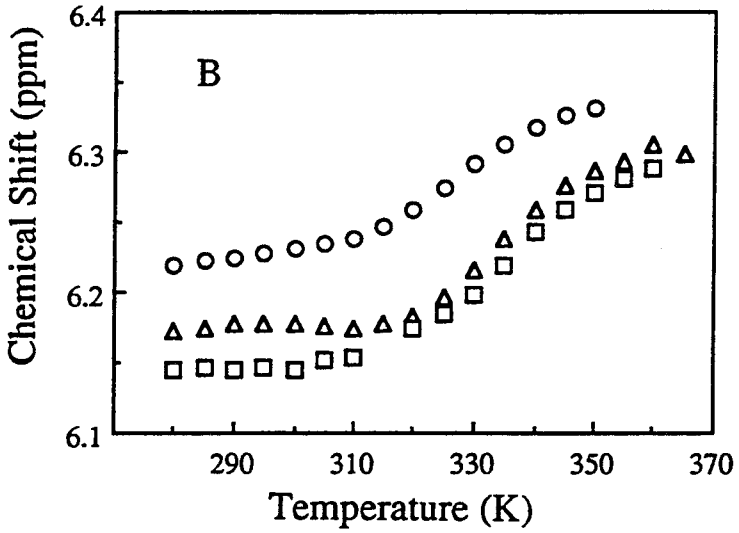
B
Chemical Shift (ppm)
6.4
6.3
6.2
6.1
290
310
330
350
370
Temperature (K)

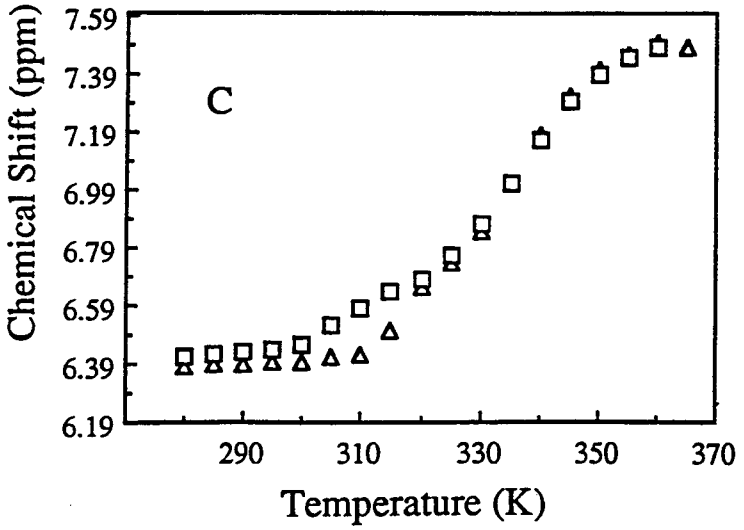
C
Chemical Shift (ppm)
7.59
7.39
7.19
6.99
6.79
6.59
6.39
6.19
290
310
330
350
370
Temperature (K)

One final interesting conclusion from the melting temperature study is that both enantiomers remain associated with the oligomer, even at the highest temperatures recorded. Table 4.3 compares the chemical shifts of the melted duplex with the values observed in both melted 1:1 complexes. While the DNA protons in all 3 melted complexes display relatively similar chemical shifts, the chemical shifts of both enantiomers of $Rh(en)_2phi^{3+}$ are still shifted relative to the spectrum of free $Rh(en)_2phi^{3+}$ at 360 K. This result reinforces the high affinity imparted to these complexes by the 3+ positive charge of the metal center.

Table 4.3. Comparison of free and bound chemical shifts for DNA H8 / H6 and phi ligand protons in the melted state.[a]

Proton	free $d(GTGCAC)_2$[b]	Λ-$Rh(en)_2phi^{3+}$: DNA[c]	Δ-$Rh(en)_2phi^{3+}$: DNA[c]
G_1 H8	8.08	8.05	8.03
T_2 H6	7.39	7.39	7.39
G_3 H8	7.86	7.76	7.77
C_4 H6	7.72	7.70	7.70
A_5 H8	8.26	8.23	8.22
A_5 H2	7.82	7.76	7.77
C_6 H6	7.53	7.57	7.56
---	---	---	---
phi (2,7)	7.71	7.50	7.49
phi (3,6)	7.89	7.68	7.66
phi (1,8)	8.36	8.00	7.98
phi (2,7)	8.45	8.19	8.17

a. All chemical shifts are listed in ppm, referenced to TSP at the corresponding temperature. b. Final temperature = 350 K. c. Final temperature = 360 K.

4.3.4. 2D-NMR experiments with 1:1 Δ-Rh(en)$_2$phi^{3+}: d(GTGCAC)$_2$.

The 1:1 Δ-Rh(en)$_2$phi^{3+} : d(GTGCAC)$_2$ complex was further investigated by 2D-NOE methods to confirm the binding site at the G_3-C_4 step, as well as to gain a more detailed picture of the intercalation site through the observation of intermolecular NOE contacts. In a NOESY spectrum of free d(GTGCAC)$_2$, an NOE is observed between each base H8 or H6 resonance to its own sugar H2'2" protons, as well as to the H2'2" protons of the nucleotide residue in the 5'-direction; this observation is consistent with a B-type conformation for the free duplex.[20,21] However, in the 200 ms NOESY spectrum of Δ-Rh(en)$_2$phi^{3+} : d(GTGCAC)$_2$, (Figure 4.5), there is a complete absence of internucleotide NOE connectivity between the C_4 H6 and G_3 H2'2" protons. This selective NOE loss therefore indicates that the distance between the C_4 H6 proton and the G_3 sugar residue has significantly increased upon binding of Δ-Rh(en)$_2$phi^{3+}. Given the long mixing time used in this experiment, such an NOE contact would be expected if the distance between the G_3 and C_4 base residues in the Δ-Rh(en)$_2$phi^{3+} : d(GTGCAC)$_2$ complex was less than 5 Å. It is noteworthy that this NOE is also absent in a 300 ms mixing time NOESY experiment (data not shown). Coincident with this loss of internucleotide connectivity, we observe new NOE cross peaks between the aromatic phi protons and the G_3 H2'2" protons. Taken together, these observations support the sequence specific intercalation of Δ-Rh(en)$_2$phi^{3+} between the G_3 and C_4 bases of the oligomer.

In attempting to elucidate further the position of Δ-Rh(en)$_2$phi^{3+} within the intercalation site, one may consider the intermolecular NOE contacts between the metal complex and DNA. However, given the small number of non-exchangeable protons on Δ-Rh(en)$_2$phi^{3+} available for such NOE contacts, the 1:1 complex would not be expected to display many intermolecular cross peaks. Also, while there are no contacts observed between the ancillary ethylene diamine protons and the DNA, this result is not surprising given the fact that, as illustrated in Chapter 3, these methylene groups do not affect the

sequence selectivity of the complex. In Figure 4.5, the only strong intermolecular NOE cross peak observed is from the phi (2,7) to the G_3 H2'2" protons above and below the intercalation site, and this interaction is marked by a stronger cross peak to the H2" proton than to H2' proton. There is also a weak cross peak evident between the phi (3,6) and G_3 H2' protons. A similar weak NOE between the phi (1,8) proton and the G_3 H2' resonance is observed in a 300 ms mixing time NOESY experiment (data not shown). There are no contacts evident in either 200 ms or 300 ms NOESY spectra between the phi (4,5) protons and any DNA protons. While these few intermolecular NOE cross peaks do not offer a full picture of the intercalation site, they do complement the absence of NOE connectivity between the G_3 and C_4 residues, and thus support the intercalation of the phi ligand between the G_3 and C_4 residues of the duplex.

4.3.5. Model building and molecular dynamics minimization.

Although the 2D-NMR experiments with Δ-$Rh(en)_2phi^{3+}$: $d(GTGCAC)_2$ do not yield sufficient distance constraints for meaningful energy minimization, such a set of distance constraints was available from the investigation of a related complex, $Rh(NH_3)_4phi^{3+}$: $d(TGGCCA)_2$, by 1D- and 2D-NMR methods.[12] As with the case of Δ-$Rh(en)_2phi^{3+}$: $d(GTGCAC)_2$, 2D NOESY experiments established that $Rh(NH_3)_4phi^{3+}$ intercalates into the hexanucleotide $d(TGGCCA)_2$ from the major groove by complete insertion of the phi ligand between the G_3 and C_4 residues. Due to the lack of non-exchangeable protons on the ancillary ligands of $Rh(NH_3)_4phi^{3+}$, there are again no NOE contacts between the ancillary ligands and DNA. However, the cross peaks observed between the phi ligand and both the G_3 and C_4 sugar residues provided constraints of < 5.5 Å for ten sets of protons. Molecular modeling was carried out in order to explore the positioning of the rigid $Rh(NH_3)_4phi^{3+}$ within this G_3-C_4 step of $d(TGGCCA)_2$.

Figure 4.5. Expansion of a 200 ms mixing time 2D-NOESY spectra at 295 K of the 1:1 Δ-$Rh(en)_2phi^{3+}$: $d(GTGCAC)_2$ complex (0.9 mM in 10 mM phosphate buffer, 20 mM NaCl, pH 7) showing the connectivities between base H8 / H6 protons and the sugar H2'2" protons. The box labeled (A) indicates the absence of internucleotide connectivity between the C_4 H6 and G_3 H2'2". Intermolecular cross peaks are also evident : (B) phi (2,7) to G_3H2'2"; and (C) phi (3,6) to G_3 H2' proton.

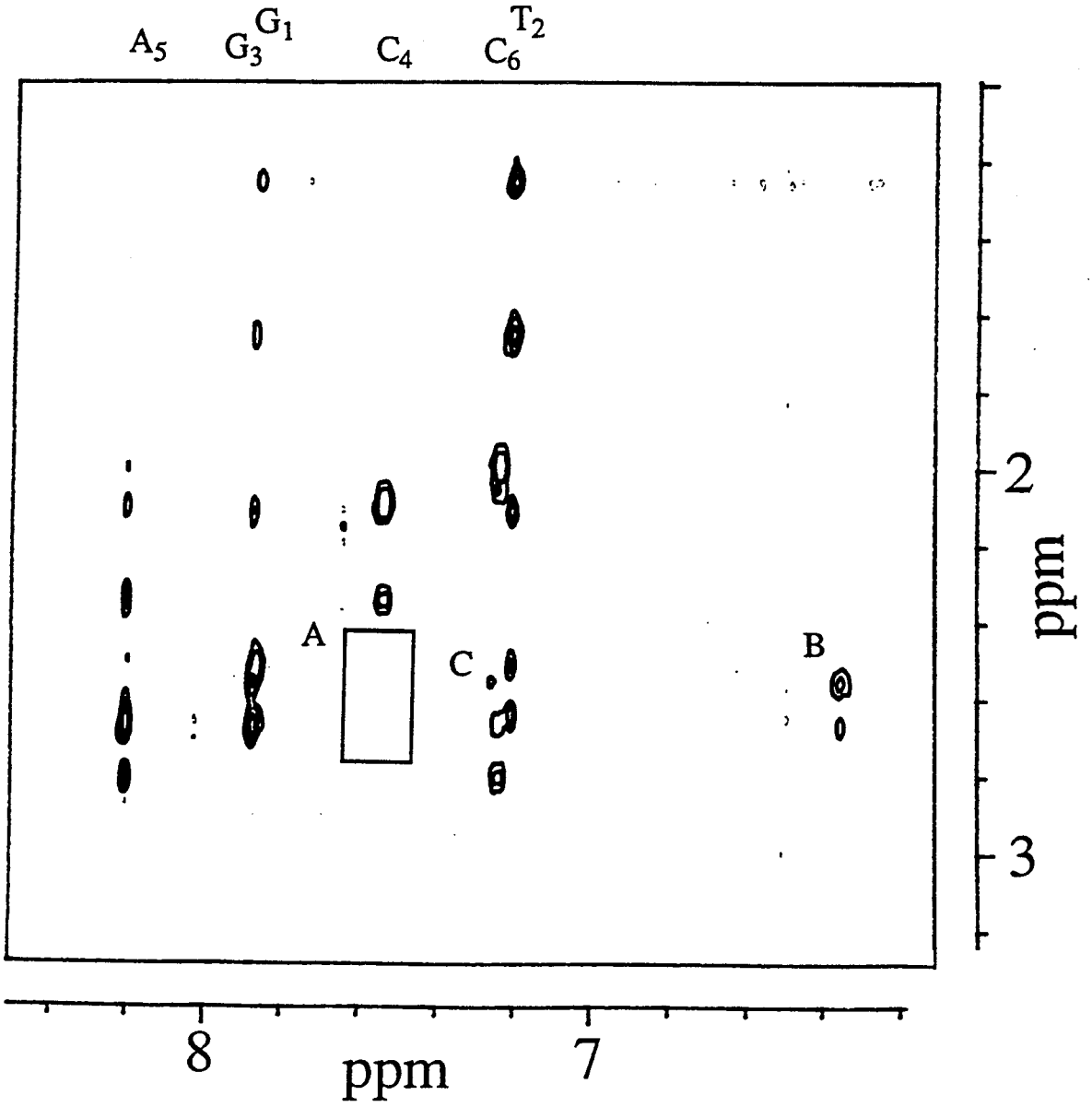
A5
G3
G1
C4
C6
T2
A
C
B
2
3
ppm
8
ppm
7

As starting points for energy minimization, two different models of the intercalation site were constructed, characterized by the state of the sugar puckers at the intercalation site. Although the crystal structures of ethidium and other classical intercalators bound to both RNA and DNA dinucleotides consistently display a mixed sugar pucker (C3'-endo at the 5'-base, C2'-endo at the 3'-base),[6,17] the lack of sequence selectivity of these molecules precludes the observation of such a mixed sugar pucker with duplex DNA. In the case of the specific intercalation of $Rh(NH_3)_4phi^{3+}$ into $d(TGGCCA)_2$, a combination of 2D-COSY and NOESY evidence confirmed that the C_4 sugar residue could be characterized in the C_2' -endo sugar pucker, but no conclusion could be drawn regarding the G_3 sugar residue. Therefore, initial models with both C_2'-endo and C_3'-endo sugar puckering at G_3 were constructed. For simplicity, these will be referred to as the C3'-endo and C2'-endo models.

Based upon plasmid DNA unwinding experiments,[9b] an unwinding angle of 20° per rhodium complex bound was used in the starting structures. For the C2'-endo model of the intercalation site, $d(TGGCCA)_2$ was built from within Insight II as a B-DNA duplex, except that a 6.76 Å rise and a -16° twist (i.e. 20° unwound) parameters were specified at the G_3-C_4 intercalation step. For the C3'-endo model of $d(TGGCCA)_2$, the coordinates at the G_3-C_4 intercalation step were based on the crystal structure of $d(CG)_2$ with the metallointercalator $Pt(terpy)HET^+$.[17] With both DNA models (C2'-endo or C3'-endo), several placements of $Rh(NH_3)_4phi^{3+}$ were examined. The rhodium complex was placed close to each strand, tilted in the site, intercalated deeply in the pocket as well as being positioned at the entry of the site.

Figure 4.6 shows the lowest energy structure with a C3'-endo starting model. Variations in the initial orientation of the metal complex in the site produced negligible differences in the final structure of lowest energy. The details of the structure of minimum energy for C2'-endo models are also quite similar, despite the difference in sugar puckering, which was maintained in the final structures. As illustrated in Figure 4.6, in all of these final models, the phi ligand is seen to stack with the purine bases in the intercalation site. The

pyrimidine bases become propeller twisted away from their initial idealized coplanar orientations, but the purine residues remain parallel to the phi ligand, maximizing stacking overlap between the purine and phi. This result is interesting in light of the noted preference of classical intercalators for 5'-pyrimidine-purine-3' steps, a sequence preference considered to maximize purine-intercalator stacking interactions.[6,17]

The energy-minimized models are also consistent with the upfield chemical shifts seen in the phi aromatic protons on binding to the hexamer. In both C2'-endo and C3'-endo models, the phi (1,8) and (2,7) protons are positioned more directly under the base pairs than the (3,6) and (4,5) protons, and the leading edge of the phi ligand extends into the minor groove of the central GC base step. The phi (1,8) and (2,7) protons are stacked between the cytosine aromatic ring, and the 5 membered ring of the guanosine aromatic base. Theoretical predictions[23] of the shielding effects of the aromatic bases suggests that placing a proton 3.4 Å above the centers of the aromatic rings should produce strong upfield shifts of the order observed experimentally (about 1 ppm). Protons at the periphery of the aromatic bases, such as the phi (3,6) and (4,5) protons, would experience smaller upfield shifts.

The model provides the rationale for the sequence selectivity of the $Rh(NH_3)_4phi^{3+}$ complex. As evident in Figure 4.6, the axial amines of the rigid complex are well positioned for hydrogen bonding to the guanine O^6 atoms. The hydrogen bonds are characterized by a 2.9 - 3.0 Å N -- O distance and a linear N-H --- O alignment for both hydrogen bonds above and below the site of intercalation. Importantly, despite deep intercalative binding in the $Rh(NH_3)_4phi^{3+}$: $d(TGGCCA)_2$ complex, no steric clash is evident between the ancillary NH_3 ligands and the DNA helix. Instead, intercalation of the phi ligand brings the ancillary axial amines into position for hydrogen bond donation.

Figure 4.6. Views perpendicular to (A) and down (B) the helical axis of an energy minimized model of $Rh(NH_3)_4phi^{3+}$ intercalated into the G_3-C_4 steps of $d(TGGCCA)_2$. Shown is an energy minimized model after starting with a mixed sugar pucker at the intercalation site (C_3'-endo model). The metal complex is shown in bold. $Rh(NH_3)_4phi^{3+}$ was manually docked into the G_3-C_4 from the major groove, constrained with the observed NOE contacts, and minimized with the Discover program using a conjugate gradients algorithm. The relative upfield shifts of the aromatic phi protons may be understood in the context of the model, where the maximum upfield shift is seen for the phi (2,7) proton resonances. The selectivity of the metal complex for 5'-GC-3' steps can also be understood based on the hydrogen bonding evident between the axial ammines of the complex and the O^6 atoms above and below the plane of intercalation.

A

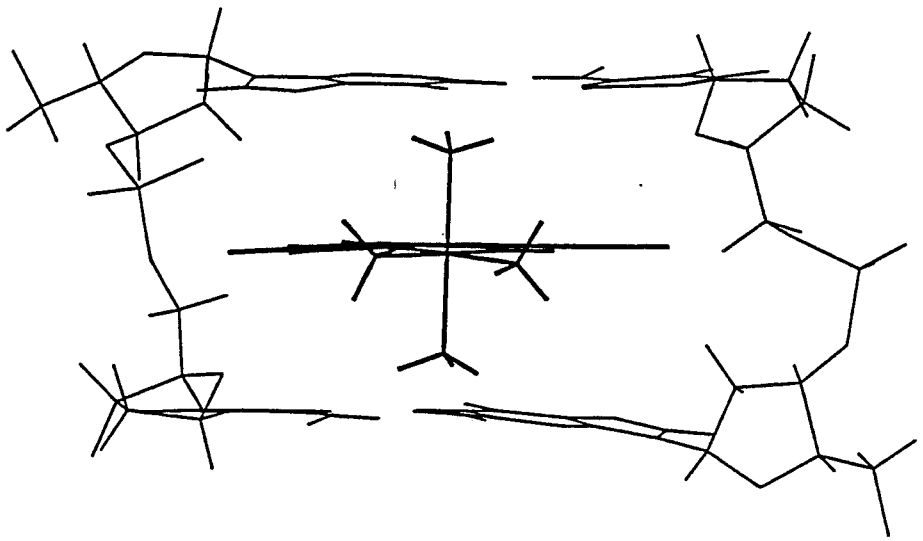

B

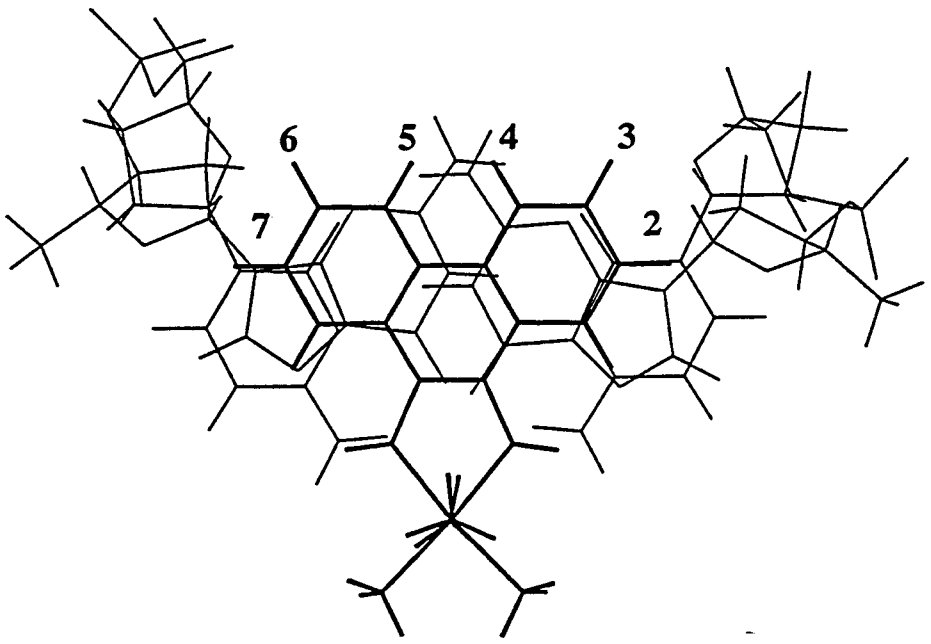

These modeling results therefore support the general mode of binding by these complexes which has been proposed for both $Rh(NH_3)_4phi^{3+}$ and $Rh(en)_2phi^{3+}$.[9b] The complexes intercalate into the DNA base stack through full insertion of the aromatic phi ligand, and this intercalation is characterized by a complete separation of the base pairs. The unstacking of the base pairs is compensated for energetically through the new stacking of guanine bases with the phi ligand. The deep intercalation of the phi ligand ideally positions the axial ammine ligands to donate hydrogen bonds to the O^6 positions of the guanine bases. It is noteworthy here that the chemical shift changes reported here for the case of Λ- and Δ-$Rh(en)_2phi^{3+}$: $d(GTGCAC)_2$ are wholly consistent with those previously reported for $Rh(NH_3)_4phi^{3+}$: $d(TGGCCA)_2$.

4.4. Discussion.

The sequence selectivity of Λ- and Δ-$Rh(en)_2phi^{3+}$ evident in the ^1H NMR results presented here are completely consistent with photocleavage results presented in Chapter 3. The low level of sequence selectivity displayed by Λ-$Rh(en)_2phi^{3+}$ in photocleavage assays is mirrored in the ^{1} H NMR spectra by the pronounced broadening and shifting of $d(GTGCAC)_2$ upon binding. Although it appears that the complex binds selectively at the 5'-TG-3' step of the oligomer, the low selectivity precludes a firm assignment. Also as predicted by photocleavage studies, Δ-$Rh(en)_2phi^{3+}$ binds to $d(GTGCAC)_2$ at the C_3-G_4 step, and disrupts the internucleotide NOE connectivity between the two bases, consistent with intercalation. Although the data presented here does not allow for the quantitative modeling of the binding site, the combination of the strong upfield chemical shifts of the phi (2,7) and (1,8) protons, the loss of internucleotide NOE connectivity and the discovery of new intermolecular NOE contacts clearly places the Δ-$Rh(en)_2phi^{3+}$ deeply within the G_3-C_4 intercalation site.

Importantly, the ^{1}H-NMR results described here provide a sound structural basis for understanding the enantioselectivity in DNA binding of $Rh(en)_2phi^{3+}$. Overall, Λ- and Δ-$Rh(en)_2phi^{3+}$ bind to $d(GTGCAC)_2$ in a very similar fashion, characterized as

classical intercalation, involving the full insertion of the heterocyclic aromatic phi ligand into the DNA base stack. The phi ligand protons of both enantiomers display similar chemical shift changes upon intercalation, and both enantiomers stabilize the helix to thermal denaturation by 5 - 10 ° K. These results are consistent with the observation in Chapter 2 that the enantiomers of $Rh(en)_2phi^{3+}$ were similar in their general characteristics of DNA binding such as plasmid unwinding and hypochromicity. These ^{1}H-NMR results therefore provide a structural validation for the concept of utilizing the $Rh(phi)^{3+}$ moiety to anchor Λ- and Δ-$Rh(en)_2phi^{3+}$ into the major groove of DNA. Once oriented with respect to the DNA helix by intercalation of the phi ligand, the enantiomers of $Rh(en)_2phi^{3+}$ provide a unique opportunity to examine the fundamental contributions of hydrogen bonding and van der Waals contacts to sequence selective DNA recognition.

The presence of high resolution structural data allows us to revisit the molecular models of Λ-and Δ-$Rh(en)_2phi^{3+}$ presented in Chapter 3 in order to question whether the models previously proposed are in fact consistent with the structural evidence presented here. In Figure 4.7, the phi ligands of both Λ- and Δ-$Rh(en)_2phi^{3+}$ are intercalated at a depth similar to that yielded by the energy minimized structure of $Rh(NH_3)_4phi^{3+}$: $d(TGGCCA)_2$. In these models, the stacking of the phi ligand is in accordance with the upfield shifts displayed by both enantiomers; the phi (2,7) and (1,8) protons are stacked to a significantly greater degree than the phi (3,6) and (4,5) protons, which nearly rest in the minor groove of the helix. Importantly, as predicted by these models, the full intercalation of the phi ligand ideally locates the ethylenediamine ligands to engage in hydrogen bonding and van der Waals contacts with the DNA major groove. The full intercalation of the phi ligand serves not to create steric clashes between ancillary ligands and DNA (*ala* shape selectivity), but in fact positions the axial amines and Λ-methylene groups in ideal positions for hydrogen bonding and van der Waals contacts. Thus, one may envision a scheme wherein relatively sequence neutral intercalative binding is followed by weaker interactions which fine-tune the specificity of the metal complex.

Figure 4.7. Molecular models Λ- and Λ-$Rh(en)_2phi^{3+}$ intercalated into 5'-GC-3' and 5'-TA-3' steps. Shown are views down the helical axis (A), as well as perpendicular to the axis (B). In order to show the depth of intercalation, the phi ligand protons have been numbered. The intercalation of both Λ-and Δ-$Rh(en)_2phi^{3+}$ is similar in depth to the energy minimized structure of $Rh(NH_3)_4phi^{3+}$ discussed in the text. Importantly, when the enantiomers of $Rh(en)_2phi^{3+}$ are intercalated in accordance with the structural data gathered via ^{1}H-NMR methods, the ancillary ethylene diamine ligands are ideally located to engage in hydrogen bonding and van der Waals contacts as described. As the views in Panel B show, Λ- and Δ-$Rh(en)_2phi^{3+}$ are again positioned for the van der Waals contacts (at 4.0 Å) and hydrogen bonding (at 3.0 Å).

A

Λ-Rh(en)$_2$phi^{3+} : 5'-TA-3' step.

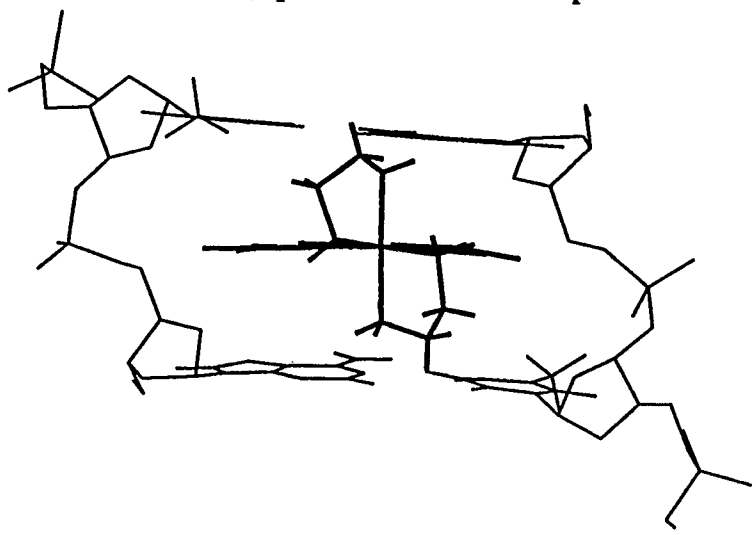

B

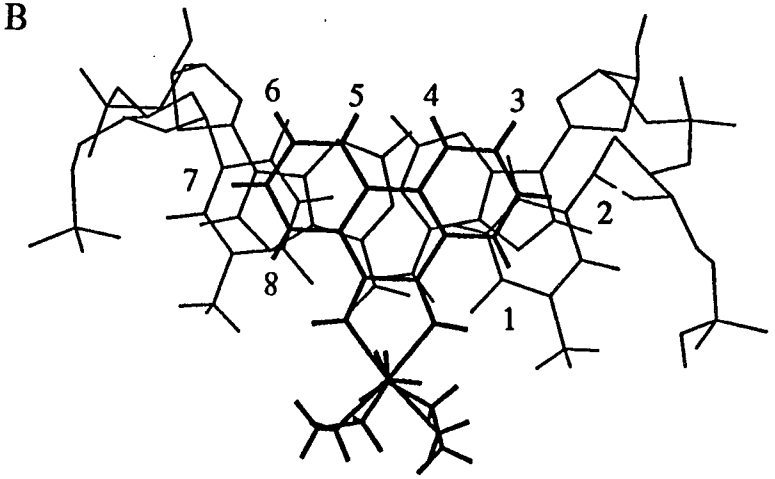

A

Δ-Rh(en)$_2$phi^{3+} : 5'-GC-3' step.

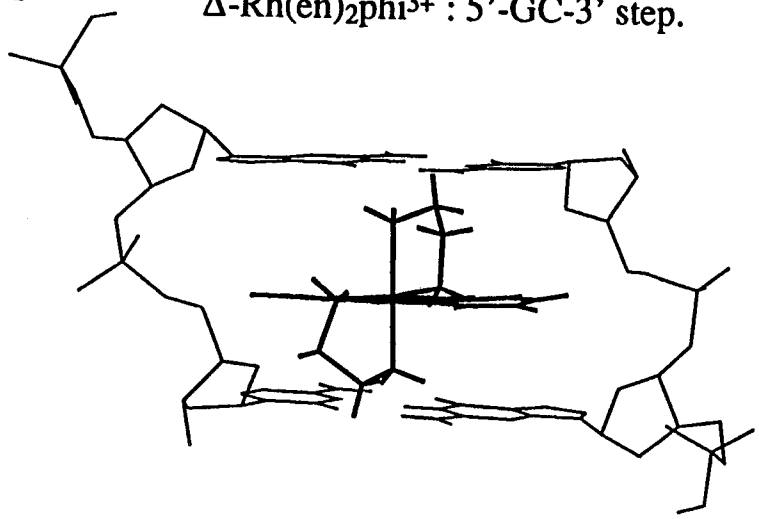

B

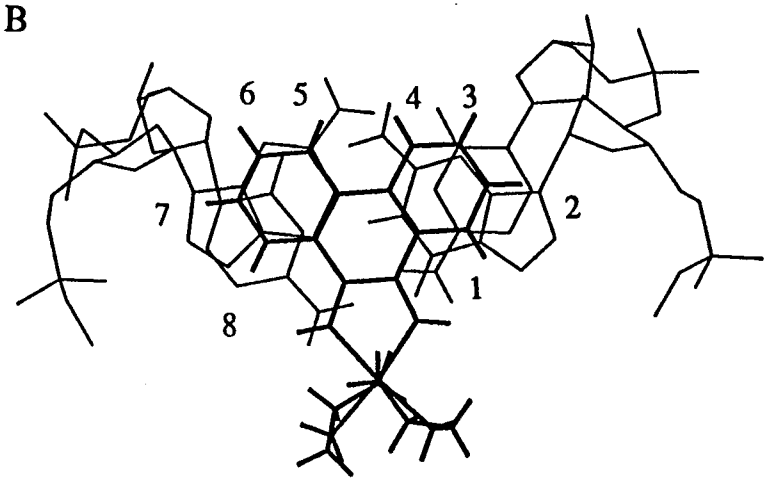

While the photocleavage of DNA by $Rh(phen)_2phi^{3+}$ produces cleavage at the 5'-residue of an intercalation site, it was noted in Chapter 3 that photocleavage by the smaller $Rh(en)_2phi^{3+}$ complexes was often characterized by cleavage at both 5'- and 3'-residues of the intercalation site. The ^1H - NMR results described here also shed light on the novel chemistry of $Rh(N_4)phi^{3+}$ ($N_4 = (NH_3)_4$, $(en)_2$, cyclen) complexes at the 3'-sugar of the intercalation site. Relative to the partial intercalation of the phi ligand in the shape selective molecule $Rh(phen)_2phi^{3+}$, the deeper intercalation of the smaller $Rh(en)_2phi^{3+}$ allows access to the 3'-sugar of the intercalation site. Cleavage at both sugar residues of an intercalation site is also noted for the complex Λ-$Rh(MGP)_2phi^{3+}$ (Figure 4.8).[26] Based upon photocleavage assays, as well as a novel assay designed to probe inherent DNA twistability, it has been proposed that the phi ligand of this complex is again allowed to fully insert due to the large degree of unwinding of DNA noted upon binding. Thus both $Rh(en)_2phi^{3+}$ and Λ-$Rh(MGP)_2phi^{3+}$ act to eliminate the constraints of the right-handed sugar phosphate backbone, albeit by vastly different means, and the net result is cleavage at both the 5'- and 3'- sugars of a DNA intercalation site.

Interestingly, molecular modeling predicts that the H2' proton is the most directly accessible proton of the 3'-sugar. Although H atom abstraction is disfavored energetically by 2 kcal/mol relative to the H3' position, the effective reactivity would be expected to be highly controlled by accessibility.[27] Furthermore, initial abstraction of the H2' atom would likely be followed by fast H atom migration from the *cis*-positioned H3' (not the *trans*-oriented H1') and thus, the overall chemistry would appear to occur at the C3' position of the sugar. Such a model might be tested through substitution of ribonucleotides into an otherwise DNA duplex, since the C2'-radical would be stabilized by substitution with the heteroatom.

Finally, the NMR evidence presented here may be discussed in reference to other studies of metallointercalators via ^{1}H-NMR; the presence of NMR data concerning the DNA binding of Δ-$Ru(phen)_3^{2+}$,[9,28] Δ-$Rh(phen)_2phi^{3+}$,[10] $Rh(NH_3)_4phi^{3+}$,[11] and now Λ- and Δ-$Rh(en)_2phi^{3+}$ allows for interesting and informative comparisons to be made among them. The chemical shift movements for these five complexes upon binding to oligonucleotides are given in Table 4.4. The resonances of the peripheral phenanthroline (4,7) and (5,6) protons of $Rh(phen)_2phi^{3+}$ show virtually no movement upon binding to DNA. In contrast, the phi proton resonances of all four $Rh(phi)^{3+}$ complexes show significant upfield shifts as a result of selective intercalation of the phi ligand into the base stack. This pattern indicates that when an ancillary phenanthroline ligand is located in the DNA groove little or no chemical shift movement is expected for the phenanthroline (4,7) or (5,6) resonances. However, the phenanthroline (4,7) and (5,6) resonances of Δ-$Ru(phen)_3^{2+}$ do show significant upfield movement in chemical shift upon oligonucleotide binding. This upfield shift indicates that one of the phenanthroline ligands is likely intercalated. Furthermore, because the binding of $Ru(phen)_3^{2+}$ to the oligonucleotide occurs with fast exchange on the NMR time scale, the upfield chemical shift movements observed for the phenanthroline protons represent the exchange-averaged movement of all three phenanthroline ligands. On this basis, the upfield shifts shown by the phenanthroline resonances of Δ-$Ru(phen)_3^{2+}$ on binding to DNA are completely consistent with the larger chemical shift movements shown by the phi ligand protons of Δ-$Rh(phen)_2phi^{3+}$, $Rh(NH_3)_4phi^{3+}$, and the enantiomers of $Rh(en)_2phi^{3+}$, all of which bind by intercalation. For comparison, intercalated proton resonances of ethidium bromide displays upfield shifts of 0.75 ppm on average.[22] With octahedral metallointercalators, as with classical organic intercalators, then, a substantial upfield chemical shift of protons on the aromatic ligand may be viewed as a signature of the intercalation of that ligand.

Table 4.4. Upfield chemical shift movements in metal complexes upon oligonucleotide binding.

Proton	Δ-Ru(phen)$_3^{2+}$ (ppm)	Δ-Rh(phen)$_2$phi^{3+} (ppm)	Rh(NH$_3$)$_4$phi^{3+} (ppm)	Λ-Rh(en)$_2$phi^{3+} (ppm)	Δ-Rh(en)$_2$phi^{3+} (ppm)
phen (2,9)	0.17	-0.18, 0.15			
phen (3,8)	0.16	-0.05, -0.18			
phen (4,7)	0.28	0.04, -0.02			
phen (5,6)	0.31	0.01			
	---	---	---	---	---
phi (1,8)		0.58	0.84	1.14	1.18
phi (2,7)		0.83	1.10	1.15	1.25
phi (3,6)		0.88	0.60	0.68	0.55
phi (4,5)		0.73	0.59	0.61	0.58

a. Data for Δ-Ru(phen)$_3^{2+}$, Δ-Rh(phen)$_2$phi^{3+}, and Rh(NH$_3$)$_4$phi^{3+} are taken from references 9 ,10, and 12 respectively.

b. Upfield movements in chemical shifts upon binding oligonucleotides are listed in this table as positive values.

b. Data are reported for Δ-Ru(phen)$_3^{2+}$, Λ- and Δ-Rh(en)$_2$phi^{3+} bound to d(GTGCAC)$_2$ and Δ-Rh(phen)$_2$phi^{3+} bound to d(GTCGAC)$_2$.

The relative upfield chemical shift movements of the intercalated ligands in these complexes reflects the fundamental differences in the means of achieving for sequence selectivity. While comparisons of absolute chemical shift changes for different ligand systems are difficult, parallels may be drawn with respect to relative shift movements for different resonances. With Δ-$Ru(phen)_3^{2+}$ and Δ-$Rh(phen)_2phi^{3+}$, steric clashes of ancillary phenanthroline protons with the DNA bases precludes the deep intercalation of the coordinated ligand; the largest chemical shift changes for these complexes are seen in the peripheral phenanthroline (5,6) and phi (3,6) protons which are located at the leading edge of the intercalating ligand. For $Ru(phen)_3^{2+}$, this results in the weak overall binding affinity of the molecule ($K_b \sim 10^3$-10^4 M^{-1}), and little, if any, sequence selectivity.[29] For $Rh(phen)_2phi^{3+}$, the larger surface area of the phi ligand provides high binding affinity even with partial intercalation, and thus the complex displays shape selective DNA binding and are probes of the sequence dependent structural polymorphism of DNA.[8,9]

Due to the small ancillary ligands of $Rh(NH_3)_4phi^{3+}$ and $Rh(en)_2phi^{3+}$, full insertion of the phi ligand is possible; the largest shifts with these complexes are seen at the phi (2,7) positions, at the side of the intercalating ligand. $Rh(NH_3)_4phi^{3+}$ and $Rh(en)_2phi^{3+}$ are therefore positioned deeply in the intercalation pocket which brings the ancillary ligands into the proper orientation to engage in hydrogen bonding and van der Waals contacts. This full insertion also permits a larger surface area for overlap with the DNA base pairs, and hence likely a larger average DNA binding affinity than $Rh(phen)_2phi^{3+}$.

The 2D-NOESY studies of these complexes may be best understood in terms of their exchange properties and sequence selectivities. Since Δ-$Rh(phen)_2phi^{3+}$, $Rh(NH_3)_4phi^{3+}$ and Δ-$Rh(en)_2phi^{3+}$ bind to DNA sites with high specificity, a sequential internucleotide NOE walk is expected to reveal a loss of NOE intensity selectively at the site of intercalation. Indeed, for $Rh(NH_3)_4phi^{3+}$ [12] and Δ-$Rh(en)_2phi^{3+}$ which are both within the slow exchange regime, a complete loss of internucleotide NOE intensity is

observed at the binding site; for Δ-Rh(phen)$_2$phi^{3+}, a loss in internucleotide NOE intensity is also observed.[10] For Ru(phen)$_3^{2+}$, the absence of this loss of NOE intensity has been taken as evidence against intercalation,[28] but with the fast exchange kinetics and lack of sequence specificity of Ru(phen)$_3^{2+}$, little reduction in internucleotide NOE intensity should be expected.

It is also noteworthy that the 2D-NOESY data reveal intermolecular NOE's for Ru(phen)$_3^{2+}$ [28] and Δ-Rh(phen)$_2$phi^{3+} [10] to AH2 protons in the minor groove; for Rh(NH$_3$)$_4$phi^{3+} no direct NOE's (without spin diffusion) can be attributed to minor groove interaction. Importantly, the 2D-NOESY data for Δ-Rh(phen)$_2$phi^{3+},[10] Rh(NH$_3$)$_4$phi^{3+},[12] and Δ-Rh(en)$_2$phi^{3+} bound to oligonucleotides indicate several intermolecular NOE contacts to major groove protons, and, in the presence of Ru(phen)$_3^{2+}$,[9] a substantial shift in the thymine methyl resonance is observed. These data are consistent with at least two binding modes for Ru(phen)$_3^{2+}$ and to some extent for Δ-Rh(phen)$_2$phi^{3+} under these conditions of high concentration and low ionic strength; the phenanthroline ligands may promote hydrophobic association in the minor groove.[29] For Rh(NH$_3$)$_4$phi^{3+} and Δ-Rh(en)$_2$phi^{3+}, both containing small saturated ancillary ligands capable only of donating hydrogen bonds, no similar minor groove association is detected. Instead binding to the oligonucleotide by these polyamine Rh(phi)$^{3+}$ complexes occurs through a single mode - deep intercalation from the major groove.

Finally, although intercalation has long been recognized as a central motif of DNA binding by numerous small molecules and drugs,[6,17] high resolution study of the structural effect of intercalation upon duplex DNA have been hindered by the low sequence selectivity and intermediate exchange kinetics of these simple intercalators.[22] The slow exchange kinetics and relatively high sequence selectivity displayed in the current study of Δ-Rh(en)$_2$phi^{3+} offers hope that similar studies with other polyamine Rh(phi)$^{3+}$ complexes will yield the first high-resolution models of intercalation into

duplex DNA.[13] This work will possibly answer several long-standing questions regarding DNA intercalation, such as whether or not the 5'-base of an intercalation step is truly locked into the C3'-endo conformation , or whether this mixed sugar pucker observed in dinucleotide crystal structures is a unique artifact of the nature of these studies. Another interesting question to be addressed is whether better stacking follows intercalation into 5'-pyrimidine-purine-3' steps, as observed in the numerous dinucleotide crystal structures. In the distance restrained energy minimization of $Rh(NH_3)_4phi^{3+}$: $d(TGGCCA)_2$, excellent stacking interactions were observed at a 5'-purine - pyrimidine - 3' step between the purine bases and the phi ligand. Again, the utility of polyamine $Rh(phi)^{3+}$ complexes in approaching these fundamental issues lies both in their relatively high specificity and exchange properties.

4.5. Conclusions.

This chapter provides structural evidence that both Λ- and Δ-Rh(en)$_2$phi^{3+} bind to DNA by the full intercalation of the heterocyclic aromatic phi ligand between the base pairs of DNA. Following this high affinity (but likely sequence neutral) binding event, the sequence selectivity of DNA binding is determined by an array of non-covalent contacts between the ancillary ethylene diamine ligands and the major groove of DNA. Importantly, the deep intercalation of the phi ligand does not cause clashes between the DNA and the small ancillary ligands, but rather, ideally positions the molecule to engage in hydrogen bonding and van der Waals contacts with the major groove of DNA. In molecular models based on this hypothesis, the axial amines of Δ-Rh(en)$_2$phi^{3+} are well positioned to make hydrogen bonding contacts to the guanine O^6 atoms above and below the intercalation site. Although Λ-Rh(en)$_2$phi^{3+} binds to DNA in essentially sequence neutral fashion, the fundamental intercalative event is similar to that with Δ-Rh(en)$_2$phi^{3+}. Therefore in addition to hydrogen bond donation, the deep intercalation of the Λ-enantiomer places the methylene groups of the ancillary ligands in the proper spatial orientation to engage in positive van der Waals contacts with the methyl groups of thymine residues. The clean 1:1 binding and slow exchange behavior of the Δ-Rh(en)$_2$phi^{3+} : d(GTGCAC)$_2$ complex are both promising indications that similar studies with other polyamine Rh(phi)$^{3+}$ complexes will provide the first high resolution structure of sequence specific intercalation.

The concept of utilizing the intercalation of the Rh(phi)$^{3+}$ moiety as an anchor in the major groove of DNA allows not only the exploration of discrete elements of molecular recognition as described here, but also points to a more general strategy for the design of sequence specific DNA binding molecules based upon metallointercalation. Finally, the current results reinforce the value of a detailed structural model in understanding DNA recognition.

Footnotes and References.

1. (a) Pyle, A. M.; Long, E. C.; Barton, J. K. *J. Amer. Chem. Soc.* **1989**, *111*, 4520. (b) Pyle, A. M.; Morii, T.; Barton, J. K. *J. Amer. Chem. Soc.* **1990**, *112*, 9432 - 9434.
2. Sitlani, A.; Long, E. C.; Pyle, A. M.; Barton, J. K. *J. Amer. Chem. Soc.* **1992**, *114*, 2303.
3. (a) Chow, C. S.; Behlen, E. S.; Uhlenbeck, O. C.; Barton, J. K. *Biochem.* **1992**, *31*, 972. (b) Chow, C. S.; Hartman, K.M.; Rawlings, S.L.; Huber, P.W.; Barton, J.K. *Biochem.* **1992**, *31*, 3534. (c) Lim, A.C.; Barton, J.K. *Biochem.* **1993** *32*, 11029-11034.
4. (a) Sitlani, A.S.; Dupureur, C.M.; Barton, J.K. *J. Am. Chem. Soc.* **1993**, *115*, 12589. (b) Campisi, D.; Morii, T.; Barton J.K. *Biochem.* **1994**, *33*, 4130.
5. (a) Brenowitz, M.; Senear, D.F.; Shea, M.A.; Ackers, G.K. *Methods Enzymol.* **1986**, *130*, 132. (b) Brenowitz, M.; Senear, D.F.; Shea, M.A.; Ackers, G.K. *Proc. Natl. Acad. Sci. U.S.A.* **1986**, *83*, 8462. (c) Senear, D.F.; Brenowitz, M.; Shea, M.A.; Ackers, G.K.Ackers *Biochem.* **1986**, *25*, 7344.
6. (a) Anderson, J.E.; Ptashne, M.; Harrison, S.C. *Nature* **1987**, *326*, 846. (b) Ptashne, M. *A Genetic Switch, Second Edition*; Cell Press, Cambridge,1992.
7. Searle, M.S. *Prog. NMR Spec.* **1993**, *25*, 403.
8. (a) Pelton, J.G.; Wemmer, D.E. *Proc. Natl Acad. Sci. U.S.A.* **1989**, *86*, 5723. (b) Wu, W.; Vanderwall, D.E.; Stubbe, J.A.; Kozarich, J.W.; Turner, C.W. *J. Amer. Chem. Soc.* **1995**, *116*, 10843. (c) Gao, X.; Patel, D.J. *Biochem.* **1989**, *28*, 751.
9. (a) Rehmann, J. P.; Barton, J. K. *Biochem.*, **1990**, *29*, 1701. (b) Rehmann, J. P.; Barton, J. K. *Biochem.*, **1990**, *29*, 1710.
10. David, S. D.; Barton, J. K. *J. Am. Chem. Soc.* **1993**, *115*, 2984.
11. Dupureur, C.M.; Barton, J.K. *J. Am. Chem. Soc.* **1993**, *116*, 1086.
12 Collins, J.G.; Shields, T.P.; Barton, J.K. *J. Am. Chem Soc.* **1994**, *116*, 9840.

13. Hudson, B.P.; Collins, J.G.; Barton, J.K. unpublished results.

14. (a) Schaefer, W. P.; Krotz, A. H.; Kuo, L.Y.; Shields, T. P.; Barton, J. K. *Acta Cryst.* **1992**, *C48*, 2071. (b) Krotz, A.H.; Kuo, L.Y.; Shields, T.P.; Barton, J.K. *J. Am. Chem Soc.* **1993** , *115*, 3877.

15. Marion, D.; Wuthrich, K. *Biochem Biophys. Res. Comm.* **1983**, *113*, 967.

16. Krotz, A.H.; Kuo, L.Y.; Barton, J.K. *Inorg. Chem* **1993**, 32, 5963.

17. Wang, A.H.J.; Nathans, J.; van der Marel, G.; van Boom, J.H.; Rich, A. *Nature* **1978**, *276*, 471.

18. Haworth, I. S.; Elcock, A. H.; Freeman, J.; Rodger, A.; Richards, W.G. *J. Biol. Mol. Struct. Dyn.* **1991**, *9*, 23.

19. (a) Veal, J.W.; Wilson, W. D. *J. Biomol. Structure & Dynamics* **1991**, *8*, 1119. (b) Weiner, S. J.; Kollman, P. A.; Nguyen, D. T.; Case, P. A., *J. Comp. Chem.*, **1986**, *7*, 230. (c) Weiner, S. J.; Kollman, P. A., Case, D. A.; Singh, U. C.; Ghio, C.; Alagana, G.; Piotete, S.; Weiner, P. *J. Am. Chem. Soc.* **1984**, *106*, 765.

20. Wuthrich, K. *NMR of Proteins and Nucleic Acids;* Wiley: New York, **1986.**

21. (a) Patel, D. J.; Shapiro, L.; Hare, D. *J. Biol. Chem.* **1986**, *261*, 1223. (b) Patel, D. J.; Shapiro, L. *J. Biol. Chem.* **1986**, *261*, 1230. (c) Patel, D. J., Shapiro, L. *Biopolymers*, **1986**, *25*, 707. (d) Liu, X. L.; Chen, H.; Patel, D. J. *J. Biomolecular NMR*, **1991**, *1*, 323.

22. (a) Feigon, J.; Denny, W. A.; Leupin, W.; Kearns, D. R. *J. Med. Chem.* **1984**, 450. (b) Patel, D. J.; Canuel, L. L. *Biopolymers* **1977**, *16*, 857. (c) Patel, D. J.; Shen, C. *Proc. Natl. Acad. Sci.* **1978**, *75*, 2553. (d) Wilson, W. D.; Krishnamoorthy, C. R.; Wang, Y. H.; Smith, J. C. *Biopolymers* **1985**, *24*, 1941. (e) Chandrasekaran, S.; Jones, R. L.; Wilson, W. D. *Biopolymers* **1985**, *24*, 1941. (f) Delbarre, A.; Gourevitch, M. I.; Gaugain, B.; Le Pecq, J. B.; Roques, B. P. *Nuc. Acids Res.* **1983**, *11*, 4467.

23 Giessner-Prettre, C.; Pullman, B. *Biochem. Biophys. Res. Commun.* **1976**, *70*, 578.

24. Cantor, C.R.; Schimmel, P.R. *Biophysical Chemistry, Part. III*; W.H. Freeman and Co.; San Francisco, 1980.

25. Becker, E.D., *High Resolution NMR : Theory and Chemical Appplications, Second Edition*; Academic Press; New York, 1980.

26. Terbreuggen, R.H.; Barton, J.K. submitted for publication.

27. Miaskiewicz, C.; Osman, R. *J. Am. Chem. Soc.* **1994**, *116*, 232-238.

28. Eriksson, M.; Leijon, M.; Hiort, C.; Norden, B.; Graslund, A. *J. Am. Chem. Soc.* **1992**, *114*, 4933; *Biochem.*, **1994**, *33*, 5031.

29. Mei, H. Y.; Barton, J. K. *Proc. Natl. Acad. Sci., USA* **1988**, *85*, 1339.

30. Based on NMR and luminescence experiments, we have proposed that $Ru(phen)_3^{2+}$ binds DNA with low overall affinity through two primary modes, partial intercalation in the major groove and hydrophobic binding against the surface of the minor groove.

Chapter 5. Conclusions and Perspectives

The design synthetic molecules capable of sequence specific recognition of DNA is an alluring field for the chemist today.[1,2] Such molecules hold promise as new pharmaceuticals, and as new tools for biotechnology. In the Barton group, we design simple, structurally defined transition metal complexes to explore the fundamental questions of how a DNA binding protein recognizes its DNA target with high affinity and specificity. We have found that these molecules recognize DNA, like proteins, through an ensemble of non-covalent contacts in the major groove.[3]

The focus of this thesis has been the sequence selective recognition of DNA by the enantiomers of $Rh(en)_2phi^{3+}$. Both enantiomers bind strongly to DNA via intercalation of the aromatic phi ligand into the major groove of DNA, and photocleave DNA upon irradiation with UV light. These small metallointercalators display a marked enantioselectivity in binding and cleavage of DNA, a remarkable feat given their small size relative to a single dinucleotide step along the DNA helix. Oligonucleotide photocleavage assays reveal that this enantioselectivity is due to an array of non-covalent interactions between the ancillary ethylene diamine ligands and the major groove of DNA. Δ-$Rh(en)_2phi^{3+}$ displays a reasonably high level of selectivity for 5'-GC-3' steps due to hydrogen bonding contacts between the axial amine ligands of the metal complex and the O^6 position of guanine residues. Although the Λ-enantiomer is also capable of donating hydrogen bonds to DNA, it is not a sequence selective molecule since it also recognizes 5'-TX-3' steps through positive van der Waals contacts with the 5-methyl group of thymine.

These elements of recognition were also explored via ^1H NMR methods. While both enantiomers interacted with the duplex $d(GTGCAC)_2$ via complete insertion of their phi ligand, the spectra of the 1:1 complexes was quite different, reflective of the enantioselectivity observed in photocleavage studies. As predicted, Δ-$Rh(en)_2phi^{3+}$

Figure 5.1. Four-base pair (bp) recognition of 5'-TGCA-3' sequences by the complex Δ–α-Rh(R,R-Me_2trien)phi^{3+}. Shown on the left is the isomeric configuration which was predicted to bind to the sequence 5'-TGCA-3' through a combination of hydrogen bonding and van der Waals interactions. On the right is shown the schematic of the recognition elements : van der Waals contacts are shown in circles, while hydrogen bonding contacts are boxed.

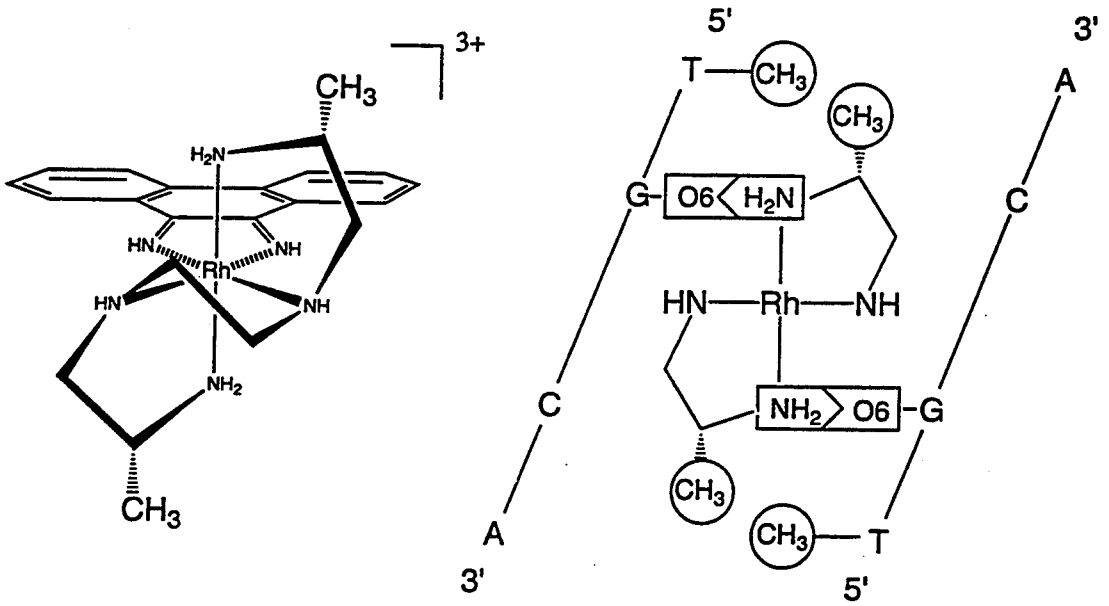
3+
CH3
H2N
HN
Rh
NH
HN
NH
NH2
CH3
5'
3'
T
CH3
CH3
A
G
O6
H2N
C
HN
Rh
NH
C
NH2
O6
G
CH3
CH3
T
A
3'
5'

Figure 5.2. Three-dimensional model of 4 bp recognition by Δ–α-Rh(R,R-Me_2trien)phi^{3+}. The sugar phosphate backbone is shown in green, the base pairs in white, and the metal complex in blue. The specific, non-covalent interactions responsible for recognition are shown in red.

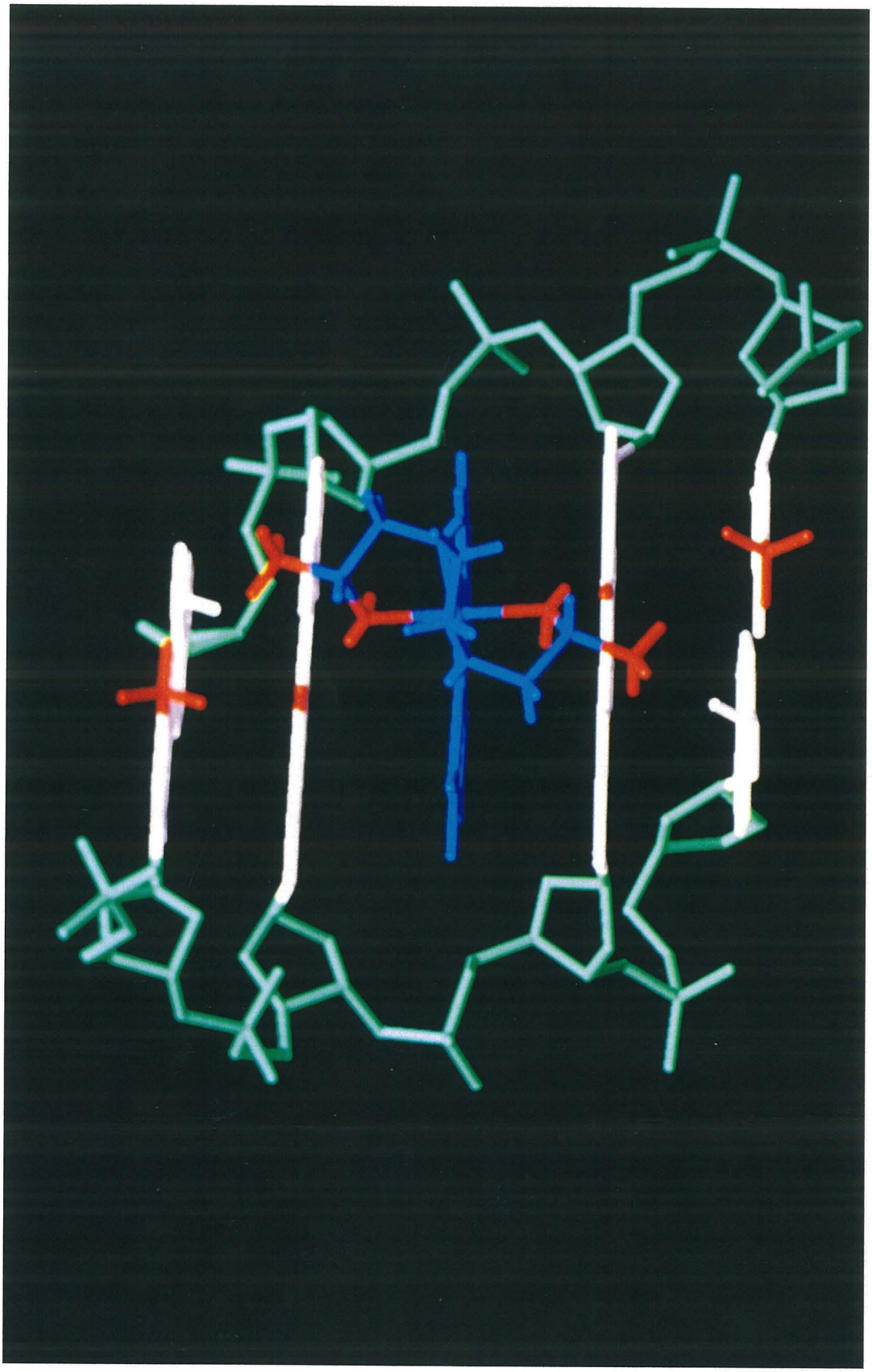

bound specifically to the central G_3-C_4 step of $d(GTGCAC)_2$, while the Λ-enantiomer bound non-specifically. Molecular models based on the NMR evidence indicates that the deep intercalation of the phi ligand serves not to create steric clashes with the DNA backbone, but in fact ideally locate the ancillary ligands of both enantiomers to engage in the proposed hydrogen bonding and van der Waals contacts.

While the overall sequence selectivity of the enantiomers of $Rh(en)_2phi^{3+}$ is low, they have provided a unique model system with which to investigate the importance of hydrogen bonding and van der Waals contacts in the recognition of DNA. The basic principles detailed here provide a means whereby sequence specific affinity may be increased in a modular fashion through the linking of several hydrogen bonding or van der Waals groups onto a larger molecule. Such a system is best represented by the complex Δ-α-$Rh(R,R\text{-}Me_2trien)phi^{3+}$ (Figure 1).[3,4] This complex is capable of 4 bp recognition based on a combination of simple hydrogen bonding and van der Waals contacts. The versatility of this complex, based upon the condensation of two amino acids with ethylene diamine to yield the derivatized trien framework, offers the possibility of incorporating any natural or unnatural amino acid. Such a scheme allows us to present a wide array of functionality to the major groove of DNA in the attempt to not only explore the importance of various recognition elements, but to develop sequence specific intercalative metal complexes in a predictive manner.

References :

1. Dervan, P. B. *Science* **1986**, *232*, 464.

2. Barton, J.K. *Science*, **1986**, *233*, 727.

3. Krotz, A.H.; Hudson, B.P.; Barton, J.K. *J. Am. Chem Soc.* **1993** , *115*, 12577.

4. Hudson, B.P.; Collins, J.G.; Barton, J.K. unpublished results.